

Dissertation

submitted to the

Combined Faculty of Natural Sciences and Mathematics
of Heidelberg University, Germany

for the degree of

Doctor of Natural Sciences

Put forward by

Markus Heller

born in: Stuttgart, Germany
Oral examination: July 21st, 2021

A Temporal Functional Renormalisation Group Approach to Non-Perturbative Quantum Dynamics

Referees: Prof. Dr. Jan M. Pawłowski
Prof. Dr. Joerg Jaeckel

Ein Zugang zu Nichtperturbativer Quantendynamik mit der Zeitlichen Funktionalen Renormierungsgruppe

In dieser Arbeit wird der Formalismus der zeitlichen funktionalen Renormierungsgruppe, der einen nichtperturbativen Zugang für die Berechnung der Dynamik von Korrelationsfunktionen in Quantenfeldtheorien darstellt, wesentlich weiterentwickelt. Zu diesem Zweck überarbeiten wir sorgfältig die Herleitung der zeitlichen Flussgleichung, wobei wir besonderes Augenmerk auf Eigenschaften legen, die sich aus einem kausalen zeitlichen Regulator ergeben. Wir nutzen die manifeste Kausalität des Formalismus, um den allgemeinen zeitlichen Fluss analytisch zu integrieren. Das Ergebnis sind neue exakte ein-loop Gleichungen für vollständig gedresste Korrelationsfunktionen. Durch weitere Ausnutzung der Kausalität leiten wir die vollständige Dyson-Schwinger-Hierarchie und den effektiven s-Kanal Vertex aus spezifischen Trunkierungen des zeitlichen Flusses her. Wir lösen das Problem der Renormierung des allgemeinen kausalen Zeitflusses. Wir zeigen, dass bestimmte Arten von kausalen Integralgleichungen durch eine explizite numerische Methode gelöst werden können. Wir lösen den integrierten Fluss numerisch in einer Trunkierung, die den Propagator der ϕ^3 -Theorie in $1 + 1$ Dimensionen enthält. Unsere Ergebnisse deuten auf das Auftreten von universeller Dynamik hin. Aufgrund der hohen Flexibilität der Approximationsschemata des zeitlichen Flusses ist die Energieerhaltung in generischen Trunkierungen nicht automatisch gewährleistet, sondern wird zu einer nicht-trivialen Eigenschaft. Wir befassen uns mit energieerhaltenden Trunkierungen, indem wir den kausalen zeitlichen Fluss des Energie-Impuls-Tensors herleiten und diesen analytisch integrieren.

A Temporal Functional Renormalisation Group Approach to Non-Perturbative Quantum Dynamics

In this work, we substantially advance the formalism of the temporal functional renormalisation group which constitutes a non-perturbative framework for computing the dynamics of correlation functions in quantum field theories. To that end we carefully revisit the derivation of the temporal flow equation, paying particular attention to properties arising from a causal temporal regulator. We use the manifest causality of the formalism to integrate the general temporal flow analytically. The result are novel one-loop exact equations for fully dressed correlation functions. Further leveraging causality, we derive the complete Dyson-Schwinger hierarchy and the s-channel effective vertex in terms of specific truncations of the temporal flow. We solve the problem of renormalising the general causal temporal flow. We demonstrate that certain types of causal integral equations can be solved by an explicit numerical method. We numerically solve the integrated flow in a truncation involving the propagator of the ϕ^3 -theory in $1 + 1$ dimensions. Our results indicate the emergence of universal dynamics. Due to the high degree of flexibility of approximation schemes of the temporal flow, energy conservation in generic truncations is not guaranteed automatically but becomes a non-trivial feature instead. We explore energy-conserving truncations by deriving the causal temporal flow of the energy-momentum tensor, which we integrate analytically.

Contents

1. Introduction	1
1.1. Motivation	1
1.2. Outline	6
1.3. Publications	8
2. The Closed Time Path	11
2.1. Time Evolution and the Contour	11
2.1.1. The Initial State and Open and Closed Quantum Systems	12
2.1.2. Time Evolution	13
2.1.3. The Contour	18
2.1.4. Causality, Unitarity and Energy Conservation in Approximations	23
2.2. Generating Functionals and the Path Integral	26
2.2.1. Generating Functionals	26
2.2.2. The Path Integral	28
2.2.3. The Basic Idea: A Closed Time Path of Variable Extent	32
3. The Temporal Functional Renormalisation Group	37
3.1. The Temporal Flow Equation	37
3.1.1. The Regulator	38
3.1.2. The Temporally Regulated Effective Action	40
3.1.3. Derivation of the Temporal Flow Equation	43
3.1.4. Initial Conditions	46
3.1.5. Truncations	47
3.1.6. The Role of the Background Field	50
3.2. Causality-Properties of the Temporal Flow	51
3.2.1. The Propagation of Fluctuations	51
3.2.2. Causality-Properties of the 1PI Correlation Functions	53
3.2.3. Implications of Causality for the Propagator	55
3.2.4. From Causality-Properties to Causal Constraints	57
3.2.5. Causality for the Connected Correlation Functions	58

3.3.	On the Numerical Solution of the Temporal Flow	59
3.4.	Conclusion	62
4.	The Analytically Integrated Causal Temporal Flow	63
4.1.	The Causal Constraints at Work	64
4.1.1.	Singular Products of Distributions	66
4.1.2.	The Degree of Locality of the Vertex Corrections	67
4.2.	Integrated Flow of the Two-Point Function	69
4.2.1.	Cubic Interactions Only	71
4.2.2.	Cubic and Quartic Interactions	73
4.3.	Integrated Flow of the One-Point Function	74
4.4.	Integrated Flow of the Effective Action	75
4.4.1.	Derivation and Discussion	75
4.4.2.	Towards a Causal Temporal Flow in Equilibrium	76
4.5.	Dyson-Schwinger Equations from the Integrated Flow	78
4.5.1.	The Sunset Diagram	80
4.5.2.	The Squint Diagram	83
4.5.3.	Dyson-Schwinger Equation for the One-Point Function	85
4.6.	s-Channel Effective Vertex from the Integrated Flow	86
4.7.	Renormalisation	89
4.7.1.	The Role of the Closed Time Path	89
4.7.2.	Renormalising the Causal Temporal Flow	90
4.7.3.	Discussion	94
4.8.	An Explicit Numerical Method for Causal Integral Equations	95
4.8.1.	The Propagator	95
4.8.2.	The s-Channel Effective Vertex	100
4.9.	Towards an Entirely Time-Local Causal Flow	100
4.10.	Conclusion	104
5.	Dynamics of the ϕ^3-Theory	107
5.1.	Truncation	108
5.2.	Dynamic Equations	109
5.3.	Observables and Initial Conditions	110
5.4.	Numerical Results for the Propagator	112
5.5.	Discussion and Comparison	115
5.5.1.	Discussion	116
5.5.2.	Comparison	118

5.6. Energy Conservation	121
5.6.1. Derivation	121
5.6.2. Numerical Result	123
5.6.3. Discussion	123
5.7. Particle Number Conservation	124
5.8. Conclusion	125
6. Towards Energy Conservation of Generic tFRG Truncations	127
6.1. The Causal Flow of the Energy-Momentum Tensor	127
6.2. Integrated Causal Flow of the Energy-Momentum Tensor	131
6.3. Conclusion	135
7. Summary and Outlook	137
A. Closed Time Path Notation and Propagator Bases	141
B. Diagrammatic Flow Equations for $\Gamma_\tau^{(3)}$ and $\Gamma_\tau^{(4)}$	145
C. Numerical Results for the Propagator from Its Integral Equation	149
Acknowledgments	153
Bibliography	155

1. Introduction

The fate of a generic many-body system driven out of equilibrium is inevitable: Eventually, it will thermalise. For closed quantum systems, reconciling this fact with their unitary time evolution poses a long-standing problem. How and when these systems reach equilibrium is interesting from a fundamental point of view and in concrete examples such as the early universe, relativistic heavy ion collisions and in tabletop experiments with ultracold atoms. Apart from being necessary to understand the final approach to equilibrium, a thorough understanding of the whole dynamical evolution allows to gain insights into new out-of-equilibrium phenomena and is crucial to make contact with experiments. For extreme initial conditions, the dynamics can become universal, revealing striking similarities between the above mentioned and a priori very different physical systems. In this work, we apply and substantially advance a non-perturbative method introduced in [6] and [7] that allows to compute non-equilibrium quantum correlation functions. It is based on the functional renormalisation group (FRG) with a temporal regulator.

1.1. Motivation

Unitary Evolution and Equilibration During the unitary evolution of closed quantum systems, none of the information contained in the initial state is lost. This seemingly contradicts the fact that in equilibrium, these systems can be described by just a few macroscopic parameters. In particular, these macroscopic parameters show no dependence on any initial conditions. In recent years, a mechanism known as Eigenstate Thermalisation Hypothesis has received renewed attention as a way to resolve this apparent contradiction. In particular, it was successfully used in [8] to demonstrate how unitary time evolution reveals the equilibrium values of few-body observables (see also the review [9]). However, while the Eigenstate Thermalisation Hypothesis constitutes a general mechanism reconciling unitary time evolution with statistical mechanics, it does not provide the means to compute the actual dynamics of observables. In this regard, diverse theoretical efforts have been devoted to developing stable approximations

to the full quantum dynamics, ranging from lattice to diagrammatic approaches (for reviews see e.g. [10–16]). Still, there are interesting questions that are out of reach of currently available methods. For instance, there is no approach that allows to compute the quantum dynamics of gauge theories. Moreover, accessing the dynamics of higher order correlations, which can be measured in experiments nowadays, poses a considerable challenge.

The Early Universe The prime example of a closed system is given by the universe itself. Its cosmological evolution and especially the dynamics of reheating after inflation received considerable attention. In fact, this is precisely the context that triggered early works on developing suitable approximations to quantum dynamics, see e.g. [17]. The hypothetical particle describing the quantum dynamical evolution of inflation is called the inflaton. During inflation, the associated inflaton field acquires a large field value which subsequently decays into particles. The ensuing dynamics was found to display features of universality out of equilibrium which are reminiscent of classical wave turbulence [18, 19]. As there is a lot of energy stored in the inflaton field, its decay produces a hot medium of particles, which is too hot for hadrons to form. Instead, quarks and gluons exist in a different phase of matter, known as the quark-gluon plasma (QGP).

The Quark-Gluon Plasma Investigating the properties of the QGP is a central aspect of studying heavy ion collisions (HICs). These systems are very attractive from a theoretical point of view since their actual microscopic description is well established. It is given by quantum chromodynamics (QCD) which is a non-abelian gauge theory. What is relevant at the scales of the QGP however are the macroscopic implications of QCD. Extracting these is already a formidable task in equilibrium since they require solving the strongly interacting regime of the quantum gauge theory.

The dynamical evolution of a HIC can be characterised as follows: Initially, two nuclei collide close to the speed of light, generating strong gluonic fields. Their ensuing decay produces quarks and gluons with a lot of energy. These thermalise locally above the QCD phase transition (crossover), creating the quark-gluon plasma. The hot plasma cools down as it expands and eventually hadronises, thereby crossing the confinement-deconfinement and the chiral phase transition of QCD.

An ab initio understanding of the QGP requires access to the dynamics and the equilibration processes of QCD. However, the direct computation of dynamics in QCD is out of reach to date. Nevertheless, a lot of progress with regard to HICs has been made.

In particular the limits of very strong and very weak QCD coupling are well controlled theoretically. The weak coupling regime is characterised by a non-perturbatively large occupancies of gluons. Accordingly, it can not be accessed in perturbation theory. Due to these large occupancies, quantum effects are strongly suppressed and a semi-classical description is justified. This semi-classical picture is used to describe the initial condition and the very early stage of a HIC. However, when the occupancies decrease during the course of the dynamics, quantum effects start to become relevant and other approximations must be employed. The QGP itself is well described hydrodynamically in terms of a low-viscosity fluid. More details regarding different approximation schemes can be found in [20, 21].

While these approaches have been very successful, open questions remain [20, 21]. In particular, it is in general non-trivial to extrapolate from the regimes that are well controlled theoretically to those present in the experiments. First and foremost, this is simply due to the fact that a HIC is a very complicated system, both from the theoretical as well as the experimental perspective. Moreover, it is an ongoing debate which values of the QCD coupling α_S are relevant for the different processes and stages of a collision. For instance, the best estimate for α_S at the onset of the hydrodynamic regime is given by $\alpha_S \approx 0.3$. This represents neither of the theoretically well controlled limits of very small or very large coupling. On top of all that, the coupling is expected to evolve dynamically itself. Microscopically, the respective time evolution is dictated by QCD and can not be accessed by currently available computational techniques.

The 2PI Approach A widely used formalism with regard to quantum dynamics is given by the 2PI approach [22, 23]. It has been successfully applied to the dynamics of scalars and fermions (see [14] and references therein). Furthermore, the 2PI framework has been used successfully to derive approximations that are valid in certain phases of a HIC. However, venturing outside of the range of validity of these approximations poses a challenge.

The underlying reason is related to a cherished feature of the 2PI approach, its self-consistency. Self-consistency refers to the fact that any 2PI approximation is specified by choosing a set of two-particle-irreducible skeleton diagrams that contribute to the 2PI effective action. Accordingly, the quantum equations of motion derived from this action by a variational principle are consistent among themselves and automatically guarantee the conservation of energy in approximations. These features are of particular importance in dynamical applications.

However, the self-consistency of the 2PI approach comes at a price: Approximations

are severely constrained as only two-particle-irreducible contributions are admissible. This poses a challenge to the application of the 2PI formalism to gauge theories. Indeed in standard perturbation theory which is based the 1PI effective action, gauge invariance is maintained at every order of the expansion. Due to the constraint of two-particle-irreducibility, the coupling expansion of the 2PI effective action¹ is missing diagrams compared to the 1PI expansion at any finite order. Thus, the relations that maintain gauge invariance at every order of the perturbative 1PI expansion can not be fulfilled. Accordingly, the corresponding local symmetry is broken [24–27]. Note that due to the same reasons, also issues in the case of global symmetries can arise [28, 29]. These issues are also intimately related to the fact that the 2PI approach does not grant direct access to the dynamics of higher order correlations.

The Objective Therefore, it is desirable to develop a complementary method, that is able – at least in principle – to describe dynamics in QCD. Necessary requirements include that it should be a non-perturbative approach compatible with gauge invariance. Moreover, it should allow to access the dynamics of over-occupied initial conditions, which are of great practical relevance, while also being able to describe the quantum regime of low occupancies, which is relevant for the late time approach to equilibrium. Furthermore, it should be possible to directly access the dynamics of higher order correlations. These are interesting from an experimental and a theoretical point of view. The framework put forward in this work enjoys these features. Due to the overall outstanding success of the 2PI framework in dynamical applications, our goal is to preserve as many of its beneficial features as possible, while at the same time generalising it sufficiently. The desired outcome is to obtain more flexible approximation schemes for quantum dynamics in general and feasible approximations for the quantum dynamics of gauge theories in particular.

The Functional Renormalisation Group Starting with the similarities, the method we discuss in this work is also based on a non-perturbative, diagrammatic, functional approach – the functional renormalisation group (FRG) [30–32]. A central object of the FRG is the regularised quantum effective action. A type of regularisation studied extensively adds a momentum dependent, mass-like regulator term to the effective action. It suppresses fluctuations and allows to integrate them out successively, one momentum shell at a time. An unfortunate consequence of such a momentum dependent mass-term is that it leads to modifications of local symmetries. While these can be controlled in

¹Note that this expansion is not necessary in practice, cf. Sec. 2.1.4.

equilibrium (cf. [33] and references therein), the issue is more subtle in dynamical applications. This is related to the fact that in their naive formulation, gauge theories contain unphysical degrees of freedom. These can cause instabilities in numerical approaches to the quantum dynamics of gauge theories.

The Temporal FRG The central idea of the approach pursued in this work is the following: Instead of employing a regularisation in momentum space, we introduce a temporal regulator. Accordingly, the present approach is called the temporal functional renormalisation group (tFRG) [1–3, 6, 7]. The corresponding flow equation for the quantum effective action can be thought of as integrating out fluctuations time slice by time slice. For related developments in the context of cosmology, see [34] and for non-equilibrium FRG applications with a standard momentum regulator see e.g. [35–51].

In particular, we will consider a causal temporal regulator, ensuring a causal time evolution of the quantum effective action. Notably, this regulator does not interfere with the local symmetries of a gauge theory since gauge theories are causal. Furthermore, as the tFRG approach is based on the 1PI effective action, it features fully dressed correlation functions of arbitrary order. Moreover, since it is a non-perturbative approach, it can naturally deal with both classical as well as quantum fluctuations.

Notably, truncations of the tFRG can be specified on the level of the individual correlation functions. On the contrary, 2PI approximations must be specified on the level of the effective action. Therefore, generic tFRG truncations are more flexible. However, there is a price to pay for this gain in flexibility. For generic tFRG truncations, the conservation of energy and the compatibility of the truncated evolution equations of the individual correlation functions are not guaranteed automatically but become a non-trivial feature instead. In this regard, the tFRG formalism displays very promising properties. First of all, it is possible to recover the self-consistent 2PI approximations from the tFRG. More generally, the conservation of energy in generic tFRG approximations can be addressed by considering the temporal flow of the energy-momentum tensor.

Universal Dynamics Apart from addressing the dynamics of quantum gauge theories, the tFRG approach is also of interest with respect to dynamics of quantum field theories in general. A particularly exciting topic in this regard is given by universality out of equilibrium. An impressive demonstration of universal dynamics is given by the fact that the decay of occupations in the early stages of a HIC was found to proceed

through processes reminiscent of classical turbulence, providing intriguing links to the time evolution of reheating in the early universe [52, 53]. The emergence of dynamic universality has been attributed to non-equilibrium attractor solutions known as non-thermal fixed points (NTFP) [54–56]. Similarly to universality in equilibrium, the scaling behaviour of correlations at these fixed points suggest a classification in terms of non-equilibrium universality classes. Interestingly, they appear to be much larger than their equilibrium counter parts, for example encompassing relativistic and non-relativistic scalar theories [57] and even gauge and scalar theories in the semi-classical regime of high occupancies [58].

Aside from leading to a remarkable convergence of theoretical efforts, dynamic universality has resulted in a close collaboration between theory and experiments. Today, the quantum dynamics of scalars and fermions are experimentally accessible in a variety of different platforms using ultracold atoms. These enabled the first experimental observations of the self-similar scaling dynamics at a NTFP [59, 60]. Furthermore, the precise control given in these experiments now allows measurements of higher-order correlations [61] and their dynamics [62]. Moreover, there is the interesting possibility of using these platforms to simulate quantum dynamics. For instance, there is a proposal to simulate reheating after inflation with ultracold atoms. [63].

NTFPs have been mainly described theoretically by two-point correlations which can be accessed in the 2PI formalism and its derivatives (see [64–67] for applications to Bose gases). However, when the time evolution becomes universal, in principle all correlators show scaling behaviour. Taking this into account, for instance using the tFRG approach, should provide a more refined picture of the universality classes associated to NTFPs. Moreover, FRG methods are well suited to perform a scaling analysis which allows to find fixed points [68]. Thus, the tFRG can contribute to the classification of temporal scaling phenomena, as it allows to find NTFP. Furthermore, apart from understanding the approach to and the dynamics at NTFPs, it is of interest to study how precisely the departure towards the equilibrium fixed point comes about. This departure is associated to an unstable direction at the NTFP which can be investigated using the tFRG.

1.2. Outline

In Ch. 2, we introduce the basics of non-equilibrium quantum field theory using the Schwinger-Keldysh closed time path. We comment on features of the Schwinger-Keldysh formalism in approximations and introduce an important concept for this work: A closed time path of variable extent.

In Ch. 3, we introduce the formalism of the temporal functional renormalisation group. We revisit the derivation of the temporal flow equation, focusing on properties and subtleties that arise from employing a causal temporal regulator. Amongst others, this allows us to clarify the role of the background field in the tFRG. We propose approaches to devise general and consistent tFRG truncations, and we discuss the causality-properties of the regulated, flowing correlation functions. Notably, we translate them into local causal constraints for the temporal flow. These causal constraints are at the heart of many results obtained in this work. We conclude this chapter by addressing some of the challenges we encountered, attempting to numerically solve the temporal flow.

In Ch. 4, we use the causal constraints to integrate the general temporal flow analytically, obtaining novel one-loop exact equations for the fully dressed correlation functions. The integration is facilitated by a locality analysis of possible vertex corrections. We then put this machinery to work and derive the complete hierarchy of Dyson-Schwinger equations as well as the s-channel effective vertex from the temporal flow. We show that the latter is able to reproduce the 2PI $1/N$ expansion at next-to-leading order. We proceed with another major novel development of the present work: We solve the problem of renormalising the causal temporal flow in general, using the ϕ^4 -theory in $3 + 1$ dimensions as a concrete example. Furthermore, we derive an algorithm that allows to solve certain causal integral equations in terms of an explicit numerical method, involving only sums over known values. Regarding the memory integrals present in the tFRG, we propose an extension of the temporal flow which uses a non-diagonal causal temporal regulator. We outline how this could give rise to entirely time-local evolution equations for the correlation functions.

In Ch. 5, we numerically solve the integrated flow in a truncation containing the propagator of the ϕ^3 -theory in $1 + 1$ dimensions. Our results indicate the emergence of universal dynamics. We discuss the numerical satisfaction of conservation of energy and particle number. Moreover, we derive a simple equation for the expectation value of the energy-momentum tensor of the ϕ^3 -theory involving only the propagator.

In Ch. 6, we address the question of energy-conservation in generic tFRG truncations by deriving the general flow of the energy-momentum tensor. We show that the causal temporal flow of the energy-momentum tensor differs by regulator terms from the general flow, and we discuss the respective implications regarding the trace anomaly of the energy-momentum tensor. We analytically integrate the causal temporal flow and show that it is consistent with the usual symmetry identity of the expectation value of the energy-momentum tensor.

We summarise our main results and give an outlook in Ch. 7. The Appendices A - C

contain material supplementing the discussions of the main text.

1.3. Publications

This dissertation has been compiled by the author alone. However, most of the presented results were obtained together with my collaborators. Elements of text taken from the publications below are not marked explicitly. They are part of Ch. 3, 4, 5 and 6 as well as of App. C. Figures taken from these publications are marked explicitly.

[1] **Flowing with the Temporal Renormalisation Group**

Lukas Corell, Anton K. Cyrol, Markus Heller, Jan M. Pawłowski
submitted to Physical Review D
Eprint: arXiv:1910.09369

[2] **Renormalised Causal Temporal Flow**

Lukas Corell, Markus Heller, Jan M. Pawłowski
In preparation.
Comment: We solve the problem of renormalising the general causal temporal flow.

[3] **Causal Temporal Flow of the Energy-Momentum Tensor**

Markus Heller, Jan M. Pawłowski
In preparation.
Comment: We derive the general flow of the energy-momentum tensor (EMT). We show that the causal temporal flow of the EMT differs by regulator terms from the general flow. We discuss the relation of this difference to the trace anomaly of the EMT. We integrate the causal temporal flow of the EMT analytically and demonstrate that it is consistent with the symmetry identity of the expectation value of the EMT.

Beyond that, Ch. 3, 4, 5 and 6 additionally contain new and extended results which are so far unpublished. We will indicate this when appropriate.

Two more articles were published before my PhD. These works were compiled during my Master studies and are not included in this dissertation.

[4] **The Goldstino Brane, the Constrained Superfields and Matter in $\mathcal{N} = 1$ Supergravity**

Igor Bandos, Markus Heller, Sergei M. Kuzenko, Luca Martucci, Dmitri Sorokin
Published in JHEP 11, 109 (2016).
Eprint: arXiv:1608.05908

[5] **Pion and η -Meson Mass Splitting at the Two-Flavour Chiral Crossover**

Markus Heller, Mario Mitter

Published in Phys. Rev. D 94, 074002 (2016).

Eprint: arXiv:1512.05241

2. The Closed Time Path

This chapter constitutes an introduction to the Schwinger-Keldysh closed time path (CTP) formalism [69, 70]. For related works and early applications, see also [71–76]. This formalism allows us to describe the dynamics of quantum field theories. The basic facts about the CTP are for example covered in [14, 77, 78]. For general textbook knowledge, see e.g. [79, 80].

In Sec. 2.1, we discuss the Schwinger-Keldysh formalism in detail, striving to provide a pedagogical discussion of the basic ideas and important concepts of the formalism. Readers familiar with these can jump directly to Sec. 2.1.4, where we discuss features of the Schwinger-Keldysh formalism in approximations and summarise important aspects of self-consistent approximations.

In Sec. 2.2, we introduce the generating functional for the correlation functions of the Schwinger-Keldysh formalism. Paying particular attention to subtleties that originate from a time path of finite extent, we represent the generating functional in terms of the path integral. Readers familiar with this construction can skip directly to Sec. 2.2.3. There, we introduce and illustrate the basic idea of the temporal FRG: A closed time path of variable extent. This idea originated in [81, 82] and was further developed by us in [1–3]. It is implemented using concepts from functional renormalisation group (FRG) theory in Ch. 3.

We collect some notation regarding the closed time path and different representations of the CTP-propagator in App. A. We work in units $c = \hbar = k_B = 1$.

2.1. Time Evolution and the Contour

At a fixed time t_0 , consider the state of a quantum system that is described by the density matrix $\rho(t_0) = \rho_{t_0}$. Furthermore, let this system interact according to the Hamiltonian $\mathcal{H}(t)$.

2.1.1. The Initial State and Open and Closed Quantum Systems

In the most general case, the Hamiltonian operator $\mathcal{H}(t)$ depends explicitly on time. Such an explicit time dependence arises for instance if a coupling is turned on or off non-adiabatically. This type of sudden change in the Hamiltonian is referred to as a quench. More generally, an explicit time dependence arises for any coupling to time-dependent external fields. Here, “external” refers to classical, non-fluctuating fields. One major application of such time-dependent external fields is given by periodically driven systems. For more details see e.g. [16].

In this work, we will not consider any continuous external perturbations. We remark that these can be described in the tFRG framework, cf. Sec. 3.1.6. The concept of a quench on the other hand will prove useful for us. Hence, we illustrate it briefly: For this example, consider a system that is described by some Hamiltonian \mathcal{H}_{eq} . Moreover, assume for the moment that the system is in equilibrium at the time t_0 . The corresponding equilibrium state is given by $\rho_{t_0} \propto e^{-\beta \mathcal{H}_{\text{eq}}}$. In order to trigger a dynamical evolution for times $t > t_0$, we perturb the system which is efficiently accomplished by a quench. This means to suddenly change the Hamiltonian. Thus in the first instance, the state stays the same but its energy changes. Therefore, ρ_{t_0} now represents an excited state with respect to the quenched Hamiltonian and a dynamical evolution ensues.

Note that the thermal state $\rho_{t_0} \propto e^{-\beta \mathcal{H}_{\text{eq}}}$ provides an example of a correlated state if \mathcal{H}_{eq} represents an interacting system. To characterise a correlated state in terms of correlation functions requires n -point functions with $n > 2$. We remark that such general correlated initial states are naturally part of the tFRG, and we discuss this in Sec. 3.1.4. Let us emphasise that in general dynamical applications, ρ_{t_0} is not an equilibrium state. For instance in Ch. 5, we will explicitly consider a far-from-equilibrium initial state in our numerical applications.

An important result with regard to correlated initial states is that any general, possibly correlated, non-equilibrium initial state that is physically meaningful can always be obtained from an instantaneous quench, cf. e.g. [83]. We explain this in more detail in Sec. 4.9. Here, we just point out the following: The limit of an instantaneous quench corresponds to an experiment in which the dynamical system is isolated to a high degree against interactions with its environment during the time scales that are of interest. Examples of such isolated systems are given by HICs and experiments with ultracold atoms, cf. e.g. [20, 67]. In these cases, using the formalism of closed, isolated quantum systems is a very good approximation [78]. Note that considering an instantaneous quench implies that we neglect the influence of the environment during the dynamics completely. All that is left of any pre-quench system-environment interactions are the

correlations of the initial state at t_0 . Importantly, the energy of the dynamical system remains constant and no information is lost during the time evolution for $t > t_0$. We remark that if we want to describe a setting in which the system and the environment are not well-isolated during the dynamical evolution of the system, then we should use the formalism of open systems [84].

2.1.2. Time Evolution

In this work, we will focus on closed, isolated systems. Thus, all the information about the state of such a quantum system is contained in the initial density matrix ρ_{t_0} . Furthermore, the time evolution of the density matrix is governed by the unitary operator \mathcal{U}

$$\rho(t) = \mathcal{U}(t, t_0) \rho_{t_0} \mathcal{U}^\dagger(t, t_0).$$

The time evolution operator is the solution to the Schrödinger equation

$$\partial_{t_2} \mathcal{U}(t_2, t_1) = -i \mathcal{H}_S(t_2) \mathcal{U}(t_2, t_1) \quad \text{with} \quad t_2 \geq t_1. \quad (2.1)$$

Here, we denote the Hamiltonian in the Schrödinger picture as $\mathcal{H}_S(t)$. Let us formally solve the Schrödinger equation (2.1), thus obtaining the time evolution operator in terms of $\mathcal{H}_S(t)$. Using the initial condition $\mathcal{U}(t_1, t_1) = \mathbb{1}$, the solution reads

$$\mathcal{U}(t_2, t_1) = \mathcal{T} \exp \left[-i \int_{t_1}^{t_2} dt \mathcal{H}_S(t) \right], \quad t_2 > t_1. \quad (2.2)$$

Here, \mathcal{T} denotes standard time-ordering, i.e. operators with later times are moved to the left. This ordering appears naturally when solving the Schrödinger equation (2.1) by iteration using the composition law (2.3). The time evolution operator evolves states causally by acting on them from the left. It has the following properties:

$$\mathcal{U}(t_2, t_1) = \mathcal{U}(t_2, t) \mathcal{U}(t, t_1) \quad \text{for} \quad t \in [t_1, t_2] \quad (2.3)$$

$$\mathcal{U}(t_1, t_1) = \mathbb{1} \quad (2.4)$$

$$\mathcal{U}^\dagger(t_2, t_1) = \mathcal{U}^{-1}(t_2, t_1) = \mathcal{U}(t_1, t_2). \quad (2.5)$$

These relations encode profoundly important physical concepts. The composition law (2.3) reflects causality: In order for a cause at t_1 to take effect at $t_2 > t_1$, it must have passed the intermediate times t chronologically. The property (2.4) follows from causality by considering $t = t_1$. It indicates that there is an initial state at which the

time evolution starts and where \mathbf{U} is trivial accordingly. Eq. (2.5) states that quantum dynamics is unitary: No information encoded in the initial state is lost during the time evolution of a closed system. The major challenge all approaches to quantum dynamics have to face is to preserve these features in approximations. The Schwinger-Keldysh formalism, which we introduce in this section, assists us tremendously in addressing this challenge.

We proceed by determining the explicit form of \mathbf{U}^\dagger , which is found by solving the hermitian conjugate of the Schrödinger equation (2.1), resulting in

$$\mathbf{U}^\dagger(t_2, t_1) = \overline{\mathcal{T}} \exp \left[i \int_{t_1}^{t_2} dt \mathcal{H}_S(t) \right], \quad t_2 > t_1, \quad (2.6)$$

where $\overline{\mathcal{T}}$ denotes anti-time-ordering, i.e. later times are moved to the right. \mathbf{U}^\dagger evolves conjugate states causally by acting on them from the right. Due to unitarity (2.5), there is also a natural interpretation of the action of \mathbf{U}^\dagger on states from the left: $\mathbf{U}^\dagger(t_2, t_1)$ with $t_2 > t_1$ evolves states backward in time. Thus, unitarity allows us to find $\mathbf{U}(t_2, t_1)$ for $t_2 < t_1$ in terms of $\mathbf{U}^\dagger(t_1, t_2)$. Combining its explicit form (2.6) with Eq. (2.2) for \mathbf{U} , we obtain an expression for the time evolution operator for both time-orderings, to wit

$$\mathbf{U}(t_2, t_1) = \begin{cases} \mathcal{T} \exp \left[-i \int_{t_1}^{t_2} dt \mathcal{H}_S(t) \right] & \text{if } t_2 > t_1 \\ \overline{\mathcal{T}} \exp \left[i \int_{t_2}^{t_1} dt \mathcal{H}_S(t) \right] & \text{if } t_2 < t_1 \end{cases}. \quad (2.7)$$

The microscopic field operators Φ_S entering in the Hamiltonian are time-independent in the Schrödinger picture. We suppress any spatial dependence and all types of indices until they are needed explicitly. For simplicity, we take Φ_S to be bosonic. The generalisation to fermions is straight forward. Note that the following discussion can be directly generalised to (possibly composite) operators by replacing Φ_S with a general operator $\mathcal{O}_S(t)$. Such operators can have an explicit time dependence in the Schrödinger picture, and we refer to [78] for more details.

We are interested in the time-dependent expectation values of the microscopic field operators Φ_S . These encode all the information about the dynamics of a quantum field theory. For a single operator, its time-dependent expectation value is computed as

follows

$$\begin{aligned}
 \langle \Phi_S(t) \rangle &= \text{Tr}[\rho(t) \Phi_S] \\
 &= \text{Tr}[\mathcal{U}(t, t_0) \rho_{t_0} \mathcal{U}(t_0, t) \Phi_S] \\
 &= \text{Tr}[\mathcal{U}(t_0, t) \Phi_S \mathcal{U}(t, t_0) \rho_{t_0}] ,
 \end{aligned}$$

where we used the basic properties of \mathcal{U} and the cyclicity of the trace. There exists a variety of different approaches to compute such time-dependent expectation values. One way to distinguish these approaches is the following: Either, the approach stays in the Schrödinger picture and employs a state-based formalism, or it uses the Heisenberg picture where the time dependence is carried by the operators. A comparison between these two different types of approaches is for example given in [85].

The Heisenberg picture allows to define time-dependent correlation functions as the expectation values of products of multiple operators, and we choose to work in this picture. In particular, we will eventually employ a functional approach to time-dependent correlation functions. The functional language will give us access to powerful functional renormalisation group techniques. Their application to quantum dynamics constitutes the major part of this work, and we start to introduce these techniques in Ch. 3. For the rest of this section, we continue to work with operators. Concretely, we proceed by defining operators in the Heisenberg picture as follows:

$$\Phi(t) := \mathcal{U}(t_0, t) \Phi_S \mathcal{U}(t, t_0) .$$

The expectation value of a single Heisenberg operator is defined as

$$\langle \Phi(t) \rangle = \text{Tr}[\Phi(t) \rho_{t_0}] = \text{Tr}[\mathcal{U}(t_0, t) \Phi_S \mathcal{U}(t, t_0) \rho_{t_0}] . \quad (2.8)$$

This guarantees $\langle \Phi(t) \rangle = \langle \Phi_S(t) \rangle$ by construction. Thus, both pictures are equivalent as they should be. Time-dependent correlation functions can now be defined by inserting further operators into the trace in Eq. (2.8). Let us remark that in this case, the equivalence of the Heisenberg and the Schrödinger picture is less obvious. This is mainly due to the fact that in the Heisenberg picture, multiple, in general different time arguments appear, whereas in the Schroedinger picture there is only a single time – the time of the state $\rho(t)$. We resolve this apparent tension in Sec. 4.9.

Now, consider again Eq. (2.8). In particular, observe the product of operators inside the trace. Reading the last expression from right to left, we start with the system in

$$\mathcal{U}(t_2, t_1) = \begin{cases} \begin{array}{c} t_1 \quad \longrightarrow \quad t_2 \\ \text{blue arrow} \end{array} & \text{if } t_2 > t_1 \\ \begin{array}{c} t_2 \quad \longleftarrow \quad t_1 \\ \text{red arrow} \end{array} & \text{if } t_2 < t_1 \end{cases}, \quad \bullet \quad \Phi_S \text{ or } \rho(t)$$

Figure 2.1.: Building blocks for the graphical representation of time-dependent correlation functions. A right-facing blue arrow denotes the time-ordered case and a left-facing red arrow the anti-time-ordered one. Operator insertions are indicated by a black dot.

its initial state specified by ρ_{t_0} . We then evolve with $\mathcal{U}(t, t_0)$ to the time t where the operator Φ_S is inserted and then back to t_0 with $\mathcal{U}(t_0, t)$. This forward-backward motion is forced upon us when considering expectation values of operators, and it encodes the causal and unitary nature of their time evolution. Products of operators such as the one in Eq. (2.8) represent the central objects of the Schwinger-Keldysh formalism.

To proceed, we would like to define time-dependent correlation functions. However, if we naively keep inserting operators into the trace in Eq. (2.8), we will not end up with a consistent description of quantum dynamics. This is due to the fact that we did not specify any ordering for the operators yet. Indeed, it is a priori not clear what operator ordering is appropriate. A historical account is for example given in [86]. Nowadays, we of course know that the appropriate operator ordering is provided by the Schwinger-Keldysh formalism, which we start to explore now.

To that end, let us just continue by inserting one more operator into the trace in Eq. (2.8) and carefully examine what we find. This will lead us to the appropriate operator ordering. Thus, we consider

$$\begin{aligned} \text{Tr}[\Phi(t_1) \Phi(t_2) \rho_{t_0}] &= \text{Tr}[\mathcal{U}(t_0, t_1) \Phi_S \mathcal{U}(t_1, t_0) \mathcal{U}(t_0, t_2) \Phi_S \mathcal{U}(t_2, t_0) \rho_{t_0}] \\ &= \text{Tr}[\mathcal{U}(t_0, t_1) \Phi_S \mathcal{U}(t_1, t_2) \Phi_S \mathcal{U}(t_2, t_0) \rho_{t_0}]. \end{aligned} \quad (2.9)$$

Reading from right to left, if $t_1 < t_2$, we evolve from the initial state at t_0 to t_2 , insert one field operator, evolve back to t_1 with the anti-time-ordered $\mathcal{U}(t_1, t_2)$, insert another field operator and then evolve further back to t_0 . If on the other hand, $t_1 > t_2$, then the middle \mathcal{U} is time ordered and evolves forward from t_2 to the later time t_1 , where the second field operator is inserted and then back to t_0 .

It is instructive to represent products of operators like in the trace of Eq. (2.9) graphically. The necessary building blocks are introduced in Fig. 2.1. A right-facing blue

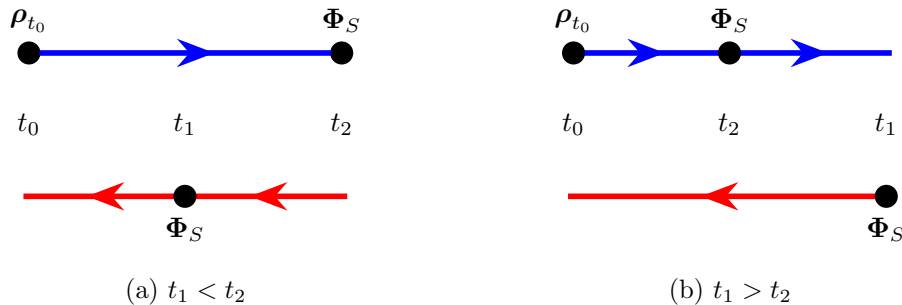


Figure 2.2.: Representations of the time-dependent correlation function (2.9) using the building blocks introduced in Fig. 2.1. On the left, $t_1 < t_2$: Starting at t_0 and following the arrows, we first encounter the operator Φ_S at the later time t_2 and then the operator Φ_S at the earlier time t_1 . Thus, this ordering of operators is anti-chronological. On the right, $t_1 > t_2$: We first encounter the operator Φ_S at the earlier time t_2 and then the operator Φ_S at the later time t_1 which corresponds to a chronological ordering.

arrow denotes the case when \mathcal{U} is time ordered and a left-facing red arrow the anti-time-ordered one. When we encounter an operator, we indicate this by a black dot. The graphical representation of the correlator in (2.9) is depicted in Fig. 2.2. On the left side we consider $t_1 < t_2$. Starting at t_0 and following the direction in which the arrows are pointing, we first encounter the operator Φ_S at the later time t_2 and then the operator Φ_S at the earlier time t_1 . Thus, this ordering of operators is anti-chronological. On right side we consider the opposite case $t_1 > t_2$. Again following the arrows, we first encounter the operator Φ_S at the earlier time t_2 and then the operator Φ_S at the later time t_1 which corresponds to a chronological ordering. Note that the rightmost operator Φ_S can be placed on the upper as well as on the lower line in Fig. 2.2. The represented correlator does not change as both cases represent the same product of operators (2.9). While this observation seems to be trivial, let us emphasise that the structure we just pointed out is rooted deeply in causality and unitarity and is crucial for the consistency of the Schwinger-Keldysh formalism. We will come back to this below Eq. (2.12).

With regard to inserting a second operator into the trace Eq. (2.8), there is also the other possibility of $\text{Tr}[\Phi(t_2) \Phi(t_1) \rho_{t_0}]$. In this case, the discussion is the same as above, just interchange $t_2 \leftrightarrow t_1$. Thus, we have found two correlation functions which are neither completely time ordered nor anti-time ordered. These are referred to as the Wightman functions or the Wightman propagators. The time-ordered and the anti-time-ordered propagator can be constructed from these two building blocks. In fact, all four of these propagators occur on the same footing if we formalise the graphical

representation introduced so far.

2.1.3. The Contour

Formalising the graphical representation introduced so far corresponds to introducing a central object of the Schwinger-Keldysh formalism: A closed time path (CTP) which constitutes a contour in the complex plane. To that end, let us recall that the question we set out to answer concerns the ordering of operators appropriate to describe quantum dynamics. Now, let us point out what Fig. 2.2 suggest: If we were to join together the upper (blue) and the lower (red) branch, we would obtain one continuous path. There are operators placed on this path and these are ordered according to the arrows on the respective branches. Thus, these operators are path ordered. Moreover, note that the times t_0, t_1, t_2 in Fig. 2.2 are part of the real number line. Hence, we are encouraged to consider the upper (blue) and the lower (red) branch to literally lie above and below the real numbers, i.e. they are infinitesimally shifted into the complex plane. Note that while we tried to motivate these steps using the graphical representation, a priori they are by no means obvious. Nevertheless, they turn out to lead to the desired result.

To proceed, we will define a path in the complex plane – the Schwinger-Keldysh closed time path. Next, we will promote time to a complex parameter on this path. This will allow us to define operators that are inserted on the path. Finally, for these operators, we will be able to define the desired path ordering.

To implement this proposal, let us introduce some notation. We denote the contour in the complex plane by $\mathcal{C}(t)$. We take its fixed starting point to be t_0 . The time in the brackets of \mathcal{C} denotes the fixed end point of the contour. We refer to the upper, blue branch of the contour as \mathcal{C}^+ and to the lower, red branch as \mathcal{C}^- . It will prove useful to denote the contour with infinite extend to the right by $\mathcal{C} := \mathcal{C}(\infty)$. As in the graphical representation, the forward branch represents time-ordered evolution and the backward branch anti-time-ordered evolution with \mathcal{U} . Note that the contour ends where it started, at t_0 . This is appropriate for the description of dynamics which represents an initial value problem.

The next step is to promote time to a parameter on \mathcal{C} . We denote a point on \mathcal{C} by \boldsymbol{t} . We refer to this as complex time or CTP time. Note that this is not to be confused with real time, which we denote by t . If the point \boldsymbol{t} lies on \mathcal{C}^+ , it is denoted by t^+ and if it lies on \mathcal{C}^- by t^- . Both of these are of course complex as well. An explicit parametrisation of the contour will not be needed for our applications, and we refer the interested reader to [15] for an example.

Now, we are ready to define field operators with CTP time arguments t^\pm as follows

$$\Phi(\mathbf{t} = t^\pm) := \Phi^\pm(t) = \Phi(t). \quad (2.10)$$

This equation requires some clarification. First let us point out that here, we are abusing the notation by taking the same symbol Φ for the real-time and the CTP time operator. Starting on the left-hand side of Eq. (2.10), we have the CTP operator which we want to define. To that end, recall that the actual, physical time is real. After all, the reason we introduced the CTP in the first place is to obtain path ordered operators. Note that any point on this complex path is uniquely specified by two types of data: Its real-time value and the branch of the path it sits on. On the left-hand side of the definition (2.10), this is encoded in the CTP time \mathbf{t} . On the right-hand side, we define new, real-time operators Φ^\pm . With the two-valued index \pm , these indicate the branch \mathcal{C}^\pm on which they are inserted. Accordingly, it is obvious what values these new operators $\Phi^\pm(t)$ should take at a given real time t : The value they take is the same value that the original operator $\Phi(t)$ takes. This is indicated by the last equality. Therefore, we have to equivalent formulations at our disposal: The first one encodes the operator ordering in terms of a complex time, while the second one encodes it in terms of a two-valued index. Depending on the application, either one or the other is preferable.

Finally, after defining operators on the CTP, we are now in a position to define the desired operator ordering: All operators that are inserted on \mathcal{C}^+ are defined to be time ordered and all operators that are inserted on \mathcal{C}^- are anti-time ordered. These notions are combined by introducing a path ordering $\mathcal{T}_{\mathcal{C}}$ along the closed time path. With regard to the ordering along \mathcal{C} , any time on \mathcal{C}^- is considered to be “later”, i.e. further along the path than all times on \mathcal{C}^+ . Accordingly, $\mathcal{T}_{\mathcal{C}}$ puts operators with “later” CTP times to the left of operators with “earlier” CTP times. Note that calling times on \mathcal{C}^- “later” can be misleading. Overall, there is of course only one physical, i.e. real time which increases towards the right.

Ordering operators along \mathcal{C} is easily visualised using the introduced graphical representation. It corresponds to starting at t_0 and following the arrows along the path. In Fig. 2.3, we depict the closed time path used for the computation of the expectation value of a single operator. The black arc in Fig. 2.3 indicates that the two branches are joined together at the latest time such that we obtain one continuous path. The large vertical distance between the path and the real time-axis is introduced for visualisation purposes. In practice, the shift is infinitesimal. More details in this regard can be found in [15, 87].

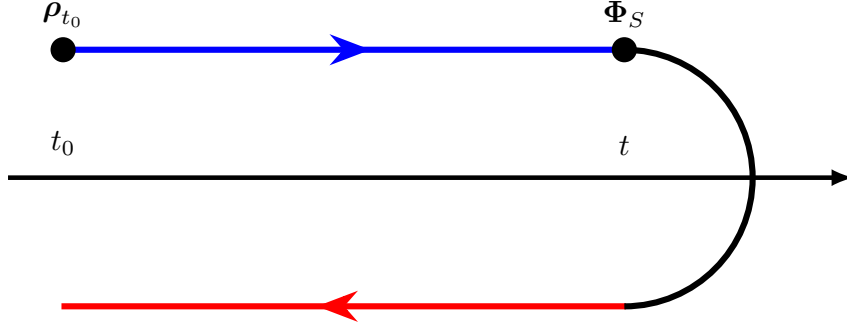


Figure 2.3.: Closed time path used to compute the time-dependent expectation value of the operator Φ_S with respect to the density matrix at the initial time t_0 which is denoted by ρ_{t_0} . The large vertical distance between the path and the real time-axis is introduced for visualisation purposes. The black arc indicates that the two branches are joined together at the latest time such that we obtain one continuous path.

Concerning the extent of the contour, observe from Fig. 2.3 that it does not need to extend any further than the latest operator insertion. This is a reflection of causality: Correlations beyond the latest time under consideration do not contribute. Nevertheless, we can always extend the path to $+\infty$ using unitarity: To that end, insert $\mathbb{1} = \mathcal{U}(t, \infty)\mathcal{U}(\infty, t)$ into the trace in Eq. (2.8) after the field operator insertion. This operator insertion corresponds to the point in time where the path in Fig. 2.3 turns around. As is obvious by the insertion of $\mathbb{1}$, this does not change the value of the respective correlation function. Note that this property is very convenient from a notational point of view: As the default, we can simply consider the extended path $\mathcal{C} := \mathcal{C}(\infty)$. Since no times larger than the latest operator insertion contribute to the time evolution, the path will “automatically” adjust its length.

Now, we collected everything necessary to define the CTP ordered correlation functions

$$\langle \mathcal{T}_{\mathcal{C}} \Phi(t_1) \cdots \Phi(t_n) \rangle := \text{Tr}[\rho_{t_0} \mathcal{T}_{\mathcal{C}} \Phi(t_1) \cdots \Phi(t_n)] . \quad (2.11)$$

As an illustrative example, consider n operators and insert m of them on \mathcal{C}^- and the remaining ones on \mathcal{C}^+ . This corresponds to the following choice for the complex times: $t_1, \dots, t_m \in \mathcal{C}^-$ and $t_{m+1}, \dots, t_n \in \mathcal{C}^+$. Moreover, for this example we consider the corresponding real times to be ordered as $t_1 < \dots < t_m < t_{m+1} < \dots < t_n$. The

respective n -point function then looks as follows

$$\begin{aligned}
 \langle \mathcal{T}_C \Phi(t_1) \cdots \Phi(t_n) \rangle &= \text{Tr}[\rho_{t_0} \overline{\mathcal{T}} \{ \Phi^-(t_1) \cdots \Phi^-(t_m) \} \mathcal{T} \{ \Phi^+(t_{m+1}) \cdots \Phi^+(t_n) \}] \\
 &= \text{Tr}[\Phi^-(t_1) \cdots \Phi^-(t_m) \Phi^+(t_n) \cdots \Phi^+(t_{m+1}) \rho_{t_0}] \\
 &= \text{Tr}[\Phi^-(t_1) \cdots \Phi^-(t_m) \Phi^-(t_n) \cdots \Phi^+(t_{m+1}) \rho_{t_0}] . \quad (2.12)
 \end{aligned}$$

The corresponding graphical representation is found by reading either the last line or the second to last line from right to left.

Let us come back to discussing the important property with regard to the latest operator insertion which we already pointed out when discussing Fig. 2.2: The value of a n -point function is independent of whether the operator with the maximal real time $t_{max} = \max(t_1, \dots, t_n)$ is inserted on C^+ or C^- . In the above example, $\Phi(t_{max}) = \Phi(t_n)$. This operator marks the rightmost point of the contour, i.e. the point where the path turns around. Thus, this operator marks the transition from time-ordering to anti-time-ordering in Eq. (2.12). The value that this operator takes is just the value the real-time operator takes. Since the ordering does not change when exchanging $\Phi^+(t_{max})$ and $\Phi^-(t_{max})$, the value of the respective n -point functions does not change.

Equations like Eq. (2.12) are known for a long time. In the discussion of cutting rules (see e.g. [88] and references therein), such equations are referred to as largest-time equations (LTEs). LTEs can be viewed as consequences of unitarity and can be shown to encode causality for the n -point functions in the sense illustrated below for the propagator. This is discussed in detail in [89–92]. For the lack of a better name, we will refer to this causality-property as the LTE property. The LTE property will be important for the developments of Sec. 4.8.

For the case of the CTP propagator, we can easily see how the LTE relates to causality. To that end, we denote the time-ordered propagator as $G^{++}(t_1, t_2) = \langle \mathcal{T} \Phi^+(t_1) \Phi^+(t_2) \rangle$. Furthermore, we will need the Wightman function $G^{+-}(t_1, t_2) = \langle \Phi^-(t_2) \Phi^+(t_1) \rangle$. Note that here, all time arguments are real. More details regarding the notation are deferred to App. A. Now we can obtain the retarded propagator as follows, making the time-

ordering explicit

$$\begin{aligned}
 G_{\text{R}}(t_1, t_2) &= G^{++}(t_1, t_2) - G^{+-}(t_1, t_2) \\
 &= \theta(t_1 - t_2) \langle \Phi^+(t_1) \Phi^+(t_2) \rangle + \theta(t_2 - t_1) \langle \Phi^+(t_2) \Phi^+(t_1) \rangle - \langle \Phi^-(t_2) \Phi^+(t_1) \rangle \\
 &= \theta(t_1 - t_2) \langle \Phi^-(t_1) \Phi^+(t_2) \rangle + \theta(t_2 - t_1) \langle \Phi^-(t_2) \Phi^+(t_1) \rangle - \langle \Phi^-(t_2) \Phi^+(t_1) \rangle \\
 &= \theta(t_1 - t_2) \langle [\Phi^-(t_1), \Phi^+(t_2)] \rangle .
 \end{aligned} \tag{2.13}$$

Going from the second to the third line, we used the LTE property. The retarded propagator is manifestly causal in the sense that it vanishes for $t_2 > t_1$. The retarded propagator is also referred to as a response function precisely for this reason: It takes into account that responses occur *after* the perturbation that caused them. Note that we could have dropped the \pm -indices completely already in the second line in Eq. (2.13). Indeed, if we are not facing any ambiguities with regard to the operator ordering, the CTP has fulfilled its purpose and can be forgotten. We remark that the CTP ordering is very useful to efficiently keep track of all necessary products of operators for a general n -point function. This is relevant for the present work since the tFRG formalism in general features correlation functions of arbitrary n . Note that in this general case, there exists a suitable generalisation of being a response function and the LTE property encodes its causality [92].

At this point, let us emphasise again the important change of perspective that occurred due to introducing the CTP: For the real-time operators $\Phi(t)$, it is their time dependence that “generates” the contour. However, it is a priori not clear what ordering prescription to impose on products of multiple operators. This is solved by defining the closed time path, the CTP operators and the corresponding path ordering. For the CTP operators $\Phi(\mathbf{t})$ and equivalently for the real-time operators $\Phi^\pm(t)$, the contour exists independently of the operators, which are placed somewhere on it.

Note that any n -point function with CTP times as in Eq. (2.11) has 2^n real-time components. For instance, consider the CTP propagator, i.e. the case of two operators. It has four components: Two of them are given by the two Wightman functions G^{+-} and G^{-+} , which we encountered in Eq. (2.9) and the discussion below. Recall that these are neither completely time-ordered nor anti-time-ordered. Note that the time-ordered propagator G^{++} and anti-time ordered propagator G^{--} occur on the same footing as the two Wightman functions. All of them are components of the CTP propagator. It turns out that in general, we need all components for a consistent formulation of quantum

dynamics. This is also nicely illustrated in [77].

Let us point out that defining the operators on the CTP can be viewed as introducing another copy of the same system. Indeed, the actual physical system is described by the operators $\Phi(t)$. To describe the dynamics of their correlations, we introduced the CTP operators $\Phi(\mathbf{t})$ which led to the set of two real-time operators Φ^\pm . However, the physical degrees of freedom of course have to stay the same. In this sense, the CTP ordered correlation functions are an overcomplete basis for time-dependent operator expectation values. This implies that the CTP quantities display a high degree of redundancy. Consider for example the CTP propagator. It has four real-time components, which in general take complex values. For the description of the dynamics in a relativistic quantum field theory, there are however only two real-time *and* real-valued propagators that are necessary. To make the degrees of freedom match, the CTP propagator has to be highly symmetric, i.e. it contains a lot of redundant information. In terms of its components, this implies that there are constraints relating them. These constraints are easily made explicit, using the notation introduced in App. A. For instance for the propagator, one crucial constraint reads

$$G^{++} + G^{--} = G^{+-} + G^{-+}. \quad (2.14)$$

Note that this constraint holds for all times. Indeed, it can be shown that this constraint is completely independent of the dynamics in general. In particular, it is therefore independent of unitarity. Let us emphasise that Eq. (2.14) holds for the classical as well as the fully resummed propagator. A detailed discussion of these facts is for example given in [90]. Additionally, there are other symmetry- and reality-constraints relating the different propagator components. These will be very useful in Sec. 4.8, and we defer their discussion to there.

Of course what immediately comes to mind regarding such a highly redundant basis is to change to a less redundant one, for instance by solving all or some of the constraints of the components. In this regard, a lot is known for the case of the propagator, and there are several useful bases available, tailored to the application at hand. We briefly introduce the bases relevant to this work in App. A. Let us remark that bases for general n are not nearly as well explored. We come back to this at the end of Sec. 3.3.

2.1.4. Causality, Unitarity and Energy Conservation in Approximations

To conclude this section, let us make some important remarks with regard to the features of the Schwinger-Keldysh formalism in approximations. To that end, let us emphasise

that the high degree of symmetry of a given CTP correlation function reflects the unitarity and causality of quantum dynamics. It is this particular structure of the CTP that leads to causal evolution equations for correlation function in perturbative [93] and non-perturbative [14] approximations. In this sense, causality can be considered a robust feature of the Schwinger-Keldysh formalism. Let us remark that the causally regulated correlation functions of the temporal FRG approach of this work enjoy causality-properties that are substantially more powerful than the standard causality-properties provided by the CTP. We introduce the causality-properties of the tFRG for the first time in Sec. 2.2.3 and discuss them in full detail in Ch. 3.

Regarding unitarity and energy conservation, it has been known for a long time that these are not nearly as robust as causality. Indeed, they are not necessarily preserved in approximations. This is related to the appearance of so called secular terms (see for example [10, 94, 95]). To understand this relation, let us first discuss secular terms. A priori, secular terms merely indicate an inconsistency in the employed approximation and appear quite generically in the description of general dynamical systems. Secular terms are defined as contributions that grow unboundedly with time and must be absent in a consistent description of the dynamics of closed quantum systems¹.

As a very basic illustration as to why secular terms appear in a generic expansion scheme applied to unitary dynamics, consider the time evolution operator for the case of a time-independent Hamiltonian: $\mathcal{U} = \exp[-i\Delta t(\mathcal{H}_0 + \lambda \mathcal{H}_{int})]$. Here, we separated the Hamiltonian into a free part \mathcal{H}_0 and an interacting part \mathcal{H}_{int} where the strength of the interaction is determined by the coupling λ . Performing a perturbative expansion with respect λ leads us to $\mathcal{U} = [1 - i\Delta t \lambda \mathcal{H}_{int} + \mathcal{O}(\lambda^2)] \exp[-i\Delta t \mathcal{H}_0]$. Clearly, the first correction due to the interaction diverges for long times. Thus if we do not choose our approximations carefully, unitarity might be lost. Moreover, unitarity is lost if the expectation value of the Hamiltonian, i.e. the energy, ceases to be real-valued. In this case, energy is no longer conserved. Thus, depending on the sign, such a term can cause damping or lead to exponential growth in time: $\mathcal{U} \propto \exp[\mp \Delta t \dots]$. Later on we will not work with the time evolution operator directly but with time dependent correlation functions. Still, similar issues persist: A generic expansion will suffer from secular terms. In general we will not be able to identify them analytically due to the complexity of the occurring hierarchies of equations. Instead, secularities will reveal themselves as instabilities in numerical approaches.

Note that the first observation regarding unitarity in expansions also suggests a reso-

¹Note that secular terms are per se not forbidden in driven system where the external driving can cause a resonance.

lution to the problem: If we manage to (partially) “resum” the perturbative series, we have a chance to obtain a bounded result. That such a procedure can be successfully applied is demonstrated by the n PI formalisms whose most prominent representative with regard to dynamical applications is given by the 2PI formalism². We introduced it briefly in Sec. 1.1 (see [10, 14] for a pedagogical introduction). The n PI formalisms are distinguished from generic expansion schemes by their self-consistency. Here, self-consistency entails that any approximation must be specified on the level of an effective action. The dynamic equations for the correlation functions are derived from this action by a variational principle.

As a concrete example, consider the 2PI effective action $\Gamma_{2\text{PI}}[\phi, G]$. It is a functional of the macroscopic field ϕ and of the fully dressed propagator G . The respective quantum equations of motion are given by $\delta\Gamma_{2\text{PI}}/\delta\phi \equiv 0$ and $\delta\Gamma_{2\text{PI}}/\delta G \equiv 0$. Furthermore, a generic variation of the 2PI effective action is of the form $\delta\Gamma_{2\text{PI}} = (\delta\Gamma_{2\text{PI}}/\delta\phi)\delta\phi + (\delta\Gamma_{2\text{PI}}/\delta G)\delta G$. This expression vanishes when evaluated on the solution of the quantum equations of motion. Note that this holds in any approximation as long as all of the quantum equations of motion are derived from the respective 2PI effective action in that approximation. This is the power of self-consistency. Now, establishing energy conservation in any approximation by standard field theoretic methods is trivial: The expectation value of the energy-momentum tensor in a given approximation is obtained by considering the variation of the 2PI effective action with regard to arbitrary space-time translations: $\delta\Gamma_{2\text{PI}} = \int_x T^{\mu\nu}(x)\partial_\mu\epsilon_\nu(x)$. Accordingly, $0 = \delta\Gamma_{2\text{PI}}|_{EoM} = -\int_x \partial_\mu T^{\mu\nu}(x)\epsilon_\nu(x)|_{EoM}$ for arbitrary $\epsilon_\nu(x)$ implies energy-momentum conservation in the approximation. Moreover, as there is an underlying variational principle, all equations derived from the effective action in the approximation are compatible with each other. Combining all of these properties results in a bounded time evolution in 2PI approximations.

We remark that the approximation must of course contain the processes relevant for the concrete dynamics with the concrete initial conditions at hand. Otherwise, also the 2PI dynamics suffers from instabilities, see e.g. [98]. Moreover, even if the time evolution remains bounded, we are not guaranteed to obtain accurate results [97, 99, 100]. At this point, let us also recall that the self-consistent “resummations” of the n PI formalisms are known to break the local symmetries of a gauge theory [24–27]. We explained this in Sec. 1.1. Due to the same reasons, also issues in the case of global symmetries can

²Note that the n PI effective actions are defined as functionals involving only fully dressed quantities. In particular, they do not rely on any perturbative expansion. Moreover, viewing them in terms of a resummed perturbative series is misleading for the following reason: The purpose of resumming a series is to extract a convergent result. This suggests that the n PI loop-expansions are convergent which they are not [96, 97].

arise [28, 29].

A detailed discussion of causality, unitarity and energy conservation in generic approximations of the temporal FRG can be found in Sec. 3.1.5.

2.2. Generating Functionals and the Path Integral

We continue our journey of exploring the Schwinger-Keldysh formalism by introducing and discussing the generating functional of correlation functions in Sec. 2.2.1. We proceed by pointing out important aspects of its path integral representation in Sec. 2.2.2. This allows us to introduce the basic idea of the tFRG framework in Sec. 2.2.3.

2.2.1. Generating Functionals

A convenient way to deal with all n -point functions simultaneously is given by the generating functional of correlation functions

$$Z[J; \rho_{t_0}] := \text{Tr} \left[\rho_{t_0} \mathcal{T}_{\mathcal{C}} \exp \left\{ i \int_{\mathcal{C}, x} \Phi(x) J(x) \right\} \right]. \quad (2.15)$$

This is the representation of the generating functional in terms of a complex time which is a parameter on \mathcal{C} . All things concerning the contour \mathcal{C} are explained in detail in Sec. 2.1. The contour integration on \mathcal{C} is defined as follows

$$\int_{\mathcal{C}, x} := \left[\int_{t_0, \mathcal{C}^+}^{\infty} dx^0 - \int_{t_0, \mathcal{C}^-}^{\infty} dx^0 \right] \int_{\mathbf{x}}, \quad (2.16)$$

Take note of the crucial minus sign which captures the orientation of the two branches. Here, x is a $D = d+1$ dimensional vector with time component x^0 and d -dimensional spatial component \mathbf{x} . The subscripts \mathcal{C}^{\pm} indicate the branch on which the time arguments are evaluated. Using relation (2.16), the integral in (2.15) reads explicitly

$$\int_{\mathcal{C}, x} \Phi(x) J(x) = \int_{t_0}^{\infty} dx^0 \int_{\mathbf{x}} (\Phi^+(x) J^+(x) - \Phi^-(x) J^-(x)).$$

Here we employed the real-time representation Φ^{\pm} of the field operators. Importantly, from here on out we will not notationally distinguish any more between real and complex times. In the real-time representation, we need two sources J^{\pm} , one for each field

operator. Accordingly, the sources are to be treated as independent. Note that the real-time representation lends itself to the introduction of a CTP metric which allows to raise and lower the CTP indices \pm , providing an efficient bookkeeping of the occurring minus signs. We defer the details to App. A.

Next, we introduce a convenient representation of the generating functional with real-time sources

$$Z[J^+, J^-; \rho_{t_0}] = \text{Tr} \left[\mathcal{U}[J^-](t_0, \infty) \mathcal{U}[J^+](\infty, t_0) \rho_{t_0} \right]. \quad (2.17)$$

This form will come in handy shortly. Here, we introduced the time evolution operator in presence of a source. It is defined by replacing $\mathcal{H}_S(t) \rightarrow \mathcal{H}_S(t) - \int_{\mathbf{x}} J^\pm(t, \mathbf{x}) \Phi_S(\mathbf{x})$ in the expression (2.7) of the time evolution operator. Notably, the operator ordering of the CTP is taken care of by the individual time evolution operators in the representation (2.17). Importantly, the time evolution operators in Eq. (2.17) do not collapse to $\mathbb{1}$ as long as $J^+ \neq J^-$. To see that this representation of the generating functional agrees with the one given in Eq. (2.15), recall that operators under (anti-)time-ordering commute by definition. Then, $Z[J^+, J^-; \rho_{t_0}] = Z[J; \rho_{t_0}]$ is easily seen using the explicit representations of $\mathcal{U}[J^\pm]$.

To obtain the CTP ordered correlation functions from the generating functional, we take functional derivatives with respect to the current. This is concisely written using the CTP time representation

$$\langle \mathcal{T}_C \Phi(x_1) \cdots \Phi(x_n) \rangle = (-i)^n \frac{\delta^n Z[J; \rho_{t_0}]}{\delta J(x_1) \cdots \delta J(x_n)} \Bigg|_{J=0}. \quad (2.18)$$

More details regarding this notation can be found in App. A, where we exemplify this definition by means of the CTP propagator. Let us comment on our choice of $J = 0$ for the CTP current in the above definition. To that end, consider $Z[J^+, J^-; \rho_{t_0}]$ as in Eq. (2.17) and recall the following: The closed time path for a n -point function with largest time t_{max} does not need to extend further than t_{max} . This is achieved by evaluating the n th functional derivative of Z at $J^+ = \bar{J} = J^-$. Indeed, in this case the time evolution operators for times beyond t_{max} cancel each other out: $\mathcal{U}[\bar{J}](t_{max}, \infty) \mathcal{U}[\bar{J}](\infty, t_{max}) = \mathbb{1}$. Moreover, the time evolution operators $\mathcal{U}[J^\pm]$ in between the field operators Φ_S of the n -point function reduce to the physical time evolution that is then governed by the single Hamiltonian $\mathcal{H}_S(t) - \int_{\mathbf{x}} \bar{J}(t, \mathbf{x}) \Phi_S(\mathbf{x})$.

We remark that a non-zero value for \bar{J} can be useful in several situations. For one, it can be used to discuss periodic driving or more general time-dependent external per-

turbations [16]. Moreover, it can be useful also in the context of closed systems. For instance, a non-zero current can be helpful to improve the convergence of approximations [101]. In non-perturbative applications, it can be used to improve the restoration of symmetries which are broken due to approximations [29]. Very similar concepts could also be of interested for the tFRG regarding the preservation of unitarity and the conservation of energy in generic tFRG truncations, cf. Sec. 3.1.5 and Ch. 6. For now though we consider $\bar{J} = 0$ which is adequate for closed systems.

2.2.2. The Path Integral

We proceed by introducing the path integral representation of the generating functional. This will provide important intuition for the developments that follow. Importantly, it will allow us to introduce the basic idea of the tFRG framework without the need to go into all the details of the tFRG formalism. These details are reserved for the chapters that follow.

To derive the path integral representation, it will prove very useful to consider the generating functional for correlation functions whose latest time t_{max} is not larger than some time τ . For now, we can think of τ as the *fixed* extent of the closed time path. Less formally, we can think of τ as the present time. We denote the respective generating functional by $Z_\tau[J; \rho_{t_0}]$. Accordingly, $Z_\tau[J; \rho_{t_0}]$ contains all time-dependent correlations between t_0 and τ . Let us emphasise that the closed time path of finite extent τ and the associated generating functionals are the central objects of this work. Their causality-properties are pivotal for all following developments and can be already observed by studying their path integral representations. Note that we recover the generating functional for all times in the limit $Z[J; \rho_{t_0}] = \lim_{\tau \rightarrow \infty} Z_\tau[J; \rho_{t_0}]$.

As the first step to derive the path integral representation, we make use of the following real-time representation of Z_τ

$$\begin{aligned} Z_\tau[J; \rho_{t_0}] &= \text{Tr} \left[\rho_{t_0} \mathcal{T}_C e^{i \int_{C(\tau), x} \Phi(x) J(x)} \right] \\ &= \text{Tr} \left[\rho_{t_0} \bar{\mathcal{T}} \left(e^{-i \int_{t_0}^\tau dx^0 \int_{\mathbf{x}} \Phi^-(x) J^-(x)} \right) \mathcal{T} \left(e^{i \int_{t_0}^\tau dx^0 \int_{\mathbf{x}} \Phi^+(x) J^+(x)} \right) \right]. \end{aligned} \quad (2.19)$$

In general, path integrals are representations of transition amplitudes between some initial and some final state. In our case, these states are given by the eigenvectors of the Heisenberg operators $\Phi(x^0 = t_0, \mathbf{x})$ and $\Phi(x^0 = \tau, \mathbf{x})$ at the initial and final time respectively. The Heisenberg operators are explicitly time dependent and so are their

eigenstates $|\varphi, t\rangle := \mathcal{U}^\dagger(t, t_0) |\varphi, t_0\rangle$. This is indeed an eigenstate of $\Phi(x)$, to wit

$$\Phi(x) |\varphi, t\rangle = \mathcal{U}^\dagger(t, t_0) \Phi_S(\mathbf{x}) \mathcal{U}(t, t_0) \mathcal{U}^\dagger(t, t_0) |\varphi, t_0\rangle = \varphi(\mathbf{x}) |\varphi, t\rangle,$$

where $|\varphi, t_0\rangle =: |\varphi\rangle$ is an eigenstate of the Schrödinger operator $\Phi_S(\mathbf{x})$. It is defined in the usual way, $\Phi_S(\mathbf{x}) |\varphi\rangle = \varphi(\mathbf{x}) |\varphi\rangle$ where the eigenstate is defined as the formal product $|\varphi\rangle := \prod_{\mathbf{x}} |\varphi(\mathbf{x})\rangle$.

Next, we express the trace in Eq. (2.19) using the eigenstates of $\Phi(x^0 = t_0, \mathbf{x})$ and insert representations of unity,

$$\mathbb{1} = \int [d\varphi] |\varphi, t\rangle \langle \varphi, t| \quad \text{with} \quad \int [d\varphi] := \int \prod_{\mathbf{x}} d\varphi(\mathbf{x}), \quad (2.20)$$

at the times t_0 and τ . To account for the operator ordering on the CTP, we label the eigenstates of Φ^\pm at t_0 as $|\varphi_0^\pm\rangle$ and at τ as $|\varphi_f^\pm, \tau\rangle$, resulting in

$$\begin{aligned} Z_\tau[J; \rho_{t_0}] &= \int [d\varphi_0^+] [d\varphi_0^-] [d\varphi_f^+] [d\varphi_f^-] \langle \varphi_0^+ | \rho_{t_0} | \varphi_0^- \rangle \times \\ &\quad \times \langle \varphi_0^- | \overline{\mathcal{T}} \left(e^{-i \int_{t_0}^\tau dx^0 \int_{\mathbf{x}} \Phi^-(x) J^-(x)} \right) | \varphi_f^-, \tau \rangle \langle \varphi_f^-, \tau | \\ &\quad \times | \varphi_f^+, \tau \rangle \langle \varphi_f^+, \tau | \mathcal{T} \left(e^{i \int_{t_0}^\tau dx^0 \int_{\mathbf{x}} \Phi^+(x) J^+(x)} \right) | \varphi_0^+ \rangle. \end{aligned} \quad (2.21)$$

Note that there are essentially three factors which we can interpret as follows: In the first line, ignoring the functional integral measures, we find the matrix elements of the initial state ρ_{t_0} in the eigenbasis of the operators Φ^\pm at t_0 . This factor contains all the initial data of our system. In general, it is not diagonal in the eigenbasis of Φ^\pm at t_0 . This is shown in a very instructive way in [14]. Now consider the third line. It represents the transition amplitude for the state $|\varphi_0^+\rangle$ into the state $\langle \varphi_f^+, \tau |$. Accordingly, the second line is a transition amplitude for the state $|\varphi_f^-, \tau\rangle$ into $\langle \varphi_0^- |$. Crucially, the states at τ must be identified according to

$$\langle \varphi_f^-, \tau | \varphi_f^+, \tau \rangle = \delta[\varphi_f^- - \varphi_f^+] := \prod_{\mathbf{x}} \delta(\varphi_f^-(\mathbf{x}) - \varphi_f^+(\mathbf{x})). \quad (2.22)$$

Let us emphasise that this condition is the functional analogue of joining the branches \mathcal{C}^+ and \mathcal{C}^- of the CTP. It represents a boundary condition for the path integral, and we discuss it in more detail after deriving the path integral.

The factors in (2.21) can now be expressed as path integrals. There are two transition amplitudes with insertions of Φ^\pm , coupled by the initial condition at t_0 and a boundary

condition at τ . The derivation proceeds along the lines of the usual time-slicing argument which is discussed in detail in [14, 80, 102]. Very briefly, we start by dividing the interval from t_0 to τ as follows $\frac{\tau-t_0}{N+1} = \Delta t$. In the end, we will take the limit $N \rightarrow \infty$. Any contributions of manipulations that give rise to non-vanishing commutator terms will be dropped immediately as these only contribute at order $\mathcal{O}(\Delta t^2)$. We factorise the exponential and insert representations of unity (2.20). A typical factor looks like

$$\begin{aligned} & \langle \varphi_{k+1}^\pm, t_{k+1} | \left(1 \pm i\Delta t \int_{\mathbf{x}} \Phi^\pm(t_k, \mathbf{x}) J^\pm(t_k, \mathbf{x}) \right) | \varphi_k^\pm, t_k \rangle \\ &= \left(1 \pm i\Delta t \int_{\mathbf{x}} \varphi_k^\pm(\mathbf{x}) J^\pm(t_k, \mathbf{x}) \right) \langle \varphi_{k+1}^\pm | \mathcal{U}(t_{k+1}, t_k) | \varphi_k^\pm \rangle . \end{aligned}$$

To proceed, we need to specify the Hamiltonian more precisely. For simplicity, we consider a scalar bosonic field. The Hamiltonian in the Schrödinger picture can then be expressed in terms of the respective field operator Φ_S and its conjugate momentum operator Π_S as follow: $\mathcal{H}_S(t) \equiv \mathcal{H}_S[\Phi_S, \Pi_S; t]$. For our purposes, it is sufficient to consider Weyl-ordered Hamiltonians for which we can integrate out the conjugate momentum fields $\Pi_k(\mathbf{x})$.

The transition amplitudes are then expressed in terms of the Lagrangian density \mathcal{L} . All arising prefactors are absorbed into the measure. As usual when taking $N \rightarrow \infty$, we interpret the sequence of fields $\{\varphi_k(\mathbf{x})\}$ as a discretisation of the field configuration $\varphi(x^0 = t_k, \mathbf{x})$ and we arrive at

$$\begin{aligned} Z_\tau[J; \rho_{t_0}] &= \int [d\varphi_0^+] [d\varphi_0^-] [d\varphi_f^+] [d\varphi_f^-] \langle \varphi_0^+ | \rho_{t_0} | \varphi_0^- \rangle \delta[\varphi^-(\tau) - \varphi^+(\tau)] \quad \times \\ & \times \int_{\varphi^-(\tau, \mathbf{x}) = \varphi_f^-(\mathbf{x})}^{\varphi^-(t_0, \mathbf{x}) = \varphi_0^-(\mathbf{x})} \mathcal{D}'\varphi^- \exp \left\{ -i \int_{t_0}^\tau dx^0 \int_{\mathbf{x}} \left(\mathcal{L}[\varphi^-(x)] + \varphi^-(x) J^-(x) \right) \right\} \\ & \times \int_{\varphi^+(t_0, \mathbf{x}) = \varphi_0^+(\mathbf{x})}^{\varphi^+(\tau, \mathbf{x}) = \varphi_f^+(\mathbf{x})} \mathcal{D}'\varphi^+ \exp \left\{ i \int_{t_0}^\tau dx^0 \int_{\mathbf{x}} \left(\mathcal{L}[\varphi^+(x)] + \varphi^+(x) J^+(x) \right) \right\} . \end{aligned} \tag{2.23}$$

The prime on the measure reminds us that $[d\varphi_0^\pm]$ and $[d\varphi_f^\pm]$ are not included, i.e.

$$\mathcal{D}'\varphi^\pm := \prod_{t_0 < x^0 < \tau} \prod_{\mathbf{x}} [d\varphi^\pm(x)] . \tag{2.24}$$

Now that we obtained the path integral representation of the generating functional, let us stress again the boundary condition at τ for the fields: $\varphi^+(\tau, \mathbf{x}) = \varphi^-(\tau, \mathbf{x})$. In Eq. (2.23), it is enforced by the δ -distribution in the first line. This boundary condition ensures causality on the level of the correlation functions by enforcing the LTE property in the path integral representation, cf. Eq. (2.12) and the discussion below it. Note that this boundary condition is often not mentioned in the literature. This is due to the fact that for many applications, it turns out not to be essential in practice. For certain applications however, it is important to take the boundary condition into account explicitly. We will discuss the details as to why this is the case in Sec. 3.3. The interested reader is also referred to [12, 103–105] for more details regarding the boundary condition and to [89–92] for more details regarding causality in the Schwinger-Keldysh formalism.

Moving on, let us make some definitions that allow to write the path integral representation of Eq. (2.23) in a more compact form. First, we introduce the CTP action

$$S_\tau[\varphi] := \int_{\mathcal{C}(\tau), x} \mathcal{L}[\varphi(x)] = \int_{t_0}^\tau dx^0 \int_{\mathbf{x}} \left(\mathcal{L}[\varphi^+(x)] - \mathcal{L}[\varphi^-(x)] \right).$$

Next, we account for the initial density matrix by using the following parametrisation

$$\langle \varphi_0^+ | \rho_{t_0} | \varphi_0^- \rangle = \frac{1}{\mathcal{N}} \exp \left[i \sum_{k=0}^{\infty} \frac{1}{k!} \alpha_k \cdot \varphi^k \right] =: \frac{1}{\mathcal{N}} \exp \left[i \mathcal{I}_{t_0}[\varphi; \alpha] \right]. \quad (2.25)$$

Here, we defined $\mathcal{I}_{t_0}[\varphi; \alpha] := \sum_{k=0}^{\infty} \frac{1}{k!} \alpha_k \cdot \varphi^k$. The n th term of the sum has the form

$$\alpha_n \cdot \varphi^n = \int_{\mathcal{C}(\tau), x_1 \dots x_n} \alpha_n(x_1, \dots, x_n) \varphi(x_1) \dots \varphi(x_n).$$

The coefficients α_k have support at t_0 only. Note that this is no approximation but simply a parametrisation that solves the constraints that the density matrix has to fulfil. For more details in this regard see [14, 78, 93] and references therein. We include the initial sources by defining a generalised action

$$S_\tau[\varphi; \alpha] := S_\tau[\varphi] + \mathcal{I}_{t_0}[\varphi; \alpha]. \quad (2.26)$$

Absorbing any potential normalisation of the density matrix into the definition of the path integral measure and combining all functional integrals and the boundary condition

as follows,

$$\int_{\mathcal{C}(\tau)} \mathcal{D}\varphi := \int [d\varphi_0^+] [d\varphi_0^-] [d\varphi_f^+] [d\varphi_f^-] \int_{\varphi^-(\tau, \mathbf{x})=\varphi_f^-(\mathbf{x})}^{\varphi^-(t_0, \mathbf{x})=\varphi_0^-(\mathbf{x})} \mathcal{D}'\varphi^- \int_{\varphi^+(t_0, \mathbf{x})=\varphi_0^+(\mathbf{x})}^{\varphi^+(\tau, \mathbf{x})=\varphi_f^+(\mathbf{x})} \mathcal{D}'\varphi^+ \delta[\varphi^-(\tau) - \varphi^+(\tau)] ,$$

we arrive at the following concise path integral representation of the generating functional

$$Z_\tau[J; \rho_{t_0}] = \int_{\mathcal{C}(\tau)} \mathcal{D}\varphi \exp \left[i \left\{ S_\tau[\varphi; \alpha] + \int_{\mathcal{C}(\tau), x} \varphi(x) J(x) \right\} \right] .$$

2.2.3. The Basic Idea: A Closed Time Path of Variable Extent

Here we introduce the basic idea of the tFRG: A CTP of variable extent. To that end, we first illustrate the causality-properties that are implied by “cutting off” the CTP at τ . These ideas will be made precise in Ch. 3, using concepts from functional renormalisation group theory. Note that until the end of this section, τ and accordingly the extent of the CTP will remain fixed.

For convenience, we now introduce the Schwinger functional which is the generating functional of the connected correlation functions

$$W_\tau[J; \rho_{t_0}] := -i \ln Z_\tau[J; \rho_{t_0}] .$$

Here, we again recover the full functional W in the limit $\tau \rightarrow \infty$. The connected correlation functions are defined as

$$W_\tau^{(n)}(x_1, \dots, x_n) := \left. \frac{\delta^{(n)} W_\tau[J; \rho_{t_0}]}{\delta J(x_1) \cdots \delta J(x_n)} \right|_{J=0} . \quad (2.27)$$

The causality-properties which we now discuss hold for both generating functionals, Z_τ and W_τ . For concreteness and later reference, we consider the connected correlation functions generated by $W_\tau[J; \rho_{t_0}]$. In the path integral representation, it is particularly apparent that we sum over fluctuations to compute correlation functions. It will be useful to think of $W_\tau[J; \rho_{t_0}]$ as summing up all fluctuations up to and including the time τ . In this sense, we did “cut off” the CTP of infinite extent at τ and only kept the information about the correlations between t_0 and τ . The crucial point is that this constitutes all the information there is regarding the full quantum dynamics that started at t_0 and progressed up to the present time τ .

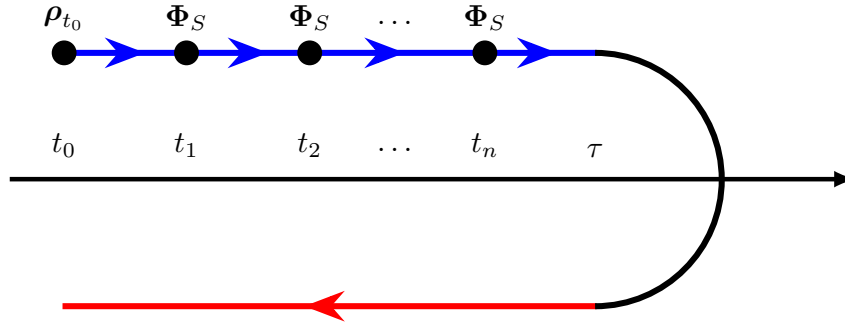


Figure 2.4.: Illustration of the causality-property (2.28): A n -point function derived from the functional W_τ with all times t_1, \dots, t_n smaller than τ is the full n -point function. Note that the time evolution operators between t_n and τ cancel after setting $J = 0$. Hence, the contour does not extend longer than the latest operator insertion.

To express this more formally, consider the following correlator $W_\tau^{(n)}(x_1, \dots, x_n)$. If all times x_1^0, \dots, x_n^0 are smaller than or equal to τ , then we obtain the full n -point function

$$W_\tau^{(n)}(x_1, \dots, x_n) = W_{\tau=\infty}^{(n)}(x_1, \dots, x_n) = W^{(n)}(x_1, \dots, x_n), \text{ for } \max\{x_1^0, \dots, x_n^0\} \leq \tau. \quad (2.28)$$

The last equality emphasises that W and W_τ only differ for times larger than τ . Thus, as long as we are interested in correlations for times smaller than or equal to τ , the functional W_τ on the “cut off” CTP contains the full dynamical information.

As an illustration of this fact, we display the component of the CTP n -point correlation function where all fields are inserted on \mathcal{C}^+ in Fig. 2.4. Note that the time evolution operators between t_n and τ , which are implied in Fig. 2.4 by the graphical representation introduced in Fig. 2.1, cancel after setting $J = 0$. Hence, the contour does not extend longer than the latest operator insertion. We remark that using the graphical notation of Fig. 2.1, the products of operators represented in Fig. 2.4 translate into the correlation function as derived from Z_τ .

Observe that τ and t_{max} need not be the same. Indeed, the contour $\mathcal{C}(\tau)$ and the functional $W_\tau[J; \rho_{t_0}]$ exist for all times between the fixed initial time t_0 and fixed latest time τ . Inserting operators on the contour corresponds to taking functional derivatives as in Eq. (2.27). The time arguments of these derivatives translate into the time arguments of the inserted operators. Accordingly, as long as we are interested in correlations for times earlier than or equal to τ , which represents the present time, we will find the full answer in $W_\tau[J; \rho_{t_0}]$.

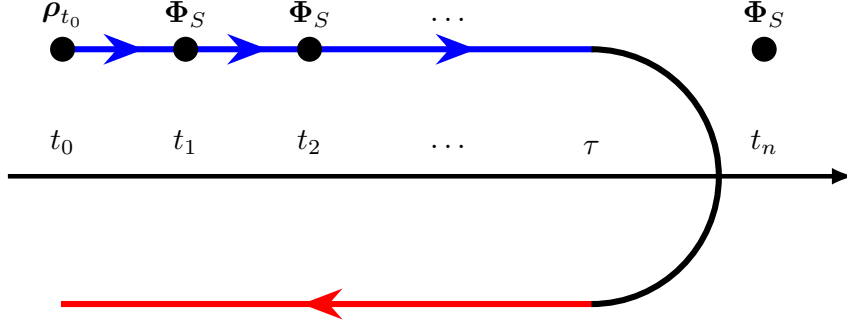


Figure 2.5.: Illustration of the causality-property (2.29): A n -point function derived from the functional W_τ with any time larger than τ vanishes. The fact that Φ_S at t_n can not be placed on the contour is best thought of in terms of the sources in Eq. (2.27). Taking a derivative with respect to a variable that is not present, namely $J(t_n > \tau)$, yields zero. If we think of τ as the present, this demonstrates causality in the sense that correlations with respect to future times vanish.

On the other hand, if we ask questions about correlations in the future of τ , i.e. if there is at least one time larger than τ , the respective correlation function vanishes

$$W_\tau^{(n)}(x_1, \dots, x_n) = 0, \quad \text{for } \max\{x_1^0, \dots, x_n^0\} > \tau. \quad (2.29)$$

This is due to the fact that the functional $W_\tau[J; \rho_{t_0}]$ does not contain any information about such future correlations. We illustrate this property in Fig. 2.5. The fact that Φ_S at t_n can not be placed on the contour is best thought of in terms of the sources in Eq. (2.27). Sources with times larger than τ are not included in $W_\tau[J; \rho_{t_0}]$. Hence, a derivative with respect to such a source vanishes.

Note that the causality-property (2.29) can be seen as a generalisation of the LTE property. Recall that on the level of the propagator, the LTE property ensures causality in the sense that the components of the CTP propagator give rise to the correct, causal retarded propagator $G_R(t, t_{max})$ which vanishes for $t_{max} > t$, cf. Eq. (2.13). The present property (2.29) is much stronger. It ensures that *all* components of the CTP propagator vanish for $t_{max} > \tau$.

Let us recall that up until now, τ and accordingly the extent of the CTP were fixed. Now, imagine that we were able to vary τ . Then we would obtain the full time evolution of the correlation functions. To see this, consider $W_{\tau=t_0}^{(n)}(x_1, \dots, x_n)$. Due to Eq. (2.29), all that this includes is the information of the initial density matrix. Then we take one τ -step and get the full correlation functions for all times smaller than τ due to

Eq. (2.28). This evolution is causal due to Eq. (2.29). The functional renormalisation group approach that we develop in the next chapter will allow us to vary τ .

3. The Temporal Functional Renormalisation Group

The objective of this chapter is to provide an introduction to the formalism of the temporal functional renormalisation group (tFRG). It was introduced in [81, 82] and substantially further developed by us in [1–3].

To that end, we revisit the derivation of the flow equation with a temporal regulator, paying particular attention to subtleties and properties that arise due to the use of a causal temporal regulator in Sec. 3.1. We discuss the initial conditions for the temporal flow and introduce truncations of the tFRG, focussing on the fate of causality, unitarity and the conservation of energy in generic tFRG truncations.

In Sec. 3.2, we discuss the causality-properties of the causally regulated correlation functions. We translate these causality-properties into causal constraints which represent a central new development of the present work and are published in [1]. The causality-properties are a distinct feature of tFRG approach. In the form of the causal constraints, they are of paramount importance for the rest of this work. Indeed, these will facilitate the analytic integration of the causal temporal flow in Ch. 4.

We address several challenges we encountered attempting to numerically solve the temporal flow in Sec. 3.3.

App. B contains flow equations in diagrammatic form that are needed for later reference.

This chapter is based on [1]. Additionally it contains new, so far unpublished results and discussions in Sec. 3.1.1, 3.1.2, 3.1.5, 3.1.6, 3.2 and Sec. 3.3.

3.1. The Temporal Flow Equation

In the last chapter, we observed that the connected correlation functions on a closed time path (CTP) of finite extent τ enjoy the causality-properties Eq. (2.28) and Eq. (2.29). These properties imply that the τ -evolution of the correlation functions corresponds to their *causal* time evolution. In this section, we employ FRG theory to formalise the idea of a CTP with variable extent and to derive the corresponding τ -evolution equation.

First, let us briefly recall what the general idea of the FRG is. For instance, consider a Euclidean quantum field theory in momentum space. There, a momentum regulator is introduced which allows to integrate out fluctuations successively, momentum shell by momentum shell. For more details and references, see Sec. 1.1. Analogously, we can think about the temporal flow as integrating out fluctuations time slice by time slice. However, let us emphasise that although there are structural similarities, there are also profound differences between flows in momentum space and flows in time. One major difference with tremendous consequences is that temporal flows must respect causality.

3.1.1. The Regulator

We proceed by introducing the temporal regulator $R_\tau(x, y)$. The corresponding regulated generating functional of CTP correlation functions, Z_τ , and the regulated Schwinger functional, W_τ , can be obtained by adding the following term to the classical action

$$\Delta S_\tau[\varphi] = \frac{1}{2} \int_{\mathcal{C}, xy} \varphi(x) R_\tau(x, y) \varphi(y). \quad (3.1)$$

Then, the regulated functionals are given by

$$Z_\tau[J; \rho_{t_0}] = \int_{\mathcal{C}} \mathcal{D}\varphi \exp \left[i \left\{ S[\varphi; \alpha] + \Delta S_\tau[\varphi] + \int_{\mathcal{C}, x} \varphi(x) J(x) \right\} \right] = e^{iW_\tau[J; \rho_{t_0}]} . \quad (3.2)$$

Here, we use the notation introduced in Sec. 2.2.2. Importantly, note that $\mathcal{C} := \mathcal{C}(\infty)$ denotes a CTP of infinite extent. The generalised action $S[\varphi; \alpha]$ was defined in Eq. (2.26). The α are general functions of the spatial coordinates with support at t_0 only. They parametrise the initial density matrix. Next, we demand that the regulator has the following properties:

- (i) $-iR_\tau(x, y)$ diverges as $\tau \rightarrow t_0$, for $x^0 = y^0 > \tau$, $\mathbf{x} = \mathbf{y}$.
- (ii) $-iR_\tau(x, y)$ is semi-positive definite. (3.3)
- (iii) $\lim_{\tau \rightarrow \infty} R_\tau(x, y) = 0$ for all (x^0, y^0) .

The property (i) implies that Z_{t_0} is determined solely in terms of the initial density matrix. The property (ii) ensures that during the τ -evolution, fluctuations are suppressed in the case where $-iR_\tau(x, y)$ is positive definite. Moreover in the case where $-iR_\tau(x, y)$ vanishes, all fluctuations contribute. Lastly, (iii) guarantees that $\lim_{\tau \rightarrow \infty} Z_\tau = Z$, i.e.

we recover the full quantum theory as $\tau \rightarrow \infty$. Using Eq. (3.2), we observe that Eq. (3.3) has the same implications for W_τ .

A regulator that fulfils these requirements is given by

$$-iR_\tau(x, y) = \begin{cases} \infty & x^0 = y^0 > \tau, \mathbf{x} = \mathbf{y} \\ 0 & \text{otherwise} \end{cases}. \quad (3.4)$$

The regulator (3.4) is referred to as the sharp regulator or the sharp cutoff. Notably, Eq. (3.4) defines a causal regulator in the sense that it suppresses all fluctuations in Eq. (3.2) for times later than the present time τ . While other regulator choices are possible in principle, we will focus on the causal regulator.

Note that the causal regulator respects the hermiticity of the generating functionals. Their hermiticity is a consequence of unitary time evolution. First, let us explain the latter fact and then come back to the role of the regulator. For the unregulated generating functionals, their hermiticity is nicely discussed in [77] which we follow. Recall the representation of Z in terms of time evolution operators with sources, to wit

$$Z[J^+, J^-; \rho_{t_0}] = \text{Tr}[\mathbf{U}^\dagger[J^-] \mathbf{U}[J^+] \rho_{t_0}]. \quad (3.5)$$

If the time evolution operator is unitary, assuming the initial density matrix is hermitian, it is easy to show that $Z[J^+, J^-, \rho_{t_0}]^\dagger = Z[J^-, J^+, \rho_{t_0}]$. For the Schwinger functional, the same reasoning implies $W[J^+, J^-, \rho_{t_0}]^\dagger = -W[J^-, J^+, \rho_{t_0}]$. Here, we assumed that the currents J^\pm are chosen to be real. This is adequate if the field operators Φ are hermitian. Now to check under which conditions the regulated functionals enjoy these properties as well, it is useful to rewrite the regulated functionals as follows

$$Z_\tau[J; \rho_{t_0}] = \exp \left[-\frac{i}{2} \int_{\mathcal{C}, xy} \frac{\delta}{\delta J(x)} R_\tau(x, y) \frac{\delta}{\delta J(y)} \right] Z[J; \rho_{t_0}] = e^{iW_\tau[J; \rho_{t_0}]} . \quad (3.6)$$

Since we know from Eq. (3.4) that $-iR_\tau \in \mathbb{R}$, it immediately follows that the causally regulated functionals enjoy the same hermiticity properties as the unregulated ones. In this sense, the causal regulator Eq. (3.4) does not interfere with unitarity. Note that unitarity can still be violated in approximations and we address this in Sec. 3.1.5. We remark that the observation regarding the hermiticity of the regulated functionals represents a new result, so far unpublished of this work.

Let us remark that a path integral representation is not required for the discussion

of flow equations. Indeed, we could adapt the approach of [106] for temporal flows as follows: Assume that the generating functional Z on the CTP is well-defined. This corresponds to the statement that the quantum theory described by Z exists and its dynamics are well-defined. Then also the Schwinger functional $Z = e^{iW}$ is well defined. The regulated versions of these functionals are then obtained by the action of the derivative operator $\exp[i/2\Delta S_\tau[\delta/\delta J]]$ as in Eq. (3.6). From these regulated functionals, the standard flow equation can be derived. Note that if we choose to follow this approach, the property (ii) in Eq. (3.3) ensures that the regulated functionals as in Eq. (3.6) are also well-defined.

Note that as opposed to standard regulators in momentum space, the sharp temporal regulator (3.4) is compatible with the local symmetries of a gauge theory. This is due to the fact that Eq. (3.4) defines a causal regulator. Since gauge theories are causal, it is clear that a causal regulator can not interfere with the symmetries of the theory. Let us illustrate this by the following argument: One way to see the violation of a local symmetry due to a momentum regulator is by observing that such a regulator corresponds to adding a momentum-dependent mass term to the classical action, analogously to Eq. (3.1). It is known that such a term quadratic in the field is not compatible with gauge invariance. However, anticipating a result that we obtain in Sec. 3.2, it can be shown that the sharp causal regulator (3.4) does not translate into any finite mass for the propagator. Essentially, this can already be observed from Eq. (3.4): The sharp causal regulator is either zero or infinity. Thus, it either does not contribute anything at all or it leads to the complete decoupling of all fluctuations. Let us remark that additional regularisation might be necessary in practice. For instance, this is the case if the theory under consideration has to be renormalised, and we discuss the renormalisation of the causal temporal flow in Sec. 4.7.

3.1.2. The Temporally Regulated Effective Action

To proceed, we introduce the effective action Γ . It is the generator of one-particle irreducible (1PI) correlation functions. These constitute a more efficient way of organising the information of the quantum theory than the connected correlators, and they are an essential ingredient of the tFRG approach. We define the regulated effective action as follows

$$\Gamma_\tau[\phi] := W_\tau[J[\phi]] - \int_{\mathcal{C},x} J[\phi](x)\phi(x) - \frac{1}{2} \int_{\mathcal{C},xy} \phi(x)R_\tau(x,y)\phi(y). \quad (3.7)$$

Here we suppressed the dependence of W_τ on the initial density matrix for the sake of a concise notation. We emphasise that the fields ϕ are free variables and the currents are determined via

$$\phi(x) = \left. \frac{\delta W_\tau[J]}{\delta J(x)} \right|_{J[\phi]}. \quad (3.8)$$

Before we derive the flow equation for Γ_τ , let us discuss some subtleties originating from the causal regulator. We remark that these have not been discussed in the literature before. To that end, let us recall that we are trying to formalise the idea of generating functionals on a CTP of finite extent τ as introduced in Sec. 2.2.3. There, we had obtained such generating functionals simply by not including any correlations for times later than τ in their definition. This is especially apparent in Eq. (2.23) and Eq. (2.24). Accordingly, these functionals do not exist for times larger than τ . Thus, there is no way of evolving these functionals to later τ solely based on the information encoded in them. This issue is absent for the functionals defined as in Eq. (3.6) where the finite extent of the CTP is achieved using the regulator. Indeed, observe that the path integral (3.2) sums over all fluctuations for all times. Furthermore, it includes sources J for all times. Hence, the correlation functions derived from it exist for all times. However, they receive no contributions for times later than the present time τ since such contributions are completely suppressed by the causal regulator. Their τ -evolution is obtained by successively removing the temporal regulator. Let us remark that when we refer to the regulated functionals Z_τ and W_τ from now on we do refer to the regulated functionals as defined in Eq. (3.6). These functionals can be evolved to later τ solely based on the information encoded in them by removing the regulator.

Now, when we define the regulated effective action Eq. (3.7), we exchange the current J for the field ϕ according to Eq. (3.8). This definition implies the following when considering a generic current J : $\phi[J](x) = \frac{\delta W_\tau[J]}{\delta J(x)} = 0$ for $x^0 > \tau$. This appears to be an issue since it would imply that Γ_τ does not exist for times later than τ . However, a more careful analysis reveals that this issue is absent and that the regulated effective action indeed exists for all times. One way to show this is to note that in Eq. (4.5), we do not use a generic current J but a very special current $J[\phi]$. It is given by taking a ϕ -derivative of Eq. (3.7),

$$J[\phi](x) = -\Gamma_\tau^{(1)}[\phi](x) - \int_{\mathcal{C},y} R_\tau(x,y)\phi(y). \quad (3.9)$$

Notably, the current $J[\phi]$ receives a contribution from the regulator. It turns out that

precisely this contribution ensures that the field ϕ can be non-vanishing everywhere. Note that the suppression of fluctuations for the correlation functions is still guaranteed. This can be seen by explicitly inserting the current (3.9) into the definition of the regulated effective action (3.7) and using the path integral representation (3.2) for W_τ . After shifting the integration variables in the path integral as follows $\varphi = \phi + f$, we obtain

$$e^{i\Gamma_\tau[\phi]} = \int_{\mathcal{C}} \mathcal{D}f \exp \left[i \left\{ S[\phi + f; \alpha] + f \cdot \Gamma_\tau^{(1)}[\phi] + \frac{1}{2} f \cdot R_\tau \cdot f \right\} \right]. \quad (3.10)$$

Here, we use a shorthand notation where the dots indicate CTP integrations. Observe that the fluctuations f are suppressed for times larger than τ thanks to the regulator, but the field ϕ is not touched by the regulator as desired. Thus, $\Gamma_\tau[\phi]$ exists for all times and is either the full effective action including all fluctuations or the initial one, determined solely in terms of the initial state. The 1PI-correlators which are the field-derivatives of the effective action, enjoy similar causality-properties and we discuss these in Sec. 3.2. Recall that the initial density matrix is accounted for by α . We discuss the initial conditions for the temporal flow in Sec. 3.1.4.

A complementary viewpoint to the above argument involving the current $J[\phi]$ and the path integral is given by introducing a smooth regulator with finite height and width determined by ε

$$-iR_{\tau,\varepsilon}(x, y) = \delta_{\mathcal{C}}(x - y) \cdot r_\varepsilon(\tau, x^0), \quad (3.11)$$

with $r_\varepsilon(\tau, x^0)$ chosen to reproduce Eq. (3.4) as $\varepsilon \rightarrow 0$. One example would be $\frac{1}{\theta_\varepsilon(\tau, x^0)} - 1$, where $\theta_\varepsilon(\tau, x^0)$ is a smooth version of the step function. Now as long as ε is finite, there are no subtleties as the regulator is not sharp. Thus, it is clear that ϕ can have support for all times and the standard FRG derivations can be applied. Then we take the causal limit $\varepsilon \rightarrow 0$ at the end. We will use such a smooth cutoff in the applications of Ch. 4, and we discuss the details of the causal limit there. Let us emphasise that the causal limit does not depend on the concrete form of $r_\varepsilon(\tau, x^0)$. We discuss this in more detail in Sec. 3.2.1. Until necessary, we suppress any potential dependence on ε .

Next, we address the hermiticity of the regulated effective action Γ_τ . In Sec. 3.1.1, we established that the causal regulator does not interfere with the hermiticity of the generating functionals. Thus, the hermiticity of Γ_τ can be established in exactly the same way as for Γ . The only subtlety that arises is due to exchanging the currents for the fields. This can be dealt with in a very elegant way, cf. [77]. For the regulated effective action, it leads to $\Gamma_\tau[\phi^+, \phi^-]^\dagger = -\Gamma_\tau[\phi^{-*}, \phi^{+*}]$. In this sense, Γ_τ is compatible

with unitarity. Note that the fields ϕ^\pm are complex in general ($\phi^\pm \neq (\phi^\pm)^*$) even if the original field operator is hermitian. A single real-time field only emerges after evaluating the effective action on $\phi^+ = \bar{\phi} = \phi^-$, cf. Sec. 3.1.6. We remark that unitarity can still be violated in approximations and we discuss this in detail in Sec. 3.1.5.

3.1.3. Derivation of the Temporal Flow Equation

We proceed by deriving the flow equation for the effective action Γ_τ . To that end, it proves useful to first derive the flow of the Schwinger functional W_τ . Note that the derivation of the temporal flow is completely identical to the derivation of the flow equation in equilibrium. In particular, it is independent of the chosen of regulator. Taking a partial τ -derivative of Eq. (3.6), we obtain

$$\begin{aligned}\partial_\tau W_\tau[J] &= \frac{1}{2} \left(-iW_\tau^{(2)}[J] + (W_\tau^{(1)}[J])^2 \right) \cdot \partial_\tau R_\tau \\ &= \frac{1}{2} \left(G_\tau[J] + (\phi[J])^2 \right) \cdot \partial_\tau R_\tau.\end{aligned}\tag{3.12}$$

The first term in the second line constitutes a definition: $G_\tau[J] := -iW_\tau^{(2)}[J]$. For the second term, we inserted the definition of the field (3.8) at generic J .

We proceed to the derivation of the flow of the effective action. Note that since ϕ is a free variable, we can consider it to be τ -dependent. Discussing this choice is deferred to Sec. 3.1.6. Taking the total τ -derivative, we obtain

$$\begin{aligned}\frac{d\Gamma_\tau[\phi]}{d\tau} &= \Gamma_\tau^{(1)}[\phi] \cdot \partial_\tau \phi + \partial_\tau \Gamma_\tau[\phi] \\ &= W_\tau^{(1)}[J[\phi]] \cdot \frac{\delta J[\phi]}{\delta \phi} \partial_\tau \phi + \partial_\tau W_\tau[J[\phi]] \\ &\quad - \frac{\delta J[\phi]}{\delta \phi} \partial_\tau \phi \cdot \phi - J[\phi] \cdot \partial_\tau \phi - \phi \cdot R_\tau \cdot \partial_\tau \phi - \frac{1}{2} \phi \cdot \partial_\tau R_\tau \cdot \phi.\end{aligned}\tag{3.13}$$

The first line just represents the definition of the total τ -derivative. We obtain the second line by applying the total τ -derivative to the effective action as defined in Eq. (3.7). Using the definition of ϕ in Eq. (3.8), the terms involving the field derivative of the current cancel and we arrive at

$$\frac{d\Gamma_\tau[\phi]}{d\tau} = \partial_\tau W_\tau[J[\phi]] - \frac{1}{2} \phi \cdot \partial_\tau R_\tau \cdot \phi - (J[\phi] + \phi \cdot R_\tau) \cdot \partial_\tau \phi.\tag{3.14}$$

Inserting the flow of the Schwinger functional (3.12) removes the terms involving the

$$G_{\tau,xy} = x \text{ --- } \textcircled{\tau} \text{ --- } y \quad \dot{R}_{\tau,xy} = x \text{ --- } \textcircled{\tau} \text{ --- } y$$

$$\Gamma_{\tau,x_1\dots x_n}^{(n)} = \text{--- } \textcircled{\tau} \text{ --- } \text{---}$$

Figure 3.1.: Graphical notation for the diagrammatic representation of flow equations. The black line with the orange circle containing τ represents the full, in general field dependent, regulated propagator $G_{\tau,xy}[\phi] = i[\Gamma_{\tau}^{(2)}[\phi] + R_{\tau}]_{xy}^{-1}$. The line with the blue square denotes the insertion of the regulator derivative $\partial_{\tau}R_{\tau,xy}$. The green circle containing τ with n lines attached to it denotes the full, field dependent and regulated n -point vertex $\Gamma_{\tau,x_1,\dots,x_n}^{(n)}[\phi]$.

regulator derivative between two fields. Recalling the expression (3.9) for the current, we identify $\Gamma_{\tau}^{(1)}[\phi]$ in the last term. Comparing Eq. (3.14) with the first line in Eq. (3.13), we arrive at the following expression for the partial τ -derivative of the effective action, commonly referred to as the flow equation

$$\partial_{\tau}\Gamma_{\tau}[\phi] = \frac{1}{2} \int_{\mathcal{C},xy} G_{\tau}[\phi](x,y) \partial_{\tau}R_{\tau}(x,y). \quad (3.15)$$

Here, $G_{\tau}[\phi] \equiv G_{\tau}[J[\phi]]$ is obtained by taking a field-derivative of the current (3.9) and using the definition of the field (3.8), to wit

$$G_{\tau}[\phi](x,y) = -i \frac{\delta^2 W_{\tau}[J]}{\delta J(x)\delta J(y)} \Big|_{J[\phi]} = \left[\frac{i}{\Gamma_{\tau}^{(2)}[\phi] + R_{\tau}} \right](x,y). \quad (3.16)$$

This relation defines the τ -dependent propagator as a functional of ϕ in terms of the second derivative of the effective action. Since this propagator is regulated, no fluctuations later than the present time τ can propagate. We discuss this in more detail in Sec. 3.2.

We continue by deriving the flow equations for the 1PI-correlators,

$$\Gamma_{\tau}^{(n)}[\phi](x_1, \dots, x_n) := \frac{\delta^n \Gamma_{\tau}[\phi]}{\delta \phi(x_1) \cdots \delta \phi(x_n)},$$

from the master flow equation for the effective action (3.15). Note that the field derivative commutes with the partial τ -derivative even if the field depends explicitly on τ . This

$$\partial_\tau \Gamma_{\tau,xy}^{(2)} = \frac{i}{2} \text{tadpole} - \frac{1}{2} \left[\text{diagram 1} + \text{diagram 2} \right]$$

Figure 3.2.: Diagrammatic representation of the general flow equation for the two-point function (cf. Eq. (3.18)) using the symbols introduced in Fig. 3.1. The first diagram is referred to as the tadpole. Using the symmetry of the propagator and the three-point function, we display the respective diagrams in a way that makes the symmetry of the regulator insertions explicit. This is useful for our applications in Ch. 4

is due to the fact that the partial derivative per definition involves keeping the other variables fixed. In particular, it is insensitive to any potential τ -dependence of the field ϕ , which we accounted for in our derivation of the flow equation (3.15). More details can be found in [106]. Taking the first ϕ -derivative of $\partial_\tau \Gamma_\tau$, using Eq. (3.16), we obtain the flow of the one-point function

$$\partial_\tau \Gamma_{\tau,x}^{(1)}[\phi] = \frac{i}{2} \int_{\mathcal{C},ab} \Gamma_{\tau,xab}^{(3)}[\phi] (G_\tau[\phi] \cdot \partial_\tau R_\tau \cdot G_\tau[\phi])_{ab}. \quad (3.17)$$

Here, we use a shorthand notation denoting space-time arguments as indices. This flow determines the τ -evolution of the regulated quantum equation of motion, $\Gamma_{\tau,x}^{(1)}[\phi]$. Thus, this flow determines the evolution of the macroscopic field ϕ . Taking a second derivative, we obtain the flow of the two-point function

$$\begin{aligned} \partial_\tau \Gamma_{\tau,xy}^{(2)}[\phi] &= \frac{i}{2} \int_{\mathcal{C},ab} \Gamma_{\tau,xyab}^{(4)}[\phi] (G_\tau[\phi] \cdot \partial_\tau R_\tau \cdot G_\tau[\phi])_{ab} \\ &\quad - \frac{1}{2} \int_{\mathcal{C},abcd} \left[\Gamma_{\tau,xab}^{(3)}[\phi] G_{\tau,ac}[\phi] (G_\tau[\phi] \cdot \partial_\tau R_\tau \cdot G_\tau[\phi])_{bd} \Gamma_{\tau,ycd}^{(3)}[\phi] + P(x,y) \right]. \end{aligned} \quad (3.18)$$

By $P(x,y,\dots)$, we denote a sum over the respective previous terms containing the remaining permutations of (x,y,\dots) .

A graphical representation of this equation is depicted in Fig. 3.2, using the symbols introduced in Fig. 3.1. For our applications in Ch. 4, we will also need the flow of the three- and four-point functions, which can be found in App. B. The fact that higher-order correlation functions enter in the flow of the lower-order ones is a general feature

of FRG equations. Typically, the flow of $\Gamma_\tau^{(n)}$ contains contributions from $\Gamma_\tau^{(n+1)}$ and $\Gamma_\tau^{(n+2)}$. Hence, we are dealing with an infinite hierarchy of coupled functional integro-differential equations. To obtain a finite set that can be solved in practice, this hierarchy has to be truncated which we discuss in Sec. 3.1.5.

3.1.4. Initial Conditions

The initial conditions for the temporal flow are provided by specifying the correlation functions included in a certain truncation at $\tau = t_0$. Specifying all

$$\Gamma_{t_0, x_1 \dots x_n}^{(n)}[\phi] \equiv \Gamma_{\tau=t_0, x_1 \dots x_n}^{(n)}[\phi] = S^{(n)}[\phi] + \mathcal{I}_{t_0}^{(n)}[\phi], \quad (3.19)$$

corresponds to completely specifying the initial density matrix $\langle \rho_{t_0} \rangle \propto \exp[i\mathcal{I}_{t_0}[\phi; \alpha]]$, cf. Eq. (2.25). Here, $\mathcal{I}_{t_0}^{(n)}$ denotes the n th field-derivative of the initial correlations \mathcal{I}_{t_0} . As will be discussed in Sec. 3.1.5, in practice we usually content ourselves with the first few lower-order correlation functions. One particularly simple choice for the initial values of the n -point functions is given by equating them to the respective derivatives of the classical action, $S_{x_1 \dots x_n}^{(n)}[\phi]$. In terms of the parametrisation (2.25) of the initial density matrix, this corresponds to $\alpha_n \equiv 0 \forall n$, i.e. $\langle \rho_{t_0} \rangle \propto \mathbb{1}$. Out of equilibrium of course much more general initial conditions are admissible. Indeed generically, the α_n are general functions of the spatial coordinates with support at the initial time t_0 . As such, the α_n allow to specify arbitrary far-from-equilibrium initial conditions. An example of initial conditions far from equilibrium is given by the initial conditions of our numerical applications in Sec. 5.3. These constitute Gaussian initial conditions which refers to setting $\alpha_{n>2} \equiv 0$. Notably, that non-Gaussian initial conditions are naturally part of the tFRG formalism. Taking into account any non-trivial $\alpha_{n>2}$ is straightforward and corresponds to considering non-trivial initial conditions for the n -point functions with $n > 2$ as given in Eq. (3.19). This high degree of flexibility regarding the initial conditions renders the tFRG approach an ideal candidate to address the dynamics of diverse physical systems in various types of conditions. We remark that including non-Gaussian initial conditions in the 2PI approach is not straightforward [107]. This is due to the fact that in $\Gamma_{2\text{PI}}[\phi, G]$, the only dynamical quantities are the macroscopic field ϕ and the propagator G . In this sense, all higher vertices are left bare. We remark that the presence of correlations of arbitrary order at t_0 in the tFRG framework is very useful with regard to renormalising the general causal temporal flow, which we discuss in Sec. 4.7.

3.1.5. Truncations

While the FRG allows for many different truncation schemes (cf. [33] and references therein), we will focus on the vertex expansion. To that end, we expand the effective action in powers of the fields ϕ around a background $\bar{\phi}$,

$$\Gamma_\tau[\phi] = \sum_{n=0}^{\infty} \frac{1}{n!} \int_{\mathcal{C}, x_1 \dots x_n} \Gamma^{(n)}(x_1, \dots, x_n)[\bar{\phi}] \prod_{j=1}^n [\phi(x_j) - \bar{\phi}(x_j)]. \quad (3.20)$$

The ‘‘coefficients’’ of this expansion are the n -point correlation functions in that background. For $n > 2$, these are also referred to as the vertices. Note that Eq. (3.20) constitutes a formal infinite series in the sense that we are agnostic about its convergence as a whole. What is relevant in practice is referred to as apparent convergence. Apparent convergence constitutes a systematic way to assess the sensitivity of the results in a given truncation with regard to truncation artefacts. The basic idea is to observe how the results obtained in a given truncation change when the truncation is enlarged by including more vertices. Apparent convergence is indicated by the fact that the results do not change significantly any more upon enlarging the truncation. What is observed in practice is that typically, the first few lower-order correlation functions suffice to obtain a satisfactory description of a given system.

Important guidance principles for devising a truncation are provided by the symmetries of the system in question. Ideally, these symmetries are neither broken by the truncation nor by the regulator. In practice, finding such symmetry-preserving truncations and regulators can be very challenging in particular with regard to local symmetries. Notably, the causal regulator (3.4) represents such a symmetry-preserving regulator for local symmetries, and we discussed this fact in Sec. 3.1.1.

With regard to devising truncations, the fact the FRG is a diagrammatic scheme proves to be very useful. For one, the contributions to the diagrams that enter in a given truncation can be given interpretations in terms of physical processes. Thus, we can use our intuition and prior experience to select contributions which are (potentially) important to describe a given process to a satisfactory degree. And indeed, as is apparent by [33] and the references therein, there is a lot of experience regarding FRG truncations for a plethora of different systems and applications.

Furthermore, FRG truncations can be systematically improved, for instance by including previously neglected correlations functions. Note that in this sense, the vertex expansion is truly an FRG scheme. Indeed, it is fundamentally distinct from other expansion schemes that are based on the smallness of some parameter. In a generic

truncation of the vertex expansion, no such small parameter exists.

Let us remark that generically, the flow in a given truncation is sensitive to the choice of regulator. The subject of optimisation of FRG flows as discussed for instance in [106] deals with minimising this spurious regulator dependence of truncations. Interestingly, the causal temporal flow of this work constitutes such an optimised flow of minimal regulator dependence, and we will come back to this fact in Sec. 3.2.

While there is a lot of experience regarding FRG truncations in equilibrium, much less is known concerning dynamical applications. Still, the same important guidance principles to devise truncations apply. For approximations of unitary quantum dynamics, these include causality, unitarity and the conservation of energy as essential ingredients. In this regard, recall the exceptional position of the self-consistent n PI approximations (e.g. 2PI) for dynamical applications. These approaches are distinguished in that they lead to a causal, bounded, energy conserving time evolution for the correlation functions in a quantum field theory. We discussed this in Sec. 2.1.4. In particular, recall that n PI approximations must be specified on the level of the effective action. In contrast, consider a generic truncation of the tFRG. As is apparent by the vertex expansion, the tFRG framework allows for very general classes of approximations that can be specified on the level of the individual correlation functions. The price we have to pay for this gain in flexibility is that energy conservation and the compatibility of the individual dynamic equations for the correlators of generic tFRG truncations are not guaranteed automatically but become non-trivial features instead. In their absence, the time evolution will show unbounded, secular growth, eventually leading to the breakdown of numerical approaches.

There are no conclusive answers yet with regard to general unitarity-preserving and energy-conserving tFRG truncations. However, it is known that there are tFRG truncations with these properties. For instance, the tFRG allows to recover 2PI approximations as particular truncations of the temporal flow, cf. Sec. 4.6. This implies that the tFRG knows about self-consistency. One perspective in this regard is the following: The tFRG formalism enforces causality in a manifest and local way, instead of enforcing self-consistency which is for instance enforced in the 2PI formalism. Thus, self-consistent tFRG truncations can be viewed as consequences of the inherent causality of the framework. We remark that it is known for the FRG that it contains 2PI and n PI approximations [6, 7, 108–110] and that these constitute so called complete resummations [111].

Regarding the conservation of energy in generic truncations, there are very concrete ideas as of how to address it. Namely by considering the causal temporal flow of the

energy-momentum tensor, which we derive in Ch. 6. As illustrated in Sec. 2.1.4, questions regarding energy conservation in approximations are linked to questions regarding unitarity. As far as the tFRG is concerned, these questions are not settled to date and constitute an area of active research. It remains to be seen whether addressing one of them, progress can be made on both fronts. What is encouraging regarding unitarity is that the causal regulator does not interfere with the hermiticity of the effective action, cf. Sec. 3.1.2. In this sense, unitarity is respected by the causal regulator. Note that unitarity can still be violated by the truncation itself. Thus, it would be interesting to see whether constraints can be derived which allow to identify unitary truncations. Complementary, constraints from unitarity could be enforced dynamically during the flow. To that end, we point out the following:

Note that similar situations regarding the breaking of unitarity are known in quantum field theory. Indeed in their naive formulation, quantum gauge theories also suffer from violations of unitarity. In the perturbative BRST quantisation of gauge theories, we typically choose to fix a gauge, breaking the gauge symmetry explicitly. Then, we introduce ghost fields which cancel all unphysical contributions to perturbative diagrams, restoring unitarity order by order in perturbation theory. Note that generalising this to non-perturbative approximations is non-trivial. Nevertheless, there are examples in equilibrium in *ab initio* FRG approaches to QCD where the symmetries which are broken by the regulator and the truncation get effectively restored at the end of the flow (see [112] and references therein). Whether these observations translate to tFRG truncations is an open problem. However, the structural similarities of the FRG and the tFRG should be very useful in this regard. In particular the underlying 1PI structure of the FRG is advantageous in this regard since it enables us to include all relevant topologies of diagrams also in non-perturbative applications.

For the Schwinger-Keldysh formalism, it is known that it has a rich cohomological structure, associated to “hidden” BRST symmetries. Note that the Schwinger-Keldysh BRST symmetries encode the causality and unitarity of quantum dynamics. Accordingly, these are already present when describing the dynamics of scalar fields. Similarly to the case of gauge theories, ghost fields can be introduced which enforce these BRST symmetries at every order of perturbation theory. To discuss Schwinger-Keldysh BRST symmetry for non-perturbative tFRG truncations requires extending the analysis performed in [89–91, 113].

We remark that the discussion regarding causality, unitarity and energy conservation in generic tFRG truncations constitutes a new result of the present work.

3.1.6. The Role of the Background Field

Now, let us discuss some important aspects regarding the background $\bar{\phi}$. In general, the effective action on the CTP depends on the macroscopic field ϕ with times on the CTP, cf. Eq. (3.20). In terms of real times, there are thus two fields ϕ^\pm and accordingly two background fields $\bar{\phi}^\pm$ a priori. However, let us recall the discussion concerning the CTP currents J^\pm below Eq. (2.18): For the generating functionals we need two currents with $J^+ \neq J^-$ in general. Then to obtain the physical time evolution, we must evaluate the CTP correlation functions derived from these generating functionals at $J^+ = \bar{J} = J^-$ where \bar{J} is a general space-time dependent real-time current. This ensures the cancellations between the forward and backward evolution on the contour where appropriate, $\mathcal{U}^\dagger[\bar{J}] \mathcal{U}[\bar{J}] = \mathbb{1}$, cf. Eq. (3.5). In particular, this ensures that for the expectation value of a single field operator, we obtain a single real-time field.

For the effective action, we traded the dependence on the currents for a dependence on the fields ϕ^\pm via Eq. (3.8). Still, the same reasoning applies: The generating functionals depend on $\phi^+ \neq \phi^-$ in general. However, the physical values of the CTP correlation functions as functionals of ϕ^\pm are obtained by evaluating them at $\phi^+ = \bar{\phi} = \phi^-$. Here, $\bar{\phi}$ now denotes a single real-time field. We remark that for the case of the standard CTP functionals, these facts are well known, see e.g. [77]. For the tFRG, they imply that general space-time-dependent backgrounds $\bar{\phi}$ are admissible in the tFRG formalism. We remark that this constitutes a new, so far unpublished result of the present work.

Now let us comment on a potential τ -dependence of the field. We took this into account in our derivation of the flow equation in Sec. 3.1.3. Such a dependence can be useful in practice. For instance in momentum space, a scale-dependent field can be used to perform scale-dependent field redefinitions (see e.g. [106] and references therein). This is useful if the relevant degrees of freedom at a given scale are composite operators of the microscopic fields. Such field redefinitions could also be done in a τ -dependent way. In this case, $\partial_\tau \bar{\phi}$ is required to integrate the flow, cf. Eq. (3.13). In this work, we do not pursue these directions further. Note that for a τ -independent field, we also obtain the flow equation (3.15). Since for a τ -independent field the total derivative of the effective action reduces to a partial one, Eq. (3.15) suffices to integrate the flow in this case.

Let us remark that the physical background in a closed system is determined by the solution to the quantum equation of motion in the absence of sources, i.e. $\Gamma_{\tau,x}^{(1)}[\bar{\phi}] = 0$, cf. Eq. (3.9). The quantum equation of motion is of course a causal equation. In particular, this implies that its solution does not involve any values of the field $\bar{\phi}(x)$ for $x^0 > \tau$. Note that this does not constitute an explicit τ -dependence of the field in the sense

discussed above. Expansions around such a solution are expected to be particularly stable [7], and the n -point functions evaluated on such a solution constitute the physical fluctuations around the physical background. However, note that we are not forced to make this choice. The FRG formalism allows us to expand the effective action around any background we like, and we will make use of this fact in the numerical applications of Ch. 5. Let us further remark that in approximations of closed systems, considering a non-vanishing background can be advantageous, cf. the discussion below Eq. (2.18).

3.2. Causality-Properties of the Temporal Flow

In this section, we discuss the causality-properties of the propagator and of the 1PI n -point functions. These properties are a distinct feature of the tFRG approach and will be very important for the rest of this work. We explain how these causality-properties arise, using the causal regulator and the structure of the flow in Sec. 3.2.1 and Sec. 3.2.2. Deriving these causality-properties from the flow represent one central result of [81, 82]. Apart from discussing of the important aspects of their original derivation, we provide additional, complementary insights. In Sec. 3.2.3 and Sec. 3.2.4, we derive further implications of causality and we translate the causality-properties into causal constraints. Note that these developments constitute a very important result of this work and are published in [1]. Combining the causality-properties of the propagator and the 1PI correlation functions, we infer the causal behaviour of the connected correlation functions as functionals of ϕ in Sec. 3.2.5.

3.2.1. The Propagation of Fluctuations

The causality-properties of the tFRG approach are intimately linked to the causal propagation of fluctuations. Here, the propagation of fluctuations is determined by the regulated propagator as given in Eq. (3.16): $G_{\tau,xy}[\phi] = i[\Gamma_{\tau}^{(2)}[\phi] + R_{\tau}]_{xy}^{-1}$. In this regard, recall that $R_{\tau,xy}$ diverges if the maximum of x^0 or y^0 is larger than τ . Thus, assuming $\Gamma_{\tau,xy}^{(2)}$ is sufficiently well-behaved for these times, the propagator vanishes upon inverting $[\Gamma_{\tau}^{(2)}[\phi] + R_{\tau}]_{xy}$, to wit

$$G_{\tau}[\phi](x, y) = 0 \quad \text{if } \max(x^0, y^0) > \tau. \quad (3.21)$$

Eq. (3.21) is a very important result for several reasons. First and foremost, it ensures that the propagator behaves in a manifestly causal way since fluctuations for times larger than τ are completely suppressed. Moreover it turns out that due to the structure

of the temporal flow, this leads to a manifest causal behaviour of *all* 1PI correlation functions. We explain this in more detail shortly in Sec. 3.2.2. We remark that this type of structure is generic for the FRG: The regularisation of fluctuations with a term that is quadratic in the fields, cf. Eq. (3.1), suffices to regulate all 1PI n -point functions thanks to the structure of the flow. Importantly, Eq. (3.21) also illustrates that if we choose to employ a smooth version of the temporal regulator, $-iR_{\tau,\varepsilon} = \delta_{\mathcal{C},xy} r_{\varepsilon,\tau x^0}$ as in Eq. (3.11), the restoration of causality in the limit $\varepsilon \rightarrow 0$ does not depend on the details of r_{ε,τ,x^0} . Indeed, all that matters in this regard is that in the limit, all fluctuations are completely suppressed. Let us remark that since the property Eq. (3.21) is due to the suppression of fluctuations by the regulator, it is not a distinctive feature of the temporal flow. Indeed, the complete suppression of fluctuations as in the property Eq. (3.21) can also be obtained for example by a sharp momentum cutoff [114, 115].

Complementary, Eq. (3.21) can also be deduced using the path integral representation of $W_\tau[J]$. To this end, we take two derivatives of $W_\tau[J]$ and evaluate it at $J[\phi]$ given by (3.9). Using the path integral representation as in Eq. (3.10), we find

$$G_\tau[\phi](x, y) \equiv -iW_\tau^{(2)}[J](x, y) \Big|_{J[\phi]} = \frac{\exp[-\frac{i}{2} \phi \cdot R_\tau \cdot \phi]}{Z_\tau[J[\phi]]} \times \\ \times \int_{\mathcal{C}} \mathcal{D}f f(x) f(y) \exp \left[i \left\{ S[\phi + f; \alpha] + f \cdot \Gamma_\tau^{(1)}[\phi] + \frac{1}{2} f \cdot R_\tau \cdot f \right\} \right]. \quad (3.22)$$

Here we again shifted $\varphi = \phi + f$ and used $\langle f \rangle = 0$. Focussing on the second line, we observe that the fluctuations f for times later than τ are completely suppressed due to $f \cdot R_\tau \cdot f$. Thus, we arrive at the same conclusion as in Eq. (3.21). Note that the regulator term in the first line of Eq. (3.22) can be cancelled with the same factor in the denominator.

Next, let us introduce the property that distinguishes the temporal FRG flow from flows in equilibrium. It is related to the cancellation of the time evolution along the forward and backward branch beyond the latest operator insertion. Recall that this occurs at $\phi^+ = \bar{\phi} = \phi^-$, cf. Sec. 3.1.6. Moreover, for times earlier than the latest operator insertion, the time evolution operators $\mathcal{U}[\bar{J}[\bar{\phi}]]$ on $\bar{\phi}$ attain their physical values. Let us emphasise that these CTP cancellations encode the causality and unitarity of quantum dynamics. For the propagator, evaluating it at $\bar{\phi}$, this implies

$$G_\tau[\bar{\phi}](x, y) = G_\infty[\bar{\phi}](x, y) \quad \text{if } \max(x^0, y^0) \leq \tau. \quad (3.23)$$

Recall that $G_\infty \equiv G_{\tau=\infty} \equiv G$, i.e. G_∞ is identical to the fully dressed propagator of the unregulated theory, G . Thus, Eq. (3.23) states that the regulated propagator equals the full result if τ is larger than or equal to the maximal time argument of the propagator. Eq. (3.23) immediately follows from the path integral representation (3.22): For the times $\max(x^0, y^0) \leq \tau$, the regulator in Eq. (3.22) vanishes. Thus, Eq. (3.22) is just the standard path integral and Eq. (3.23) follows upon evaluating on $\bar{\phi}$.

Let us reiterate that it is the property (3.23) which distinguishes the temporal FRG flow from flows in equilibrium. The suppression of fluctuations as in the property Eq. (3.21) can also be obtained using a sharp momentum cutoff. However, Eq. (3.23) does not hold for a flow in momentum space with a sharp regulator. For instance, consider an infrared regulator suppressing fluctuations below an infrared energy scale k . In this case, the n -point functions do not cease to flow for external momenta p that were already passed by the flow parameter k , i.e. for $p > k$ [114, 115].

3.2.2. Causality-Properties of the 1PI Correlation Functions

To derive the causality-properties of the 1PI n -point functions from the temporal flow, we use Eq. (3.21) and Eq. (3.23) from Sec. 3.2.1. Let us remark that if we do not want to keep referring back to the path integral as we did in Sec. 3.2.1, we can instead take the following approach: Assume that Eq. (3.21) and Eq. (3.23) are fulfilled. Using these properties and the arguments to be presented shortly, we derive the causality-properties for the 1PI correlators. Then we verify that indeed, Eq. (3.21) and Eq. (3.23) are consistent with these properties. We remark that for the applications of this work, the technical details of the following derivations are not relevant. What is important are the properties themselves which encode important physical concepts.

The first causality-property concerns the case when τ has not yet reached the maximal time of the n -point function: If any time argument is larger than τ , we find

$$\partial_\tau \Gamma_\tau^{(n)}[\phi](x_1, \dots, x_n) = 0 \quad \text{if } \max\{x_1^0, \dots, x_n^0\} > \tau. \quad (3.24)$$

This can be shown in an inductive way by analysing the diagrams on the right-hand side of the flow equation (3.15). To that end, one additional assumption has to be made. We require the initial vertices $\Gamma_{t_0}^{(n)}$ to be diagonal in time. Physically, this encodes the locality of the microscopic interactions. On a technical level, this condition ensures that an external time that is larger than τ reaches the internal propagators of the diagrams. Hence, these diagrams vanish using Eq. (3.21). Note that due to the properties of the regulator (3.3), Eq. (3.24) holds at $\tau = t_0$ by definition, which is the base case for the

induction over τ . For more technical details, we refer to [82].

Thus, fluctuations are suppressed as long as there is an external time later than the cutoff. Put differently, the flow has not yet advanced to these times and the n -point functions therefore just remain at their initial values, i.e.

$$\Gamma_\tau^{(n)}[\phi](x_1, \dots, x_n) = \Gamma_{t_0}^{(n)}[\phi](x_1, \dots, x_n) \quad \text{if } \max\{x_1^0, \dots, x_n^0\} > \tau, \quad (3.25)$$

Note that this is different than for the connected correlation functions. The propagator for instance vanishes for these times, cf. Eq. (3.21). However, this difference is to be expected. This is due to the fact that the 1PI correlation functions are derived from the quantum effective action Γ_τ . Through a perturbative expansion, the effective action can be viewed as the classical (initial) action $S[\phi; \alpha]$ plus corrections due to fluctuations. Accordingly, if all fluctuations are suppressed, we expect the 1PI correlators to reduce to their initial values $\Gamma_{t_0}^{(n)}$. More details in regarding the causality-properties of the connected correlators as functionals of ϕ are deferred to Sec. 3.2.5. In summary, Eq. (3.24) and Eq. (3.25) encode the causality of the temporal flow. A graphical illustration of the property Eq. (3.25) was given in Fig. 2.5.

The second property we want to recover encodes the CTP cancellations. Evaluating at $\phi^+ = \bar{\phi} = \phi^-$, we expect the time evolution along the forward branch \mathcal{C}^+ and backward branch \mathcal{C}^- beyond the latest operator insertion to cancel out since for these times, the operator ordering does not change any more. In terms of the flow, this means that as soon as τ has passed the latest time, the flow vanishes

$$\partial_\tau \Gamma_\tau^{(n)}[\bar{\phi}](x_1, \dots, x_n) = 0 \quad \text{if } \max\{x_1^0, \dots, x_n^0\} < \tau. \quad (3.26)$$

This property can be derived along the lines of [82], using the integrated flow. Here, we provide a similar argument, focusing directly on the flow itself. First note that all external times are smaller than $t_{max} := \max\{x_1^0, \dots, x_n^0\}$ by assumption. The only place where times larger than t_{max} can appear is in the loop integrals of the diagrams on the right-hand side of the flow equation. A priori, these CTP integrals run from t_0 along \mathcal{C}^+ to infinity and back along \mathcal{C}^- to t_0 . Due to the suppression by the regulator, we already know that no contributions for times later than τ occur. Accordingly, the upper boundary of all CTP integrals can be set to τ . Now Eq. (3.26) states that when evaluated on $\phi^+ = \bar{\phi} = \phi^-$, also the parts of the integrals between $t_{max} < \tau$ and τ vanish. To derive this result, we expand all fully dressed vertices in terms of the initial vertices and the fully dressed propagators. Now evaluating on $\bar{\phi}$, we know from Eq. (3.23) that the operator ordering for the propagator does not change for times later than or equal to

its maximal time argument. This implies that all CTP integrations beyond t_{max} cancel out and we arrive at Eq. (3.26).

In terms of the n -point functions, Eq. (3.26) implies that these do not change any more as soon as τ has passed their latest time argument. For $t_{max} = \tau$ however, the flow is non-zero and the n -point functions jump from their initial to their full values at which they remain

$$\Gamma_{\tau}^{(n)}[\bar{\phi}](x_1, \dots, x_n) = \Gamma_{\infty}^{(n)}[\bar{\phi}](x_1, \dots, x_n) \quad \text{if } \max\{x_1^0, \dots, x_n^0\} \leq \tau. \quad (3.27)$$

Note that Eq. (3.26) and Eq. (3.27) encode the causality and unitarity of quantum dynamics. In practice, one useful consequence is that after evaluating at $\bar{\phi}$, the upper boundaries of all CTP integrals of the diagrams on the right-hand side of the flow equation can be set to t_{max} . A graphical illustration of the property Eq. (3.27) was given in Fig. 2.4.

We observe that the causality-properties of the propagator as introduced in Sec. 3.2.1 are consistent with the causality-properties of the temporal flow. To that end, we use the known relation for the propagator: $G_{\tau,xy}[\phi] = i[\Gamma_{\tau}^{(2)}[\phi] + R_{\tau}]_{xy}^{-1}$. and Eq. (3.25) and Eq. (3.27).

3.2.3. Implications of Causality for the Propagator

We proceed by collecting important consequences of the causal structure of the flow for the propagator. Combining Eq. (3.21) and Eq. (3.23), we get

$$G_{\tau}[\bar{\phi}](x, y) = G[\bar{\phi}](x, y)\theta(\tau - x^0)\theta(\tau - y^0), \quad (3.28)$$

where $G[\bar{\phi}](x, y) \equiv G_{\infty}[\bar{\phi}](x, y)$ is the full propagator. A useful way of writing the above relation is as follows

$$G_{\tau}[\bar{\phi}](x, y) = \left[\frac{i}{\Gamma^{(2)}[\bar{\phi}] + R_{\tau}} \right] (x, y). \quad (3.29)$$

Notably, the regulated propagator on $\bar{\phi}$ depends only on the *full* two-point function $\Gamma^{(2)} \equiv \Gamma_{\infty}^{(2)}$ on $\bar{\phi}$. This surprising property is deeply rooted in the locality and causality of the present cutoff procedure. Furthermore, it is linked to the functional optimisation of the FRG. In [106], it has been shown that optimised FRG flows have a related property: For an optimal regulator, the regulator variation of the two-point function perpendicular to the direction of the optimised flow vanishes: $\delta_{\perp} \Gamma_k^{(2)} = 0$. Thus, the regulator dependence of the final result is minimised. This can be understood by think-

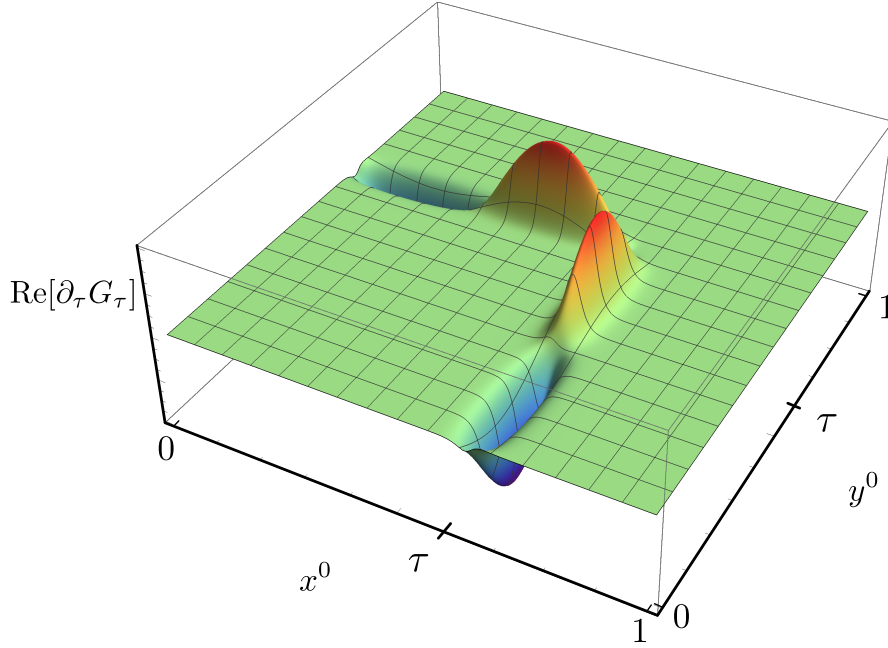


Figure 3.3.: Illustration of the causal structure of the τ -derivative of the propagator, $\partial_\tau G_\tau$, cf. Eq. (3.31). For visualisation purposes, we introduced a finite width to the contributing δ - and θ -functions. The oscillations stem from the real part of the free propagator. Both field operators are inserted on \mathcal{C}^+ . Observe that the causal structure leads to a localisation of $\partial_\tau G_\tau$ at τ . Starting from t_0 , the flow propagates this local shape outward, turning G_τ into the full propagator in the process.

ing about the FRG flow in terms of a literal flow in the space of theories. Provided we have a suitable metric in this space, the above property translates to travelling the minimal distance possible from the initial condition to the full theory [106]. The local and causal temporal regularisation discussed in the present work shares this property.

Taking a τ -derivative of Eq. (3.29) gives another very important identity

$$\partial_\tau G_\tau[\bar{\phi}](x, y) = i \int_{\mathcal{C}, z_1 z_2} G_\tau[\bar{\phi}](x, z_1) \partial_\tau R_\tau(z_1, z_2) G_\tau[\bar{\phi}](z_2, y). \quad (3.30)$$

In contrast to standard flows with momentum regulators, the term proportional to $\partial_\tau \Gamma_\tau^{(2)}$ is absent. Eq. (3.30) has important implications on the general structure of the causal temporal flow equations and is crucial for the approach. Note that if we decide to use a smooth regulator $R_{\tau, \varepsilon}$, we simply replace $\theta \rightarrow \theta_\varepsilon$ in the equations of this section. The absence of the $\partial_\tau \Gamma_\tau^{(2)}$ -term also at finite ε should stabilise the (integrated) flow in

numerical approaches. We address challenges we faced attempting to numerically solve the flow in Sec. 3.3.

Using Eq. (3.28), we can express the τ -derivative of the propagator on $\bar{\phi}$ as

$$\partial_\tau G_\tau[\bar{\phi}](x, y) = G_\infty[\bar{\phi}](x, y) \partial_\tau \left[\theta(\tau - x^0) \theta(\tau - y^0) \right]. \quad (3.31)$$

A visualisation of the τ -dependence in Eq. (3.31) is depicted in Fig. 3.3. Applying the τ -derivative to the θ -functions in the bracket, we obtain terms of the form $\delta \cdot \theta$. For illustration purposes, we introduce a finite width for the δ - and θ -functions and take $G_\infty[\bar{\phi}]$ to be the free propagator, cf. Sec. 5.3. In Fig. 3.3, we show its real part. Both field operators are inserted on the \mathcal{C}^+ branch of the CTP but other insertions give a similar picture as does the imaginary part. At $x^0 = \tau$, $\partial_\tau G_\tau$ in y^0 -direction carries the oscillating shape of the real part of the free propagator. However, as soon as $y^0 > \tau$, the τ -derivative of the propagator vanishes. The same holds if we interchange x^0 and y^0 . Observe that the causal structure leads to a localisation of the τ -derivative of the propagator at τ . Starting from t_0 , the flow propagates this local shape outward, turning G_τ into the full propagator in the process.

3.2.4. From Causality-Properties to Causal Constraints

In this section, we derive the causal constraints that the temporal flow obeys. Note that this represents a central new development of the present work which is published in [1].

To that end, we summarise the implications of causality collected thus far: The flow only contributes when the present time τ is equal to the maximal time of the respective n -point function. At this point, the n -point function jumps from its initial value to its full value. Thus, the causal constraint for the regulated n -point functions reads

$$\begin{aligned} \Gamma_\tau^{(n)}[\bar{\phi}](x_1, \dots, x_n) &= \Gamma_{t_0}^{(n)}[\bar{\phi}](x_1, \dots, x_n) \\ &+ \Delta\Gamma^{(n)}[\bar{\phi}](x_1, \dots, x_n) \prod_{i=1}^n \theta(\tau - x_i^0), \end{aligned} \quad (3.32)$$

with $\Delta\Gamma^{(n)} := \Gamma^{(n)} - \Gamma_{t_0}^{(n)}$. Here, $\theta(\tau - x_i^0)$ is defined such that it is zero for $x_i^0 > \tau$ and one otherwise. The difference between the initial and the full n -point function, $\Delta\Gamma^{(n)}$, is given by the (integrated) flow. Ignoring some subtleties regarding the τ -dependence which we will discuss shortly, we can think of $\Delta\Gamma^{(n)}$ as the diagrams on the right-hand side of the flow equation.

The causal constraint (3.32) allows us to deuce the constraints posed on the flow.

However, as it is written above, Eq. (3.32) only holds for $\varepsilon \rightarrow 0$. For ε finite, the step functions generally appear to some power m_i . This is due to the fact that during the flow, the vertices, the propagators and the regulator can jump at the same time. This generates contributions of the form $\delta(\tau - x^0)\theta^{m_i}(\tau - x^0)$. The δ -distribution stems from the τ -derivative. The power m_i depends on the specific contribution in question, but it can always be determined explicitly. To resolve such products, we need to introduce smooth versions of the distributions, δ_ε and θ_ε . This corresponds to replacing the sharp cutoff with a smooth version $R_\tau \rightarrow R_{\tau,\varepsilon}$. A detailed discussion is deferred to Ch. 4. For the flow, the causal constraint takes the form

$$\partial_\tau \Gamma_\tau^{(n)}[\bar{\phi}](x_1, \dots, x_n) = \Delta \Gamma^{(n)}[\bar{\phi}](x_1, \dots, x_n) \partial_\tau \left[\prod_{i=1}^n \theta(\tau - x_i^0) \right]. \quad (3.33)$$

Again, $m_i = 1$ holds after $\varepsilon \rightarrow 0$. As an illustration, consider $n = 2$. Then Eq. (3.33) carries the same local causal structure as the propagator (cf. Eq. (3.31)) which we depicted in Fig. 3.3. Starting from t_0 , this local shape propagates outward turning $\Gamma_\tau^{(2)}$ into the full two-point function in the process. We can think analogously about the flow of a general n -point function.

Let us briefly outline how the causal constraints can be used to integrate the flow analytically. Recall the diagrammatic representation of the flow of the two-point function in Fig. 3.2. The line with the regulator derivative $G_\tau \partial_\tau R_\tau G_\tau$ enters in all diagrams. This also holds for the higher n -point functions, see e.g. Fig. B.2 and Fig. B.3. Using (3.30), this line can be replaced by the τ -derivative of the propagator which contains a δ -distribution due to (3.31). Furthermore, the causal constraint (3.32) provides us with the τ -dependence of the vertices. Thus, the entire τ -dependence of the flow of any n -point functions is completely encoded in terms of products of δ - and θ -functions. Properly defining these products of distributions, we can perform the integration over τ analytically. We discuss this in detail in Ch. 4.

3.2.5. Causality for the Connected Correlation Functions

Here we provide more details regarding the two facts that, for any time larger than τ , the connected correlators $W_\tau^{(n)}[J[\phi]]$ vanish while the 1PI n -point functions $\Gamma_\tau^{(n)}[\phi]$ remain at their initial value which is non-zero in general. Indeed, these two properties are consequences of one another. This is immediately seen recalling how the two types

$$W_{\tau, x_1 x_2 x_3}^{(3)} = -i \begin{array}{c} x_1 \\ | \\ \textcircled{\tau} \\ | \\ \textcircled{\tau} \\ / \quad \backslash \\ \textcircled{\tau} \quad \textcircled{\tau} \\ | \quad | \\ x_2 \quad x_3 \end{array}$$

Figure 3.4.: Diagrammatic representation of the connected, regulated three-point function using the symbols introduced in Fig. 3.1. It is given by the regulated 1PI three-point function with regulated propagators as external legs.

of correlators are related. The important point is that due to

$$-i \frac{\delta}{\delta J} = G_{\tau}[\phi] \cdot \frac{\delta}{\delta \phi},$$

the connected correlators are expressed in terms of 1PI n -point functions with regulated propagators at their external legs. These regulated propagators at the external legs are also present for the higher order connected n -point functions and ensure that they vanish if any external time of the connected correlation function is larger than τ . While the internal 1PI vertices attain their initial values in this case, the external, regulated propagators force the entire diagram to vanish. We remark that this observation has not been discussed before in the literature. A graphical illustration of this observation can be found in Fig. 3.4 where we diagrammatically represent the connected three-point function $W_{\tau}^{(3)}$ using the symbols introduced in Fig. 3.1.

3.3. On the Numerical Solution of the Temporal Flow

We already introduced the idea that the temporal flow can always be integrated analytically. Note that for other types of flows, this is only possible in certain special cases, while it is generic for the temporal flow. Before this fact was clarified, we attempted to solve the temporal flow numerically. In these attempts, we faced several issues which we discuss in this section. Note that at that time, the results of Sec. 3.2.3 and Sec. 3.2.4 were either not yet obtained or not yet fully understood.

The first problem that has to be addressed concerns the causal regulator (3.4). Numerically, we can represent it only approximately, using a representation as in Eq. (3.11) where the regulator has a finite height and width determined by the parameter ε . The

regulated propagator is then obtained from $G_{\tau,\varepsilon} = i[\Gamma_{\tau,\varepsilon}^{(2)} + R_{\tau,\varepsilon}]^{-1}$. For any finite ε this entails that there are acausal contributions to the flow which potentially lead to numerical instabilities. Assuming these are controlled, the causal limit has to be taken numerically, performing several runs with decreasing ε . Similarly to lattice computations, a scaling analysis should allow the extrapolation to the causal results. During our efforts, our numerical computations never reached this stage.

This is due to another, much more subtle problem. It concerns the proper definition of $\Gamma_{t_0}^{(2)}$. Since the issues we are going to address are already present for a Gaussian initial state, we set $\alpha_{n>2} \equiv 0$ for the following discussion. Then, $\Gamma_{t_0}^{(2)} = S^{(2)} + \alpha_2$. Thus, we are dealing with the classical kinetic operator on the CTP with initial condition α_2 . This derivative operator must be defined with care, properly taking into account the CTP boundary condition at the endpoint of the CTP. This boundary condition states that the branches \mathcal{C}^+ and \mathcal{C}^- of the CTP must be joined such that we obtain one continuous path, i.e. the latest points on \mathcal{C}^+ and \mathcal{C}^- have to be identified. Note that this condition arises automatically in the derivation of the CTP path integral, cf. Eq. (2.22) and the discussion below Eq. (2.24). If this boundary condition is not taken into account, $\Gamma_{t_0}^{(2)}$ is not invertible and the classical CTP propagator $G_{\text{cl}} = i[\Gamma_{t_0}^{(2)}]^{-1}$ cannot be obtained. The proper, invertible operator can be defined by a careful discretisation of the free CTP path integral. For a derivative operator that is first order in time, the result can be found in [12, 103] and for a second-order time derivative in [104]. The latter case is also discussed very pedagogically in [105]. We focus on the second-order operator.

In terms of real times, $\Gamma_{t_0}^{(2)}$ is a *non-diagonal* CTP matrix. The non-diagonal entries are crucial to obtain an invertible operator and originate from the CTP boundary condition. Note that the initial condition α_2 also contains off-diagonal contributions if the initial state is a mixed state. For a pure state however, the initial condition only contributes to the diagonal of $\Gamma_{t_0}^{(2)}$. The continuum notation common in the literature hides these non-diagonal entries, see e.g. Eq. (3.10). Note that in approaches like the 2PI formalism these issues do not arise since the propagator does not need to be inverted in order to compute the dynamics. The same is true for the integrated temporal flow. To numerically solve the temporal flow however, $\Gamma_{t_0}^{(2)}$ is required. Then, the regulated propagator is obtained by numerical inversion of $G_{\tau,\varepsilon} = i[\Gamma_{\tau,\varepsilon}^{(2)} + R_{\tau,\varepsilon}]^{-1}$. This inversion has to be performed each time we want to advance τ . Thus, it represents a numerical bottleneck. Unaware of the proper definition of $\Gamma_{t_0}^{(2)}$, the naive idea to get hold of it is to attempt to invert G_{cl} numerically. However, for a field theory with a classical kinetic operator of the form $S^{(2)}[\bar{\phi} = 0] = -(\partial^\mu \partial_\mu + m_0)$, this is not possible. For instance, naively discretising G_{cl} for a relativistic scalar field, cf. Sec. 5.3, leads to a non-invertible propagator matrix.

After resolving these issues, numerically solving the temporal flow is still challenging. To that end, assume that we properly define $\Gamma_{t_0}^{(2)}$ such that we can obtain the regulated propagator by numerical inversion. Recall that the CTP propagator in terms of real times is a block matrix, cf. Eq. (A.3), containing the four components $G^{\pm\pm}$ and $G^{\pm\mp}$. We call this propagator basis the \pm -basis. As discussed at the end of Sec. 2.1.3, this representation is highly redundant, encoding two independent real-valued functions in terms of four interdependent complex-valued ones. Numerically, this redundant basis wastes valuable resources. In particular, it consumes a lot of memory and increases the computing time.

In principle, this issue can be circumvented by changing to a propagator basis where no redundancies are present. For the 2PI formalism or for the integrated flow, this can be achieved using the completely real basis, cf. Eq. (A.4). However, such a type of basis is not readily available for the derivative operator $\Gamma_{t_0}^{(2)}$. Furthermore, even if such a basis can be found, we have to be very careful in tFRG applications. This is due to the fact that the discontinuities present in the completely real basis can coincide with the discontinuity of $R_{\tau,\varepsilon}$ and $\partial_\tau R_{\tau,\varepsilon}$.

Apart from being demanding in terms of resources, the \pm -basis is plagued by instabilities in numerical applications. This is due to the fact that the CTP cancellations for times smaller than the latest operator insertion which are crucial for the overall consistency have to occur numerically. Of course, these cancellations are never exact in a numerical application with finite precision. The completely real basis does not suffer from these instabilities as all CTP constraints are resolved in this basis and we are dealing with real integrals over real-valued functions. We explicitly observed these types of instabilities in our numerics when solving the integrated flow: Our computations in the \pm -basis were plagued by instabilities which got cured once we switched to the completely real basis.

Let us remark that the different bases for the propagator are well understood, and it is known how to obtain completely real equations if products or convolutions of two-time quantities are involved. This can be accomplished using the Langreth rules [78]. However, the contributions to the temporal flow and to the integrated flow generically involve contour integrals with multi-time integrands that can not be reduced to simple convolutions, cf. Eq. (3.18). These contributions arise due to the vertices. For numerical applications, it is important to reduce these contour integrals to real integrals. This could be done along the lines of [116]. Possible bases for general CTP n -point functions are analysed in detail in [117].

3.4. Conclusion

In this chapter, we introduced the tFRG formalism and discussed its manifest local and causal structure in detail. This includes several recent, so far unpublished developments.

To that end, we revisited the derivation of the temporal flow equation. Paying particular attention to subtleties and properties originating from the employed causal regulator, we clarified that general space-time dependent backgrounds are admissible in the tFRG approach. Moreover, we showed that the causal regulator leads to regulated generating functionals which respect the hermiticity enjoyed by their unregulated counterparts. This hermiticity is related to unitarity which can still be broken by the choice of truncation, and we outlined how the unitarity of generic tFRG truncations could be addressed using the BRST-symmetries of the CTP. We discussed the initial conditions for the temporal flow and showed that arbitrary far-from-equilibrium, non-Gaussian initial conditions are an intrinsic feature of the tFRG.

We proceeded with a discussion of the causality-properties of the temporal flow and their implications for the temporally regulated correlation functions. Apart from illustrating their original derivation, we provided additional, complementary insights. Using these causality-properties, we derived causal constraints that are obeyed by the correlation functions and their flow. These constitute an important result of the present work since they facilitate the analytic integration of the temporal flow. We reconciled the the causality-properties of the connected correlation functions with the ones of the 1PI correlators.

We addressed several challenges we encountered attempting to numerically solve the temporal flow.

4. The Analytically Integrated Causal Temporal Flow

In this chapter, we present some of the major results of the present work.

First, we continue developing the causal constraints introduced in Sec. 3.2. To that end, we discuss the particular role of local contributions to the flow in detail in Sec. 4.1. This analysis facilitates the analytic integration of the flow of the two-point function in Sec. 4.2. Remarkably, the integrated flow constitutes a novel one-loop exact functional relation valid for general theories. We remark that Sec. 4.1 and 4.2 contain parts of [1].

We present the integrated flow of the one-point function in Sec. 4.3 and the integrated flow of the effective action in Sec. 4.4. There, we also propose an extension of the tFRG formalism designed to directly access equilibrium properties of quantum field theories. We remark that Sec. 4.3 and 4.4 constitute new, so far unpublished results of the present work.

In Sec. 4.5, we derive the complete hierarchy of Dyson-Schwinger equations (DSEs) solely from the temporal flow. This constitutes a substantial extension of the discussion given in [1] and is, to the best of our knowledge, the first time that such a derivation has been accomplished [118].

In Sec. 4.6, we derive a truncation of the temporal flow that includes an effective vertex that leads to an s-channel resummation for the propagator. We show that this truncation is able to reproduce the 2PI $1/N$ -expansion at next-to-leading order. We remark that this result is known [6, 7]. Here however, we provide a different derivation, using the causal constraints of this work.

In Sec. 4.7, we solve the problem of renormalising the general causal temporal flow, using the ϕ^4 -theory in $3+1$ dimensions as a concrete example. This constitutes a major novel development of this work. Sec. 4.7 is in parts based on [2].

In Sec. 4.8, we derive an algorithm that allows to explicitly solve certain causal integral equations that appear in the integrated flow. This possibility has, to the best of our knowledge, not been noticed in the literature so far. We remark that while this fact was stated by us in [1], the detailed derivation of Sec. 4.8 constitutes a new, so far unpublished result of the present work.

Regarding the memory integrals present in the tFRG, we propose an extension of the temporal flow which uses a non-diagonal causal temporal regulator in Sec. 4.9. Placing the flow on an S-shaped contour, we outline how this procedure could give rise to entirely time-local evolution equations for the correlation functions. This proposal constitutes a new, so far unpublished result of the present work.

We conclude in Sec. 4.10.

4.1. The Causal Constraints at Work

In this section, we use the causality-properties and the causal constraints obtained in Sec. 3.2 to classify possible contributions to the flow. As an illustrative example and for later use, we consider the flow of the two-point function, Eq. (3.18). We evaluate the flow at $\phi^+ = \bar{\phi} = \phi^-$ which we do not denote explicitly any more from now on. Using the important relation (3.30), we replace the line with the cutoff insertion $G_\tau \partial_\tau R_\tau G_\tau$ by $-i \partial_\tau G_\tau$ in the flow equation for $\Gamma_\tau^{(2)}$, to wit

$$\begin{aligned} \partial_\tau \Gamma_{\tau,xy}^{(2)} &= \frac{1}{2} \int_{\mathcal{C},ab} \Gamma_{\tau,xyab}^{(4)} * \partial_\tau G_{\tau,ab} \\ &+ \frac{i}{2} \int_{\mathcal{C},abcd} \Gamma_{\tau,xab}^{(3)} * [G_{\tau,ac} \partial_\tau G_{\tau,bd} + \partial_\tau G_{\tau,ac} G_{\tau,bd}] * \Gamma_{\tau,ycd}^{(3)}. \end{aligned} \quad (4.1)$$

Using the symmetry of the propagator and the three-point functions, we made the symmetry of the appearance of the τ -derivative manifest in the second line, cf. Fig. 3.2. Here, we introduce an important notation for this work, $*$, the star-product. It indicates that the distributions carrying the τ -dependence are replaced by regularised versions, $\delta \rightarrow \delta_\varepsilon$ and $\theta \rightarrow \theta_\varepsilon$. When the regularisation with ε is not denoted explicitly, the $*$ -product implies it. The regularisation of the distributions with ε originates from the use of a smooth regulator $R_{\tau,\varepsilon}$ (cf. Eq. (3.11)) which we discussed in Sec. 3.2. The regularisation in terms of ε is necessary to properly deal with contributions to the flow that arise when the discontinuities of the propagator, the regulator and the n -point functions coincide. As will become clear in this section, these are in fact the only contributions to the flow. This fact is intimately linked to the locality of the causal regulator which implies the local causal constraints through the structure of the flow.

To develop the causal constraints further, we consider the diagram involving the four-point function in Eq. (4.1). This diagram is referred to as the tadpole. First, we focus on the τ -derivative of the propagator. Using the implications of causality for the

propagator, in particular Eq. (3.28), we know that the τ -dependent propagator is given by $G_{\tau,ab} = G_{ab} \theta_{\tau a} \theta_{\tau b}$. Hence, its τ -derivative reads

$$\partial_{\tau} G_{\tau,ab} = G_{ab} (\delta_{\tau a} \theta_{\tau b} + \theta_{\tau a} \delta_{\tau b}). \quad (4.2)$$

Here, $\theta_{\tau a} = \theta(\tau - a^0)$ and analogously for $\delta_{\tau a}$. We illustrated this causal structure in Fig. 3.3. Now for this example, consider a local contribution to the four-point function that contains $\delta_{\mathcal{C}}(x^0 - a^0) \delta_{\mathcal{C}}(x^0 - b^0)$. Such a local part of the vertex together with Eq. (4.2) gives rise to

$$2 \lim_{\varepsilon \rightarrow 0} \theta_{\varepsilon}(\tau - x^0) \delta_{\varepsilon}(\tau - x^0) = 2 \frac{1}{2} \delta(\tau - x^0).$$

The factor of two is due to the two terms in Eq. (4.2), whereas the factor of $1/2$ arises from properly resolving the product of distributions. Importantly, evaluating these types of products of δ - and θ -functions leads to a prefactor times a δ -function. To determine the correct prefactor, the points of coincidence of the involved distributions have to be treated properly, and we discuss this in Sec. 4.1.1.

The involved distributions allow us to constrain possible contributions to the flow. To that end, compare Eq. (4.2) to the causal constraint for the flow of the two-point function, cf. Eq. (3.33). The causal constraint implies that the flow is non-zero if and only if τ is equal to the maximal external time argument

$$\partial_{\tau} \Gamma_{\tau,xy}^{(2)} = \Delta \Gamma_{xy}^{(2)} (\delta_{\tau x} \theta_{\tau y} + \theta_{\tau x} \delta_{\tau y}). \quad (4.3)$$

Notably, the flow must generate a δ -function containing τ and an *external* time argument. For the causal structure of the tadpole as given in Eq. (4.2), this implies that the only non-vanishing contributions to the tadpole come from the *local* parts of the four-point function. This is due to the fact that these local parts contain CTP δ -functions, e.g. $\delta_{\mathcal{C},xa} \delta_{\mathcal{C},xb}$, making the involved internal times coincide with the respective external ones for all times. For diagrams with multiple vertices as the second term in Eq. (4.1), the non-local part of the vertex can contribute as well as long as there is also a local contribution from another vertex.

To make the important local contributions explicit, we distinguish the contributions from the flow accordingly,

$$\Delta \Gamma_{\tau,x_1 \dots x_n}^{(n)} = \Delta \Gamma_{\text{nl},x_1 \dots x_n}^{(n)} \prod_{i=1}^n \theta(\tau - x_i^0) + \Delta \Gamma_{\text{local},\tau,x_1 \dots x_n}^{(n)}. \quad (4.4)$$

Here, the local part is defined to contain all terms with $\delta_{\mathcal{C}}(x_i^0 - x_j^0)$, $i \neq j$. Accordingly for the non-local part, no coincident points of discontinuities occur. In particular, this implies that all θ -functions involving external time arguments, $\theta(\tau - x_i^0)$, appear to the power of one. For the local part however this is not the case. In general, its τ -dependence is of the form $\prod_{i=1}^n \theta_{\varepsilon}^{m_i}(\tau - x_i^0)$. We will show how to determine the exponents m_i in explicit examples in Sec. 4.5 and Sec. 4.6. Importantly, given a specific contribution to the flow, the m_i are always known explicitly.

Let us emphasise again that the presence of local contributions is necessary to obtain a non-vanishing contribution to the flow. This fact is deeply rooted in the local and causal regularisation employed in this work and is made manifest in terms of the local causal constraints (4.4). In concrete applications, this property leads to tremendous simplifications as the number of admissible contributions to the flow is greatly reduced.

Adding the initial n -point function to Eq. (4.4), we express the whole correlator as

$$\Gamma_{\tau, x_1 \dots x_n}^{(n)} = \Gamma_{t_0, x_1 \dots x_n}^{(n)} + \Delta \Gamma_{\tau, x_1 \dots x_n}^{(n)}. \quad (4.5)$$

Note that here, we indicate the fact that the τ -dependence of the local part of the correlator still has to be determined by the subscript τ in $\Delta \Gamma_{\tau, x_1 \dots x_n}^{(n)}$. This is in contrast to the parametrisation 3.32 introduced in the previous chapter. In particular, by

$$\Delta \Gamma^{(n)} = \Delta \Gamma_{\text{nl}}^{(n)} + \Delta \Gamma_{\text{local}}^{(n)}, \quad (4.6)$$

we denote the contribution from the flow where the whole τ -dependence has been determined and $\varepsilon \rightarrow 0$ was taken. Note that there is no subscript τ in Eq. (4.6). In contrast for $\Delta \Gamma_{\tau}^{(n)}$ as in Eq. (4.5), ε is finite and the τ -dependence still has to be determined.

4.1.1. Singular Products of Distributions

To determine the correct prefactor of a general product of δ - and θ -functions, we use the following identity [115, 119]

$$\lim_{\varepsilon \rightarrow 0} f[\theta_{\varepsilon}(\tau - x^0)] \delta_{\varepsilon}(\tau - x^0) = \delta(\tau - x^0) \int_0^1 dx f[x]. \quad (4.7)$$

Eq. (4.7) allows us to compute the correct prefactor for expressions of the type

$$\lim_{\varepsilon \rightarrow 0} [\theta_{\varepsilon}(\tau - x^0)]^n \delta_{\varepsilon}(\tau - x^0) = \delta(\tau - x^0) \int_0^1 dx x^n = \frac{1}{n+1} \delta(\tau - x^0). \quad (4.8)$$

Let us emphasise that in order for Eq. (4.7) to apply, the δ - and θ -functions in Eq. (4.7) have to share the same regularisation ε . Crucially for our applications, we can use the same regularisation ε for the distributions in the propagator and in all n -point functions since their regularisation originates from the regularisation of the causal temporal regulator, $R_\tau \rightarrow R_{\tau,\varepsilon}$. This implies that the product (4.8) is uniquely defined. We remark that the naive assignment of a certain value to $\theta(0)$ leads to incorrect results in general.

4.1.2. The Degree of Locality of the Vertex Corrections

Now that we know how to deal with singular products of distributions, we will determine when such products can arise. To that end, we analyse the vertex corrections that get generated by the temporal flow and determine for which types of interactions local parts can arise. The result we will obtain is that local parts arise when there are microscopic four-point interactions. On the contrary, if there are microscopic three-point interactions only, the flow does not generate any local vertex corrections. Let us emphasise that the following arguments do not depend on the field content of theory. Hence, we use the ϕ^3 - and the ϕ^4 -theory as explicit – and general – examples.

The ϕ^3 -Theory Here, we outline a proof that in a theory with microscopic three-point interactions only, no local vertex corrections occur. Accordingly, the only local vertex present is given by the initial $\Gamma_{t_0}^{(3)}$. To that end, let us first clarify which parts of $\Gamma_{t_0}^{(3)}$ are relevant to the present case. For a general correlated initial state, $\Gamma_{t_0}^{(3)}$ receives contributions from the classical vertex $S^{(3)}$ and contributions from the coefficients α_n which parametrise the initial density matrix, cf. Eq. (2.25). What is relevant for the following argument is the topology of the diagrams that can be constructed from a given vertex. This property is not influenced by the α_n and we consider $\Gamma_{t_0}^{(3)} = S^{(3)}$ accordingly.

We proceed by showing that the flow does not generate any local vertex corrections. First, consider the flow of the three-point function. In particular focus on the triangle diagrams, i.e. the second line of Fig. B.2. Starting with the classical vertices, the flow generates the vertex corrections

$$\Delta\Gamma^{(3)}(x_1, x_2, x_3) \propto (\lambda_3)^3 G(x_1, x_2)G(x_1, x_3)G(x_2, x_3) + \dots, \quad (4.9)$$

where the dots stand for other diagrams as well as vertex corrections in the triangle. Here, λ_3 is the classical three-point coupling. The space-time dependence of Eq. (4.9) is simply given by a product of propagators. Evidently, this product does not contain

temporal or spatial δ -functions as long as it is well-defined. We remark that the τ -dependence of the correlators is irrelevant for this argument.

We add that in dimensions $d \geq 1 + 5$, the product of propagators in Eq. (4.9) is not well-defined any more at $x_1 = x_2 = x_3$. The respective terms are proportional to $\delta_{\mathcal{C}}(x_1 - x_2) \delta_{\mathcal{C}}(x_2 - x_3)$ and hence add to the classical coupling. This is nothing but the standard renormalisation. We discuss the renormalisation of the temporal flow in detail in Sec. 4.7. In the numerical applications of Ch. 5, we consider the ϕ^3 -theory in $d = 1 + 1$ and these intricacies are absent.

Thus, we have established that the vertex correction Eq. (4.9) has no local pieces. Furthermore, any other vertex correction to the three-point function can be iteratively constructed from this diagram and the respective ones for the higher correlation functions. For example the flow of the three-point function generates a four-point function from the box diagram in the flow of $\Gamma_{\tau}^{(4)}$, cf. the fourth line in Fig. B.3. This four-point function couples back into the flow of the other n -point functions and in particular into the flow of $\Gamma_{\tau}^{(3)}$ as can be seen from the first line in Fig. B.2. However, none of these diagrams can generate $\delta_{\mathcal{C}}$ -functions as all legs are connected by propagators. In conclusion, the vertices in the ϕ^3 -theory have no local parts, except the classical vertex $S^{(3)}$, i.e.

$$\Delta\Gamma_{\text{local}}^{(n)}(x_1, \dots, x_n) \equiv 0, \quad \forall n > 2. \quad (4.10)$$

This will greatly simplify the analytic integration of the temporal flow in the ϕ^3 -theory as the local contributions are absent and no $*$ -product has to be evaluated.

The ϕ^4 -Theory The absence of local vertex corrections of the ϕ^3 -theory does not continue to hold in general theories. We elucidate the generic structure within the ϕ^4 -theory. In this case, it can be shown that all n -point functions contain local parts. To that end, consider the fish diagrams with classical vertices which is the analogue of Eq. (4.9)

$$\begin{aligned} \Delta\Gamma^{(4)}(x, y, z_1, z_2) = & \frac{i}{2} (\lambda_4)^2 \left[G^2(x, y) \delta_{\mathcal{C}}(x - z_1) \delta_{\mathcal{C}}(y - z_2) \right. \\ & + G^2(x, y) \delta_{\mathcal{C}}(x - z_2) \delta_{\mathcal{C}}(y - z_1) \\ & \left. + G^2(x, z_1) \delta_{\mathcal{C}}(x - y) \delta_{\mathcal{C}}(z_1 - z_2) \right] \\ & + \dots, \end{aligned} \quad (4.11)$$

where λ_4 is the classical four-point coupling. This vertex correction is self-consistently generated by the flow of the four-point function, cf. the second line in Fig. B.3. In Eq. (4.11), the dots stand for other diagrams as well as vertex corrections to the fish diagrams. The diagrams in Eq. (4.11) are evidently local. Analogously to before, this basic diagrammatic structure enters in the iterative construction of the vertex corrections of the four- and the higher n -point functions.

Furthermore, Eq. (4.11) can also contribute to the three-point function. The three-point function is absent in the ϕ^4 -theory for $\bar{\phi} = 0$, but it is present for $\bar{\phi} \neq 0$ or in a theory with additional microscopic ϕ^3 -vertices. In any event, under the presence of a microscopic four-vertex, the three-point function receives local corrections. In the presence of local vertex corrections, we will need to consider the $*$ -product.

4.2. Integrated Flow of the Two-Point Function

To analytically integrate the general temporal flow of the two-point function, we use the results established in Sec. 4.1. To that end, we write Eq. (4.1) as

$$\begin{aligned} \partial_\tau \Gamma_{\tau,xy}^{(2)} = \partial_\tau \left[\frac{1}{2} \int_{\mathcal{C},ab} \Gamma_{\tau,xyab}^{(4)} G_{\tau,ab} + \frac{i}{2} \int_{\mathcal{C},abcd} \Gamma_{\tau,xab}^{(3)} G_{\tau,ac} G_{\tau,bd} \Gamma_{\tau,ycd}^{(3)} \right] - \frac{1}{2} \int_{\mathcal{C},ab} \partial_\tau \Gamma_{\tau,xyab}^{(4)} * G_{\tau,ab} \\ - \frac{i}{2} \int_{\mathcal{C},abcd} \partial_\tau \Gamma_{\tau,xab}^{(3)} * G_{\tau,ac} G_{\tau,bd} \Gamma_{\tau,ycd}^{(3)} - \frac{i}{2} \int_{\mathcal{C},abcd} \Gamma_{\tau,xab}^{(3)} G_{\tau,ac} G_{\tau,bd} * \partial_\tau \Gamma_{\tau,ycd}^{(3)}. \end{aligned} \quad (4.12)$$

This relates to the fact that the flow equation for the effective action can be rewritten as a total τ -derivative and an RG improvement term,

$$\partial_\tau \Gamma_\tau = \frac{i}{2} \text{Tr} \left[\partial_\tau \ln \left[\Gamma_\tau^{(2)} + R_\tau \right] \right] - \frac{1}{2} \text{Tr} \left[\partial_\tau \Gamma_\tau^{(2)} \cdot G_\tau \right], \quad (4.13)$$

where we have suppressed the field dependence. While such a rewriting is not required for applications, it carries much of the structure of the flow equation: Typically, the first term is dominant while the second term generates sub-leading RG-improvements.

The total derivative in the first line of (4.12) can be integrated directly. No singular products of distributions occur and the $*$ -product reduces to the standard one. Thus for these terms, we can take $\varepsilon \rightarrow 0$. For the other terms we use the results of Sec. 4.1.

Recall the following causal constraint,

$$\partial_\tau \Gamma_{\tau,xy}^{(2)} \propto \delta_{\tau x} \theta_{\tau y} + \theta_{\tau x} \delta_{\tau y}. \quad (4.14)$$

To generate δ -functions in the external time arguments, the flow of the vertices in Eq. (4.12), $\partial_\tau \Gamma_{\tau,xyab}^{(4)}$, $\partial_\tau \Gamma_{\tau,xab}^{(3)}$ and $\partial_\tau \Gamma_{\tau,ycd}^{(3)}$, have to contain adequate local contributions. To determine them for the tadpole, we consider the causal constraint (4.4) for $n = 4$

$$\partial_\tau \Gamma_{\tau,xyab}^{(4)} = \Delta \Gamma_{\text{nl},xyab}^{(4)} \partial_\tau [\theta_{\tau x} \theta_{\tau y} \theta_{\tau a} \theta_{\tau b}] + \partial_\tau \Delta \Gamma_{\text{local } \tau,xyab}^{(4)}. \quad (4.15)$$

Hence, there are two ways to generate δ -functions in the external time arguments:

- (i) *Contributions from the non-local part of the vertex:* $\Delta \Gamma_{\text{nl}}^{(4)}$ can only contribute if the τ -derivative hits a θ -function with an external time argument. If it hits an internal argument, the causal constraint of the flow (4.14) is not satisfied and the respective contribution vanishes. This leads us to the following causal structure:

$$\Delta \Gamma_{\text{nl},xyab}^{(4)} [\delta_{\tau x} \theta_{\tau y} + \theta_{\tau x} \delta_{\tau y}] \theta_{\tau a} \theta_{\tau b}, \quad (4.16)$$

The product in Eq. (4.16) is the standard one.

- (ii) *Contributions from the local part of the vertex:* Contributions from $\Delta \Gamma_{\text{local } \tau}^{(4)}$ have to be computed with care. As for Eq. (4.16), we receive contributions from $\partial_\tau \theta(\tau - x_i^0)$. Since additional factors $\theta(\tau - x_i^0)$ may be present, the $*$ -product has to be evaluated. Here, $i = 1, 2$ and $x_1^0 = x^0$, $x_2^0 = y^0$.

Moreover, also contributions from the τ -derivative of θ -functions with an internal time argument z_j^0 have to be considered as $\Delta \Gamma_{\text{local } \tau}^{(4)}$ carries contributions with the following δ -functions: $\delta_{\mathcal{C}}(x_i^0 - z_j^0)$ with $j = 1, 2$ and $z_1^0 = a^0$, $z_2^0 = b^0$ and the x_i^0 as above. These terms also satisfy the causal constraint Eq. (4.15). Again, the $*$ -product has to be considered due to the potential occurrence of additional θ -functions.

Analogously, the contributions from the three-point functions are identified using the causal constraint (4.4) for $n = 3$.

Now we are in a position to integrate the flow of the two-point function analytically. The causal constraint (4.3) dictates that this flow must carry the following causal structure: $\delta_{\tau x} \theta_{\tau y} + \theta_{\tau x} \delta_{\tau y}$. Considering $x_0 > y_0$ singles out the first term where the flow is only

non-vanishing for $\tau = x_0$. For $y_0 < x_0$, the flows is only non-vanishing for $\tau = y_0$. For a concise derivation of the final result, we use that the two-point function is symmetric and consider $x^0 > y^0$. We remark that the final result will also be valid on the diagonal $x^0 = y^0$. Moreover, we assume that the renormalisation has already been performed. In particular this implies that products of propagators do not give rise to any additional local contributions as discussed below Eq. (4.9). We discuss the renormalisation of the tFRG in detail in Sec. 4.7.

The integrated flow of the two-point function is given by

$$\Gamma^{(2)}(x, y) = \Gamma_{t_0}^{(2)}(x, y) + \lim_{\xi \rightarrow 0^+} \int_{t_0}^{x^0 + \xi} d\tau \partial_\tau \Gamma_\tau^{(2)}(x, y). \quad (4.17)$$

Recall that we evaluated the flow on $\phi^+ = \bar{\phi} = \phi^-$. Accordingly, we can use the causality-property (3.26): There are no contributions to the flow when τ is larger than the maximal external time. The infinitesimal shift with ξ has been introduced to ensure that our integration picks up the contribution from $\delta_{\tau x}$. For the times considered in Eq. (4.17), $\Gamma^{(2)} \equiv \Gamma_{\tau=\infty}^{(2)} \equiv \Gamma_{\tau=x^0}^{(2)}$ is the full two-point function. Here, the last equivalence again follows using the CTP cancellations. Thus, the upper boundaries of the CTP integrals in the diagrams on the right hand side of the flow equation can be set to x^0 . Let us remark that due to the causal property (3.25), we also have $\Gamma_{\tau=x^0-\xi}^{(n)} \equiv \Gamma_{t_0}^{(n)}$. Thus we could change the lower integral boundary in Eq. (4.17) as follows: $t_0 \rightarrow x^0 - \xi$. We remark that the lower boundaries of the CTP integrals on the right hand side of the flow equation start at t_0 . These integrals are referred to as memory integrals and we investigate them more closely in Sec. 4.9.

4.2.1. Cubic Interactions Only

We now apply the above arguments to the two-point function of the ϕ^3 -theory. Integrating the flow results in an integral equation for the correlation functions. In fact, as a particularity of the ϕ^3 -theory, we directly obtain the Dyson-Schwinger equation (DSE) for the two-point function. This is to be expected since we are integrating a one-loop equation and the DSE in the ϕ^3 -theory is one-loop exact. Thus, the following derivation serves a consistency check of our approach. Furthermore, it demonstrates that the inherent locality and causality of the tFRG lead to considerable simplifications in computations. We emphasise that these simplifications are also present in numerical applications.

We insert the right-hand side of the flow (4.12) in (4.17) to integrate it. This leads us

to a vanishing tadpole contribution,

$$\frac{1}{2} \int_{\mathcal{C}, ab \leq x^0} \left[\Gamma_{xyab}^{(4)} G_{ab} - \Gamma_{t_0, xyab}^{(4)} G_{t_0, ab} - \Delta \Gamma_{nl, xyab}^{(4)} G_{ab} \right] = 0. \quad (4.18)$$

The first two terms stem from the total derivative in (4.12). For the third term, we used that the four-point function in the ϕ^3 -theory receives no local corrections, cf. Eq. (4.10), and the $*$ -product reduces to the standard one accordingly. Recall that the full four-point function is given by $\Gamma^{(4)} = \Gamma_{t_0}^{(4)} + \Delta \Gamma_{nl}^{(4)} + \Delta \Gamma_{local}^{(4)}$. Since $S^{(4)} = 0$ in the ϕ^3 -theory, the initial vertex $\Gamma_{t_0}^{(4)} = S^{(4)} + \mathcal{I}_{t_0}^{(4)}$ is determined solely in terms of the initial correlations \mathcal{I}_{t_0} , cf. Eq. (3.19). Here, we defined $\mathcal{I}_{t_0}^{(n)} := \delta^n \mathcal{I}_{t_0} / \delta \phi_1 \dots \delta \phi_n$. Thus in total, the full vertex reduces to $\Gamma^{(4)} = \mathcal{I}_{t_0}^{(4)} + \Delta \Gamma_{nl}^{(4)}$. The non-local vertex corrections are cancelled by the third term in Eq. (4.18). Concerning the initial correlations, recall that these have support at t_0 only. Therefore,

$$\int_{\mathcal{C}, ab \leq x^0} \mathcal{I}_{t_0, xyab}^{(4)} G_{ab} \equiv \int_{\mathcal{C}, ab \leq x^0} \mathcal{I}_{t_0, xyab}^{(4)} G_{t_0, ab}, \quad (4.19)$$

and the initial correlations cancel with the term in Eq. (4.18) containing G_{t_0} . We remark that the latter pattern is generic: The terms involving G_{t_0} ensure that the right-hand side of the integrated flow of $\Gamma^{(n)}$ vanishes if all external times are set to t_0 . This corresponds to the fact that at t_0 , all correlators are determined in terms of their initial conditions. Keeping this in mind, we absorb terms involving G_{t_0} into the initial conditions $\Gamma_{t_0}^{(n)}$ from now on.

We emphasise that the property Eq. (4.18) is unique to the present tFRG approach and is a consequence of the employed local and causal regularisation. For other regulator choices and in particular for the common momentum and frequency regulators, the tadpole contribution is non-vanishing. To obtain the DSE for the two-point function from the integrated flow in such a setting, the DSE for the four-point function has to be inserted into the tadpole and the computation proceeds from there.

Next, we consider the contributions from the three-point functions in (4.12). Their flow, $\partial_\tau \Gamma^{(3)}$, receives contributions from the non-local vertex corrections proportional to $\delta_{\tau x}$ and $\delta_{\tau y}$ only, cf. Eq. (4.16). Moreover, the term proportional to $\delta_{\tau y}$ does not contribute as the cutoff time in this term, $\tau = y^0$, is smaller than the external time x^0 by assumption. For the non-local parts, the $*$ -product is absent and we can integrate them directly. The total τ -derivative can be trivially integrated. In summary, the τ -integration

of the flow (4.12) leads us to

$$\begin{aligned}\Gamma_{xy}^{(2)} &= \Gamma_{t_0,xy}^{(2)} + \frac{i}{2} \int_{\mathcal{C},abcd \leq x^0} \left[\Gamma_{xab}^{(3)} - \Delta\Gamma_{nl,xab}^{(3)} \right] G_{ac} G_{bd} \Gamma_{ycd}^{(3)} \\ &= \Gamma_{t_0,xy}^{(2)} + \frac{i}{2} \int_{\mathcal{C},abcd \leq x^0} \Gamma_{t_0,xab}^{(3)} G_{ac} G_{bd} \Gamma_{ycd}^{(3)}.\end{aligned}\quad (4.20)$$

Eq. (4.20) is the DSE as derived from an initial action $\Gamma_{t_0} = S + \mathcal{I}_{t_0}$. Considering $\mathcal{I}_{t_0} \equiv 0$ implies $\Gamma_{t_0}^{(3)} = S^{(3)}$ and $\Gamma_{t_0}^{(2)} = S^{(2)}$. In this case, Eq. (4.20) reduces to the standard Dyson-Schwinger equation

$$\Gamma_{xy}^{(2)} = S_{xy}^{(2)} - \frac{i\lambda}{2} \int_{\mathcal{C},cd \leq x^0} G_{ac} G_{bd} \Gamma_{ycd}^{(3)}.\quad (4.21)$$

4.2.2. Cubic and Quartic Interactions

In this subsection, we derive a central result of this work – the integrated flow of the two-point function in a theory with microscopic four-point interactions. In particular the following result applies to the ϕ^4 -theory for vanishing and non-vanishing backgrounds and to a theory that contains both microscopic three- and four-point interactions.

To that end, we have to take into account local contributions to the flow of the three- and four-point function. We first consider the latter

$$\begin{aligned}& \frac{1}{2} \int_{\mathcal{C},ab \leq x^0} \left[\Gamma_{xyab}^{(4)} G_{ab} - \Gamma_{t_0,xyab}^{(4)} G_{t_0,ab} - \Delta\Gamma_{nl,xyab}^{(4)} G_{ab} - \Delta\Gamma_{local,xyab}^{(4)} * G_{ab} \right] \\ &= \frac{1}{2} \int_{\mathcal{C},ab \leq x^0} \left[\Gamma_{t_0,xyab}^{(4)} G_{ab} + \left(\Delta\Gamma_{local,xyab}^{(4)} - \Delta\Gamma_{local,xyab}^{(4)} * \right) G_{ab} \right].\end{aligned}$$

In the first line, the first two terms again come from the total derivative in (4.12). For these, no *-product is present. The second term is absorbed into $\Gamma_{t_0}^{(2)}$, cf. the discussion below Eq. (4.19). The last two terms are the contributions from $\partial_\tau \Gamma_\tau^{(4)}$, cf. Eq. (4.15). Note that in the last term, $\Delta\Gamma_{local}^{(4)} * G$ is a shorthand for $\lim_{\xi \rightarrow 0^+} \int_{t_0}^{x^0 + \xi} d\tau \partial_\tau \Delta\Gamma_{local}^{(4)} \tau * G_\tau$. To get to the second line, recall again that the full four-point function is given by $\Gamma^{(4)} = \Gamma_{t_0}^{(4)} + \Delta\Gamma_{nl}^{(4)} + \Delta\Gamma_{local}^{(4)}$. Thus, the non-local parts in the third term of the first line cancel with the non-local parts of the full vertex. The remaining contributions from the total derivative are given by the initial vertex and the local part. These appear

in the second line. The contributions involving the three-point function are obtained analogously. In particular, we perform the same steps as for the ϕ^3 -theory taking into account the local contributions. Putting everything together, we are lead to a remarkable novel result: A one-loop exact functional relation for the two-point function valid for general theories

$$\begin{aligned} \Gamma_{xy}^{(2)} - \Gamma_{t_0,xy}^{(2)} &= \frac{1}{2} \int_{\mathcal{C}, ab \leq x^0} \left[\Gamma_{t_0,xyab}^{(4)} G_{ab} + \left(\Delta \Gamma_{\text{local},xyab}^{(4)} - \Delta \Gamma_{\text{local},xyab}^{(4)*} \right) G_{ab} \right] \\ &+ \frac{i}{2} \int_{\mathcal{C}, abcd \leq x^0} \left[\Gamma_{t_0,xab}^{(3)} G_{ac} G_{bd} \Gamma_{ycd}^{(3)} + \left(\Delta \Gamma_{\text{local},xab}^{(3)} - \Delta \Gamma_{\text{local},xab}^{(3)*} \right) G_{ac} G_{bd} \Gamma_{ycd}^{(3)} \right]. \end{aligned} \quad (4.22)$$

We emphasise that other functional relations for correlation functions do not have a generic one-loop form. For example the Dyson-Schwinger equation for the propagator is only one-loop exact in the ϕ^3 -theory, while it is two-loop exact in the ϕ^4 -theory. For future reference, we point out that the first terms on the right-hand side in the first and second line of Eq. (4.22) are the one-loop diagrams in the DSE of the two-point function. The vertex corrections in the second terms in both lines generate the respective two-loop terms. A detailed discussion is deferred to Sec. 4.5.

Note that, using the same reasoning, $\partial_\tau \Gamma_\tau^{(n)}$ can be integrated analytically for any n and the result will be one-loop exact as well. We remark that this is only seemingly in contradiction with the proof that such one-loop exact functional relations do not exist in [111]. The present approach implicitly escapes one of the presuppositions there (no integral over parameters such as the cutoff time) via Eq. (4.7).

4.3. Integrated Flow of the One-Point Function

Using the same reasoning as in Sec. 4.2, we can integrate the flow of the one-point function which was given in Eq. (3.17). As the derivation proceeds completely in parallel to the one for the two-point function, we just give the final result

$$\Gamma_x^{(1)} - \Gamma_{t_0,x}^{(1)} = \frac{1}{2} \int_{\mathcal{C}, ab \leq x^0} \left[\Gamma_{t_0,xab}^{(3)} G_{ab} + \left(\Delta \Gamma_{\text{local},xab}^{(3)} - \Delta \Gamma_{\text{local},xab}^{(3)*} \right) G_{ab} \right]. \quad (4.23)$$

This constitutes a new result not published in [1]. Eq. (4.23) is the full quantum equation of motion for the field $\bar{\phi}$ valid for general theories. Its solution is obtained by solving $\Gamma_x^{(1)}[\bar{\phi}] = 0$, which is an integro-differential equation. The derivatives enter via the

kinetic operator contained in the initial one-point function. For instance if we take the classical action for a relativistic scalar field as the initial action, this reads schematically $S_x^{(1)}[\bar{\phi}] = -(\partial^\mu \partial_\mu + m_0^2)\bar{\phi}_x + V^{(1)}[\bar{\phi}]$. Here, $V^{(1)}[\bar{\phi}]$ is the first field-derivative of the classical potential V evaluated at $\bar{\phi}$. Note that if there are microscopic four-point interactions present, $\Gamma_{t_0}^{(3)}$ receives contributions of the form $S^{(4)} \cdot \bar{\phi}$. The vertex corrections $\Delta\Gamma_{\text{local}}^{(3)}$ on the right-hand side are absent if we consider microscopic three-point interactions only. As discussed in Sec. 4.1.2, this is no approximation, but holds in the full quantum theory. Indeed dropping the vertex corrections, Eq. (4.23) agrees with the DSE of the one-point function in the ϕ^3 -theory. Note that if there are microscopic four-point interactions, the vertex corrections do not vanish in general. For the concrete example of the DSE, we discuss the vertex corrections that produce the respective two-loop term in Sec. 4.5.3.

4.4. Integrated Flow of the Effective Action

We derive and discuss the integrated flow of the effective action in Sec. 4.4.1. Sec. 4.4.2 proposes an extension of the tFRG formalism designed to directly access the equilibrium properties of quantum field theories. We remark that this constitutes a recent development whose details are the subject of ongoing discussions. The present section constitutes new, so far unpublished results of the present work.

4.4.1. Derivation and Discussion

Using the arguments of Sec. 4.2, we integrate the flow of the effective action. By partial integration, this flow can be rewritten as in Eq. (4.13), to wit

$$\partial_\tau \Gamma_\tau[\phi] = -\frac{i}{2} \partial_\tau \int_{\mathcal{C},x} \ln G_{\tau,xx}[\phi] - \frac{1}{2} \int_{\mathcal{C},xy} \partial_\tau \Gamma_{\tau,xy}^{(2)}[\phi] * G_{\tau,xy}[\phi].$$

Integrating the flow leads to

$$\Gamma[\bar{\phi}] - \Gamma_{t_0}[\bar{\phi}] = -\frac{i}{2} \int_{\mathcal{C},x} \ln G_{xx}[\bar{\phi}] - \frac{1}{2} \int_{\mathcal{C},xy} \Gamma_{xy}^{(2)}[\bar{\phi}] * G_{xy}[\bar{\phi}]. \quad (4.24)$$

Let us emphasise that the functionals in Eq. (4.24) are evaluated at $\phi^+ = \bar{\phi} = \phi^-$. As discussed in Sec. 3.1.6, this is necessary to obtain the physical time evolution. In particular, this entails that the time evolution operators along the forward and backward branch of the CTP cancel where appropriate. Now in the case of Eq. (4.24), this

implies that both terms on the right-hand side vanish. The technical reason is that CTP traces over correlators on $\bar{\phi}$ vanish. Thus, we are left with $\Gamma[\bar{\phi}] = \Gamma_{t_0}[\bar{\phi}]$. This is easily understood by recalling the definitions of the effective action and the generating functional Z :

$$\exp \{i\Gamma[\bar{\phi}]\} = Z[\bar{J}[\bar{\phi}]; \rho_{t_0}] = \text{Tr} \rho_{t_0} \equiv \exp \{i\Gamma_{t_0}[\bar{\phi}]\}. \quad (4.25)$$

This implies that if the initial density matrix is normalised, the effective action on the diagonal $\phi^+ = \bar{\phi} = \phi^-$ vanishes. This is a known result of the CTP formalism, cf. for example [77]. Thus, Eq. (4.24) constitutes no generating functional.

4.4.2. Towards a Causal Temporal Flow in Equilibrium

Consider an equilibrium state $\rho_{t_0} \equiv e^{-\beta \mathcal{H}}$. Then, Eq. (4.25) corresponds to the thermodynamic partition sum or to the free energy respectively. Since Eq. (4.25) is just a trivial identity, it provides no means to actually compute the involved quantities.

A possible way forward in this regard is given by extending the contour $\mathcal{C} = \mathcal{C}^+ \cup \mathcal{C}^-$ used so far by adding a vertical track of length β at t_0 . Adopting the notation of [78], we denote to this vertical part by \mathcal{C}^M . Here, the ‘‘M’’ refers to ‘‘Matsubara’’, commemorating his contributions to the imaginary-time formalism of equilibrium quantum field theory. In the imaginary-time formalism, only the track \mathcal{C}^M is present. For the case at hand however, the total contour is given by $\mathcal{C}_{\text{tot}} = \mathcal{C}^M \cup \mathcal{C}^+ \cup \mathcal{C}^-$. This type of extended contour is of course known for a long time [71]. Amongst others, it is used in the real-time formalism of equilibrium quantum field theory (see e.g. [78, 87] for an introduction).

Let us briefly introduce the contour \mathcal{C}^M . Note that in general, \mathcal{C}^M describes out-of-equilibrium initial states. To see this, we write the initial density matrix as follows:

$$\rho_{t_0} =: \exp \{-\beta \mathcal{H}^M\} = \exp \left\{ -i \int_{t_0^M}^{t_\beta^M} dt^M \mathcal{H}^M \right\}. \quad (4.26)$$

Here, the times t^M take values on the contour \mathcal{C}^M . It is defined as a path in the complex plane that is oriented such that the difference between its initial point t_0^M and its final point t_β^M is given by $t_\beta^M - t_0^M = -i\beta$. Note that the ‘‘Hamiltonian’’ \mathcal{H}^M does not depend on t^M . Indeed, it is just a parametrisation of the initial density matrix very similar to the one given in Eq. (2.25). Thus, Eq. (4.26) encodes a general out-of-equilibrium state. We remark that incorporating the initial conditions in terms of the vertical track \mathcal{C}^M has the disadvantage that it leads to more components of the contour ordered correlators which now are path ordered with respect to \mathcal{C}_{tot} . For example, the propagator becomes

a 3×3 contour matrix, see e.g. [78, 87]. Thus for general dynamical applications, it is usually more convenient to include the initial density matrix simply via the initial conditions of the dynamic equations.

Now let us consider equilibrium. There, we want Eq. (4.26) to describe a thermal state. Accordingly, β now has the interpretation of the inverse temperature. Notably, to describe thermal equilibrium, (anti-) periodic boundary conditions have to be imposed for (fermionic) bosonic fields on \mathcal{C}_{tot} [89]. These boundary conditions give rise to the KMS relations fulfilled by the thermal correlation functions. The KMS relations encode the time-translational invariance of the equilibrium correlators. Thus, using \mathcal{C}_{tot} with appropriate boundary conditions, we have direct access to equilibrium correlators at real times. We remark that the same boundary conditions have to be imposed in the imaginary time formalism for the fields on \mathcal{C}^{M} . Moreover, let us remark that in order to access correlators at real times in the imaginary time formalism, analytic continuation has to be performed. Depending on the choice of continuation, the different components that are present explicitly in the real-time formalism are recovered [120].

Now, importantly for the tFRG approach, the effective action can be defined just as before, cf. Eq. (3.7), simply replacing $\mathcal{C} \rightarrow \mathcal{C}_{\text{tot}}$. Moreover, the derivation of the temporal flow equation on \mathcal{C}_{tot} is identical to the one given in Sec. 3.1.3. We remark that the path integral representation of the effective action on \mathcal{C}_{tot} can be derived in complete analogy to the discussion in Sec. 2.2.2. Next, we address the choice of regulator. At the heart of the tFRG approach are the causal constraints that the regulated, flowing correlation functions obey. To preserve them, we regulate fluctuations on the horizontal part \mathcal{C} of the extended contour $\mathcal{C}_{\text{tot}} = \mathcal{C}^{\text{M}} \cup \mathcal{C}$ with the causal temporal regulator. For the Matsubara branch \mathcal{C}^{M} , a possible choice would be to use a standard momentum regulator. Of particular importance is the regularisation of IR fluctuations which become relevant in the vicinity of phase transitions, and a momentum regulator on \mathcal{C}^{M} can provide this type of regularisation. Moreover, it can act as a UV regulator as well. We remark that such a combined flow in time and momentum can be useful for dynamical applications as well. Note that the entire regulator on \mathcal{C}_{tot} should comply with the equilibrium constraints, i.e. the KMS conditions. For FRG applications that use a momentum regulator on \mathcal{C} , it is known how to accomplish this, see e.g. [121].

Let us remark that in equilibrium, the Fourier conjugate of the time direction, the frequency p^0 , is at our disposal. However, this has to be taken with a grain of salt: While causality is manifest in the time domain, it is somewhat obscured in Fourier space. There, it manifests itself in terms of the analyticity properties of the correlators, see e.g. [92]. Choosing a regulator function in frequency and spatial momentum in accordance with

these analyticity properties is subtle. Generically, such a regulator introduces spurious poles for the propagator, potentially spoiling causality and unitarity, see e.g. [122] and references therein. Working out the details regarding a combined time and momentum flow on \mathcal{C}_{tot} is left to future work.

Assume for the moment that the just outlined extension of the tFRG framework is possible and leads to a sensible generalisation of the integrated flow of the effective action (4.24). Then all integrals in Eq. (4.24) run over \mathcal{C}_{tot} . Causality still dictates that contributions only involving \mathcal{C} vanish. Now however there are additional, non-zero contributions coming from \mathcal{C}^{M} . Thus, there is a non-vanishing contribution from the first term on the right-hand side of Eq. (4.24): $\int_{\mathcal{C}^{\text{M}},x} \ln G_{xx}$. This contribution passes the first straightforward consistency check: Replace $G \rightarrow G_{\text{cl}}$, considering perturbation theory. There, this term leads to the correct temperature dependent one-loop correction to the effective potential [87, 93]. On a non-perturbative level, we remark that the term $\int_{\mathcal{C}^{\text{M}},x} \ln G_{xx}$ is present in the n PI effective actions [26].

The interesting part is of course given by the higher loop-corrections generated by the flow and contained in the second term on the right-hand side of Eq. (4.24). For this term, additionally to contributions involving \mathcal{C}^{M} only, also cross-terms with \mathcal{C} arise. A first consistency check would be given by deriving the DSEs from the integrated flow of the effective action $\Gamma[\bar{\phi}, \phi^{\text{M}}]$. We remark that for numerical applications, it is important to derive real-time equations from the contour integrals on \mathcal{C}_{tot} and we comment on this in Sec. 4.8.

Further developing the formalism proposed in this section is left to future work.

4.5. Dyson-Schwinger Equations from the Integrated Flow

Dyson-Schwinger equations (DSEs), also referred to as gap equations, are integral equations for the correlation functions. For an introduction, see e.g. [123, 124]. Like the flow equations, DSEs also form an infinite coupled hierarchy of functional equations. What enters in the DSEs are the classical (initial) vertices as well as the fully dressed propagator and the fully dressed n -point functions. In general, all of the above depend on the field ϕ . We represent them diagrammatically as in Fig. 4.1. To have a concise discussion, we consider $\Gamma_{t_0}^{(n)} = S^{(n)}$ in this section. The results of this section are trivially extended to general initial states by replacing $S^{(n)} \rightarrow \Gamma_{t_0}^{(n)}$ in the end.

In the FRG context, the DSEs can be viewed as integrated flow equations [106]. It is thus natural to expect that they can be recovered from the integrated flow. We observed this already for the ϕ^3 -theory in Sec. 4.2 and Sec. 4.3. For the ϕ^3 -theory, this was an

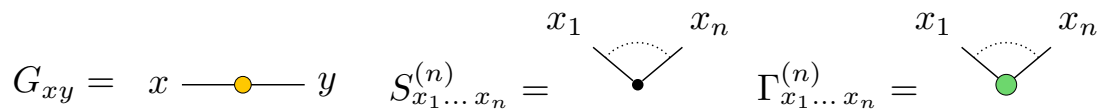


Figure 4.1.: Symbols used for the diagrammatic representation of Dyson-Schwinger equations. The black line with the orange circle represents the fully dressed propagator $G_{xy}[\phi] = i[\Gamma^{(2)}[\phi]]_{xy}^{-1}$. The small black circle with n lines attached to it denotes the classical n -point vertex $S_{x_1\dots x_n}^{(n)}[\phi]$. The green circle with n lines attached to it denotes the fully dressed n -point vertex $\Gamma_{x_1\dots x_n}^{(n)}[\phi]$.

immediate result of the analytic integration of the temporal flow since its DSEs are one-loop exact. In general theories this is not the case. In the present section, we derive the DSEs for a scalar field theory in the presence of three- and four-point interactions. In particular, this derivation applies to the ϕ^4 -theory in the symmetric and in the broken phase. Note that in the broken phase, $S^{(3)} = S^{(4)} \cdot \phi$. If both microscopic three- and four-point interactions are present then replace $S^{(3)} \rightarrow S^{(3)} + S^{(4)} \cdot \phi$.

A diagrammatic representation of the respective DSE for the two-point function can be found in Fig. 4.2. Comparing this to the integrated flow (4.22), we observe that it already contains the first two diagrams of the DSE, i.e. the one-loop contributions. The local vertex corrections in the integrated flow generate the two-loop diagrams in the DSE. These are the sunset diagram (third diagram in Fig. 4.2) and the squint diagram (last diagram in Fig. 4.2). To obtain these diagrams from the causal flow, we analyse the flow equations of the three- and of the four-point function, cf. B.2 and B.3 and determine the relevant vertex corrections: $\Delta\Gamma_{\text{local}\tau}^{(3)}$ and $\Delta\Gamma_{\text{local}\tau}^{(4)}$. Two-loop contributions to the two-point function are generated by one-loop contributions in $\Gamma^{(3)}$ and $\Gamma^{(4)}$. These are given by the total derivative terms in the respective flow equations. Reproducing the correct prefactors of the two-loop diagrams in the DSE is a highly non-trivial consistency check of our method. In this regard, we will observe that the causal constraints of the tFRG framework prevent an overcounting of perturbative contributions.

We remark that this section constitutes a substantial extension of the analysis performed in [1]. In the discussion of the DSEs there, all vertices have been identified with the classical ones. On the contrary here, we derive the *full* DSEs involving the fully dressed vertices.

In Sec. 4.5.1 and Sec. 4.5.2, we derive the DSE of the two-point function from the integrated flow. In Sec. 4.5.3, we derive the DSE of the one-point function and observe that we did in fact recover the entire hierarchy of DSEs for all n -point functions from the temporal flow. Let us emphasise that the result of this section constitutes, to the

$$\Gamma_{xy}^{(2)} = S_{xy}^{(2)} + \frac{1}{2} \text{tadpole} + \frac{i}{2} x \text{fish} + \frac{i}{6} x \text{sunset} - \frac{1}{2} x \text{squint} y$$

Figure 4.2.: Dyson-Schwinger equation for $\Gamma^{(2)}$ using the symbols explained in Fig. 4.1. The first diagram is referred to as the tadpole, the third one as the sunset and the last one as the squint.

best of our knowledge, the first derivation of the DSEs solely in terms of the FRG [118]. This derivation is facilitated using the inherent locality and causality of the tFRG approach. For the following discussion, we will assume that the theory has already been renormalised. In particular, products of propagators do not give rise to additional local contributions, cf. Sec. 4.1.2.

4.5.1. The Sunset Diagram

The sunset diagram is obtained from the fish diagrams in the flow of the four-point function. The fish diagrams can be found in the second line in Fig. B.3. The fish diagram is the only topology that can generate the sunset diagram. As before, the symmetry of the diagrams with respect to the regulator insertion allows us to group together some terms. The group of two diagrams displayed in Fig. B.3 will contribute one total derivative. Apart from the explicitly displayed fish diagrams, there are two more groups of two diagrams with permuted external arguments such that the whole sum is completely symmetric in the external arguments.

Replacing the line with the cutoff insertion $G_\tau \partial_\tau R_\tau G_\tau$ by $-i \partial_\tau G_\tau$ in $\partial_\tau \Gamma_\tau^{(4)}$, we obtain

$$\begin{aligned} & \frac{i}{2} \left[\partial_\tau \left(\Gamma_{\tau,xa12}^{(4)} G_{\tau,13} G_{\tau,24} \Gamma_{\tau,yb34}^{(4)} \right) - \partial_\tau \Gamma_{\tau,xa12}^{(4)} * G_{\tau,13} G_{\tau,24} \Gamma_{\tau,yb34}^{(4)} \right. \\ & \left. - \Gamma_{\tau,xa12}^{(4)} G_{\tau,13} G_{\tau,24} * \partial_\tau \Gamma_{\tau,yb34}^{(4)} + (a \leftrightarrow b) + (a \leftrightarrow y) \right]. \end{aligned} \quad (4.27)$$

CTP integrations over the internal arguments, i.e. repeating indices, are implied and we use a shorthand notation replacing $z_1 \rightarrow 1$ and so on. Note that the notation $(a \leftrightarrow b)$ refers to all explicitly displayed previous terms. Since we are dealing with a vertex correction that contributes to the two-point function, we consider w.l.o.g. $x^0 > y^0$. This allows us to drop all terms that do not lead to $\delta_{\tau x}$ due to the causal constraint of $\partial_\tau \Gamma_\tau^{(2)}$ (cf. Eq. (4.14)), e.g. the first term in the second line of Eq. (4.27). To determine the

vertex correction $\Delta\Gamma_{\text{local}\tau}^{(4)\text{fish}}$, we integrate (4.27) from t_0 to τ' and relabel $\tau' \rightarrow \tau$, to wit

$$\begin{aligned} & \frac{i}{2} \left[\Gamma_{t_0,xa12}^{(4)} G_{\tau,13} G_{\tau,24} \Gamma_{\tau,yb34}^{(4)} + \left(\Delta\Gamma_{\text{local}\tau,xa12}^{(4)} - \Delta\Gamma_{\text{local}\tau,xa12}^{(4)*} \right) G_{\tau,13} G_{\tau,24} \Gamma_{\tau,yb34}^{(4)} \right. \\ & \left. + (a \leftrightarrow b) + (a \leftrightarrow y) \right]. \end{aligned}$$

Here, we already used that the non-local vertex corrections cancel, cf. Sec. 4.2. The relevant one-loop contribution is given by the terms containing the initial vertex. Here, $\Gamma_{t_0,xa12}^{(4)} = -\lambda_4 \delta_{\mathcal{C},xa} \delta_{\mathcal{C},a1} \delta_{\mathcal{C},12}$, and we identify

$$\Delta\Gamma_{\text{local}\tau,xyab}^{(4)\text{fish}} = -\lambda_4 \frac{i}{2} \left[\delta_{\mathcal{C},xa} G_{\tau,a3} G_{\tau,a4} \Gamma_{\tau,yb34}^{(4)} + (a \leftrightarrow b) + (a \leftrightarrow y) \right]. \quad (4.28)$$

In the next step, we insert the vertex correction (4.28) into the tadpole in the integrated flow of the two-point function (4.22). To evaluate $(\Delta\Gamma_{\text{local}}^{(4)\text{fish}} - \Delta\Gamma_{\text{local}}^{(4)\text{fish}*}) G$, recall that

$$\Delta\Gamma_{\text{local}}^{(4)*} G = \lim_{\xi \rightarrow 0^+} \int_{t_0}^{x^0 + \xi} d\tau \partial_\tau \Delta\Gamma_{\text{local}\tau}^{(4)} * G_\tau.$$

Due to the causal constraint, only terms that generate $\delta_{\tau x}$ have to be considered. This is not the case when the τ -derivative hits $\Gamma_\tau^{(4)}$ in (4.28), but only when it hits one of the propagators. Recall that their τ -dependence is given by $G_{\tau,ab} = G_{ab} \theta_{\tau a} \theta_{\tau b}$, cf. Eq. (3.28). Thus, we are left with

$$\begin{aligned} \partial_\tau \Delta\Gamma_{\text{local}\tau,xyab}^{(4)\text{fish}} * G_{\tau,ab} &= -\lambda_4 \frac{i}{2} \left[2 \lim_{\varepsilon \rightarrow 0} \partial_\tau (\theta_{\varepsilon,\tau x}^2) \theta_{\varepsilon,\tau x} G_{x3} G_{x4} \Gamma_{\tau,yb34}^{(4)} G_{xb} \theta_{\varepsilon,\tau 3} \theta_{\varepsilon,\tau 4} \theta_{\varepsilon,\tau b} \right. \\ & \left. + \lim_{\varepsilon \rightarrow 0} \partial_\tau (\theta_{\varepsilon,\tau x}^2) \delta_{\mathcal{C},xy} G_{x3} G_{x4} \Gamma_{\tau,ab34}^{(4)} G_{ab} \theta_{\varepsilon,\tau 3} \theta_{\varepsilon,\tau 4} \theta_{\varepsilon,\tau a} \theta_{\varepsilon,\tau b} \right]. \quad (4.29) \end{aligned}$$

Here, the regularisation of the distributions with ε is made explicit. Recall that it is implied by the $*$ -product, cf. the discussion below Eq. (4.1).

Let us explain Eq. (4.29). To that end, consider the first term inside the bracket. The factor of two appears since the second term in (4.28) gives the same contribution as the first one. Observe that right next to the τ -derivative, there is an ‘additional’ factor of $\theta_{\varepsilon,\tau x}$ which is generated by the interplay of the local vertex correction with the propagator that is already present in the tadpole, $\delta_{\mathcal{C},xa} G_{\tau,ab} = G_{\tau,xb}$. To compute the product $\delta_{\varepsilon,\tau x} \theta_{\varepsilon,\tau x}^2$, we use the results of Sec. 4.1.1. In particular, the identity (4.8)

allows us to determine the proper limit

$$\lim_{\varepsilon \rightarrow 0} \partial_\tau (\theta_{\varepsilon, \tau x}^2) \theta_{\varepsilon, \tau x} = \lim_{\varepsilon \rightarrow 0} 2 \delta_{\varepsilon, \tau x} \theta_{\varepsilon, \tau x}^2 = \frac{2}{3} \delta_{\tau x}. \quad (4.30)$$

The second line in (4.29) comes from the third term in (4.28). Its structure is different compared to the first term in (4.29). In fact, it gives no contribution to the sunset at all. Importantly, no additional factor $\theta_{\varepsilon, \tau x}$ is produced. Thus, we have $\lim_{\varepsilon \rightarrow 0} 2 \delta_{\varepsilon, \tau x} \theta_{\varepsilon, \tau x} = \delta_{\tau x}$ and this term cancels in $(\Delta\Gamma_{\text{local}}^{(4)\text{fish}} - \Delta\Gamma_{\text{local}}^{(4)\text{fish}} *) G$. We remark that this does not imply the absence of diagrams of such topologies in the integrated flow general. Indeed, considering perturbation theory, this term potentially contributes to the ‘double tadpole’, schematically given by $\delta_{\mathcal{C}, xy} G_{\text{cl}, xa}^2 G_{\text{cl}, aa}$. Here, G_{cl} is the classical propagator. In our approach however this contribution is contained completely in the first term in Eq. (4.22), the tadpole with the fully dressed propagator. This is easily seen by expanding the fully dressed tadpole perturbatively. It also follows directly from topological considerations of the diagrams in the DSE, cf. Fig. 4.2: Diagrams other than the tadpole do not generate the ‘double tadpole’ topology. We emphasise that expanding the fully dressed tadpole already correctly reproduces the *complete* perturbative tadpole contribution. Therefore, it is imperative for the consistency of the tFRG formalism that no additional contributions to this perturbative diagram arise. In this sense, the second line of the vertex correction (4.29) is a very dangerous term. The fact that it drops out due to the causal and local nature of the temporal flow is a demonstration of the consistency of the tFRG approach.

Performing the τ -integration, we arrive at

$$\begin{aligned} & \frac{1}{2} \left(\Delta\Gamma_{\text{local}, xyab}^{(4)\text{fish}} - \Delta\Gamma_{\text{local}, xyab}^{(4)\text{fish}} * \right) G_{ab} \\ &= \frac{1}{2} \left((-\lambda_4) \frac{i}{2} \left[2 \left(1 - \frac{2}{3} \right) \right] G_{x3} G_{x4} \Gamma_{yb34}^{(4)} \right) G_{xb} \\ &= \frac{i}{6} S_{xa12}^{(4)} G_{ab} G_{13} G_{24} \Gamma_{yb34}^{(4)}. \end{aligned}$$

This is the *full* sunset diagram as in the DSE in Fig. 4.2. Notably, the prefactor is correct. To derive this result, we made heavy use of the causal constraints. Identifying the relevant vertex corrections was achieved through partial integration. An interesting take-away of this derivation is that not all terms that pass the causal constraints end up contributing. Technically speaking, a non-trivial $*$ -product is not enough to survive the integration of the flow. Additional θ -functions coming from a different part of the

diagram are necessary. This fact is crucial for the consistency of the tFRG formalism as it implies the absence of overcounting of perturbative diagrams. Note that this type of structure appears even more clearly if we perform no partial integration in $\partial_\tau \Gamma_\tau^{(2)}$. Then, the internal propagator $\partial_\tau G_{\tau,ab}$ of the tadpole carries the δ -functions involving τ . To obtain a non-vanishing contribution to the flow, the vertex must connect these internal to the external times. A term containing only $\delta_{\mathcal{C},xy}$ can not achieve this.

4.5.2. The Squint Diagram

The squint diagram is the last missing part of the DSE of $\Gamma^{(2)}$, cf. Fig. 4.2. It is the most complicated diagram to derive, since it contains three- and four-point functions. To obtain it from the flow, we have to collect the relevant contributions from the respective flow equations.

The Three-Point Function Consider the flow of the three-point function. The relevant diagrams are displayed in the first line of Fig. B.2. There are in total three groups of two diagrams leading to three total derivatives. Proceeding in parallel to the derivation for the sunset, we identify the vertex corrections

$$\Delta\Gamma_{\text{local},\tau,xab}^{(3)\text{ squint}} = -\lambda_4 \frac{i}{2} \left[\delta_{\mathcal{C},xa} G_{\tau,a3} G_{\tau,a4} \Gamma_{\tau,b34}^{(3)} + (a \leftrightarrow b) + (b \leftrightarrow x) \right]. \quad (4.31)$$

Similarly to before, the third term cancels in the integrated flow and the other two give the same contribution. Furthermore, the relevant τ -dependence of this contribution is the same as the one for the sunset. Thus, evaluating the $*$ -product leads to a factor $2/3$ as in (4.30). Overall, we get the following contribution to the integrated flow

$$\begin{aligned} & \frac{i}{2} \left(\Delta\Gamma_{\text{local},xab}^{(3)\text{ squint}} - \Delta\Gamma_{\text{local},xab}^{(3)\text{ squint}} * \right) G_{ac} G_{bd} \Gamma_{ycd}^{(3)} \\ &= \frac{i}{2} \left((-\lambda_4) \frac{i}{2} \left[2 \left(1 - \frac{2}{3} \right) \right] G_{x3} G_{x4} \Gamma_{b34}^{(3)} \right) G_{xc} G_{bd} \Gamma_{ycd}^{(3)} \\ &= -\frac{1}{6} S_{xa12}^{(4)} G_{13} G_{24} \Gamma_{b34}^{(3)} G_{ac} G_{bd} \Gamma_{ycd}^{(3)}. \end{aligned} \quad (4.32)$$

This is the contribution to the squint diagram from the vertex correction of the three-point function. Note that we still need to collect the squint-contribution from $\partial_\tau \Gamma_\tau^{(4)}$.

Let us remark that the third contribution of Eq. (4.31) that drops out in the integrated flow for the squint diagram and does not generate the squint topology. Instead, again expanding perturbatively, it produces a double bubble: $G_{\text{cl},xa}^2 G_{\text{cl},ay}^2$. However, the

complete perturbative double bubble contribution is already generated by the relevant one-loop diagram which is the second diagram in Fig. 4.2. To see this, replace $\Gamma^{(3)}$ in the one-loop diagram with the perturbative swordfish diagram (cf. the first line in Fig. B.2) and expand the propagator perturbatively. The swordfish diagram is the first vertex correction to the three-point function involving the four-point function. The fact that the respective term in Eq. (4.31) does not contribute therefore again demonstrates the consistency of the tFRG approach.

The Four-Point Function To collect the so far missing contribution to the squint diagram, we consider the flow of the four-point function. The relevant diagrams are displayed in the first line of Fig. B.3. The computation is still straightforward. However now, there are a lot more contributions than before. The reason being that the relevant topology on the one hand is generated when the field-derivative hits a propagator in the first line of $\partial_\tau \Gamma_\tau^{(3)}$, cf. Fig. B.2. Additionally, it is generated when the derivative hits a three-point vertex of the triangle diagrams in the second line of Fig. B.2. In total, there are twelve groups of three diagrams leading to twelve total derivatives. Not all of them contribute to the squint.

There are two groups of three diagrams where both external arguments, x and y , are located at the four-point function and there is the same number of diagrams where they are located at the two three-point functions. These do not give rise to the squint topology. In fact, similarly to the case of the ‘double tadpole’, these topologies do not contribute to the integrated flow through the vertex corrections we are discussing. By a perturbative expansion of the propagator, we observe that the complete perturbative contributions of these topologies arise from corrections to the propagator in the one-loop diagrams of the DSE, cf. Fig. 4.2.

Furthermore, there are four groups of three diagrams where y is located at the four-point function but these do not contribute for $x^0 > y^0$. Thus, we are left with four groups of three diagrams leading to four total derivatives. Continuing analogously to before, these give rise to the relevant vertex correction

$$\begin{aligned} \Delta \Gamma_{\text{local } \tau, xyab}^{(4) \text{ squint}} = \lambda_4 \frac{1}{2} & \left[\delta_{\mathcal{C}, xa} G_{\tau, a1} G_{\tau, a2} \Gamma_{\tau, y13}^{(3)} G_{\tau, 34} \Gamma_{\tau, b24}^{(3)} + (a \leftrightarrow b) \right. \\ & \left. + (b \leftrightarrow y) + (a \leftrightarrow b \text{ then } a \leftrightarrow y) \right]. \end{aligned}$$

With regard to the $*$ -product, the structure is the same as before and we get a factor of $2/3$ as in (4.30). Here, all terms of the vertex correction (4.33) survive. Due to the symmetry of the propagators and vertices, they all give the same contribution after

contracting with $G_{\tau,ab}$ in the tadpole. Hence, we arrive at

$$\begin{aligned}
 & \frac{1}{2} \left(\Delta \Gamma_{\text{local},xyab}^{(4)\text{squint}} - \Delta \Gamma_{\text{local},xyab}^{(4)\text{squint}*} \right) G_{ab} \\
 &= \frac{1}{2} \left(\lambda_4 \frac{1}{2} \left[4 \left(1 - \frac{2}{3} \right) \right] G_{x1} G_{x2} \Gamma_{y13}^{(3)} G_{34} \Gamma_{b24}^{(3)} \right) G_{xb} \\
 &= -\frac{1}{3} S_{xa56}^{(4)} G_{51} G_{62} \Gamma_{y13}^{(3)} G_{34} \Gamma_{b24}^{(3)} G_{ab}. \tag{4.33}
 \end{aligned}$$

After a suitable relabelling of internal arguments, we add the two contributions (4.32) and (4.33) to get the *full* squint diagram with the correct prefactor of $-\frac{1}{6} - \frac{1}{3} = -\frac{1}{2}$, cf. Fig. 4.2.

Thus, we derived all diagrams of the DSE of the two-point function as displayed in Fig. 4.2 from the causal temporal flow.

4.5.3. Dyson-Schwinger Equation for the One-Point Function

To obtain the DSE for the one-point function, we consider its integrated flow (4.23). As before, the one-loop contribution is already present in the integrated flow. Furthermore, we already identified the relevant vertex correction, namely the vertex correction from the three-point function contributing to the squint, Eq. (4.31). In the flow of the one-point function, it is just closed with G_{ab} , to wit

$$\begin{aligned}
 & \frac{1}{2} \left(\Delta \Gamma_{\text{local},xab}^{(3)\text{squint}} - \Delta \Gamma_{\text{local},xab}^{(3)\text{squint}*} \right) G_{ab} \\
 &= \frac{1}{2} \left((-\lambda_4) \frac{i}{2} \left[2 \left(1 - \frac{2}{3} \right) \right] G_{x3} G_{x4} \Gamma_{b34}^{(3)} \right) G_{xb} \\
 &= \frac{i}{6} S_{xa12}^{(4)} G_{13} G_{24} G_{ab} \Gamma_{b34}^{(3)}.
 \end{aligned}$$

Indeed, this is the *full* two-loop contribution to the DSE of the one-point function, cf. [124]. All other terms are already present in the integrated flow (4.23).

Let us recall that the flow has to be evaluated on $\phi^+ = \bar{\phi} = \phi^-$ for the causal constraints to apply, cf. Sec. 3.2.4. In particular this implies that we can in general not take variations $\delta/\delta\phi^\pm$ of the integrated flow of $\Gamma^{(n)}[\bar{\phi}]$ to derive the integrated flow of $\Gamma^{(n+1)}[\bar{\phi}]$. For the case of the DSEs however, this is possible. Since the DSE for the one-point function is the master DSE from which all other DSEs can be derived, we therefore obtained the entire hierarchy of DSEs from the integrated flow.

The reason that having access to the variations $\delta/\delta\bar{\phi}$ suffices to derive the DSEs from the master DSE on $\bar{\phi}$ is related to the origin of the DSEs. The DSEs are symmetry identities encoding the fact that we are free to reparametrise the fields with which we choose to describe our system. In the quantum theory, this is encoded in the field reparametrisation invariance of the path integral measure [123]. Whether we refer to the CTP measure, a real-time measure or to a regulated measure does not influence the topologies of diagrams that enter in the DSEs.

4.6. s-Channel Effective Vertex from the Integrated Flow

In this section, we discuss a non-perturbative truncation of the temporal flow that includes vertex dynamics of the four-point function in the form of an effective vertex Γ^s . For the propagator, this truncation corresponds to a resummation of propagator-bubbles, $i/2\lambda_4 G^2$, in the s-channel. Schematically, $i/2\lambda_4 G^2 \cdot i/2\lambda_4 G^2 \cdots i/2\lambda_4 G^2$. This type of resummation is used extensively in the literature, in particular in the 2PI approach to quantum dynamics [125–130]. There, this type of resummation is obtained at next-to-leading (NLO) order in the $1/N$ expansion where N is the number of field components. It is known that this resummation can be recovered from the FRG by considering the flow of the Bethe-Salpeter equation for the effective vertex [108, 110, 131]. This has also been demonstrated for the tFRG [6, 7]. Here, we present a different derivation, focusing on the causal constraints that were introduced by us in [1], cf. also Sec. 3.2.4 and 4.1.

First, we integrate the flow of the four-point function. A graphical representation of $\partial_\tau \Gamma_\tau^{(4)}$ can be found in Fig. B.3. We obtain

$$\Gamma^{(4)} = \Gamma_{t_0}^{(4)} + \frac{i}{2} \Gamma_{t_0}^{(4)} \cdot G^2 \cdot \Gamma^{(4)} + \frac{i}{2} \left(\Delta\Gamma_{\text{local}}^{(4)} \cdot - \Delta\Gamma_{\text{local}}^{(4)} * \right) G^2 \cdot \Gamma^{(4)} + P + \text{rest} . \quad (4.34)$$

For a concise representation, we suppressed all space-time dependencies. The first term on the right-hand side is the classical (initial) vertex. The second term is the fish diagram with one classical (initial) and one full vertex. The bubble resummation we want to derive is contained in this diagram. The third term is the fish diagram with vertex corrections $\Delta\Gamma_{\text{local}}^{(4)}$. These lead to more general types of resummations, which we do not consider here. The P represents a sum over the the remaining contributions with permuted arguments and “rest” refers to contributions involving $\Gamma^{(3)}$ and $\Gamma^{(n>4)}$, cf. Fig. B.3.

To derive the bubble resummation, we make the following ansatz for the four-point

function

$$\Gamma_{xyab}^{(4)} \Big|_{\text{bubble}} = \Gamma_{t_0,xyab}^{(4)} + \left[\Gamma_{xy}^s \delta_{\mathcal{C},xa} \delta_{\mathcal{C},yb} + (a \leftrightarrow b) + (a \leftrightarrow y) \right]. \quad (4.35)$$

It proves useful to included all three channels in the ansatz of the vertex. The first term in the bracket is the s-channel, the second one is the u-channel and the last one is the t-channel. Thus, Eq. (4.35) has the full bose-symmetry of the four-point function under permutation of its arguments. Inserting Eq. (4.35) into Eq. (4.34) and neglecting the vertex corrections $\Delta\Gamma_{\text{local}}^{(4)}$, we find

$$\begin{aligned} & \Gamma_{xy}^s \delta_{\mathcal{C},xa} \delta_{\mathcal{C},yb} + (a \leftrightarrow b) + (a \leftrightarrow y) \\ = & \left[\frac{i}{2} (-\lambda_4)^2 G_{xy}^2 - \frac{i}{2} \lambda_4 G_{x1}^2 \Gamma_{1y}^s \right] \delta_{\mathcal{C},xa} \delta_{\mathcal{C},yb} - i\lambda_4 G_{xy} G_{xb} \Gamma_{yb}^s \delta_{\mathcal{C},xa} \\ & + (a \leftrightarrow b) + (a \leftrightarrow y). \end{aligned} \quad (4.36)$$

Observe that the last term in the second line has a different topology than the previous terms. It is local only with respect to x and a and non-local concerning y and b where the bubble resummation is inserted. While such a term gives non-vanishing contributions to the integrated flow, these contributions do not contribute to Γ^s itself. They can be included in an extended truncation of the form

$$\Gamma_{xyab}^{(4)} \Big|_{\text{ext}} = \Gamma_{t_0,xyab}^{(4)} + \Gamma_{xyab}^{(4)} \Big|_{\text{bubble}} + \left[\Gamma_{xyb}^{(4)} \delta_{\mathcal{C},xa} + (a \leftrightarrow b) + (a \leftrightarrow y) + (a \leftrightarrow x) \right].$$

Exploring such extended truncations is left to future work.

We determine Γ_{xy}^s by comparing the left- and right-hand side in Eq. (4.36)

$$\Gamma_{xy}^s = \frac{i}{2} \lambda_4^2 G_{xy}^2 - \frac{i}{2} \lambda_4 G_{x1}^2 \Gamma_{1y}^s. \quad (4.37)$$

Iterating this equation, we observe that it is a formal geometric series, and we define the effective coupling,

$$\lambda_{\text{eff},xy} := \frac{\lambda_4}{1 + i\lambda_4/2 G_{xy}^2},$$

as a shorthand for this series.

Next, we determine the correct prefactor when Eq. (4.37) is inserted into the flow of

the two-point function. Here, instead of using the result of Sec. 4.2, we prefer not to perform the partial integration. Instead, our starting point is the flow of the two-point function as given in Eq. (4.1). The relevant part for the present discussion is

$$\partial_\tau \Gamma_{\tau,xy}^{(2)} = \frac{1}{2} G_{ab} \Gamma_{\tau,xyab}^{(4)} * \partial_\tau (\theta_{\tau a} \theta_{\tau b}). \quad (4.38)$$

Considering w.l.o.g. $x^0 > y^0$, we use that the causal constraint for the two-point function (cf. Eq. (4.3)) implies $\partial_\tau \Gamma_{\tau,xy}^{(2)} \propto \delta_{\tau x} \theta_{\tau y}$. Inserting the ansatz (4.35) for the four-point function into Eq. (4.38) and using the causal constraint, we observe that the last term of Eq. (4.35) does not contribute to the integrated flow. Indeed, these topologies are already contained entirely in the fully dressed tadpole which originates from the classical (initial) vertex in $\Gamma_\tau^{(4)}$. The other two terms of Eq. (4.35) give the same contribution due to the symmetry of the propagator. The τ -dependence of $\Gamma_{\tau,xy}^s$ can be determined from Eq. (4.37). The square of the regulated propagator contains $\theta_{\varepsilon,\tau x}^2$, and this is the only τ -dependence relevant for the evaluation of the $*$ -product. Recalling Eq. (4.8), we find that this causal structure leads to an overall factor of $1/3$. Thus, we arrive at the following result for the integrated flow of the two-point function with the bubble effective vertex

$$\begin{aligned} \Gamma_{xy}^{(2)} - \Gamma_{t_0}^{(2)} &= -\frac{\lambda_4}{2} \delta_{\mathcal{C},xy} G_{xx} + \frac{i}{6} \lambda_4^2 G_{xy}^3 - \frac{i}{6} \lambda_4 G_{x1}^2 \Gamma_{1y}^s G_{xy} \\ &= -\frac{\lambda_4}{2} \delta_{\mathcal{C},xy} G_{xx} + \frac{i}{6} \lambda_4 \lambda_{\text{eff},xy} G_{xy}^3. \end{aligned} \quad (4.39)$$

The second term in the first line is the sunset diagram with classical vertices, and $i/6$ is the correct prefactor reproducing the whole perturbative contribution. Expanding λ_{eff} generates the resummation of bubbles in the s-channel. Since the prefactor is the correct perturbative prefactor, Eq. (4.39) contains the entire contribution of the s-channel bubbles.

We remark that Eq. (4.39) contains the full tadpole. This is due to the fact that we considered $\Gamma_{t_0,xyab}^{(4)}$ in the ansatz for the vertex. From the perspective of the $1/N$ expansion, the full tadpole contains arbitrary orders in $1/N$. This becomes apparent if we define the rescaled coupling $\lambda_4 =: \bar{\lambda}_4 / \sqrt{3N}$. We remark that the coupling $\bar{\lambda}_4$ is denoted as λ in [14]. Using this rescaling, makes the fact explicit that the contributions to the term containing λ_{eff} match the result of the 2PI $1/N$ -expansion at NLO [14]. The prefactor of the tadpole at NLO order is given by $(N+2)/6N$. Rescaling in Eq. (4.22), we find here $(2\sqrt{3N})^{-1}$ which clearly includes contributions beyond NLO. We can project out the

higher order contributions if need be by modifying Eq. (4.35), replacing $\Gamma_{t_0}^{(4)} \rightarrow \Gamma_{t_0}^{(4)} \Big|_{\text{NLO}}$.

4.7. Renormalisation

We solve the problem of renormalising the general causal temporal flow.

This section is in parts based on [2].

4.7.1. The Role of the Closed Time Path

Regarding the renormalisation of unitary quantum dynamics, it is known that it can be accomplished with the usual vacuum counter terms [132, 133]. In particular, this entails that renormalisation is a time-independent problem which is concerned solely with the initial state. Therefore, we can work in momentum space. For concreteness, we consider a relativistic scalar field theory. The respective propagators are given by

$$\begin{aligned} G_{\text{cl}}^{\pm\pm}(p^0, \mathbf{p}) &= \pm \frac{i}{p^2 - m_0^2 \pm i\epsilon} + 2\pi f_0(|p^0|) \delta(p^2 - m_0^2), \\ G_{\text{cl}}^{\pm\mp}(p^0, \mathbf{p}) &= 2\pi \left[\theta(\mp p^0) + f_0(|p^0|) \right] \delta(p^2 - m_0^2). \end{aligned} \quad (4.40)$$

In equilibrium f_0 must be thermal. For dynamical applications, this need not be the case. First observe that due to $\delta(p^2 - m_0^2)$, the components $G_{\text{cl}}^{\pm\mp}$ are only non-vanishing on-shell. The same is true for the terms in $G_{\text{cl}}^{\pm\pm}$ involving the distribution f_0 . Notably, the only off-shell contributions arise from the vacuum sector of the theory which features only in $G^{\pm\pm}$. It is a non-trivial consequence of the CTP formalism that this structure is preserved in resummations, cf. e.g. [87, 93]. Accordingly, the fully resummed propagator G and the self-energy $\Sigma := \Gamma^{(2)} - \Gamma_{t_0}^{(2)}$ can be decomposed analogously to Eq. (4.40), to wit

$$G(x, y) = G_{\text{vac}}(x, y) + G_{\text{dyn}}(x, y). \quad (4.41)$$

Note that this is a feature of the CTP and in particular does not depend on the coordinates in which we choose to work. Here, all terms that do not involve f are collected in G_{vac} and all others in G_{dyn} . Importantly, note that the distributions f of any finite energy system are UV finite: $f \xrightarrow{p \rightarrow \infty} 0$. Accordingly, G_{dyn} does not lead to any UV divergencies. The fact that $G_{\text{vac}}^{\pm\mp} \equiv 0$ implies that all UV divergencies of a renormalisable theory can be absorbed into the diagonal parts of the classical kinetic operator on the CTP, $S^{(2)\pm\pm}$ and into the diagonal CTP vertices present in the classical action,

e.g. $S^{(4)\pm\pm\pm\pm}$ in the ϕ^4 -theory.

4.7.2. Renormalising the Causal Temporal Flow

Now we derive the renormalised (integrated) causal temporal flow. To that end, observe the following: Due to the suppression by the regulator, the flow at t_0 is determined in terms of the initial conditions $\Gamma_{t_0}^{(n)}$. Performing one τ -step $\Delta\tau$, the correlators $\Gamma_{t_0+\Delta\tau}^{(n)}$ for times earlier or equal to $t_0 + \Delta\tau$ jump to their final value including all fluctuations. Importantly however,

$$\Gamma_{t_0+\Delta\tau}^{(n)}(x_1, \dots, x_n) \Big|_{x_1^0, \dots, x_n^0 = t_0} = \Gamma_{t_0}^{(n)}(x_1, \dots, x_n),$$

since the flow does not contribute to the initial values of the correlators. The fluctuations which enter in e.g. $\Gamma_{t_0+\Delta\tau}^{(n)}(x_1, \dots, x_n) \Big|_{x_1^0 = t_{max} = t_0 + \Delta\tau}$ are determined by the one-loop diagrams on the right-hand side of the flow equations. Analogously to the self-energy, we define

$$\Sigma^{(n)} := \Gamma^{(n)} - \Gamma_{t_0}^{(n)}.$$

Thus, $\Sigma^{(n)}$ parametrises the diagrams contributing to the (integrated) flow. For concreteness, we now consider the ϕ^4 -theory in the symmetric phase. In $3 + 1$ dimensions, only the two- and the four-point function have to be renormalised. For the two-point function, we have

$$\Gamma^{(2)} - \Gamma_{t_0}^{(2)} =: \Sigma \equiv \Sigma^{(2)} = \frac{1}{2} \Gamma^{(4)} * G + \text{finite}.$$

Here, we use the shorthand notation $\Gamma^{(4)} * G = \lim_{\xi \rightarrow 0^+} \int_{t_0}^{x_0 + \xi} d\tau \Gamma_{\tau}^{(4)} * \partial_{\tau} G_{\tau}$. Finite contributions involving $\Gamma^{(3)}$ are not displayed explicitly. As in the decomposition (4.41) of the propagator, we define

$$\Sigma^{(2)} = \Sigma^{(2)} \Big|_{\text{vac}} + \Sigma^{(2)} \Big|_{\text{dyn}},$$

with

$$\Sigma^{(2)} \Big|_{\text{vac}} = \frac{1}{2} \left(\Gamma^{(4)} * G \right) \Big|_{\text{vac}}, \quad \Sigma^{(2)} \Big|_{\text{dyn}} = \Sigma^{(2)} - \Sigma^{(2)} \Big|_{\text{vac}}.$$

Per definition, the projection of the self-energy onto the vacuum can be absorbed in the parameters of the classical action which is part of the initial conditions. Accordingly,

the renormalised initial conditions are defined as follows:

$$\Gamma_{t_0, \text{ren}}^{(2)} := \left(\Gamma_{t_0}^{(2)} + \Sigma^{(2)} \right) \Big|_{\text{vac}}. \quad (4.42)$$

The renormalised (integrated) flow then reads

$$\Gamma^{(2)} - \Gamma_{t_0, \text{ren}}^{(2)} = \Sigma^{(2)} \Big|_{\text{dyn}}. \quad (4.43)$$

We continue with the renormalisation of the four-point function

$$\Gamma^{(4)} - \Gamma_{t_0}^{(4)} = \frac{i}{2} \Gamma^{(4)} * G^2 * \Gamma^{(4)} + \text{finite}.$$

Finite contributions to the (integrated) flow are not displayed explicitly, cf. Fig. B.3. Here, we use the shorthand notation

$$\Gamma^{(4)} * G^2 * \Gamma^{(4)} = \lim_{\xi \rightarrow 0^+} \int_{t_0}^{x^0 + \xi} d\tau \Gamma_{\tau}^{(4)} * (\partial_{\tau} G_{\tau} G_{\tau} + G_{\tau} \partial_{\tau} G_{\tau}) * \Gamma_{\tau}^{(4)}.$$

The renormalised (integrated) flow is then given by

$$\Gamma^{(4)} - \Gamma_{t_0, \text{ren}}^{(4)} = \Sigma^{(4)} \Big|_{\text{dyn}}, \quad (4.44)$$

with the renormalised initial condition for the four-point function,

$$\Gamma_{t_0, \text{ren}}^{(4)} := \left(\Gamma_{t_0}^{(4)} + \Sigma^{(4)} \right) \Big|_{\text{vac}}. \quad (4.45)$$

The projections of the four-point self-energy are given by

$$\Sigma^{(4)} \Big|_{\text{vac}} = \frac{i}{2} \left(\Gamma^{(4)} * G^2 * \Gamma^{(4)} \right) \Big|_{\text{vac}}, \quad \Sigma^{(4)} \Big|_{\text{dyn}} = \Sigma^{(4)} - \Sigma^{(4)} \Big|_{\text{vac}}.$$

The important result of this procedure is the following: Since only fluctuations in terms of $(\dots) \Big|_{\text{dyn}}$ contribute to the (integrated) flows (4.43) and (4.44), these are manifestly UV finite.

Let us discuss the renormalised initial conditions (cf. Eq. (4.42) and (4.45)) in more

detail. Evaluating the projections onto the vacuum, we obtain

$$\begin{aligned}\Gamma_{t_0,\text{ren}}^{(2)} &= \left(\Gamma_{t_0}^{(2)} + \Sigma^{(2)}\right)\Big|_{\text{vac}} = S^{(2)} + \frac{1}{2}\Gamma_{t_0,\text{ren}}^{(4)} \cdot G_{\text{ren}} \quad \Rightarrow \quad G_{\text{ren}} = \text{i}\left(\Gamma_{t_0,\text{ren}}^{(2)}\right)^{-1}, \\ \Gamma_{t_0,\text{ren}}^{(4)} &= \left(\Gamma_{t_0}^{(4)} + \Sigma^{(4)}\right)\Big|_{\text{vac}} = S^{(4)} + \frac{\text{i}}{2}\Gamma_{t_0,\text{ren}}^{(4)} \cdot G_{\text{ren}}^2 \cdot \Gamma_{t_0,\text{ren}}^{(4)}.\end{aligned}\quad (4.46)$$

Here, we used the fact that the projection on the vacuum removes all dynamical contributions and that all UV divergences are absorbed in the parameters of $S^{(2)}$ and $S^{(4)}$. What is left over are per definition renormalised quantities. Notably, the renormalised correlators appear fully dressed in Eq. (4.46). Thus, there are no subdivergencies that need to be accounted for. We remark that this remarkable result relies on the one-loop exact nature of the flow. We emphasise that in Eq. (4.46), we already evaluated the $*$ -product: The projection on the vacuum implies that only the initial, maximally local part of the correlators contributes. Collecting all contributions from $\partial_\tau G_{\tau,\text{vac}}$ that get generated by the maximally local vertices leads to terms of the form $2\delta_{\tau x} * \theta_{\tau x} = \delta_{\tau x}$. Note that there are CTP integrals present in Eq. (4.46) implied by the dots.

Let us consider Eq. (4.46) in a concrete example. We remark that Eq. (4.46) does not rely on the availability of a Fourier representation. However, renormalisation is most intuitively discussed in momentum space. There, we have access to the following parametrisation

$$\begin{aligned}\Gamma_{t_0,\text{ren}}^{\pm\pm} &=: Z_R(p^2)p^2 - m_R^2 \pm \text{i}\epsilon \quad \Rightarrow \quad G^{\pm\pm} = \pm \frac{\text{i}}{Z_R(p^2)p^2 - m_R^2 \pm \text{i}\epsilon}, \\ \Gamma_{t_0,\text{ren}}^{\pm\pm\pm\pm} &=: \mp(\lambda_R + \Gamma_R^{(4)}).\end{aligned}\quad (4.47)$$

We parametrise the vertex such that there is a momentum-independent piece λ_R and a rest. We emphasise that Eq. (4.47) takes into account all relevant CTP components. To that end, recall that the fully dressed propagator fulfils the constraint

$$\sum_{\substack{\alpha=\pm \\ \beta=\pm}} G_{\alpha\beta} = 0,$$

which features all of its components (cf. Eq. (2.14)). Accordingly, the dressings $Z^{\alpha\beta}$ for G^{++} and G^{--} must agree. Moreover, we know that $G^{\pm\mp}$ do not get renormalised at all, cf. Eq. (4.40), and their dressings therefore vanish. By the same argument, we arrive at the same conclusion for the vertices: Only the classically present CTP-diagonal

components get dressed. Note that from the perspective of the FRG, this is highly non-trivial. Indeed, the flow of non-classical tensor structures is non-vanishing in general [33]. The CTP correlators however are highly constrained by causality and unitarity. In this sense, these constraints give rise to non-renormalisation theorems, cf. e.g. [90]. Using the parametrisation Eq. (4.47), Eqs. (4.46) become

$$\begin{aligned}
 m_R^2 - m_0^2 &= p^2(Z_R - 1) \mp \frac{1}{2} \left(\lambda_R + \Gamma_R^{(4)} \right) \cdot G_{\text{vac}}^{\pm\pm} , \\
 \frac{1}{p^2}(Z_R - 1) + \frac{dZ_R}{dp^2} &= \mp \frac{1}{2p^2} \frac{d}{dp^2} \left[\left(\lambda_R + \Gamma_R^{(4)} \right) \cdot G_{\text{vac}}^{\pm\pm} \right] , \\
 \mp \left(\lambda_R - \lambda_0 + \Gamma_R^{(4)} \right) &= \frac{i}{2} \left[\lambda_R + \Gamma_R^{(4)} \right] \cdot \left(G_{\text{vac}}^{\pm\pm} \right)^2 \cdot \left[\lambda_R + \Gamma_R^{(4)} \right] .
 \end{aligned} \tag{4.48}$$

Providing the initial conditions for Eq. (4.46) or Eq. (4.48) at some scale μ^2 respectively corresponds to a choice of renormalisation scheme. For instance, consider the following on-shell like renormalisation scheme

$$\begin{aligned}
 \Gamma_{t_0, \text{ren}}^{\pm\pm} \Big|_{p^2=m_R^2} \stackrel{!}{=} 0 &\Rightarrow Z_R \Big|_{p^2=m_R^2} = 1 , \quad m_R^2 - m_0^2 = \frac{1}{2} \left[\Gamma_{t_0, \text{ren}}^{\pm\pm\pm\pm} \cdot G_{\text{vac}}^{\pm\pm} \right] \Big|_{p^2=m_R^2} , \\
 \frac{d\Gamma_{t_0, \text{ren}}^{\pm\pm}}{dp^2} \Big|_{p^2=m_R^2} \stackrel{!}{=} 0 &\Rightarrow \frac{dZ_R}{dp^2} \Big|_{p^2=m_R^2} = \mp \frac{1}{2m_R^2} \left[\frac{d\Gamma_R^{(4)}}{dp^2} \cdot G_{\text{vac}}^{\pm\pm} \right] \Big|_{p^2=m_R^2} , \\
 \Gamma_{t_0, \text{ren}}^{\pm\pm\pm\pm} \Big|_{\substack{p_1^2=m_R^2 \\ p_2^2=m_R^2 \\ p_3^2=m_R^2}} \stackrel{!}{=} 0 &\Rightarrow \mp(\lambda_R - \lambda_0) = \left\{ \pm\Gamma_R^{(4)} + \frac{i}{2} \Gamma_{t_0, \text{ren}}^{\pm\pm\pm\pm} \cdot \left(G_{\text{vac}}^{\pm\pm} \right)^2 \cdot \Gamma_{t_0, \text{ren}}^{\pm\pm\pm\pm} \right\} \Big|_{\substack{p_1^2=m_R^2 \\ p_2^2=m_R^2 \\ p_3^2=m_R^2}} .
 \end{aligned}$$

Here, we chose $\mu^2 = m_R^2$.

Note that the present discussion readily extends to general renormalisable theories. The renormalisation of the general causal temporal flow is thus solved. To derive this remarkable result, the one-loop structure of the flow was crucial. Moreover, the fact that the causal temporal flow leaves the initial conditions untouched is important.

4.7.3. Discussion

This result is of great practical relevance. Indeed, the renormalisation of unitary quantum dynamics in practice has been an unresolved problem at large [107, 134, 135]. For instance in the 2PI approach, it is known how to renormalise using subtractions, but this procedure is cumbersome due to “hidden” divergencies [136–138]. These arise since only the macroscopic field and the propagator appear in the formalism. Thus, these are fully dressed but all vertices are left bear. Still, the UV structure of the theory is of course what it is. For instance if the coupling gets renormalised, this has to be accounted for somehow. However, since no independent vertex exists in the 2PI formalism, these divergencies are “hidden” in the resummations of the field and the propagator. Compared to general n PI effective actions, the 2PI effective action has a comparatively simple structure. Hence, it is possible to uncover these “hidden” divergencies and renormalise 2PI approximations by subtractions à la BPHZ. Regarding the renormalisation of the 2PI approach in dynamical in applications in practice, we remark that in some cases only the leading quadratic divergencies are subtracted [125, 126, 139].

We remark that higher n PI effective actions get exceedingly more complicated and it is, to the best of our knowledge, not known how to renormalise them with counter terms à la BPHZ [140]. A renormalisation procedure demonstrated to work for the 4PI effective action in equilibrium uses the FRG in momentum space [140]. For similar results regarding the 2PI formalism, see [100, 110].

We remark that all dynamical effects are included in $(\dots)|_{\text{dyn}}$ by definition. In particular, this includes the possibility of IR divergences. This is an example where an additional momentum regulator can be useful, and the tFRG allows such combined flows in momentum space and time, cf. Sec. 4.4.2.

We remark that effective field theories need not be renormalisable. Then there can be additional divergencies not present in the vacuum [141]. Note that in an effective field theory, already the CTP action in the vacuum in general has non-diagonal CTP vertices. In this sense, effective CTP theories belong into the realm of open systems [90].

Note that in the present case, the structure of the renormalised and the unrenormalised dynamic equations is the same. Typically, this is also observed in the 2PI approach. A notable exception is given by [142]. This can be understood as follows: In [142], the renormalised initial state is prepared by an evolution starting in the free theory at $t = -\infty$. We discuss such preparations of initial states in Sec. 4.9.

4.8. An Explicit Numerical Method for Causal Integral Equations

We use causality to develop an algorithm that allows to solve integral equations like the equation for the effective vertex (4.37) or the dynamic integral equation for the propagator (4.49) in an explicit manner. The latter equation is referred to as the Dyson equation. We remark that the following derivation relies solely on the causality as encoded in the CTP. Therefore, this algorithm can be employed in general dynamical applications independent of the tFRG method. Regarding the Dyson equation, we stated this fact in [1] and provided numerical evidence for our assertion, cf. App. C. The following discussion providing the detailed derivation as well as the discussion regarding the effective vertex are new, so far unpublished result of this work.

4.8.1. The Propagator

In general, we can parametrise the full two-point function in terms of a classical (initial) piece plus corrections: $\Gamma^{(2)} = \Gamma_{t_0}^{(2)} + \Sigma$. Here, we define the self-energy Σ . Thus, we obtain the general Dyson equation

$$G(x, y) = G_{\text{cl}}(x, y) + i \int_{\mathcal{C}, z_1 z_2} G_{\text{cl}}(x, z_1) \Sigma(z_1, z_2) G(z_2, y), \quad (4.49)$$

where we used $G_{\text{cl}} = i(\Gamma_{t_0}^{(2)})^{-1}$ and $G = i(\Gamma^{(2)})^{-1}$. Note that in the tFRG framework, the self-energy is given by the integrated flow. For the following derivation, we use the \pm -basis for the CTP correlators. We introduced this basis in App. A, but we will discuss all of the properties relevant to the present derivation in this section. It is a real-time basis, and the CTP ordering is encoded in terms of two-valued indices $\alpha = \pm$. Accordingly, the real-time propagator G is a 2×2 matrix containing the time-ordered propagator G^{++} , the anti-time-ordered propagator G^{--} and the two Wightman functions G^{+-} and G^{-+} . This matrix structure readily extends to all two-time CTP quantities. In this basis, the contour integrals in Eq. (4.49) become real-time integrals of CTP matrices, to wit

$$(G_{xy})^{\alpha\beta} = (G_{\text{cl},xy})^{\alpha\beta} + i (G_{\text{cl},xz_1})^{\alpha\gamma} (\Sigma_{z_1 z_2})_{\gamma\delta} (G_{z_2 y})^{\delta\beta}. \quad (4.50)$$

CTP indices are raised and lowered using the CTP metric $c_{\alpha\beta} = \text{diag}(1, -1)_{\alpha\beta}$ and sums (integrals) over repeating CTP (space-time) indices are implied. In the \pm -basis,

the causality and unitarity of the time evolution operator are encoded in terms of the high degree of redundancy present in the CTP tensors in combination with appropriate cancellations of terms due to the minus signs of the CTP metric. For instance, the four components of the propagator constitute four complex-valued functions encoding two real-valued functions. Thus, any of the component matrices already contains the full information. The other components are then obtained by symmetry and complex conjugation. Recall that the CTP cancellations imply that no times beyond the latest external time t_{max} contribute to CTP integrals. Since the propagator, the two-point function and the self-energy are symmetric for bosonic fields, we can consider w.l.o.g. $x^0 \geq y^0$. Then the integrals implicit in Eq. (4.50) are non-vanishing only for $z_1, z_2 \leq x^0$.

To proceed, we first collect some useful properties of the CTP propagator: The hermiticity of the Schwinger functional, cf. Sec. 3.1.1, implies for the propagator

$$(G^{\alpha\beta}(x, y))^* = G^{(-1)\cdot\alpha (-1)\cdot\beta}(x, y),$$

where $\alpha, \beta \in \{\pm 1\}$. For example, $(G^{+-}(x, y))^* = G^{-+}(x, y)$. The symmetry of the propagator implies for its components

$$G^{\alpha\beta}(y, x) = G^{\beta\alpha}(x, y).$$

Moreover, we will make use of the LTE property, cf. Eq. (2.12) and the discussion below it: The operator ordering of a CTP n -point functions is independent of the CTP branch on which the operator with the latest time is inserted. This implies

$$G^{+-}(t_x > t_y, t_y) = G^{--}(t_x > t_y, t_y), \quad G^{-+}(t_x > t_y, t_y) = G^{++}(t_x > t_y, t_y), \quad (4.51)$$

where we suppress the dependence on spatial arguments. Furthermore, the LTE property implies that at coincident times, i.e. along their respective diagonals, all components agree. We proceed by discretising time. Then, Eq. (4.50) becomes a matrix equation with respect to time, and Eq. (4.51) can be summarised as follows

$$(G_{i \geq j, j})^{\alpha\beta} = (G_{i \geq j, j})^{(-1)\cdot\alpha\beta}, \quad (4.52)$$

where (i, j) are discrete time indices. It is a non-trivial fact of the CTP formalism that Σ enjoys the same properties [78]. With regard to a more subtle point note that on the diagonal, (4.52) holds for a discretisation of the continuum propagator. Put differently, if we start with the CTP action on a lattice, derive the kinetic operator and invert it, the resulting propagator contains terms violating Eq. (4.51) on the diagonal which vanish in

the continuum limit, cf. [12]. This fact is related to the issues discussed in Sec. 3.3.

We proceed with the most important step of this derivation: We show that the discrete Dyson equation is an explicit equation for the lower triangular part of the discrete propagator. We remark that the conjugate equation containing $G\Sigma G_{\text{cl}}$ is explicit for the upper triangular part. Discretising Eq. (4.50), we obtain

$$(G_{ij})^{\alpha\beta} = (G_{\text{cl},ij})^{\alpha\beta} + iw_a w_b (G_{\text{cl},ia})^{\alpha\gamma} (\Sigma_{ab})_{\gamma\delta} (G_{bj})^{\delta\beta}. \quad (4.53)$$

Here, the weights w arise from the discretisation of the integrals and we do not need to specify them further for the following discussion. Recall that G_{cl} is the solution to the classical equation of motion and is thus known explicitly for all times. Now we show that for $i \geq j$, the entry (i, j) of G on the left-hand side does not involve G_{ij} on the right-hand side. Apart from the explicitly present G , the self-energy also contains the propagator. First, we deal with the G that occurs explicitly. To that end, recall that internal times are restricted to be smaller than or equal to the largest external time due to CTP cancellations, i.e. $a, b \leq i$. With regard to G_{ij} , the only term relevant in the sum over b is $b = i$, to wit

$$[(G_{\text{cl}} \cdot \Sigma)_{ii}]_{\delta}^{\alpha} (G_{i \geq j, j})^{\delta\beta} = [(G_{\text{cl}} \cdot \Sigma)_{ii}]^{\alpha+} \left((G_{i \geq j, j})^{+\beta} - (G_{i \geq j, j})^{-\beta} \right). \quad (4.54)$$

Note that ii refers to the i^{th} diagonal entry of $(G_{\text{cl}} \cdot \Sigma)_{ii}$, i.e. no sum over i is implied here. In Eq. (4.54), we used the LTE property (4.52) for the self-energy in every summand of the sum over a implicit in $(G_{\text{cl}} \cdot \Sigma)_{ii}$. All of these terms are of the form

$$\begin{aligned} (\Sigma_{a, i \geq a})_{\gamma\delta} &= (\Sigma_{a, i \geq a})_{\gamma(-1)\cdot\delta} \\ \Rightarrow [(G_{\text{cl}} \cdot \Sigma)_{ii}]^{\alpha+} &= [(G_{\text{cl}} \cdot \Sigma)_{ii}]^{\alpha-}. \end{aligned}$$

Using the LTE property (4.52) for $G_{i \geq j, j}$ in Eq. (4.54), we find that the two terms in the bracket cancel. Next, we deal with the self-energy. Using the same types of arguments, it follows that the sum over a in $[G_{\text{cl},ia}]_{\gamma}^{\alpha} [(\Sigma \cdot G)_{aj}]^{\gamma\beta}$ only runs up to $a \leq i - 1$. Hence, the entries of the self-energy Σ_{ab} that appear on the right-hand side of Eq. (4.53) are given by $(a \leq i - 1, b \leq i - 1)$. In summary this implies that to compute $G_{i \geq j, j}$ using Eq. (4.53), the latest time index of the propagator that occurs on the right-hand side is $i - 1$. Accordingly, the lower triangular part of G is determined by sums over explicitly known values. Let us remark that the LTE property for n -point functions (cf. Eq. (2.12)) implies that for any discretised CTP integral extending up to the latest external time index i_{max} , this latest point does in fact not contribute. Thus as a consequence of

causality, discrete CTP integrals need not extend beyond $i_{max} - 1$.

Next, we discuss the algorithm that allows us to solve the discrete Dyson equation (4.53) in the form of an explicit numerical method, involving only sums over already known values: We start with the initial conditions $(G_{00})^{\alpha\beta}$ and compute $(\Sigma_{00})^{\alpha\beta}$. Visually, we think about one component $(G_{i \geq j, j})^{\alpha\beta}$ as a square with $G_{00}^{\alpha\beta}$ being the upper left corner, and $i > j$ places us in the lower triangular part. We perform the first time step down to compute $(G_{10})^{\alpha\beta}$. Note that the latest contribution off the diagonal, i.e. $(i_{max}, j \leq i_{max} - 1)$ on the left-hand side of Eq. (4.53) involves $(G_{b \leq i_{max} - 1, j \leq i_{max} - 1})^{\alpha\beta}$ on the right-hand side. We use the symmetry of the propagator to obtain $(G_{01})^{\alpha\beta}$. Then we can take one time step to the right. In the present case, we arrive at the diagonal $(G_{11})^{\alpha\beta}$ whose computation involves entries up to $(G_{b \leq i_{max} - 1, i_{max}})^{\alpha\beta}$. We remark that for terms of the self-energy involving CTP integrals, the latest indices involved on the right-hand side of the Dyson equation can reduce further. Now we have computed the propagator in a square of size $i_{max} \times i_{max}$. This allows to compute the values of the self-energy in this square. Due to causality, the earliest time at which these values of the self-energy are needed to advance the propagator is at $i_{max} + 1$. We can continue the time evolution in this fashion: Compute the next values for the propagator, making one step down and continuing chronologically to the right up until the last entry before the diagonal. Symmetrise the propagator and advance to the diagonal. Use these new propagator values to compute the respective entries of the self-energy and symmetrise. Then, both are determined in an square of size $(i_{max} + 1) \times (i_{max} + 1)$. Note that the discussed procedure can be visualised as walking on the causal structure of the flow implied by the causal constraint as in Fig. 3.3. We remark that the above algorithm for the propagator can be used in generic tFRG truncations.

We emphasise that the above naive implementation in terms of the \pm -basis is not suited for numerical applications as it is prone to be unstable. This is due to the fact that the CTP cancellations that happen for the non-vanishing entries are never numerically exact. Since the exact cancellations are crucial for the overall consistency, their absence for instance causes functions that must be real-valued to become complex and an instability ensues. We observed this explicitly in our numerics. This issue was resolved once we switched to the completely real basis in terms of F and ρ , cf. App. A. This is due to the fact that the completely real basis solves the CTP constraints. Accordingly, the redundancies present in the \pm -basis are removed entirely. Apart from improving the stability, this also greatly reduces the overhead by reducing memory consumption and the number of operations used. Note that the integral equations for F and ρ can of course also be solved explicitly. After all, what we used to derive the explicit time-

stepping algorithm is causality and unitarity.

Note that the described algorithm can be further optimised. For instance, the symmetries of the propagator and the self-energy are ideally exploited on the level of the employed data structure. In particular, memory can be saved if entries that can be inferred by symmetry are not actually stored but are obtained by an appropriate mapping of the respective indices.

We remark that the conclusions of this section also apply if instead of solving the classical equation of motion for the propagator in terms of $G_{\text{cl}} = i(\Gamma_{t_0}^{(2)})^{-1}$, we use the fact that $\Gamma_{t_0}^{(2)}$ is a differential operator. This leads to a variant of the Dyson equation (4.49) that is an integro-differential equation. This formulation is very common in the literature and our numerical results of Ch. 5 are obtained in this way. Note that in App. C, we demonstrate numerically that the solution of the integro-differential version of the Dyson equation agrees with the solution obtained by using the outlined algorithm. In fact, these results indicate that the explicit time-stepping algorithm for the integral equation leads to improved convergence properties compared to the one used to solve the integro-differential equation.

We remark that in general, the dynamic equations for the correlation functions are integral equations. The above analysis suggests to investigate these causal integral equations carefully. Note that the fact that the Dyson equation factorises into a piece known for all relevant times, G_{cl} , and a rest, $\Sigma \cdot G$, is crucial for the explicit algorithm to be available. Indeed to compute $G_{i_{\text{max}} \geq j, j}$, we need to know $G_{\text{cl}, i_{\text{max}} \geq j, j}$. For instance to compute the entry G_{20} , we need $G_{\text{cl}, 20}$ and $G_{\text{cl}, 21}$. Note that this is perfectly compatible with causality as the latest external time index in this case is 2. Thus, if there is a known quantity as the left (right) factor, Dyson-type equations can be solved by the explicit numerical method in their lower (upper) triangular part. Note that such a factorisation is not possible in general. For instance for the fish diagram, $\Gamma_{1000}^{(4)} \propto \Gamma_{1000}^{(4)} G_{00}^2 \Gamma_{0000}^{(4)}$. Still, there definitely is a potential for the occurrence of simplifications also in more general cases. Note that for these general cases, the usual Langreth rules (cf. e.g. [78]) which allow to decompose convolutions and products of two-time quantities leading to real-time integrals do not suffice when genuine, independent vertices are present. For contour integrals with general multi-argument integrands on \mathcal{C}_{tot} ($\mathcal{C}_{\text{tot}} = \mathcal{C}^{\text{M}} \cup \mathcal{C}^+ \cup \mathcal{C}^-$, cf. Sec. 4.4.2), this could be done along the lines of [116]. A detailed analysis of basis choices for general n -point functions can be found in [117].

4.8.2. The s-Channel Effective Vertex

Analysing the structure of the CTP integrals in the general flow of the two-point function is beyond the scope of this work. Here, we demonstrate that the equation for the effective vertex (4.37) can be solved explicitly.

The respective contribution to the propagator G_{xy} is given by $\tilde{\Sigma}_{xy} := 1/3\Gamma_{xy}^s G_{xy}$, cf. Eq. (4.39). Discretising time, we know that for $G_{i_{max} \geq j, j}$, the self-energy in the Dyson equation appears as $\Sigma_{a \leq i_{max}-1, b \leq i_{max}-1} \propto \Gamma_{a \leq i_{max}-1, b \leq i_{max}-1}^s G_{a \leq i_{max}-1, b \leq i_{max}-1}$ with

$$\begin{aligned} \Gamma_{a \leq i_{max}-1, b \leq i_{max}-1}^s &= \frac{i}{6} \lambda_4 \left[G_{a \leq i_{max}-1, b \leq i_{max}-1}^2 \right. \\ &\quad \left. - \lambda_4 G_{a \leq i_{max}-1, c \leq i_{max}-2}^2 \Gamma_{c \leq i_{max}-2, b \leq i_{max}-1}^s \right]. \end{aligned} \quad (4.55)$$

Note that here, a discrete CTP integral over c is implied. Thus, we are dealing with the same structure as in the Dyson equation: The integrand factorises into a known left factor and a rest. Hence, the algorithm of Sec. 4.8.1 applies and Eq. (4.55) can be solved in terms of an explicit time-stepping for the lower triangular part of Γ^s . This is an important result of this work. To the best of our knowledge, this has not been discussed in the literature so far. This result is of great practical relevance as it improves the stability and the performance for one of the most used approximations regarding unitary dynamics.

4.9. Towards an Entirely Time-Local Causal Flow

In this section, we investigate more closely the lower boundaries of the CTP integrals that feature in the diagrams on the right-hand side of the flow. We remark that the present section constitutes recent developments whose details are the subject of ongoing discussions.

Let us recall that the flow $\partial_\tau \Gamma_{\tau, 1 \dots n}^{(n)}$ has a causal structure of the form $\delta_{\tau_1} \theta_{\tau_2} \dots \theta_{\tau_n} +$ permutations. In particular, this structure is local in time. The CTP integrals however do not get localised. These extend from t_0 to t_{max} , cf. Eq. (3.18). These types of integrals are referred to as memory integrals. Their appearance is common in general applications of quantum dynamics [14, 78, 142]. Physically, these account for the correlations build up between t_0 and t_{max} in an interacting system. In fact, this can be made more concrete using the results of Sec. 2.2. They originate from the matrix elements of the time evolution operator that connect the earliest operator insertion at t_{min} to the density matrix at t_0 .

In practice, these integrals allocate a lot of computational resources. With regard to storage capacities this can get out of hand quickly, consuming $\mathcal{O}(100)$ gigabytes of memory. One procedure to alleviate this memory problem is to successively ignore the contributions from earlier times. This is justified if the correlations in time decay fast enough. For which times this assumption holds must in principle be checked explicitly for each case at hand. Thus, it is desirable to reduce the integration range of the memory integrals in a more systematic way. In principle, this should be possible at least to a degree. To that end, recall that in the Schrödinger picture, there is only a single time – the time of the state $\rho(t)$ and time evolution can be formulated without memory integrals. Thus, the time dependent correlations of the interacting theory can be encoded in a manifestly time-local way.

When considering time-dependent correlations in the Heisenberg picture however, the locality of unitary quantum dynamics appears to be lost. Fundamentally, we know that it can not be lost in any closed system due to the fact the Heisenberg and the Schrödinger picture are equivalent. This fact is also referred to as the Quantum Regression Theorem (QRT) [84, 143]. Following the presentation there, observe that

$$\Omega(t_1, t_2) := \mathcal{U}(t_1, t_2) \rho(t_2) \Phi_S \mathcal{U}(t_2, t_1), \quad (4.56)$$

at fixed t_2 and regarded as a function of t_1 , fulfils the same time evolution equation as the density matrix $\rho(t_1)$. Note that Ω in general does not obey the same constraints as ρ . Moreover, Ω can be used to express two-time averages as follows

$$\text{Tr}[\rho(t_0) \Phi(t_2) \Phi(t_1)] = \text{Tr}[\Omega(t_1, t_2) \Phi_S]. \quad (4.57)$$

Thus, for fixed t_2 and given $\rho(t)$ for all t , the propagator can be computed like a single-time quantity: We start at a fixed t_2 and compute Ω for all t_1 . Then we move to the next time, $t_2 + \Delta t$, thus performing the computation in time-slices. In particular, no memory integrals are present in this representation. Then by induction and defining suitable $\Omega^{(n)}$, we can keep adding one time argument after the other.

This poses the question if such a formulation without memory integrals can be found in our diagrammatic approach, which takes place in the Heisenberg picture. To that end, observe that Eq. (4.56) implies that we should keep moving the density matrix to the earliest operator insertion at t_{min} instead of referring back to t_0 . Indeed, we can imagine adjusting the initial state such that all correlations of interest can be inferred from times between t_{min} and t_{max} . While the details of such a reformulations are not fully developed, the tFRG formalism offers a unique perspective to address it. In particular

intriguing is the fact that Eq. (4.57) and $\partial_\tau G_{\tau,12} = G_{12}(\delta_{\tau 1}\theta_{\tau 2} + \theta_{\tau 1}\delta_{\tau 2})$ suggest to compute the dynamics of the propagator in time-slices.

One crucial question in such a set-up concerns relating the initial states at t_0 and t_{\min} . Note that if for instance $\rho(t_0)$ describes a Gaussian state, the correlations build up during any non-trivial time evolution will lead to a non-Gaussian state $\rho(t_{\min})$. An important result with regard to correlated initial states is that any general, possibly correlated, non-equilibrium initial state that is physically meaningful can always be obtained from an instantaneous quench, cf. e.g. [83]. To that end, consider two Hamiltonians: The Hamiltonian $\mathcal{H}_{\text{prep}}(t)$ is used to prepare the initial state. For now, we can consider it to be a fictitious quantity introduced for the purposes of the discussion. By $\mathcal{H}_{\text{dyn}}(t)$, we denote the Hamiltonian that generates the dynamics we want to investigate. At the time $t = -\infty$, imagine the constituents of a given system to be well separated such that they can be considered as non-interacting. Then, using an external, time dependent potential that is part of $\mathcal{H}_{\text{prep}}(t)$, we drive the system out of equilibrium and force it to interact. Hence, this system evolves from an uncorrelated initial state until it equilibrates at later times. In equilibrium, the system becomes time-translational invariant again. In particular this implies that the propagator takes the form

$$G^{+-}(t, t') = \frac{1}{\omega} \left(\frac{1}{2} + f_0 \right) \cos [\omega(t - t')] + \frac{i}{2\omega} \sin [\omega(t - t')],$$

Here we use G^{+-} as an explicit example, but the other propagator components are of the same form, cf. (5.9) and App. A. By ω , we denote the dispersion relation, and we suppressed any momentum dependence. Note that we can always tune $\mathcal{H}_{\text{prep}}(t)$ in precisely such a way to produce a specific equilibrium state that contains precisely the correlations of interest. In particular, we can arrange for occupation numbers f_0 far from equilibrium. At t_0 we then turn off the Hamiltonian $\mathcal{H}_{\text{prep}}(t)$ and turn on the Hamiltonian $\mathcal{H}_{\text{dyn}}(t)$, starting the dynamics we want to investigate. Thus, the Hamiltonian $\mathcal{H}(t)$ describing the whole experiment is given by $\mathcal{H}(t) = \theta(t_0 - t) \mathcal{H}_{\text{prep}}(t) + \theta(t - t_0) \mathcal{H}_{\text{dyn}}(t)$. Therefore, at t_0 there is a sudden discontinuous change in the Hamiltonian. This is referred to as a quench which is a concept we introduced in Sec. 2.1.1. In the present case, the quench is instantaneous. Note that in actual experiments, the Hamiltonian $\mathcal{H}_{\text{prep}}$ is of course not fictitious. For general considerations however, we do not need to know it explicitly, and correlated initial states parametrise our ignorance with respect to $\mathcal{H}_{\text{prep}}$.

Now, consider starting the evolution at t_- in the past and let it evolve to the present time $\tau > t_-$. In light of the previous discussion, whether we pause the time evolution for a moment at $t_- < t_0 < \tau$ or whether we perform an instantaneous quench at t_0

are physically indistinguishable as far as times $t > t_0$ are concerned. This allows us to obtain the initial conditions at t_0 such that both evolutions agree for times greater than t_0 . For instance for the two-point function

$$\mathcal{I}_{t_0,xy}^{(2)} = \mathcal{I}_{t_-,xy}^{(2)} + \Sigma_{t_0,xy}.$$

Here, \mathcal{I}_t encodes the correlations of the density matrix at t , cf. Eq. (3.19) and $\mathcal{I}^{(n)}$ denotes its n th field derivative. We remark that similar discussions with respect to the preparation of the initial state can be found in [142, 144] with a particular emphasis on renormalisation and in [83] in the context of correlated initial states.

In the tFRG approach, the self-energy is determined in terms of the integrated flow, $\Sigma_{t_0} \equiv \Sigma_{\tau=t_0}$. Notably, the tFRG approach allows us to match the initial correlations for all n -point functions,

$$\mathcal{I}_{t_0,x_1\dots x_n}^{(n)} = \mathcal{I}_{t_-,x_1\dots x_n}^{(n)} + \Sigma_{t_0,x_1\dots x_n}^{(n)},$$

since we know all the integrated flows $\Sigma_{t_0,x_1\dots x_n}^{(n)}$. Note that due to the instantaneous quench at t_0 , contributions from the integrated flow that started at t_- get removed. For instance, consider

$$\Gamma_{\tau}^{(2)} - \Gamma_{t_-}^{(2)} = \overset{\tau}{t_-}(\Sigma)_{t_-}^{\tau} = \overset{t_0}{t_-}(\Sigma)_{t_-}^{t_0} + \overset{\tau}{t_0}(\Sigma)_{t_0}^{\tau} + \overset{t_0}{t_-}(\Sigma)_{t_0}^{\tau} + \overset{\tau}{t_0}(\Sigma)_{t_-}^{\tau}. \quad (4.58)$$

By the notation $\overset{\tau}{t_0}(\Sigma)_{t_-}^{t_0}$, we denote that Σ_{xy} is non-vanishing for $t_0 \leq x^0 \leq \tau$ and for $t_- \leq y^0 \leq t_0$. Thus, we split the total self-energy into four blocks. The block $\overset{\tau}{t_0}(\Sigma)_{t_0}^{\tau}$ can either be obtained from an evolution starting at t_0 in terms of the initial condition $\mathcal{I}_{t_0}^{(2)}$ that contains $\overset{t_0}{t_-}(\Sigma)_{t_-}^{t_0} \equiv \Sigma_{\tau=t_0}$ as well as from an evolution starting at t_- where the initial condition is given by $\mathcal{I}_{t_-}^{(2)}$. The other two blocks in Eq. (4.58) are not readily accessible for the evolution that starts at t_0 . From the perspective of $\overset{\tau}{t_-}(\Sigma)_{t_-}^{\tau}$, these are removed by the quench.

If we are interested in these correlations, we propose the following strategy: So far, the causal regulator R_{τ} suppresses only contributions to the flow for times larger than τ . Now we generalise this to $R_{\tau_{min},\tau_{max}}$ which is defined to vanish for times $\tau_{min} \leq t \leq \tau_{max}$, while it suppresses all fluctuations outside this interval. If we keep the regulator diagonal, then this defines a square of size $\Delta\tau \times \Delta\tau$ with $\Delta\tau := \tau_{max} - \tau_{min}$. Assuming that the causal constraints of the temporal flow generalise to this regulator, this implies that a general n -point function is non-vanishing inside a hyper-cube of size $(\Delta\tau)^n$. For two-time quantities, this constitutes a tiling of the time-plane by squares.

With the results already established, it is clear that we can tile along the time-diagonal using R_τ . To obtain the off-diagonal blocks, the \mathcal{S} -path considered in [145] could be used. The \mathcal{S} -path is a contour that extends from t_0 to the right *and* to the left. For concreteness, consider $t_0 = 0$. The correlation functions ordered on this S-shaped path can therefore have positive and negative time arguments. This is related to the microscopic reversibility of unitary dynamics. Thus, the \mathcal{S} -path allows us to evolve forward and backward in time. The extended causal regulator $R_{\tau_{min}, \tau_{max}}$ should then ensure that both the forward and the backward evolution are causal. Note that to access the off-diagonal blocks, we need to shift the regulator off the diagonal. Thanks to the presence of n -point functions of arbitrary order, the temporal flow should allow us to match all initial conditions appropriately. Assuming that this procedure can be shown to be consistent, the limit $\Delta\tau \rightarrow 0$ could lead to fully time-local evolution equations for the correlation functions. In particular, no memory integrals would be present in this formulation. Developing these ideas further is left to future work.

4.10. Conclusion

We presented several substantial advancements for the tFRG framework. One central result are novel one-loop exact relations for the fully dressed correlation functions that were derived by analytically integrating the causal temporal flow. The procedure we presented uses the causality-properties of the tFRG approach in a very immediate way in terms of constraints on the temporal flow. We derived the general integrated flow of the one- and two-point function and of the effective action. Note that the employed procedure readily extends to any n -point function.

The analytic integration of the flow revealed the particular importance of local vertex corrections. Our analysis demonstrates that these are absent in a theory with microscopic three-point interactions only. On the contrary if there are microscopic four-point interactions, then all vertices receive corrections containing local parts.

Using the causal constraints, we derived the full hierarchy of Dyson-Schwinger equations from the causal temporal flow. Reproducing the correct prefactors of the two-loop terms in the DSEs of the one- and two-point function constitutes a highly non-trivial demonstration of the internal consistency of the tFRG framework. By a perturbative expansion of the propagator and the vertices, we observed that certain topologies that are absent in the analysed vertex corrections are in fact created by the one-loop terms in the DSE. This demonstrates that the causal constraints prevent an overcounting of perturbative contributions.

We proposed an extension of the tFRG formalism designed to directly access equilibrium properties of quantum field theories. To that end, we analysed the integrated flow of the effective action and suggested a generalisation of the causal temporal flow to the contour known from real-time thermal field theory.

Using the causal constraints, we obtained a non-perturbative truncation of the integrated flow containing an s-channel effective vertex. We showed that our result is able to reproduce the 2PI $1/N$ expansion at next-to-leading order.

We solved the problem of renormalising the causal temporal flow in general. Its renormalisation is concerned with the initial conditions alone. Due to the one-loop structure of the flow, the absence of subdivergencies is manifest. For the concrete example of the ϕ^4 -theory in $3 + 1$ dimensions, we explicitly derived the corresponding renormalised initial conditions.

We derived an algorithm that allows to solve causal integral equations like the Dyson equation for the propagator or the Bethe-Salpeter equation for the effective vertex in terms of an explicit numerical method, involving only sums over known values.

We identified the origin of the memory integrals present in the (integrated) flow. We discussed how to match correlated, i.e. non-Gaussian initial states at different times in the tFRG framework. To develop entirely time-local evolution equations for the correlation functions, we proposed a flow on an S-shaped contour using a non-diagonal temporal regulator.

5. Dynamics of the ϕ^3 -Theory

In this chapter, we discuss the numerical solution of the integrated flow. To this end, we employ a truncation including the propagator of the ϕ^3 -theory in 1 + 1 dimensions. The classical action is given by

$$S[\varphi] = \int_{\mathcal{C},x} \left\{ \frac{1}{2} \partial^\mu \varphi(x) \partial_\mu \varphi(x) - \frac{m_0^2}{2} \varphi(x)^2 - \frac{\lambda}{3!} \varphi(x)^3 \right\}. \quad (5.1)$$

Such a theory is an ideal test case for the present approach. Moreover, it is also of interest from a physical point of view since the insights from cubic interactions are necessary with respect to non-abelian gauge theories. There, both microscopic three- and four-point vertices are present. Although the former are momentum dependent, the scalar field theory with action Eq. (5.1) allows for the same scattering processes which are absent in the ϕ^4 -theory. Furthermore, we are interested in studying the emergence of universal dynamics in the ϕ^3 -theory. Far-from-equilibrium universality is well documented for the ϕ^4 -theory, where it is observed in the relativistic and non-relativistic case [57]. It is also found in systems containing both scalars and fermions (see e.g. [146]) and in gauge theories in the semi-classical regime of high occupancies (e.g. [52, 53]). Universal dynamics can be characterised by the scaling behaviour of the correlations of a system in time and space, and we find indications thereof in our numerical results for the propagator.

We discuss our truncation and the respective (integrated) flow equation in Sec. 5.1. In Sec. 5.2, we obtain two corresponding dynamic equations: an integro-differential equation and an integral equation. The respective initial conditions that we use to solve these equations and the observables that we consider can be found in Sec. 5.3. We present and discuss our numerical results for the propagator in Sec. 5.4. The conservation of energy is discussed in Sec. 5.6 and particle number conservation is addressed in Sec. 5.7.

In App. C, we present and discuss numerical results for the propagator obtained by solving its integral equation, using the explicit numerical method derived in Sec. 4.8. We conclude in Sec. 5.8. This chapter is based on [1]. Additionally, it features extended discussions in Sec. 5.1, 5.5 and 5.6.

5.1. Truncation

We employ a truncation including the dynamics of the propagator with classical three-point functions. Thus, the vertex reads

$$\Gamma_\tau^{(3)}(x, a, b) = S^{(3)}(x, a, b) = -\lambda \delta_C(x - a) \delta_C(a - b). \quad (5.2)$$

Additionally, we set $\Gamma_\tau^{(n)} = 0$ for all $n > 3$. These higher order correlations are for example part of a thermal state given by a density matrix of the form $\rho \propto \exp^{-\beta \mathcal{H}_{\text{eq}}}$ with the Hamiltonian \mathcal{H}_{eq} . Hence, the Gaussian initial state which takes into account only one- and two-point correlations at t_0 may be understood as the result of a quench which drives the system out of equilibrium. We introduced the concept of a quench in Sec. 2.1.1. In this approximation, we study the emergence of universal dynamics in the ϕ^3 -theory. In previous 2PI studies of the ϕ^4 -theory (e.g. [125, 126]), universal dynamics was observed starting from Gaussian initial conditions. Thus, these can be considered as well motivated. Let us emphasise again that including non-Gaussian initial conditions is straightforward in the tFRG framework in the form of $\Gamma_{\tau=t_0}^{(n>2)}$, cf. Sec. 3.1.4.

We further remark that since we do not consider the dynamics of the expectation value of the field, the employed truncation corresponds to fixing $\bar{\phi} \equiv 0$ which is no solution to the quantum equation of motion $\Gamma^{(1)}[\bar{\phi}] = 0$ of the ϕ^3 -theory. Formally this choice poses no issue since the background around which the effective action is expanded can be chosen freely in the tFRG approach, cf. Sec. 3.1.6. Moreover, the over-occupied initial condition we will consider (cf. Sec. 5.3) imply that quantum fluctuations are subleading. This is well established for the ϕ^4 -theory, cf. e.g. [125]. In this work, we will not perform an analysis involving the dynamics of the field. In this sense, we assume that the vacuum instability of the ϕ^3 -theory does not constitute a problem regarding the emergence of universal dynamics in the semi-classical regime. Keep in mind that as a classical theory, the ϕ^3 -theory is perfectly well-defined. We present our numerical results for the propagator in Sec. 5.4. These show no sign of an instability.

Now let us proceed with the flow of the two-point function in the truncation at hand. As discussed in Sec. 3.1.6, we evaluate the flow on $\phi^+ = \bar{\phi} = \phi^-$ to obtain the physical time evolution and do not denote this explicitly any more. Inserting the vertex (5.2) into the flow (3.18), we obtain

$$\partial_\tau \Gamma_{\tau,xy}^{(2)} = -\frac{1}{2} \int_{\mathcal{C},abcd} S_{xab}^{(3)} G_{\tau,ac} (G_\tau \cdot \partial_\tau R_\tau \cdot G_\tau)_{bd} S_{ycd}^{(3)} + (x \leftrightarrow y).$$

Using the identity (3.30) to replace the line with the cutoff insertion with the propagator, we are left with

$$\partial_\tau \Gamma_\tau^{(2)}(x, y) = \frac{i\lambda^2}{2} \partial_\tau G_\tau^2(x, y). \quad (5.3)$$

Integrating over τ is now straightforward. Due to our simple truncation, the flow (5.3) is a total τ -derivative and we obtain

$$\Gamma^{(2)}(x, y) = \Gamma_{t_0}^{(2)}(x, y) + \frac{i\lambda^2}{2} G^2(x, y). \quad (5.4)$$

Note that we absorbed the contribution containing G_{t_0} in $\Gamma_{t_0}^{(2)}$, cf. the discussion below Eq. (4.19). Let us emphasise that the tFRG flow can be integrated in generic truncations, where the flow is no total derivative in general. This is due to the local causal structure intrinsic to the tFRG, cf. Ch. 4. The general integrated flow of the two-point function in the ϕ^3 -theory is given in Eq. (4.20). Indeed, if we replace the full and the initial vertex in Eq. (4.20) according to our truncation with $S^{(3)}$, we immediately obtain Eq. (5.4).

5.2. Dynamic Equations

Here we discuss two different possibilities how Eq. (5.4) can be solved. For both of them, we can use that $\Gamma_{t_0}^{(2)} = S^{(2)} + \alpha_2$ in the present truncation. $S^{(2)}$ denotes the classical kinetic operator of the action (5.1). α_2 parametrises the initial conditions and is not needed explicitly for what follows. One possibility is to solve Eq. (5.4) as an integro-differential equation by applying it to the full propagator G . This approach is very common in the literature. In our case, it yields the following equation

$$[\partial_x^2 + m_0^2] G(x, y) = -i\delta_{\mathcal{C}}(x - y) + \frac{i\lambda^2}{2} \int_{\mathcal{C}, z} G^2(x, z) G(z, y). \quad (5.5)$$

Another possibility is to define the inverse of $S^{(2)}$,

$$\int_{\mathcal{C}, z} S^{(2)}(x, z) G_{\text{cl}}(z, y) = i\delta_{\mathcal{C}}(x - y),$$

where we denote the inverse by G_{cl} . Here, G_{cl} is just the classical propagator. In the present truncation, this corresponds to the solution of the free equation of motion which is known analytically. Contracting (5.4) with G_{cl} from the left and G from the right, we

obtain the integral equation

$$G(x, y) = G_{\text{cl}}(x, y) - \frac{\lambda^2}{2} \int_{\mathcal{C}, z_1 z_2} G_{\text{cl}}(x, z_1) G^2(z_1, z_2) G(z_2, y). \quad (5.6)$$

Integral equations like Eq. (5.6) are implicit equations. A standard way of solving them is by some type of fixed point iteration. For the case at hand however, it turns out that we can do better. The underlying reason is that Eq. (5.6) is a *causal* equation. A detailed discussion of this fact and its implications is given in Sec. 4.8, where we use causality to demonstrate how to solve equations like (5.6) in terms of an explicit numerical method, involving only sums over known values.

Let us briefly address the numerical solution of the equations (5.5) and (5.6). At a first glance, the integro-differential equation (5.5) can be solved faster since there is one time integral less compared to the integral equation. Demanding however that the results have the same accuracy, this changes. Due to the derivative, a higher resolution is needed to achieve the same accuracy as with the integral equation. More details can be found in App. C.

An important feature of the employed truncation can be observed by exchanging the spatial coordinates for momenta using the Fourier transformation in both Eq. (5.5) and Eq. (5.6): The time evolution of the propagator has a dependence on the external momenta. This is important to obtain scattering processes between different momentum modes and hence a non-trivial dynamical evolution. Note that the corresponding truncation in the ϕ^4 -theory does not have this property. Indeed, it would only contain the tadpole diagram with a classical vertex which is independent of external momenta.

We further remark that equations Eq. (5.5) and Eq. (5.6) can also be obtained as the lowest-order in the 2PI loop expansion of the ϕ^3 -theory. The respective contribution to the 2PI effective action is given by the sunset vacuum graph, cf. e.g. [14]. Indeed, it is known that the tFRG framework can reproduce 2PI approximations by a suitable choice of truncation, cf. [6, 7] and Sec. 4.6. Let us emphasise that this is not the case generically since the tFRG framework allows for truncations that do not correspond to 2PI resummations, cf. e.g. Sec. 4.5.

5.3. Observables and Initial Conditions

For the numerical solution of the integrated flow, we express the CTP propagator G in terms of the statistical propagator F and the spectral function ρ . These are defined as the expectation value of the anti-commutator and commutator of the field operator

respectively. More details can be found in App. A. We address issues we faced when using the \pm -basis for the propagator in our numerics in Sec. 3.3. The upshot is that it is prone to numerical instabilities and consumes a lot more computing resources than the completely real basis in terms of F and ρ .

The statistical propagator already allows us to discuss relevant observables such as the occupation number f and the dispersion relation ω . In non-equilibrium situations however, there is no unique definition. We employ an approach very common in the literature making use of the following decomposition of the equal time statistical propagator (cf. e.g. [14]),

$$F(t, t, \mathbf{p}) = \frac{f(t, \mathbf{p}) + \frac{1}{2}}{\omega(t, \mathbf{p})}.$$

Here, we use a mixed position and momentum space where only the spatial coordinates are transformed to momenta. The occupation number can be computed as

$$f(t, \mathbf{p}) + \frac{1}{2} = \sqrt{\partial_t \partial_{t'} F(t, t', \mathbf{p}) F(t, t', \mathbf{p})} \Big|_{t=t'}, \quad (5.7)$$

and for the dispersion relation we find

$$\omega(t, \mathbf{p}) = \sqrt{\frac{\partial_t \partial_{t'} F(t, t', \mathbf{p})}{F(t, t', \mathbf{p})}} \Big|_{t=t'}. \quad (5.8)$$

A nice property of the definitions (5.7) and (5.8) is that they coincide with their equilibrium counterparts in the case when the propagator enjoys time-translational invariance. This is easy to verify, inserting the expression F_{cl} given below in Eq. (5.9) into Eq. (5.7) and Eq. (5.8) respectively.

Next we discuss the initial conditions. For the integral equation (5.6), these conditions are encoded in the solution of the classical equation of motion G_{cl} . In the present truncation and in terms of F_{cl} and ρ_{cl} , this is given by

$$F_{\text{cl}}(t, t', \mathbf{p}) = \frac{1}{\omega_{\mathbf{p}}} \left(\frac{1}{2} + f_0(\mathbf{p}) \right) \cos [\omega_{\mathbf{p}}(t - t')], \quad \rho_{\text{cl}}(t, t', \mathbf{p}) = \frac{1}{\omega_{\mathbf{p}}} \sin [\omega_{\mathbf{p}}(t - t')]. \quad (5.9)$$

Here, $f_0(\mathbf{p})$ and $\omega_{\mathbf{p}} = \sqrt{\mathbf{p}^2 + m_0^2}$ denote the occupations and the dispersion at the initial time respectively.

For the integro-differential equation (5.5), we have to provide values for F and ρ and

their first derivatives at the initial time. In analogy to the previous case, we use for the statistical propagator

$$F(t, t', \mathbf{p})|_{t=t'=t_0} = \frac{1}{\omega_{\mathbf{p}}} \left(\frac{1}{2} + f_0(\mathbf{p}) \right), \quad \partial_t F(t, t', \mathbf{p})|_{t=t'=t_0} = 0,$$

$$\partial_t \partial_{t'} F(t, t', \mathbf{p})|_{t=t'=t_0} = \omega_{\mathbf{p}} \left(\frac{1}{2} + f_0(\mathbf{p}) \right),$$

and the spectral function

$$\rho(t, t', \mathbf{p})|_{t=t'=t_0} = 0, \quad \partial_t \rho(t, t', \mathbf{p})|_{t=t'=t_0} = 1,$$

$$\partial_t \partial_{t'} \rho(t, t', \mathbf{p})|_{t=t'=t_0} = 0.$$

Note that the initial conditions for the spectral function can not be chosen freely. They are fixed by the equal-time commutation relations.

For the results shown in the next section, we choose initial conditions far from equilibrium. Explicitly, we consider a (sharp) box for the initial occupancies $f_0(\mathbf{p})$ of the form

$$f_0(\mathbf{p}) = \frac{\tilde{N}}{\lambda} \theta(Q_0 - |\mathbf{p}|).$$

In particular, we will use $\tilde{N} = 100$ for the occupancy parameter \tilde{N} , and $\tilde{\lambda} = \lambda/m_0^2 = 0.01$ for the dimensionless coupling of the three-point function. Thus, the momentum modes below the scale Q_0 are highly over-occupied while the modes above Q_0 are not occupied at all. Furthermore, we will identify the characteristic momentum scale with the bare mass: $Q_0 = m_0$. Such over-occupied initial conditions have been demonstrated to lead to universal dynamics in the ϕ^4 -theory (cf. e.g. [125, 126]), and the above parameters are virtually identical to the parameters chosen there.

5.4. Numerical Results for the Propagator

The results of this section were obtained solving the integro-differential version of the dynamic equation (5.5) in terms of F and ρ . Their evolution equations are derived in a straightforward way from (5.5) using the expression (A.4) for the propagator and the details can be found in [14]. We solve these equations in spatial momentum space, using the initial conditions discussed in Sec. 5.3. In our numerics, the spatial momenta take

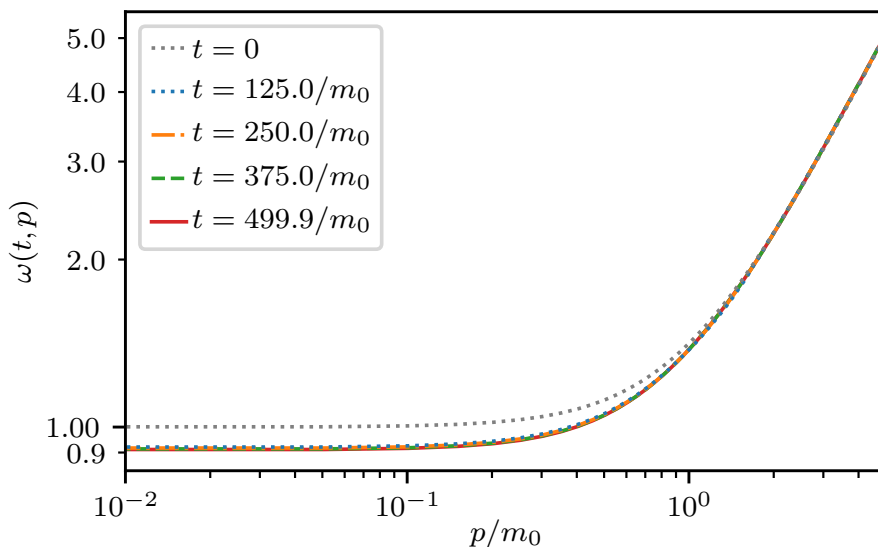


Figure 5.1.: Dispersion relation as defined in (5.8) at the indicated times. The grey dashed line corresponds to the dispersion at the initial time. At zero-momentum, we read off the mass of the interacting theory to be $m \approx 0.9m_0$ relative to the bare mass. This figure is taken from [1].

values in the range $|\mathbf{p}| \in [0, 5]$ which is resolved using an equidistant grid of $N_{|\mathbf{p}|} = 100$ points. This corresponds to a grid spacing of $\Delta|\mathbf{p}| = 0.05$. Both times take values in $t \in [0, 500]$ which is resolved using $N_t = 8000$ points. This corresponds to grid spacing of $\Delta t = 0.0625$. All dimensionful quantities are measured in units of m_0 .

A first interesting result is the time evolution of the dispersion relation which is shown in Fig. 5.1. At small momenta, the dispersion decreases with time. This region is dominated by the mass. For zero momentum, we can therefore read off the mass m of the interacting theory. Compared to the bare mass m_0 , we find $m \approx 0.9m_0$. For higher momenta, where the mass is negligible, the dispersion agrees for all times.

In Fig. 5.2, we show the time evolution of the occupation number for the same times as the dispersion relation. Naturally, the initial sharp box is smoothed out over the course of the dynamics since the occupancies are redistributed over the range of momenta. The momentum regime around $p/m_0 \approx 2$ is particularly interesting. In this regime, we may identify a power law decay of the occupation number.

$$f(t, \mathbf{p}) \propto |\mathbf{p}|^{-\kappa}.$$

For an estimate of the exponent κ , we define the following momentum- and time-

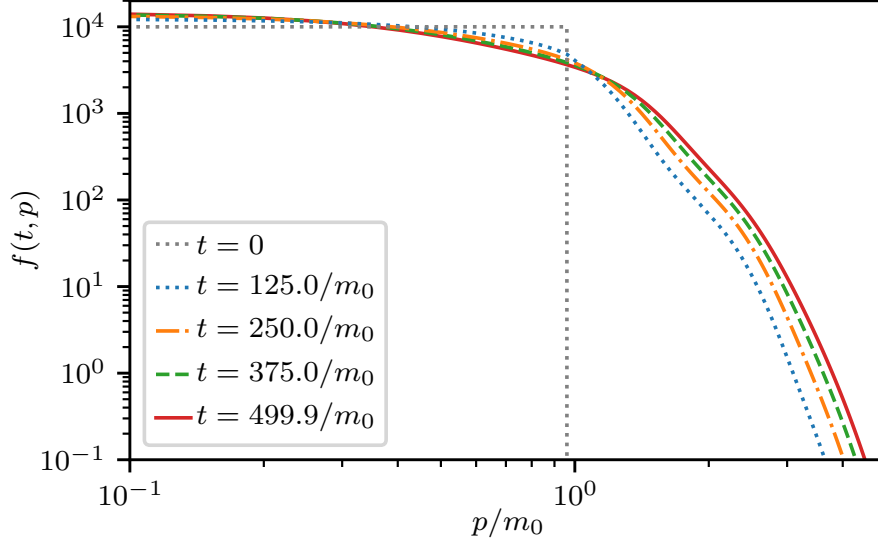


Figure 5.2.: Occupation number as defined in (5.7) at the indicated times. The grey dashed line corresponds to the initial distribution. For later times, the initial box is smoothed out, and we find indications for a self-similar scaling regime around $p/m_0 \approx 2$, exhibiting a power law decay. This figure is taken from [1].

dependent exponent

$$\kappa(t, p) = -p \partial_p \ln f(t, p). \quad (5.10)$$

This exponent is shown for different times in Fig. 5.3. It is approximately constant in the momentum range $p/m_0 \in [1.8, 2.1]$. At later times, this constant scaling regime is more pronounced. At $t = 499.9/m_0$, we find

$$\kappa \in [5.57, 5.69], \quad \frac{p}{m_0} \in [1.8, 2.1]. \quad (5.11)$$

Additionally to the suggested power law behaviour, the exponent is similar for all times considered. This potentially signals the emergence of self-similar temporal scaling, although the regime is rather small.

In such regimes, the time evolution can be characterised by the following self-similar scaling of the occupancies (see eg. [57, 67]),

$$f(t_{\text{ref}}, |\mathbf{p}|) = \left(\frac{t}{t_{\text{ref}}} \right)^{-\alpha} f \left[t, \left(\frac{t}{t_{\text{ref}}} \right)^{-\beta} |\mathbf{p}| \right]. \quad (5.12)$$

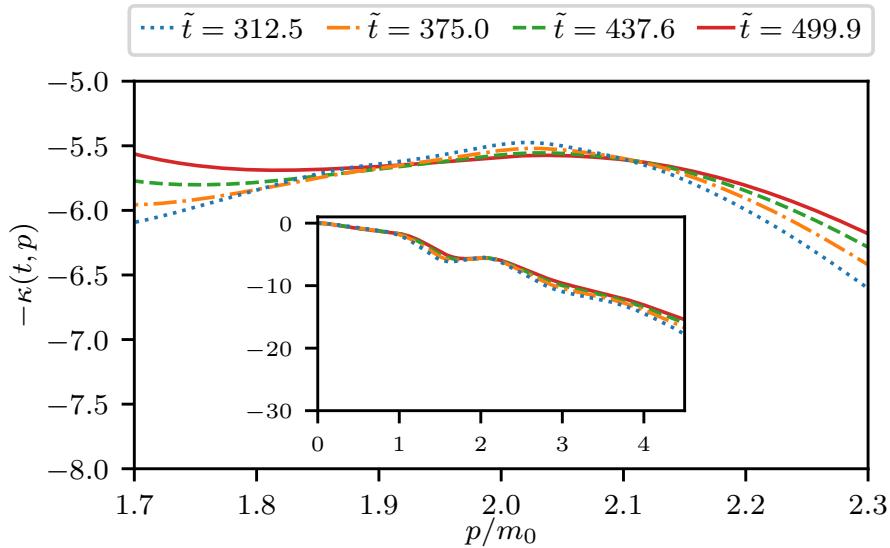


Figure 5.3.: Momentum-dependent exponent of the occupation number as defined in (5.10) for various times $\tilde{t} = tm_0$. For $p/m_0 \in [1.8, 2.1]$, the exponent is approximately constant. At later times, this constant regime is more pronounced. For the time $t = 499.9/m_0$, we find $\kappa \in [5.57, 5.69]$. The inset shows the momentum-dependent exponent for the full available momentum range. This figure is taken from [1].

Here, α moves the distribution along the y -axis and β moves it along the x -axis. We compute these exponents for the times $tm_0 = 312.5, 375.0, 437.6$, using a least squares fit with respect to the occupancies at the reference time $t_{\text{ref}} = 499.9/m_0$. In the regime $p/m_0 \in [1.8, 2.1]$, their respective values are given by $\alpha = 0.82, 1.03, 1.39$ and $\beta = -0.02, 0.02, 0.09$. For convenience and future reference, we additionally display these findings in Tab. 5.1.

As a first consistency check, we display the occupations rescaled according to the self-similar scaling ansatz (5.12), using the exponents as in Tab. 5.1, in Fig. 5.4. The rescaled occupation numbers (left) can be compared to the original ones (right). The momentum range where the exponent κ is approximately constant is indicated with vertical dashed lines. The rescaled occupation numbers match in this momentum range in accordance with a self-similar time evolution.

5.5. Discussion and Comparison

In this section, we critically assess the results obtained in Sec. 5.4, focusing on the potential emergence of universal dynamics. We discuss the respective results in Sec. 5.5.1

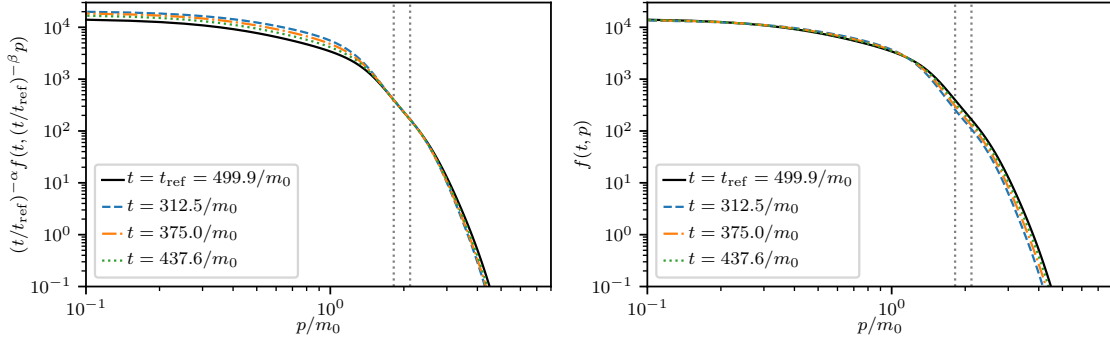


Figure 5.4.: Left: Occupation numbers rescaled according to Eq. (5.12). The used values for the scaling exponents are as in Tab. 5.1. The scaling regime is assumed to occur in the momentum range $p/m_0 \in [1.8, 2.1]$, which is marked by vertical dashed lines. Right: Original occupation numbers for the same times. These figures are taken from [1].

and compare them to the literature in Sec. 5.5.2.

5.5.1. Discussion

First, observe that the values of the exponents α and β still change with time, cf. Tab. 5.1. In particular, α is changing while $\beta \approx 0$ for the available times. Time dependent exponents indicate that the potential scaling regime is not yet fully developed. Note that nevertheless, the scaling collapse in Fig. 5.4 appears satisfactory to the naked eye. Hence, while the collapse serves as a first consistency check, a more careful analysis is needed to establish that the scaling regime has indeed been reached. To that end it is useful to continue to monitor the exponents as a function of time since they become time-independent in the scaling regime, cf. e.g. [126]. Accordingly, it would be beneficial to continue the dynamics to later times. While going to later times poses

$t m_0$	α	β
312.5	0.82	-0.02
375.0	1.03	0.02
437.6	1.39	0.09

Table 5.1.: Values of the exponents α and β of an assumed self-similar dynamical evolution at the indicated times according to Eq. (5.12), obtained employing a least squares fit with respect to the occupancies at the reference time $t_{\text{ref}} = 499.9/m_0$.

no fundamental issue, the presented results contain the latest times accessible with the computing infrastructure that was available to us at the time. Thus in the following, we assume that there exists a universal scaling regime at later times. We remark that the values of the scaling exponents can still change considerably until they settle at their fixed point values [126]¹.

Note that uncertainties of the least squares fit that is used to extract the exponents could be improved if the available momentum interval would be larger and more pronounced. It is known that either one or both can occur in the universal regime at later times, cf. e.g. [147, 148]². We found indications that the power law in momentum is more pronounced at later times in Fig. 5.3. Concerning the approach to the universal regime, it is reassuring that our exponents increase monotonically as a function of time. A monotonic approach to the fixed point values was also observed in [126].

Apart from using a higher-performance computing infrastructure, a faster emergence of the universal regime would be helpful. Typically, it is expected that the dynamics become faster when using larger couplings, cf. e.g. [126]. Considering larger couplings however caused our numerics to break down. A possible explanation is that quantum fluctuations become too large and the instability of the ϕ^3 -theory reveals itself. From the ϕ^4 -theory however, it is known that the semi-classical picture persists for a large range of couplings [125, 126]. With our current results however, we are not able to settle this question for the ϕ^3 -theory.

Another possibility is that the observed instability signals the necessity of including vertex dynamics. Indeed, it has been previously reported in the literature that the 2PI loop expansions can suffer from instabilities for over-occupied initial conditions and/or large couplings [98]. On the other hand, it has been demonstrated that 2PI approximations including vertex dynamics in the form of a Bethe-Salpeter effective vertex like (4.37) are stable for many different types of initial conditions [125–130]. In particular in the case of over-occupied initial conditions, it has been shown that the dynamical effective vertex decreases over several orders of magnitude at lower momenta which balances the typically observed strong increase of occupations in the same momentum regime, contributing to the stability of the dynamics [125, 126].

Note that in the 2PI approach, this effective vertex is derived using a $1/N$ expansion at next-to-leading order, N being the number of field components. Thus, employing it at the value $N = 1$ which is relevant for the present discussion is questionable at best from the perspective of the $1/N$ expansion. And indeed, it has been demonstrated

¹The exponents α , β and the occupation numbers for times earlier than the universal regime can be found in Appendix 3.C of [139] which contains an extended discussion of the results obtained in [126].

²Cf. also Appendix 3.C of [139].

numerically that using the effective vertex at $N = 1$ can lead to inaccurate results [149]. Let us interpret these findings from the perspective of the tFRG: We know that we can derive the effective vertex from the flow of the four-point function, cf. Sec. 4.6. As is typical in FRG truncations, there is no small expansion parameter that controls the approximation, cf. Sec. 3.1.5. Hence, there is a priori no reason not to use the s-channel effective vertex also for $N = 1$. Then, if the obtained results are not satisfactory, we conclude that the employed truncation misses important contributions and that it should be improved.

A systematic improvement for the present case would be to include non-trivial vertex dynamics of the ϕ^3 -theory in terms of an effective vertex as well as in terms of genuine vertex dynamics. The latter refers to the following: The extended truncation contains an independent vertex that couples back into its (integrated) flow, as opposed to an effective vertex that is constructed solely from the propagator. Let us remark that for the ϕ^3 -theory, the first vertex corrections that should be included are of course the ones of the three-point function.

5.5.2. Comparison

Now let us come back to our findings for the propagator and then into the context of non-thermal fixed points (NTFPs) [54–56] which is well documented in the case of the ϕ^4 -theory, see e.g. [57, 125, 126].

Let us emphasise that comparing our results of the ϕ^3 -theory in $1+1$ dimensions with 2PI studies such as [125, 126] which consider the massless ϕ^4 -theory in $3+1$ dimensions is well motivated. Indeed, recall that non-equilibrium universality classes are remarkable large, encompassing for example relativistic and non-relativistic theories [57] and even gauge and scalar theories in the classical regime of high occupancies [58]. Furthermore, it is known from analytic investigations in kinetic theory that there are cases where scaling exponents can be independent of the dimensionality of the system. Moreover, it is possible for them to agree for three- and four-point interactions [57, 66, 150].

Thus, universality does allow to compare systems that a priori appear to be very different. As opposed to universality in equilibrium, it has been demonstrated that no fine-tuning is necessary to trigger universality out of equilibrium [59]. However, let us emphasise that whether a NTFP is approached at all during the course of the dynamics and if so, which NTFP is approached certainly depends on the class of employed initial conditions [56, 59, 148]. What precisely constitutes a certain class, not to mention a classification of classes of initial conditions, is not settled to date. The initial conditions used in the present case (cf. Eq. (4.11)) are virtually identical to the ones considered in

[125, 126] and in [57]. Classical statistical simulations are employed in the latter case., while the first to references are 2PI computations.

Let us remark that 1+1 dimensions are a peculiar case. This already becomes apparent at the level of kinematics: Scattering is severely constrained in 1 + 1 dimensions due to energy- and momentum conservation [147]. This poses a problem with regard to analytic estimates for the exponents obtained in kinetic theory, which describes the transport of conserved quantities by (quasi-)particles: If there are no transport processes associated to the observed scaling, there is a priori no reason why kinetic theory should give accurate predictions. It turns out that the results reported in the literature in this regard are ambivalent. Naively extrapolating results from higher dimensions agrees for some cases with experimental observations, while it differs in others [59, 60]. There are also reported deviations when comparing to simulation results, cf. e.g. [147]. Thus, the details of 1 + 1 dimensions in general are not settled yet.

Next let us come to our expectations regarding the dynamics. These originate from comparing with the 2PI studies [125, 126, 139] in the massless ϕ^4 -theory in 3 + 1 dimensions in an approximation that includes an effective vertex. The dynamics there was observed to approach a non-thermal fixed point (NTFP) at which a so called dual cascade of the occupations f emerges [57, 125, 126]. This dual cascade is characterised by the transport of particles to low momenta (IR) while energy is transported to large momenta (UV). Accordingly, two scaling regimes with different exponents emerge. Notably, the particle transport leads to the growth of occupations in the low momentum regime by several orders of magnitude.

However, looking at Fig. 5.2, we do not observe a strong growth of occupations in the IR. Moreover considering Fig. 5.3, we find no indications of a second scaling regime. The absence of a second scaling regime could be due to the fact that we do not consider vertex dynamics. Typically, these are needed to generate the second scale that allows a second cascade to form [151]. This would imply that our truncation (5.2) just does not capture the processes relevant for the emergence of a dual cascade. Thus, we can not trigger the respective dynamics even though we use strongly over-occupied initial conditions.

The lack of a strong increase of occupations for the low momentum modes might be due to a lack of energy injected into the system. Additionally, the energy might not be injected at the relevant scale to trigger the strong growth of low momentum modes [151]. When increasing the initial occupations or when disengaging the identification $Q_0 = m_0$ to inject the energy at a different scale, we encountered instabilities in our numerics³.

³We remark that considering $Q_0 \neq m_0$ would also provide a second scales.

Possible reasons for these instabilities are the same as outlined before: Large fluctuations around a non-stable minimum and/or the necessity of including vertex corrections for over-occupied initial conditions.

All in all, the dynamic of occupations in our case, cf. Fig. 5.2, does not conform to the NTFP with a dual cascade. Note that the distributions in Fig. 5.2 are not thermal either. Thus, we are dealing with a different NTFP. This is further substantiated by observing that the obtained value for the momentum exponent $\kappa \in [5.57, 5.69]$ (cf. Eq. (5.11)) is comparatively large. For one, this becomes apparent if we compare it to the case of $|\mathbf{p}|^{-1}$ of the free propagator in the mixed representation, cf. Eq. (5.9). Part of the difference between this canonical scaling dimension and the one of the interacting theory is called the anomalous dimension. For the NTFP with the dual cascade, a small anomalous dimension is observed [57, 125, 126].

If we extrapolate the estimates obtained from kinetic theory (cf. [54, 57, 66]) to $1+1$ dimensions, we conclude that a value of κ as observed here requires a large anomalous dimension. This could be explained by the fact that we are in $1+1$ dimensions. Recall that infrared fluctuations are enhanced in lower dimensions, whereas ultraviolet fluctuations are suppressed. Thus if the observed scaling is an infrared phenomenon, our findings would be qualitatively consistent with the extrapolated kinetic theory results. To that end, we have to determine what the relevant scale is, defining the IR and UV regimes for the case at hand. A natural choice for the case of over-occupied initial conditions is given by the characteristic momentum scale, $Q_0 = m_0$ in our case. The scaling observed in Fig. 5.3 takes place at scales larger than $Q_0 = m_0$. This indicates that we are in the UV regime. If the observed fixed point is associated to processes in the UV, this implies that either this NTFP is not well described by kinetic theory or that there are so far unknown kinetic theory predictions in $1+1$ dimensions with which the observed differences can be understood. In the latter case, we conclude that we can not simply extrapolate the respective results to $1+1$ dimensions. With our current results however, we are not able to settle these questions.

We conclude this section, proposing directions for future work. Pressing issues are to clarify what types of scaling solutions to the equations (5.5) and (5.6) exist, what exponents these do imply and what their interpretation is in terms of physical processes; in the ϕ^3 -theory in general and in $1+1$ dimensions in particular. To that end, a careful analysis along the lines of [54, 57, 66] should be carried out. A complementary strategy would be to perform a fixed point search using the (integrated) tFRG flow or the FRG with a momentum cutoff as in [152]. To that end, the causal temporal flow in terms of dimensionless variables should be derived. Note that the transport of conserved charges

implies a proportionality between the exponents $\alpha \propto \beta$ if energy or particle number are conserved locally in the momentum range where scaling is observed. To that end, it should be checked whether there is a local conservation law for the scaling observed here.

It would be interesting to consider the following extended truncations in the ϕ^3 -theory: Including the time evolution of the field $\bar{\phi}$ using Eq. (4.23) allows to address whether the vacuum instability of the theory poses a challenge to the emergence of universal dynamics in general and in the semi-classical regime of high occupancies in particular. For a 2PI approach that discusses the dynamics of the field in the ϕ^4 -theory, see e.g. [125]. Furthermore, it would be interesting to include vertex dynamics in the ϕ^3 -theory as discussed at the end of Sec. 5.5.1.

5.6. Energy Conservation

In this section, we discuss the non-trivial and important consistency check of energy conservation. As a peculiarity of the ϕ^3 -theory, it is possible to derive an expression for the energy solely in terms of the propagator which we present in Sec. 5.6.1. We present the numerical result for the energy using the results of the propagator from Sec. 5.4 in Sec. 5.6.2. We discuss our findings in Sec. 5.6.3.

5.6.1. Derivation

The total energy is obtained by computing the expectation value of the time-time component of the energy-momentum tensor $T_{\mu\nu}$, which is obtained from the effective action via

$$\langle T_{\mu\nu}(x) \rangle = \frac{2}{\sqrt{-g(x)}} \left. \frac{\delta \Gamma[\phi, g]}{\delta g^{\mu\nu}(x)} \right|_{g^{\mu\nu}=\eta^{\mu\nu}}. \quad (5.13)$$

In Eq. (5.13), the metric $g^{\mu\nu}$ is identified with the Minkowski metric $\eta^{\mu\nu}$. The flow of $\langle T_{\mu\nu} \rangle$ can be derived from the metric variation of $\partial_\tau \Gamma_\tau$ and will be discussed in Sec. 6.1. Here, we follow closely derivations also found in the 2PI framework, e.g. [98, 125]

Concentrating on $\langle T_{00} \rangle$, we first compute the classical energy T_{00} by replacing the effective action with the classical one in Eq. (5.1). This leads us to

$$T_{00} = \partial_0 \varphi \partial_0 \varphi - g_{00} \left(\frac{1}{2} \partial_\mu \varphi \partial^\mu \varphi - \frac{1}{2} m_0^2 \varphi^2 - \frac{\lambda}{3!} \varphi^3 \right) \equiv \mathcal{H}[\varphi],$$

which is just the classical Hamiltonian \mathcal{H} . To obtain its expectation value, we use the following relation (see e.g. [106])

$$\left\langle \prod_{i=1}^n \varphi(x_i) \right\rangle = \prod_{i=1}^n \left[\int_{\mathcal{C}, z_i} G[\phi](x_i, z_i) \frac{\delta}{\delta \phi(z_i)} + \phi(x_i) \right]. \quad (5.14)$$

Considering a generic background $\bar{\phi}$ ($\phi^+ = \bar{\phi} = \phi^-$), the expectation value of the classical Hamiltonian takes the form

$$\begin{aligned} \langle T_{00}(x) \rangle &= \mathcal{H}[\bar{\phi}] + \frac{1}{2} \lim_{y \rightarrow x} \left[\partial_{x^0} \partial_{y^0} G(x, y) + (-\partial_{\mathbf{x}}^2 + m_0^2) G(x, y) \right] \\ &+ \frac{\lambda}{2} \bar{\phi}(x) G(x, x) + \frac{i\lambda}{3!} \int_{\mathcal{C}, z_1 z_2 z_3} \Gamma^{(3)}(z_1, z_2, z_3) \prod_{i=1}^3 G(x, z_i), \end{aligned} \quad (5.15)$$

suppressing the field dependence of the propagator and the three-point function. To arrive at this expression, we used Eq. (3.16) to evaluate the ϕ -derivative of the propagator as follows

$$\frac{\delta}{\delta \phi(z_1)} G[\phi](x, y) = i \int_{\mathcal{C}, z_2 z_3} G[\phi](x, z_2) \Gamma^{(3)}[\phi](z_1, z_2, z_3) G[\phi](z_3, y).$$

Moreover, we employed $\langle (\partial_{x^0} \varphi_x)(\partial_{x^0} \varphi_x) \rangle = \lim_{y \rightarrow x} \partial_{x^0} \partial_{y^0} \langle \varphi_x \varphi_y \rangle$ to separate the time derivatives from the microscopic fields φ .

Expression Eq. (5.15) already allows to compute the energy for our results of Sec. 5.4. However, due to the simple one-loop structure of the Dyson-Schwinger equations in the ϕ^3 -theory, we can simplify this considerably without any approximations, taking into account the fully dressed vertex $\Gamma^{(3)}$ as follows: Note that the last term in Eq. (5.15) is the vacuum sunset term. Its one loop subgraph appears in the DSE (4.21) of the two-point function in the ϕ^3 -theory. Contracting the DSE (4.21) with the propagator leads us to

$$\frac{i\lambda}{3!} \int_{\mathcal{C}, z_1 z_2 z_3} \Gamma^{(3)}(z_1, z_2, z_3) \prod_{i=1}^3 G(x, z_i) = \frac{1}{3} \int_{\mathcal{C}, z} \left[S^{(2)}(x, z) - \Gamma^{(2)}(x, z) \right] G(z, x).$$

The second term on the right-hand side is proportional to an irrelevant, field-independent constant, namely $(\Gamma^{(2)} \cdot G)_{xx} = i \delta_{\mathcal{C}, xx}$, while the first one simply changes the prefactors of the first two terms involving the propagator on the right-hand side of Eq. (5.15).

Performing a Fourier transform with respect to the spatial coordinates, we arrive at

$$\begin{aligned} \langle T_{00}(t) \rangle &= \mathcal{H}[\bar{\phi}] + \frac{5}{6} \lim_{t \rightarrow t'} \partial_t \partial_{t'} \int_{\mathbf{p}} G(t, t'; \mathbf{p}) + \frac{1}{6} \int_{\mathbf{p}} (\mathbf{p}^2 + m_0^2) G(t, t; \mathbf{p}) \\ &\quad + \frac{\lambda}{2} \bar{\phi}(t) \int_{\mathbf{p}} G(t, t, \mathbf{p}). \end{aligned} \quad (5.16)$$

The factor in front of the propagator in the third term in the first line is just the square of the classical (initial) dispersion: $\omega_{\mathbf{p}}^2 = \mathbf{p}^2 + m_0^2$. Note that the different prefactors of the two propagator terms in the first line in Eq. (5.16) arise since there is a relative minus sign between the temporal part of $(S^{(2)} \cdot G)_{xx}$ and the part containing the dispersion, whereas these contributions appear with the same signs in the energy.

Importantly, observe that the explicit occurrence of $\Gamma^{(3)}$ has dropped out in Eq. (5.16). We emphasise that this remarkably simple expression is no approximation but the complete result for the ϕ^3 -theory. Compared to Eq. (5.15) which contains the vertex, Eq. (5.16) has the advantage that it is easier and more accurately evaluable numerically since it only contains one integral. We remark Eq. (5.16) is trivially self-consistent with any approximation of the dynamics of the three-point function since the three-point function does not enter explicitly. Note that Eq. (5.16) readily extends to all components of the expectation value of the energy momentum tensor $\langle T_{\mu\nu} \rangle$.

5.6.2. Numerical Result

Using the fact that $\rho(t, t, \mathbf{p}) = 0$ in general and that $\bar{\phi} \equiv 0$ in our truncation, the expression (5.16) simplifies, and we find for the total energy in our truncation

$$E(t) = \langle T_{00}(t) \rangle \Big|_{\bar{\phi} \equiv 0} = \frac{5}{6} \lim_{t \rightarrow t'} \partial_t \partial_{t'} \int_{\mathbf{p}} F(t, t'; \mathbf{p}) + \frac{1}{6} \int_{\mathbf{p}} (\mathbf{p}^2 + m_0^2) F(t, t; \mathbf{p}).$$

As was already mentioned, the truncation employed in this chapter corresponds to the lowest order in the 2PI loop expansion. The latter is known to maintain energy conservation. However, this may be violated in numerical implementations. As a consistency check, we show the relative error of the total energy in Fig. 5.5. After an initial period of small oscillations, the error stabilises at around 10^{-4} and the total energy is conserved.

5.6.3. Discussion

To understand the initial period of oscillations, recall the discussion in Sec. 4.9: Any general non-equilibrium initial state that is physically meaningful corresponds to an

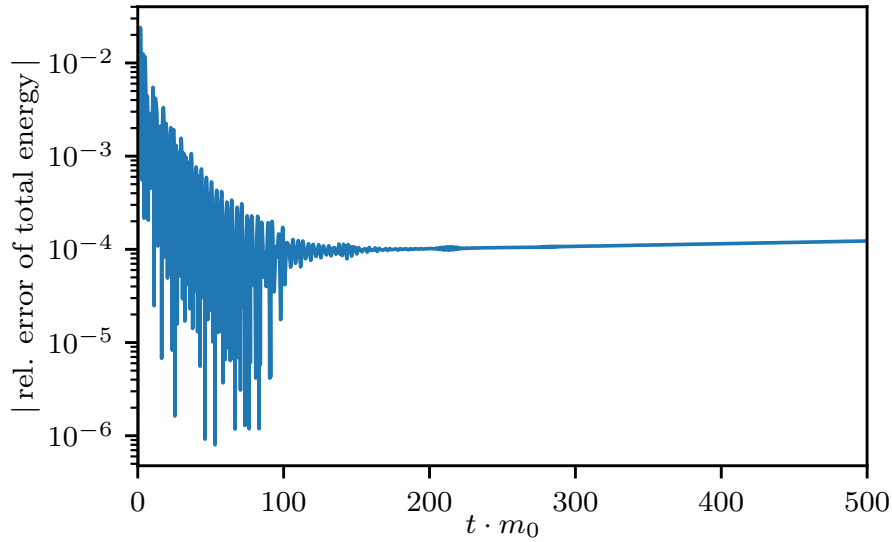


Figure 5.5.: Relative error of the total energy with respect to the initial total energy $|\frac{[E(t)-E(0)]}{E(0)}|$. After an initial period of small oscillations, the relative error stabilises at around 10^{-4} . Thus, energy is conserved. This figure is taken from [1].

instantaneous quench at t_0 . Accordingly, the energy for $t > t_0$ is conserved. Due to the sudden switching of the instantaneous quench, the state remains the same but its energy changes abruptly. Accordingly, it is to be expected that the energy is particularly sensitive to discretisation artefacts at t_0 . Our interpretation is to attribute the initial oscillations in Fig. 5.5 to this effect. However, keep in mind that Fig. 5.5 shows the relative error of the total energy. Thus, the observed oscillations are indeed small and a testament to the sufficiently high precision of the present computation.

5.7. Particle Number Conservation

For the discussion of particle number conservation, we use the following quantity:

$$\Delta f(t) = \frac{\int_p f(t,p) - f(0,p)}{\int_p |f(t,p) - f(0,p)|}. \quad (5.17)$$

It measures the sum of positive and negative flow of particle numbers normalised to the total flow. Put differently, at a given time t , it measures the change of the area enclosed by the occupations relative to the initial occupations (cf. Fig. 5.2), normalised to the total change. We show the quantity $\Delta f(t)$ in Fig. 5.6, and we find that the total

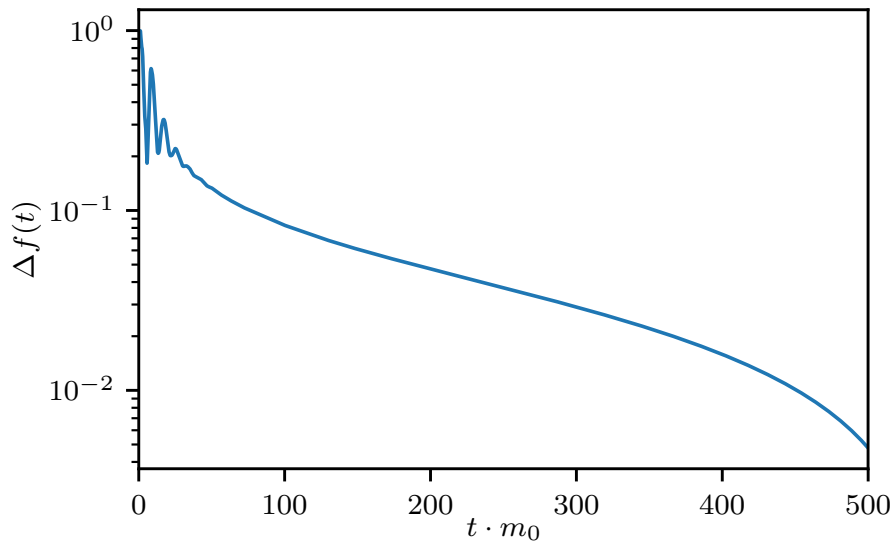


Figure 5.6.: Sum of positive and negative flow of particle numbers normalised to the difference of positive and negative flow (total flow) of particle numbers as defined in (5.17). After initial oscillations, the total particle number is conserved. This figure is taken from [1].

particle number is conserved.

5.8. Conclusion

We presented numerical solutions of the integrated flow in a truncation involving the propagator of the ϕ^3 -theory in 1 + 1 dimensions. Using over-occupied initial conditions, we found indications for the emergence of universal dynamics where the occupation numbers decay as a power law in momentum space. We obtained values in the range $\kappa \in [5.57, 5.69]$ for the momentum power law exponent κ at the time $t = 499.9/m_0$. Assuming a self-similar scaling behaviour for the temporal evolution, we found the following values for the corresponding exponents: $\alpha = 0.82, 1.03, 1.39$ and $\beta = -0.02, 0.02, 0.09$. The three values per exponent correspond to the times $tm_0 = 312.5, 375.0, 437.6$ respectively.

Critically assessing these results indicated that the potential scaling regime is not yet fully developed. To address the existence of a universal regime, the evolution should be continued to later times in future work. Assuming the existence of such a scaling regime, we compared our results to the literature. While this comparison indicates tensions between our results and the scaling discussed in the literature, these can not be resolved with the results currently available to us. Possible explanations for these obser-

vations include the absence of vertex dynamics in our truncation and the peculiarity of $1 + 1$ dimensions due to kinematic restrictions. We also discussed numerical instabilities that we encountered when varying the initial conditions and argued that these instabilities suggest the necessity of including vertex dynamics. As an important consistency check of our numerical implementation, we demonstrated that energy is conserved in our numerics. We also numerically demonstrated the conservation of the total particle number.

We derived the expectation value of the energy-momentum tensor in the ϕ^3 -theory and showed that it can be expressed solely in terms of the propagator and the macroscopic field. In particular, the three-point function does not contribute explicitly to the energy.

We implemented the explicit numerical method introduced in the last chapter for the integral equation of the propagator. We demonstrated numerically that this solution agrees with the one obtained by solving the equivalent, commonly used integro-differential equation for the propagator. Our results indicate that the explicit time-stepping algorithm for the integral equation leads to improved convergence properties compared to the one used to solve the integro-differential equation.

6. Towards Energy Conservation of Generic tFRG Truncations

We address energy conservation in generic tFRG truncations. To that end, we derive the flow of the energy-momentum tensor (EMT), and we discuss our result with regard to the trace anomaly of the EMT in Sec. 6.1. In Sec. 6.2, we perform a non-trivial consistency check of the obtained causal temporal flow of the EMT by analytically integrating this flow and showing that it is consistent with the symmetry identity of the expectation value of the EMT.

This chapter is in parts based on [3].

6.1. The Causal Flow of the Energy-Momentum Tensor

Here, we derive the flow of the EMT from the flow of the effective action, closely following the derivation of [153]. To that end, we compute

$$\partial_\tau T_{\tau, \mu\nu}[\phi](x) = \frac{2}{\sqrt{-g(x)}} \frac{\delta}{\delta g^{\mu\nu}(x)} \partial_\tau \Gamma_\tau[\phi, g] \Big|_{g^{\mu\nu}=\eta^{\mu\nu}} .$$

The derivative with respect to the metric $g^{\mu\nu}(x)$ is evaluated at the Minkowski metric $\eta^{\mu\nu}$. Here, $g := \det g_{\mu\nu}$ is the determinant of the metric. It proves useful to define the following derivative operator

$$\frac{1}{\sqrt{-g(x)}} \frac{\delta}{\delta g^{\mu\nu}(x)} (\dots) \Big|_{g^{\mu\nu}=\eta^{\mu\nu}} =: (\dots)'_{x, \mu\nu} .$$

We further introduce the following notation for CTP integrals with a volume element adequate for general curved backgrounds and the corresponding δ -distribution

$$\text{Tr}_a := \int_{\mathcal{C}, a} \sqrt{-g(a)}, \quad \mathbb{1}_{ab} := \frac{1}{\sqrt{-g(a)}} \delta_{\mathcal{C}, ab} .$$

In particular, this implies $\text{Tr}_a \mathbb{1}_{ab} = 1$. Using

$$\frac{\delta \sqrt{-g(a)}}{g^{\mu\nu}(b)} = -\frac{1}{2} \sqrt{-g(a)} g_{\mu\nu}(a) \delta_{\mathcal{C},ab}, \quad \frac{\delta \sqrt{-g(a)}}{\delta g^{\mu\nu}(b)} = -\frac{\delta}{\delta g^{\mu\nu}(a)} \frac{1}{\sqrt{-g(b)}},$$

it is straightforward to derive

$$(\text{Tr}_a)'_{x,\mu\nu} = -\frac{1}{2} g_{x,\mu\nu} \text{Tr}_a \mathbb{1}_{xa}, \quad (\mathbb{1}_{ab})'_{x,\mu\nu} = \frac{1}{2} (\sqrt{-g_x})^2 g_{x,\mu\nu} \mathbb{1}_{xa} \mathbb{1}_{ab}. \quad (6.1)$$

Note that for the right-hand side of $(\mathbb{1}_{ab})'_{x,\mu\nu}$, no sum (integral) over a is implied. Moreover, we introduced $g_{\mu\nu}(x) = g_{x,\mu\nu}$ and $g(x) = g_x$.

To determine the metric derivative of $\partial_\tau \Gamma_\tau$, we suppress the τ - and the field-dependence, to wit

$$\partial_\tau T_{\tau,\mu\nu}[\phi](x) = 2 (\partial_\tau \Gamma_\tau[\phi, g])'_{x,\mu\nu} = \left(\text{Tr}_a \text{Tr}_b G_{ab} \dot{R}_{ab} \right)'_{x,\mu\nu} \quad (6.2)$$

Here, we introduced $\partial_\tau R_\tau = \dot{R}$. Now, we obtain four contributions from the metric derivative. The derivatives of the traces can be evaluated according to Eq. (6.1). The derivative of \dot{R} requires no special attention. For the propagator, we must be careful: We know that the propagator is inversely related to the two-point function. Taking into account the metric dependence, this reads $\text{Tr}_2(\Gamma^{(2)} + R)_{12} G_{2b} = i \mathbb{1}_{1b}$. Here, we use a shorthand notation $z_1 \rightarrow 1$. To derive the metric derivative of the propagator, we consider

$$\begin{aligned} \text{Tr}_1 \left\{ G_{a1} \left[(\text{Tr}_2 G_{12}^{-1} G_{2b})'_{x,\mu\nu} \right] \right\} &= \text{Tr}_1 G_{a1} (\mathbb{1}_{1b})'_{x,\mu\nu} \\ &\Leftrightarrow \\ \text{Tr}_1 \left\{ G_{a1} \left[(\text{Tr}_2)'_{x,\mu\nu} G_{12}^{-1} G_{2b} \right] \right\} + \text{Tr}_1 \left\{ G_{a1} \left[\text{Tr}_2 (G_{12}^{-1})'_{x,\mu\nu} G_{2b} \right] \right\} &= \frac{1}{2} g_{x,\mu\nu} G_{ax} \mathbb{1}_{bx} \\ &+ \text{Tr}_1 \left\{ G_{a1} \left[\text{Tr}_2 G_{12}^{-1} (G_{2b})'_{x,\mu\nu} \right] \right\}. \end{aligned}$$

The term involving the derivative $(\text{Tr}_2)'_{x,\mu\nu}$ contributes $-1/2 g_{x,\mu\nu} G_{bx} \mathbb{1}_{ax}$. Thus, we find

$$(G_{ab})'_{x,\mu\nu} = i \text{Tr}_1 \text{Tr}_2 \left[G_{a1} \left(\Gamma_{12}^{(2)} + R_{12} \right)'_{x,\mu\nu} G_{2b} \right] + \frac{1}{2} g_{x,\mu\nu} (G_{ax} \mathbb{1}_{bx} + (a \leftrightarrow b)).$$

Note that the second term in $(G_{ab})'_{x,\mu\nu}$ cancels with the metric derivative of the traces

in Eq. (6.2). Thus, we arrive at the following expression for the flow of the EMT

$$\dot{T}_{x,\mu\nu} = \text{Tr}_{ab} G_{ab} (\dot{R}_{ab})'_{x,\mu\nu} + i \text{Tr}_{ab} \left(G \cdot \dot{R} \cdot G \right)_{ab} \left(\Gamma_{ab}^{(2)} + R_{ab} \right)'_{x,\mu\nu} \quad (6.3)$$

Here, we defined $\text{Tr}_{1\dots n} = \text{Tr}_1 \cdots \text{Tr}_n$. We remark that the above derivation is independent of the regulator. Accordingly, the same result is obtained for flows in momentum space. For the causal regulator used in this work, we can further simplify the flow of the EMT. To that end, we use that the metric dependence of the causal regulator is given by

$$-iR_{\tau,ab} = r_{\tau,x} \mathbb{1}_{ab}. \quad (6.4)$$

For the causal regulator (3.4), $r_{\tau,x}$ is either $+\infty$ or vanishes. In particular, Eq. (6.4) implies that the metric derivative of R_τ and $\partial_\tau R_\tau$ is the same. This allows us to further simplify Eq. (6.3). To that end, we use

$$\text{Tr}_{ab} G_{ab} (\dot{R}_{\tau,ab})'_{x,\mu\nu} = \frac{1}{2} (\sqrt{-g_x})^2 g_{x,\mu\nu} G_{xx} \dot{r}_{\tau,x} \Big|_{g_{\mu\nu}=\eta_{\mu\nu}}.$$

Next, we evaluate the flow at $\phi^+ = \bar{\phi} = \phi^-$. This allows us to use a remarkable property of the tFRG framework: $\partial_\tau G_\tau[\bar{\phi}] = i(G_\tau \partial_\tau R_\tau G_\tau)[\bar{\phi}]$. It was derived in Sec. 3.2.3. This allows us to combine the two terms in Eq. (6.3) involving the regulator, leading to a total τ -derivative. Thus, we need to determine $\partial_\tau (\int_{\mathcal{C},a} R_{\tau,xa} G_{\tau,xa})$. To evaluate this integral, we use

$$-i \int_{\mathcal{C},a \leq x^0} (\Gamma_{\tau,xa}^{(2)}[\bar{\phi}] + R_{\tau,xa}) G_{\tau,ay}[\bar{\phi}] + i \int_{\mathcal{C},a \leq x^0} \Gamma_{\tau,xa}^{(2)}[\bar{\phi}] G_{\tau,ay}[\bar{\phi}] = \begin{cases} 0 & \text{if } x^0 \leq \tau \\ \delta_{\mathcal{C},xy} & \text{if } x^0 > \tau \end{cases}. \quad (6.5)$$

This identity is derived as follows: Since all involved quantities are symmetric with respect to their space-time indices, we consider w.l.o.g. $x^0 > y^0$, and we use that on $\bar{\phi}$, times beyond the latest external time do not contribute to a CTP integral. If $x^0 \leq \tau$, the regulator vanishes and the remaining terms cancel. If $x^0 > \tau$, we use the fact that

the regulated propagator is the inverse of $-i(\Gamma_\tau^{(2)} + R_\tau)$ for all τ , to wit

$$-i \int_{\mathcal{C}, a \leq x^0} (\Gamma_{\tau, xa}^{(2)}[\bar{\phi}] + R_{\tau, xa}) G_{\tau, ay}[\bar{\phi}] = \delta_{\mathcal{C}, xy} .$$

The second term in Eq. (6.5) vanishes for $x^0 > \tau$ since the two-point function in this case equals $\Gamma_{t_0}^{(2)}$ which is diagonal and $G_{\tau, xy}$ vanishes. The causality-properties we used here have been derived in Sec. 3.2.

Therefore, we arrive at the remarkable fact that the metric derivatives of the causal regulator do not contribute to the flow of the EMT, which now reads

$$\partial_\tau T_{\tau, x, \mu\nu}[\bar{\phi}] = \frac{1}{2} \text{Tr}_{ab} T_{\tau, xab, \mu\nu}^{(2)}[\bar{\phi}] \partial_\tau G_{\tau, ab}[\bar{\phi}] . \quad (6.6)$$

Here, we defined $T_{\tau, xab, \mu\nu}^{(2)}[\phi] := 2 (\Gamma_{\tau, ab}^{(2)}[\phi])'_{x, \mu\nu}$. Eq. (6.6) constitutes an important result of the present work.

There are several ways in which the flow of the EMT can be used to address energy conservation in generic tFRG truncations. For instance, we can use the flow of the EMT to close a truncation. This entails to relate different correlators present in the truncation, using the flow of the EMT. Complementary, the (integrated) flow of the EMT could be used numerically to correct for potential violations of energy conservation. We remark that a suitable generalisation of the procedure discussed in [29] could also be attractive. The general idea would be to alleviate potential violations of energy conservation caused by the truncation by using a suitably constructed background $\bar{\phi}$.

We remark that Eq. (6.6) is of the same form as the standard flow equation for composite operators, cf. e.g. [33]. Note that this is generally not the case for the flow of the EMT. Indeed, in general the flow of the EMT is given by Eq. (6.3). The metric derivatives of the regulator present there are related to the so called trace anomaly. This refers to the following: In a classical theory that is scale-invariant, the trace of the EMT vanishes. In general, the corresponding quantum theory need not be scale-invariant. In this case, the classical vanishing of the trace of the EMT is broken by a quantum anomaly. This is for instance the case if the classical theory has to be renormalised in order to define the corresponding quantum theory.

In terms of the FRG, this implies the following: Consider to initialise the flow in a classically traceless theory that has a trace anomaly. If the flow of the EMT would be given by an equation of the form Eq. (6.6), the flow of the trace of the EMT would always vanish as a consequence classical tracelessness. Thus, Eq. (6.6) is not the correct equation in this case, but Eq. (6.3) must be used. On the other hand, if we initialise the

flow in the quantum theory, then the trace is non-vanishing from the start and Eq. (6.6) can be used.

For the causal temporal flow of this work, this can be understood by recalling the following: The unitary quantum dynamics described by the causal temporal flow does not alter the UV properties of the theory at hand. Thus, if we use renormalised initial conditions (cf. Sec. 4.7), the flow of the EMT is given by Eq. (6.6). On the other hand, if we choose to use (partially) unrenormalised initial conditions, we need to introduce an additional regularisation other than the causal temporal regulator. For instance, we can use a momentum regulator R_k which then leads to a combined momentum and temporal flow of the EMT of the form Eq. (6.3).

Note that in order to arrive at Eq. (6.6), the property $\partial_\tau G_\tau[\bar{\phi}] = i(G_\tau \partial_\tau R_\tau G_\tau)[\bar{\phi}]$ was crucial. In light of the previous discussion, this property holds only if we do not need to renormalise. This does not come as a surprise. Indeed, if we did not renormalise properly, products of propagators contain local parts (cf. Sec. 4.1.2) modifying the causality-properties of the temporal flow.

6.2. Integrated Causal Flow of the Energy-Momentum Tensor

Here, we integrate the causal flow of the EMT (cf. Eq. (6.6)) analytically. To that end, we introduce the shorthand notation

$$T_{xab,\mu\nu}^{(2)}[\bar{\phi}] * G_{ab}[\bar{\phi}] = \lim_{\xi \rightarrow 0^+} \int_{t_0}^{x^0 + \xi} d\tau T_{\tau,xab,\mu\nu}^{(2)}[\bar{\phi}] * \partial_\tau G_{\tau,ab}[\bar{\phi}],$$

where we make use of the *-product defined in Sec. 4.1. This allows us to express the integrated flow of the EMT as follows

$$T_{x,\mu\nu}[\bar{\phi}] - T_{t_0,x,\mu\nu}[\bar{\phi}] = \frac{1}{2} \text{Tr}_{ab} T_{xab,\mu\nu}^{(2)}[\bar{\phi}] * G_{ab}[\bar{\phi}]. \quad (6.7)$$

From Ch. 4, we know about the particular importance of local contributions to the flow. Accordingly, we define

$$T_{\tau,xab,\mu\nu}^{(2)} = T_{t_0,xab,\mu\nu}^{(2)} + \Delta T_{\tau,xab,\mu\nu}^{(2)} = T_{t_0,xab,\mu\nu}^{(2)} + \Delta T_{\text{nl},xab,\mu\nu}^{(2)} \theta_{\tau x} \theta_{\tau a} \theta_{\tau b} + \Delta T_{\text{local } \tau,xab,\mu\nu}^{(2)}.$$

Here, all contributions containing $\delta_{\mathcal{C}}$ -functions are contained in $\Delta T_{\text{local } \tau}^{(2)}$. Comparing with Eq. (6.7), we observe that $\Delta T_{\text{nl}}^{(2)}$ does not contribute to the integrated flow since

it does not fulfil the causal constraint of the EMT

$$\partial_\tau T_{\tau,x,\mu\nu}[\bar{\phi}] \propto \delta_{\tau x} \theta_{\tau x}. \quad (6.8)$$

Next, we discuss a non-trivial consistency check of Eq. (6.7): Here, we focus on T_{00} , i.e. the energy. To determine the right-hand side of Eq. (6.7), we use the diagrammatic representation of $T_{xab,00}^{(2)}[\bar{\phi}]$ which we obtain from the symmetry identity that encodes the conservation of energy in the quantum theory. Its derivation for the ϕ^3 -theory can be found in Sec. 5.6.1. Here, we consider a relativistic scalar field theory with microscopic three- and four-point interactions. Its classical Hamiltonian is given by

$$\mathcal{H}_x[\varphi] = \frac{1}{2} [\partial_{x_0}^2 + (-\partial_{\mathbf{x}}^2) + m^2] \varphi_x^2 + \frac{\lambda_3}{3!} \varphi_x^3 + \frac{\lambda_4}{4!} \varphi_x^4.$$

Using Eq. (5.14), we obtain for its expectation value

$$\begin{aligned} \langle \mathcal{H}_x[\varphi] \rangle &= T_{x,00}[\phi] = \mathcal{H}_x[\phi] + \frac{1}{2} \left[\mathcal{H}^{(2)}[\phi] G_x \right] + \lambda_4 \frac{i}{6} \left[\phi G_x^3 \Gamma^{(3)} \right] \\ &+ \lambda_3 \frac{i}{6} \left[G_x^3 \Gamma^{(3)} \right] + \lambda_4 \frac{1}{8} G_{xx}^2 - \lambda_4 \frac{1}{8} \left[G_x^4 \Gamma^{(3)} G \Gamma^{(3)} \right] + \lambda_4 \frac{i}{24} \left[G_x^4 \Gamma^{(4)} \right]. \end{aligned} \quad (6.9)$$

The second term in the first line contains the application of the kinetic operator ($\mathcal{H}^{(2)}[0]$) to the propagator as in the respective term in Eq. (5.15). In total, the second term in Eq. (6.9) reads

$$\frac{1}{2} \left[\mathcal{H}^{(2)}[\phi] G_x \right] = \frac{1}{2} \left[\mathcal{H}^{(2)}[0] G_x \right] + \lambda_3 \frac{1}{2} \left[\phi G_x \right] + \lambda_4 \frac{1}{4} \left[\phi^2 G_x \right] \quad (6.10)$$

The notation $[\phi^n G_x^m F]$ suppress the dependence on any internal space-time indices. Here, the fields always appear as ϕ_x^n and the m left most propagators of a diagram are given by $G_{x1} \cdots G_{xm}$ such that

$$[\phi^n G_x^m F] = \phi_x^n G_{x1} \cdots G_{xm} F_{1\dots m},$$

where $F_{1\dots m}$ is the rest of the diagram. For instance,

$$[G_x^4 \Gamma^{(3)} G \Gamma^{(3)}] = G_{x1} G_{x2} G_{x3} G_{x4} \Gamma_{125}^{(3)} G_{56} \Gamma_{634}^{(3)},$$

looks like a combination of the squint and the sunset diagram, cf. Fig. 4.2. Sums (integrals) over repeating internal indices are implied. It is convenient to give names to the individual diagrams in Eq. (6.9). The term involving G^2 is called the eight. We refer

to the terms involving G^3 as the sunset terms. The term with G^4 and $\Gamma^{(4)}$ is called the basketball. The term involving G^4 and $\Gamma^{(3)}$ is called the squint-sunset.

To identify the relevant contributions of Eq. (6.9) to $T_{xab}^{(2)}$, we use the integrated flow (6.7) and the causal constraint Eq. (6.8): Only terms that generate at least one $\delta_{\mathcal{C}}$ can contribute to the integrated flow. Thus, none of the field-derivatives of the terms in the second line in Eq. (6.9) have to be considered. The relevant local contributions to $T_{00}^{(2)}$ are given by

$$T_{\text{local},xab}^{(2)} = \mathcal{H}_{xab}^{(2)}[\phi] + \Delta T_{\text{local},xab}^{(2)}. \quad (6.11)$$

Here, $\mathcal{H}_{xab}^{(2)}[\phi] = \delta\mathcal{H}_x[\phi]/\delta\phi_a\delta\phi_b$. Note that the derivatives of the kinetic term for G are also non-local while the other two terms in Eq. (6.10) generate local contributions. In total, we obtain

$$\begin{aligned} \Delta T_{\text{local},xab}^{(2)} = & \lambda_3 \frac{i}{2} \left[G_x^2 \Gamma_a^{(3)} \delta_{\mathcal{C},xb} + (a \leftrightarrow b) \right] + \lambda_4 \frac{i}{2} \left[\phi G_x^2 \Gamma_a^{(3)} \delta_{\mathcal{C},xb} + (a \leftrightarrow b) \right] \\ & + \lambda_4 \frac{1}{2} \left[G_x \delta_{\mathcal{C}xa} \delta_{\mathcal{C}xb} \right] + \lambda_4 \frac{i}{6} \left[G_x^3 \Gamma_a^{(4)} \delta_{\mathcal{C},xb} + (a \leftrightarrow b) \right] - \lambda_4 \frac{1}{2} \left[G_x^3 \Gamma_a^{(3)} G \Gamma^{(3)} \delta_{\mathcal{C},xb} + (a \leftrightarrow b) \right] \end{aligned} \quad (6.12)$$

The first term is generated from $[\phi G_x]$. The second and the third term are generated from $[\phi^2 G_x]$. The last two terms are due to $[\phi G_x^3 \Gamma^{(3)}]$. Note that for all these term, at least one field must be hit by the ϕ -derivative to generate a local contribution.

Now we can reintroduce the τ -dependence and insert Eq. (6.11) into the integrated flow Eq. (6.7). Notably, the indices ab of all terms in Eq. (6.11) get closed by the τ -derivative of the propagator, $\partial_\tau G_{\tau,ab}$. Thus, $\mathcal{H}_{\tau,xab}^{(2)}[\bar{\phi}] * G_{\tau,ab}[\bar{\phi}]$ gives rise to $[\mathcal{H}^{(2)}[\bar{\phi}] G_x]$. Note that $\bar{\phi}_x$ does not contribute any $\theta_{\tau x}$ and the $*$ -product reduces to the standard one for $\mathcal{H}_{\tau,xab}^{(2)}$. For the diagrams of $\Delta T_{\text{local},xab}^{(2)}$, the $*$ -product has to be evaluated. To that end, observe that closing the first two terms in Eq. (6.12) gives rise to the sunset terms. The remaining terms generate the eight, the basketball and the squint-sunset. The corresponding contributions from the $*$ -product can be found in Tab. 6.1. Combining the factors of Tab. 6.1 with the ones already present in Eq. (6.12) and the overall factor of

diagram	$\partial_\tau G_{\tau,ab} * \Delta T_{\text{local } \tau, xab}^{(2)}$	factor
eight	$\partial_\tau G_{\tau,ab} * G_{\tau,xx} \delta_{\mathcal{C},xa} \delta_{\mathcal{C},xb}$	2/4
sunset	$[\partial_\tau G_{\tau,ab} * G_{\tau,x}^2 \delta_{\mathcal{C},x(a\leftrightarrow b)} \Gamma_{\tau,a}^{(3)}]$	2/3
basketball	$[\partial_\tau G_{\tau,ab} * G_{\tau,x}^3 \delta_{\mathcal{C},x(a\leftrightarrow b)} \Gamma_{\tau,a}^{(4)}]$	2/4
squint-sunset	$[\partial_\tau G_{\tau,ab} * G_{\tau,x}^3 \delta_{\mathcal{C},x(a\leftrightarrow b)} \Gamma_{\tau,a}^{(3)} G_\tau \Gamma_\tau^{(3)}]$	2/4

Table 6.1.: Factors due to the evaluation of the *-product for the respective diagrams. The *-product was defined in Sec. 4.1. Here, $[\dots \delta_{\mathcal{C},x(a\leftrightarrow b)} \dots] = [\dots \delta_{\mathcal{C},xb} \dots] + [\dots \delta_{\mathcal{C},xa} \dots]$, cf. Eq. (6.12).

1/2 of the flow, cf. Eq. (6.7), the integrated flow of the EMT reads

$$\begin{aligned}
 T_{x,00}[\bar{\phi}] - T_{t_0,x,00}[\bar{\phi}] &= \frac{1}{2} \left[\mathcal{H}^{(2)}[\phi] G_x \right] + \lambda_4 \frac{i}{6} \left[\phi G_x^3 \Gamma^{(3)} \right] \\
 &+ \lambda_3 \frac{i}{6} \left[G_x^3 \Gamma^{(3)} \right] + \lambda_4 \frac{1}{8} G_{xx}^2 - \lambda_4 \frac{1}{8} \left[G_x^4 \Gamma^{(3)} G \Gamma^{(3)} \right] + \lambda_4 \frac{i}{24} \left[G_x^4 \Gamma^{(4)} \right].
 \end{aligned} \tag{6.13}$$

To determine $T_{t_0,x,00}[\bar{\phi}]$, recall that it is given by $T_{\tau=t_0,x,00}[\bar{\phi}]$. By comparing with Eq. (6.9), we observe that for $\tau = t_0$, there is the classical energy $\mathcal{H}_x[\bar{\phi}]$ as well as the energy of the initial correlations $\mathcal{I}_{t_0}^{(n)}$ which enter in $\Gamma_{t_0}^{(n)} = S^{(n)} + \mathcal{I}_{t_0}^{(n)}$, cf. Eq. (3.19). Note that in Eq. (6.13), we tacitly absorbed all contributions to the integrated flow involving G_{t_0} into the initial condition. Thus, all that is left of the initial energy in Eq. (6.13) is given by the classical energy $\mathcal{H}_x[\bar{\phi}]$. We remark that the diagrams on the right-hand side of Eq. (6.13) contain the energy of the initial correlations. We remark that Eq. (6.13) readily extends to all components of the EMT.

Eq. (6.13) is a remarkable demonstration of the consistency of the tFRG formalism: The integrated causal temporal flow of the EMT is consistent with the symmetry identity (6.9) of the expectation value of the EMT. Recall that this symmetry identity encodes the conservation of energy and momentum in the quantum theory. This section again demonstrates the power of the causal constraints inherent to the tFRG. These constraints greatly simplified the above derivation as the number of relevant diagrammatic contributions was reduced dramatically. As a consequence of the consistency of the tFRG

formalism, evaluating the respective $*$ -products of the local contributions to the flow gives rise to the correct prefactors for all appearing diagrams.

6.3. Conclusion

We derived the flow of the energy-momentum tensor for general regulators. Using the causal temporal regulator, the general flow reduced to the known flow of composite operators. This equation is known to miss important contributions if there is a trace anomaly. We resolved this tension by pointing out the role of renormalised initial conditions for the causal temporal flow.

We integrated the causal flow of the energy-momentum tensor analytically and demonstrated that it is consistent with the usual symmetry identity of the expectation value energy-momentum tensor.

7. Summary and Outlook

In this work, we substantially advanced the framework of the temporal functional renormalisation group (tFRG) which constitutes a non-perturbative method that grants access to the dynamics of correlation functions in quantum field theory. Leveraging causality, we demonstrated that the general causal temporal flow can be integrated analytically, leading to novel one-loop exact equations for the fully dressed correlation functions. The integration is facilitated using local causal constraints which are a distinct feature of the tFRG approach. These constraints make the causality of quantum dynamics manifest. They constrain the admissible causal structures that appear in the flow equation and in the causally regulated correlation functions. Their origin stems from the usage of a sharp temporal regulator which suppresses fluctuations beyond the present time.

We revisited the derivation of the temporal flow equation, carefully paying attention to properties and subtleties that originate from the causal temporal regulator. In doing so, we clarified that general space-time dependent backgrounds are admissible in the tFRG approach, and we showed that the causal regulator respects the unitarity of quantum dynamics. Since the tFRG allows for very general classes of non-perturbative approximations, unitarity can be violated in generic truncations of the infinite hierarchy of flow equations. For these cases, we proposed to restore unitarity by taking into account the BRST-symmetries of the Schwinger-Keldysh closed time path on which the dynamical correlation functions are defined.

We discussed the derivation of the causality-properties enjoyed by the regulated, flowing correlators. From these properties, we derived the causal constraints for the temporal flow which allow the analytic integration thereof. In this process, we discovered that the structure of the microscopic interactions present in a given theory dictates the degree of locality of all vertex corrections generated by the flow. In particular, we showed that a microscopic three-point interaction alone does not lead to any local corrections for any vertex. On the other hand, as soon as there is a microscopic four-point interaction present, all vertices receive local corrections. Accordingly, a scalar field theory with microscopic three- and four-point vertices served as an explicit – and general – example, for which we demonstrated the analytic integration of the flow of the one- and the two-

point function and of the effective action. We remark that the analytic integration of the temporal flow readily extends to higher correlation functions. Let us emphasise that the analytic integration of other flow equations is only possible in certain special cases, while it is generic for the causal temporal flow, and its causal constraints are essential in this regard. For the flow itself, these lead to challenges with regard to its numerical integration and we discussed these in detail. We emphasise that these challenges are absent for the analytically integrated flow.

We derived the complete hierarchy of Dyson-Schwinger equations as a particular truncation of the temporal flow, using the manifest causality of the tFRG formalism. Reproducing the correct prefactors of the two-loop terms in the Dyson-Schwinger equations constitutes a highly non-trivial demonstration of the internal consistency of the tFRG framework. Moreover, we derived a truncation of the integrated flow containing an s -channel effective vertex. We showed that our result is able to reproduce the 2PI $1/N$ expansion at next-to-leading order.

We solved the problem of renormalising the causal temporal flow in general. Its renormalisation is concerned with the initial conditions alone. Due to the one-loop structure of the flow, the absence of subdivergencies is manifest. For the concrete example of the ϕ^4 -theory in $3 + 1$ dimensions, we explicitly derived the corresponding renormalised initial conditions.

We derived an algorithm that allows to solve certain types of causal integral equations like the Dyson equation for the propagator or the Bethe-Salpeter equation for the effective vertex in the form of an explicit numerical method, involving only sums over known values. We verified numerically that this algorithm reproduces the solution of the commonly used integro-differential for the propagator. Our results indicate that the explicit method for the integral equation leads to improved convergence properties compared to the one used to solve the integro-differential equation.

We identified the origin of the memory integrals present in the (integrated) temporal flow. We discussed how to match correlated, i.e. non-Gaussian initial states at different times in the tFRG framework. We outlined how entirely time-local evolution equations for the correlation functions could be obtained from the temporal flow, using a non-diagonal regulator that is designed to ensure a causal time evolution forward and backward in time.

We numerically solved the integrated flow in a truncation of the ϕ^3 -theory in $1 + 1$ dimensions. Using over-occupied initial conditions, we found indications for the emergence of universal dynamics for the propagator, and we determined the corresponding momentum power law and the temporal scaling exponents. Comparing our observations to the

literature indicated tensions which can not be resolved within the currently available results. Possible explanations for the observed tensions include the absence of vertex dynamics in our truncation and the peculiarity of $1 + 1$ dimensions due to kinematic restrictions.

We addressed the conservation of energy in generic tFRG truncations. As these truncations can be specified on the level of the individual correlators, they do not in general correspond to an approximation that can be obtained from an effective action. Thus, conservation of energy is not guaranteed automatically but becomes a non-trivial feature instead. In this regard, we derived the flow of the energy-momentum tensor for general regulators. Using the causal temporal regulator, the general flow reduced to the known flow of composite operators. This equation is known to miss important contributions if there is a trace anomaly. We resolved this tension by pointing out the role of renormalised initial conditions for the temporal flow. We integrated the causal flow of the energy-momentum tensor analytically and demonstrated that it is consistent with the usual symmetry identity of the expectation value of the energy-momentum tensor.

With regard to future work, there are several interesting avenues to pursue. One long-term goal of the tFRG framework is to compute the dynamics of quantum gauge theories from first principles. This is relevant to describe quantum dynamics in the standard model and in QCD in particular. To that end, the dynamics of an abelian gauge theory with and without matter in terms of scalars and fermions should be addressed. The next major milestone would be to consider the quantum dynamics of Yang-Mills theory. With regard to universal dynamics, the tFRG framework allows to extend the scaling analysis known from the propagator to the fully dressed vertices. This could contribute to a more refined picture of dynamic universality classes. In this regard, the temporal flow equation in terms of dimensionless variables should be derived. Moreover, there is the interesting possibility to explore equilibrium applications of the tFRG according to the proposal outlined in this work. The causal temporal flow of the energy-momentum tensor derived in this work provides a solid starting point to explore general unitary and energy-conserving tFRG truncations. The manifest causality and the one-loop exact nature of the (integrated) causal temporal flow will certainly be beneficial in all these endeavours.

A. Closed Time Path Notation and Propagator Bases

In this appendix, we discuss the CTP notation and introduce CTP propagator bases relevant for the present work. Note that in this appendix, we do not notationally distinguish between complex times, i.e. times on the CTP and real times. Which case applies can be inferred from the context. More details regarding the CTP can be for example found in [12, 14, 77, 93, 154].

First, let us introduce the δ -distribution on the contour $\mathcal{C} = \mathcal{C}^+ \cup \mathcal{C}^-$

$$\delta_{\mathcal{C}}(x - y) := \delta_{\mathcal{C}}(x^0 - y^0) \delta(\mathbf{x} - \mathbf{y}),$$

where

$$\delta_{\mathcal{C}}(x^0 - y^0) := \begin{cases} \delta(x^0 - y^0) & \text{if } x^0 \text{ and } y^0 \text{ on } \mathcal{C}^+ \\ -\delta(x^0 - y^0) & \text{if } x^0 \text{ and } y^0 \text{ on } \mathcal{C}^- \\ 0 & \text{else} \end{cases}.$$

With this definition, we get $\int_{\mathcal{C}, x} \delta_{\mathcal{C}}(x) = 1$. Functional differentiation for CTP quantities is defined as

$$\frac{\delta J(x)}{\delta J(y)} := \delta_{\mathcal{C}}(x - y).$$

It is useful to consider connected correlation functions which are generated by the Schwinger functional

$$W[J; \rho_{t_0}] := -i \ln Z[J; \rho_{t_0}].$$

The one-point function, also often referred to as the macroscopic field, is given by

$$\bar{\phi}(x) := \left. \frac{\delta W[J; \rho_{t_0}]}{\delta J(x)} \right|_{J=0} = \langle \Phi(x) \rangle.$$

Note that for a single operator at $J = 0$, there is no difference between inserting it on \mathcal{C}^+ or \mathcal{C}^- . Before evaluating the functional derivatives however, the real-time currents J^+ and J^- are not equal in general. Accordingly, as long as $J^+ \neq J^-$, there are two independent, in general complex-valued, real-time fields ϕ^+, ϕ^- , cf. e.g. [77]. The physical field $\bar{\phi}$ is given by evaluating $\delta W/\delta J$ at $J^+ = J^-$, and setting both real-time currents to zero constitutes a valid choice. The respective real-time field $\bar{\phi}$ is then real-valued.

Next, we continue to define the propagator

$$G(x, y) = -i \left. \frac{\delta^2 W[J; \rho_{t_0}]}{\delta J(x) \delta J(y)} \right|_{J=0} = \langle \mathcal{T}_{\mathcal{C}} \Phi(x) \Phi(y) \rangle - \bar{\phi}(x) \bar{\phi}(y).$$

We can make the time-ordering on the CTP explicit by defining a contour step-function,

$$\theta_{\mathcal{C}}(x^0 - y^0) := \begin{cases} \theta(x^0 - y^0) & \text{if } x^0, y^0 \in \mathcal{C}^+ \\ \theta(y^0 - x^0) & \text{if } x^0, y^0 \in \mathcal{C}^- \\ 1 & \text{if } x^0 \in \mathcal{C}^-, y^0 \in \mathcal{C}^+ \\ 0 & \text{if } x^0 \in \mathcal{C}^+, y^0 \in \mathcal{C}^- \end{cases},$$

where

$$\theta(x^0 - y^0) := \begin{cases} 1 & \text{if } x^0 > y^0 \\ 0 & \text{if } x^0 < y^0 \end{cases}.$$

In particular, $d\theta_{\mathcal{C}}(x^0 - y^0)/dx^0 = \delta_{\mathcal{C}}(x^0 - y^0)$. Thus, we can express the CTP propagator as

$$G(x, y) = \theta_{\mathcal{C}}(x^0 - y^0) \langle \Phi(x) \Phi(y) \rangle + \theta_{\mathcal{C}}(y^0 - x^0) \langle \Phi(y) \Phi(x) \rangle - \bar{\phi}(x) \bar{\phi}(y).$$

From the definition of the contour step-function, we get

$$\langle \mathcal{T}_C \Phi(x) \Phi(y) \rangle = \begin{cases} \theta_{xy} \langle \Phi(x) \Phi(y) \rangle + \theta_{yx} \langle \Phi(y) \Phi(x) \rangle & \text{if } x^0, y^0 \in \mathcal{C}^+ \\ \theta_{xy} \langle \Phi(y) \Phi(x) \rangle + \theta_{yx} \langle \Phi(x) \Phi(y) \rangle & \text{if } x^0, y^0 \in \mathcal{C}^- \\ \langle \Phi(x) \Phi(y) \rangle & \text{if } x^0 \in \mathcal{C}^-, y^0 \in \mathcal{C}^+ \\ \langle \Phi(y) \Phi(x) \rangle & \text{if } x^0 \in \mathcal{C}^+, y^0 \in \mathcal{C}^- \end{cases}. \quad (\text{A.1})$$

Here, we introduced the notation $\theta_{xy} = \theta(x^0 - y^0)$. The first line is the time-ordered propagator also known as the Feynman propagator. The second line is the anti-time-ordered propagator also known as the Dyson propagator. The two lower lines are referred to as Wightman functions or Wightman propagators. It is clear that the Wightman functions can be used to express the time-ordered and anti-time-ordered propagators.

So far, we considered times on the CTP, i.e. complex times. For some applications, a representation in terms of real-time quantities is however more convenient. To that end, we introduce the component notation

$$G^{\pm\pm}(x, y) = -i \frac{\delta W[J; \rho_{t_0}]}{\delta J_{\pm}(x) \delta J_{\pm}(y)} \Big|_{J=0}.$$

Thus, instead of working with times on the CTP, we can use real times and keep track of the CTP ordering using the two-valued index \pm . We call this basis the \pm -basis. The corresponding metric is

$$c_{\alpha\beta} = \begin{pmatrix} 1 & 0 \\ 0 & -1 \end{pmatrix}_{\alpha\beta}, \quad (\text{A.2})$$

such that $J^+ = J_+$ and $J^- = -J_-$. The propagator with real time arguments is then given by the matrix

$$G(x, y) = \begin{pmatrix} G^{++}(x, y) & G^{+-}(x, y) \\ G^{-+}(x, y) & G^{--}(x, y) \end{pmatrix}. \quad (\text{A.3})$$

As mentioned in Sec. 2.1, not all of its components are independent. From the explicit

time-ordering given in Eq. (A.1), we can directly verify the constraint

$$G^{++}(x, y) + G^{--}(x, y) = G^{+-}(x, y) + G^{-+}(x, y).$$

This can be written in more compactly as follows, using the metric (A.2),

$$\sum_{\substack{\alpha=\pm \\ \beta=\pm}} G_{\alpha\beta}(x, y) = 0.$$

There exist several common bases choices for G which can be obtained from a linear transformation of the matrix G , cf. e.g. [154]. Moreover, there is the completely real basis which involves the expectation values of the commutator and anti-commutator of two field operators [14]. These are real-time, real-valued functions, to wit

$$\begin{aligned} \langle \mathcal{T}_C \Phi(x) \Phi(y) \rangle &= \frac{1}{2} \langle \{\Phi(x), \Phi(y)\} \rangle (\theta_C(x^0 - y^0) + \theta_C(y^0 - x^0)) \\ &\quad - \frac{i}{2} \langle [\Phi(x), \Phi(y)] \rangle (\theta_C(x^0 - y^0) - \theta_C(y^0 - x^0)). \end{aligned}$$

We define $\text{sgn}_C(x^0 - y^0) := \theta_C(x^0 - y^0) - \theta_C(y^0 - x^0)$ and obtain

$$\begin{aligned} F(x, y) &:= \frac{1}{2} \langle \{\Phi(x), \Phi(y)\} \rangle - \bar{\phi}(x)\bar{\phi}(y) \\ \rho(x, y) &:= i \langle [\Phi(x), \Phi(y)] \rangle. \end{aligned}$$

F is called the statistical propagator and ρ is called the spectral function. Then, the CTP propagator can then be expressed as

$$G(x, y) = F(x, y) - \frac{i}{2} \rho(x, y) \text{sgn}_C(x^0 - y^0). \quad (\text{A.4})$$

The completely real basis is particularly advantageous in numerical applications. We discuss this fact and the issues with the basis (A.3) in numerical applications in Sec. 3.3.

$$\begin{aligned}
 \partial_\tau \Gamma_{\tau,xya}^{(3)} = & -\frac{1}{4} \left[\begin{array}{c} x \\ \tau \\ y \end{array} \begin{array}{c} \tau \\ \tau \end{array} \begin{array}{c} a \\ \tau \end{array} + \begin{array}{c} x \\ \tau \\ y \end{array} \begin{array}{c} \tau \\ \tau \end{array} \begin{array}{c} a \\ \tau \end{array} + P(x, y, a) \right] \\
 & - i \left[\begin{array}{c} x \\ \tau \\ y \end{array} \begin{array}{c} \tau \\ \tau \end{array} \begin{array}{c} a \\ \tau \end{array} + \begin{array}{c} x \\ \tau \\ y \end{array} \begin{array}{c} \tau \\ \tau \end{array} \begin{array}{c} a \\ \tau \end{array} + \begin{array}{c} x \\ \tau \\ y \end{array} \begin{array}{c} \tau \\ \tau \end{array} \begin{array}{c} a \\ \tau \end{array} \right] \\
 & + \frac{i}{2} \begin{array}{c} \tau \\ \tau \end{array} \begin{array}{c} a \\ \tau \end{array}
 \end{aligned}$$

Figure B.2.: General flow equation for $\Gamma_\tau^{(3)}[\phi]$. Symbols as in Fig. B.1. The diagrams in the first line are referred to as swordfish diagrams. The diagrams in the second line are referred to as triangle diagrams. By $P(x, y, \dots)$, we denote a sum over the respective previous terms containing the remaining permutations of (x, y, \dots) .

$$\begin{aligned}
 \partial_\tau \Gamma_{\tau,xyab}^{(4)} = & \left\{ -\frac{i}{4} \left[\begin{array}{c} x \\ \tau \\ y \end{array} \begin{array}{c} \tau \\ \tau \\ \tau \end{array} \begin{array}{c} a \\ b \end{array} \right] + \begin{array}{c} x \\ \tau \\ y \end{array} \begin{array}{c} \tau \\ \tau \\ \tau \end{array} \begin{array}{c} a \\ b \end{array} + \begin{array}{c} x \\ \tau \\ y \end{array} \begin{array}{c} \tau \\ \tau \\ \tau \end{array} \begin{array}{c} a \\ b \end{array} \right] \\
 & - \frac{1}{16} \left[\begin{array}{c} x \\ \tau \\ y \end{array} \begin{array}{c} \tau \\ \tau \\ \tau \end{array} \begin{array}{c} a \\ b \end{array} + \begin{array}{c} x \\ \tau \\ y \end{array} \begin{array}{c} \tau \\ \tau \\ \tau \end{array} \begin{array}{c} a \\ b \end{array} \right] \\
 & - \frac{1}{12} \left[\begin{array}{c} x \\ \tau \\ y \end{array} \begin{array}{c} \tau \\ \tau \\ \tau \end{array} \begin{array}{c} a \\ b \end{array} + \begin{array}{c} x \\ \tau \\ y \end{array} \begin{array}{c} \tau \\ \tau \\ \tau \end{array} \begin{array}{c} a \\ b \end{array} \right] + P(x, y, a, b) \left. \vphantom{\partial_\tau \Gamma_{\tau,xyab}^{(4)}}} \right\} \\
 & + 3 \left[\begin{array}{c} x \\ \tau \\ y \end{array} \begin{array}{c} \tau \\ \tau \\ \tau \end{array} \begin{array}{c} a \\ b \end{array} + \begin{array}{c} x \\ \tau \\ y \end{array} \begin{array}{c} \tau \\ \tau \\ \tau \end{array} \begin{array}{c} a \\ b \end{array} + \begin{array}{c} x \\ \tau \\ y \end{array} \begin{array}{c} \tau \\ \tau \\ \tau \end{array} \begin{array}{c} a \\ b \end{array} + \begin{array}{c} x \\ \tau \\ y \end{array} \begin{array}{c} \tau \\ \tau \\ \tau \end{array} \begin{array}{c} a \\ b \end{array} \right] \\
 & + \frac{i}{2} \begin{array}{c} \tau \\ \tau \\ \tau \end{array} \begin{array}{c} a \\ b \end{array}
 \end{aligned}$$

Figure B.3.: General flow equation for $\Gamma_\tau^{(4)}[\phi]$. Symbols as in Fig. B.1. The diagrams in the second line are referred to as fish diagrams. The diagrams in the fourth line are referred to as box diagrams. By $P(x, y, \dots)$, we denote a sum over the respective previous terms containing the remaining permutations of (x, y, \dots) .

C. Numerical Results for the Propagator from Its Integral Equation

We present results for the propagator of the ϕ^3 -theory in $1 + 1$ dimensions, cf. Ch. 5 for details. In particular, we solve the Dyson equation (5.6) for the propagator, which constitutes a causal integral equation of the type discussed in Sec. 4.8. Accordingly, the algorithm derived there can be applied to solve this integral equation in terms of an explicit time-stepping. Notably, this involves only sums over known values. We remark that typically, these types of integral equations are solved by some type of fixed point iteration. We compare the results of the explicitly solved integral equation to the numerical solution of the commonly used integro-differential equation for the propagator (5.5). We refer to the corresponding programs as the explicit solver and the differential solver respectively.

The initial conditions and the parameters used to obtain the results shown in this section are the same as those discussed in in Sec. 5.3 and Sec. 5.4. To solve the integro-differential equation (5.5), we use a symmetric discretisation of the second-order time-derivative. This allows us to use the simple explicit Euler method to compute the solution. More details can be found e.g. in [14, 139]. All integrals are computed using a trapezoidal rule.

In all of the following figures, we show the statistical propagator F . It is the real part of the propagator, cf. App. A. In particular, we consider $F(0, t, p = 4.04m_0)$. In Fig. C.1, we show the solution for F for three different time-step sizes $\Delta\tilde{t} = \Delta t \cdot m_0$ as obtained from the differential solver. For a decreasing step size, the curves get closer to each other. We do not observe an instability for the step sizes used. In Fig. C.2, we show the solution for F as obtained from the explicit solver for the same times as in Fig. C.1 and the same step sizes. We observe that the curves are perfectly on top of each other for all shown step sizes. This indicates that, the explicit solver converges faster than the differential one.

We proceed by showing that both methods agree for sufficiently small step sizes. This can be seen from Fig. C.3, where we compare both solvers for the smallest available step size. Let us emphasise that the same agreement is obtained, comparing the largest

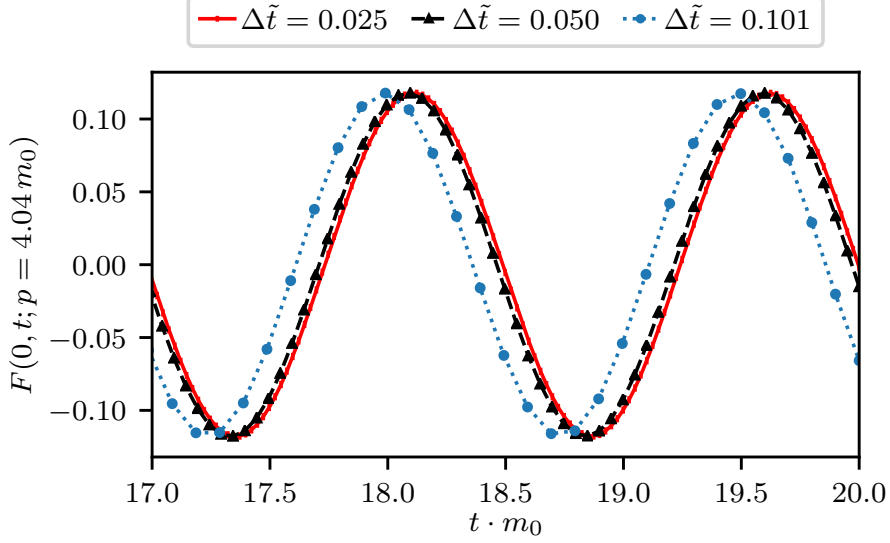


Figure C.1.: Time evolution of the statistical propagator F obtained using the *differential solver* for various time resolutions $\Delta\tilde{t} = \Delta t \cdot m_0$. The curves get closer to each other for decreasing time-step size. This figure is taken from [1].

step size for the explicit solver with the smallest one of the differential solver. Hence, we demonstrated that explicitly solving the Dyson equation by the algorithm derived in Sec. 4.8 agrees to numerical precision with the commonly used integro-differential approach. This has, to the best of our knowledge, not been discussed in the literature before. Taking a closer look at Fig. C.3, we see that the black dashed line is still slightly shifted compared to the red one. This again indicates the faster convergence of the explicit solver. The faster convergence comes at the price of an additional time integral that has to be computed. However, the differential solver requires a smaller time-step size to produce results of the same accuracy. For the results shown in this appendix for $\Delta\tilde{t} = 0.025$ for the differential solver and $\Delta\tilde{t} = 0.101$ for the explicit solver, the runtime of both solvers is comparable (same order of magnitude). While we did not perform a detailed quantitative analysis of the required computation time, solving the integral equation (5.6) explicitly certainly improves the numerical stability and the required computation time as compared to iterating it since the explicit method only involves sums over known values. It would be interesting to perform a quantitative comparison between the explicit and the differential solver, assessing which outperforms the other.

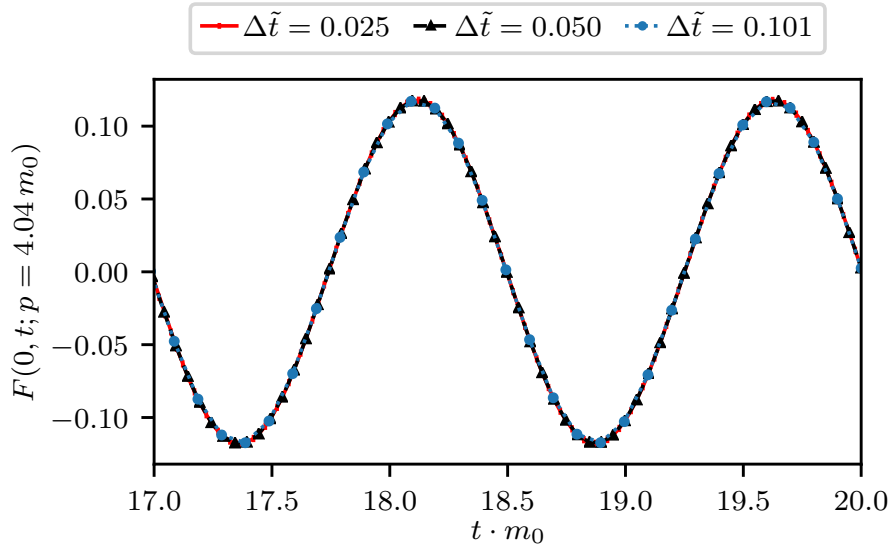


Figure C.2.: Time evolution of the statistical propagator F obtained using the *explicit solver* for various time resolutions $\Delta \tilde{t} = \Delta t \cdot m_0$. The curves are perfectly on top of each other. This indicates the faster convergence of the explicit solver as compared to the differential one. This figure is taken from [1].

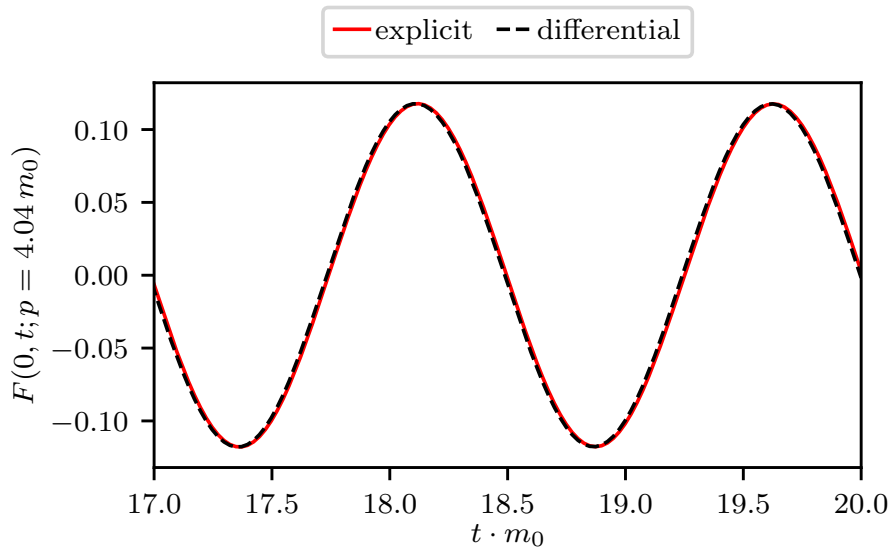


Figure C.3.: Time evolution of the statistical propagator F obtained using the differential and explicit solver for $\Delta \tilde{t} = \Delta t \cdot m_0 = 0.025$. Both solvers agree to numerical precision for small enough time-step size. This figure is taken from [1].

Acknowledgments

There are a lot of people whose support, in one way or another, allowed me to complete this work, and I am truly grateful to all of you. Having said that, clearly the following list of acknowledgements can not be exhaustive.

I thank my supervisor Jan M. Pawlowski. This work would not have been possible without your constant support. My understanding of physics in general and of the ideas laid out in this work in particular greatly benefited from the many discussions we had. I enjoyed working with you and I appreciate the fact that you were always up for a little fun.

I thank Joerg Jaeckel for being my second referee.

I thank my two collaborators Anton K. Cyrol and Lukas Corell. I greatly profited from the expertise that you shared with me. Moreover, I really enjoyed that we were not merely colleagues.

I thank Thomas Gasenzer, Aleksandr Mikheev, Christian-Marcel Schmied and Linda Shen for discussing various aspects of non-equilibrium physics with me.

I thank the staff at the Institute for Theoretical Physics, at the ITP library, at the Heidelberg Graduate School For Physics and at ISOQUANT for their work.

I thank ISOQUANT and the HGSPF for their financial support.

I thank Anton K. Cyrol, Bruno Faigle-Cedzich, Lukas Kades, Julian Urban and Felix Ziegler for critically reading parts of this manuscript.

I thank the entire crew of the Dachzimmer for the nice atmosphere at the office. I appreciate what I learned from you. Moreover, I appreciate the fact that we also did not talk about physics from time to time.

I thank them and the extended circle of fellow students and colleagues for the early coffee breaks and the late lunches, for the conferences, the lectures and the talks, for the mornings, the evenings and the occasional late nights. Thank you.

I thank my family for their unconditional support.

I thank my friends for their open ears and open hearts and for all our joyous and light-hearted moments.

I thank Eva for everything. Always.

Bibliography

- [1] L. Corell, A. K. Cyrol, M. Heller, and J. M. Pawłowski, “Flowing with the Temporal Renormalisation Group”, (2019), arXiv: 1910.09369.
- [2] L. Corell, M. Heller, and J. M. Pawłowski, ”Renormalised Causal Temporal Flow”, in preparation.
- [3] M. Heller, and J. M. Pawłowski, ”Causal Temporal Flow of the Energy-Momentum Tensor”, in preparation.
- [4] I. Bandos, M. Heller, S. M. Kuzenko, L. Martucci, and D. Sorokin, “The Goldstino brane, the constrained superfields and matter in $\mathcal{N} = 1$ supergravity”, JHEP 11, 109 (2016), arXiv: 1608.05908.
- [5] M. Heller, and M. Mitter, “Pion and η -meson mass splitting at the two-flavour chiral crossover”, Phys. Rev. D 94, 074002 (2016), arXiv: 1512.05241.
- [6] T. Gasenzer, and J. M. Pawłowski, “Towards far-from-equilibrium quantum field dynamics: A functional renormalisation-group approach”, Phys. Lett. Sect. B 670, 135–140 (2008), arXiv: 0710.4627.
- [7] T. Gasenzer, S. Keßler, and J. M. Pawłowski, “Far-from-equilibrium quantum many-body dynamics”, Eur. Phys. J. C 70, 423–443 (2010), arXiv: 1003.4163.
- [8] M. Rigol, V. Dunjko, and M. Olshanii, “Thermalization and its mechanism for generic isolated quantum systems.”, Nature 452, 854–8 (2008), arXiv: 0708.1324.
- [9] L. D’Alessio, Y. Kafri, A. Polkovnikov, and M. Rigol, “Review From Quantum Chaos and Eigenstate Thermalization to Statistical Mechanics and Thermodynamics”, Adv. Phys. 65, 239–362 (2016), arXiv: 1509.06411v3.
- [10] J. Berges, “Introduction to Nonequilibrium Quantum Field Theory”, in Aip conf. proc. Vol. 739 (Sept. 2005), pp. 3–62, arXiv: 0409233.
- [11] T. Gasenzer, “Ultracold gases far from equilibrium”, Eur. Phys. J. Spec. Top. 168, 89–148 (2009), arXiv: 0812.0004.

- [12] A. Kamenev, and A. Levchenko, “Keldysh technique and non-linear sigma-model: basic principles and applications”, *Adv. Phys.* 58, 197–319 (2009), arXiv: 0901.3586.
- [13] S. Hermanns, K. Balzer, and M. Bonitz, “Few-particle quantum dynamics -- Comparing nonequilibrium Green functions with the generalized Kadanoff-Baym ansatz to density operator theory”, in *J. phys. conf. ser.* Vol. 427 (2013), arXiv: 1211.6959.
- [14] J. Berges, ”Nonequilibrium Quantum Fields: From Cold Atoms to Cosmology”, 2015, arXiv: 1503.02907.
- [15] P. Millington, and A. Pilaftsis, “Perturbative nonequilibrium thermal field theory”, *Phys. Rev. D* 88, 085009 (2013), arXiv: 1211.3152.
- [16] J. Eisert, M. Friesdorf, and C. Gogolin, “Quantum many-body systems out of equilibrium”, *Nat. Phys.* 11, 124 (2014), arXiv: 1408.5148.
- [17] F. Cooper, and E. Mottola, “Initial-value problems in quantum field theory in the large- N approximation”, *Phys. Rev. D* 36, 3114–3127 (1987).
- [18] R. Micha, and I. I. Tkachev, “Relativistic Turbulence: A Long Way from Preheating to Equilibrium”, *Phys. Rev. Lett.* 90, 121301 (2003), arXiv: hep-ph/0210202.
- [19] R. Micha, and I. I. Tkachev, “Turbulent thermalization”, *Phys. Rev. D* 70, 043538 (2004), arXiv: hep-ph/0403101.
- [20] J. Berges, M. P. Heller, A. Mazeliauskas, and R. Venugopalan, ”Thermalization in QCD: Theoretical approaches, phenomenological applications, and interdisciplinary connections”, 2020, arXiv: 2005.12299.
- [21] W. Busza, K. Rajagopal, and W. van der Schee, “Heavy Ion Collisions: The Big Picture, and the Big Questions”, *Annu. Rev. Nucl. Part. Sci.* 68, 339–376 (2018), arXiv: 1802.04801.
- [22] G. Baym, and L. P. Kadanoff, “Conservation laws and correlation functions”, *Phys. Rev.* 124, 287–299 (1961).
- [23] J. M. Cornwall, R. Jackiw, and E. Tomboulis, “Effective action for composite operators”, *Phys. Rev. D* 10, 2428–2445 (1974).
- [24] A. Arrizabalaga, and J. Smit, “Gauge-fixing dependence of Phi-derivable approximations”, *Phys. Rev. D* 66, 065014 (2002), arXiv: 0207044.
- [25] M. E. Carrington, G. Kunstatter, and H. Zaraket, “2PI effective action and gauge invariance problems”, *Eur. Phys. J. C* 42, 253–259 (2003), arXiv: 0309084.

-
- [26] M. E. Carrington, and Y. Guo, “Techniques for n-particle irreducible effective theories”, *Phys. Rev. D* 83, 016006 (2011), arXiv: 1010.2978.
- [27] T. Zöller, “Nonequilibrium formulation of abelian gauge theories”, PhD thesis (Darmstadt, Tech. Hochsch., 2013).
- [28] A. Pilaftsis, and D. Teresi, “Symmetry Improved CJT Effective Action”, *Nucl. Phys. B* 874, 594–619 (2013), arXiv: 1305.3221 [hep-ph].
- [29] B. Garbrecht, and P. Millington, “Constraining the effective action by a method of external sources”, *Nucl. Phys. B* 906, 105 (2016), arXiv: 1509.07847.
- [30] C. Wetterich, “Exact evolution equation for the effective potential”, *Phys.Lett. B* 301, 90–94 (1993).
- [31] U. Ellwanger, “Flow equations for N point functions and bound states”, *Z. Phys. C* 62, 503–510 (1994), arXiv: hep-ph/9308260.
- [32] T. R. Morris, “The Exact renormalization group and approximate solutions”, *Int. J. Mod. Phys. A* 9, 2411–2450 (1994), arXiv: hep-ph/9308265.
- [33] N. Dupuis, L. Canet, A. Eichhorn, W. Metzner, J. Pawłowski, M. Tissier, and N. Wschebor, “The nonperturbative functional renormalization group and its applications”, *Phys. Rep.* (2021), arXiv: 2006.04853.
- [34] M. Pietroni, “Flowing with Time: a New Approach to Nonlinear Cosmological Perturbations”, *JCAP* 0810, 036 (2008), arXiv: 0806.0971.
- [35] S. G. Jakobs, V. Meden, and H. Schoeller, “Nonequilibrium Functional Renormalization Group for Interacting Quantum Systems”, *Phys. Rev. Lett.* 99, 150603 (2007), arXiv: cond-mat/0702494.
- [36] J. Berges, and G. Hoffmeister, “Nonthermal fixed points and the functional renormalization group”, *Nucl. Phys. B* 813, 383–407 (2009), arXiv: 0809.5208.
- [37] S. G. Jakobs, M. Pletyukhov, and H. Schoeller, “Nonequilibrium functional renormalization group with frequency-dependent vertex function: A study of the single-impurity Anderson model”, *Phys. Rev. B* 81, 195109 (2010), arXiv: 0911.5502.
- [38] L. Canet, H. Chate, B. Delamotte, and N. Wschebor, “Non-perturbative renormalization group for the Kardar-Parisi-Zhang equation”, *Phys. Rev. Lett.* 104, 150601 (2010), arXiv: 0905.1025.
- [39] D. M. Kennes, S. G. Jakobs, C. Karrasch, and V. Meden, “Renormalization group approach to time-dependent transport through correlated quantum dots”, *Phys. Rev. B* 85, 085113 (2012), arXiv: 1111.6982.

- [40] L. Canet, H. Chate, B. Delamotte, and N. Wschebor, “Non-perturbative renormalisation group for the Kardar-Parisi-Zhang equation: general framework and first applications”, *Phys. Rev. E* **84**, 061128 (2011), arXiv: 1107.2289.
- [41] J. Berges, and D. Mesterhazy, “Introduction to the nonequilibrium functional renormalization group”, *Nucl. Phys. Proc. Suppl.* **228**, 37–60 (2012), arXiv: 1204.1489.
- [42] L. M. Sieberer, S. D. Huber, E. Altman, and S. Diehl, “Dynamical Critical Phenomena in Driven-Dissipative Systems”, *Phys. Rev. Lett.* **110**, 195301 (2013), arXiv: 1301.5854.
- [43] D. Mesterházy, J. H. Stockemer, L. F. Palhares, and J. Berges, “Dynamic universality class of Model C from the functional renormalization group”, *Phys. Rev. B* **88**, 174301 (2013), arXiv: 1307.1700.
- [44] L. M. Sieberer, S. D. Huber, E. Altman, and S. Diehl, “Nonequilibrium functional renormalization for driven-dissipative Bose-Einstein condensation”, *Phys. Rev. B* **89**, 134310 (2014), arXiv: 1309.7027.
- [45] L. Canet, B. Delamotte, and N. Wschebor, “Fully developed isotropic turbulence: nonperturbative renormalization group formalism and fixed point solution”, *Phys. Rev. E* **93**, 063101 (2016), arXiv: 1411.7780.
- [46] D. Mesterházy, J. H. Stockemer, and Y. Tanizaki, “From quantum to classical dynamics: The relativistic $O(N)$ model in the framework of the real-time functional renormalization group”, *Phys. Rev. D* **92**, 076001 (2015), arXiv: 1504.07268.
- [47] A. Chiocchetta, A. Gambassi, S. Diehl, and J. Marino, “Universal short-time dynamics: boundary functional renormalization group for a temperature quench”, *Phys. Rev. B* **94**, 174301 (2016), arXiv: 1606.06272.
- [48] C. Duclut, and B. Delamotte, “Frequency regulators for the nonperturbative renormalization group: A general study and the model A as a benchmark”, *Phys. Rev. E* **95**, 012107 (2017), arXiv: 1611.07301.
- [49] M. Tarpin, L. Canet, and N. Wschebor, “Breaking of scale invariance in the time dependence of correlation functions in isotropic and homogeneous turbulence”, *Phys. Fluids* **30**, 055102 (2018), arXiv: 1707.06809.
- [50] M. Tarpin, L. Canet, C. Pagani, and N. Wschebor, “Stationary, isotropic and homogeneous two-dimensional turbulence: a first non-perturbative renormalization group approach”, *J. Phys. A* **52**, 085501 (2019), arXiv: 1809.00909.

-
- [51] H. Schoeller, “Dynamics of open quantum systems”, arXiv:1802.10014 (2018), arXiv: 1802.10014.
- [52] J. Berges, K. Boguslavski, S. Schlichting, and R. Venugopalan, “Turbulent thermalization process in heavy-ion collisions at ultrarelativistic energies”, Phys. Rev. D 89, 074011 (2014), arXiv: 1303.5650.
- [53] J. Berges, K. Boguslavski, S. Schlichting, and R. Venugopalan, “Universal attractor in a highly occupied non-Abelian plasma”, Phys. Rev. D 89, 114007 (2014), arXiv: 1311.3005.
- [54] J. Berges, A. Rothkopf, and J. Schmidt, “Nonthermal fixed points: Effective weak coupling for strongly correlated systems far from equilibrium”, Phys. Rev. Lett. 101 (2008), arXiv: 0803.0131.
- [55] J. Berges, and G. Hoffmeister, “Nonthermal fixed points and the functional renormalization group”, Nucl. Phys. B 813, 383–407 (2009).
- [56] J. Berges, and D. Sexty, “Strong versus weak wave-turbulence in relativistic field theory”, Phys. Rev. D - Part. Fields, Gravit. Cosmol. 83 (2011), arXiv: 1012.5944.
- [57] A. Piñeiro Orioli, K. Boguslavski, and J. Berges, “Universal self-similar dynamics of relativistic and nonrelativistic field theories near nonthermal fixed points”, Phys. Rev. D - Part. Fields, Gravit. Cosmol. 92 (2015), arXiv: 1503.02498.
- [58] J. Berges, K. Boguslavski, S. Schlichting, and R. Venugopalan, “Universality far from equilibrium: From superfluid bose gases to heavy-ion collisions”, Phys. Rev. Lett. 114, 061601 (2015), arXiv: 1408.1670.
- [59] M. Prüfer, P. Kunkel, H. Stobel, S. Lannig, D. Linnemann, C.-M. Schmied, J. Berges, T. Gasenzer, and M. K. Oberthaler, “Observation of universal dynamics in a spinor Bose gas far from equilibrium”, Nature 563, 217–220 (2018), arXiv: 1805.11881.
- [60] S. Erne, R. Bücker, T. Gasenzer, J. Berges, and J. Schmiedmayer, “Universal dynamics in an isolated one-dimensional Bose gas far from equilibrium”, Nature 563, 225–229 (2018).
- [61] T. Schweigler, V. Kasper, S. Erne, I. Mazets, B. Rauer, F. Cataldini, T. Langen, T. Gasenzer, J. Berges, and J. Schmiedmayer, “Experimental characterization of a quantum many-body system via higher-order correlations”, Nature 545, 323–326 (2017).

- [62] M. Prüfer, T. V. Zache, P. Kunkel, S. Lannig, A. Bonnin, H. Strobel, J. Berges, and M. K. Oberthaler, “Experimental extraction of the quantum effective action for a non-equilibrium many-body system”, *Nat. Phys.* 16, 1012–1016 (2020), arXiv: 1909.05120.
- [63] A. Chatrchyan, K. T. Geier, M. K. Oberthaler, J. Berges, and P. Hauke, “Analog reheating of the early universe in the laboratory”, (2020), arXiv: 2008.02290.
- [64] C. Scheppach, J. Berges, and T. Gasenzer, “Matter-wave turbulence: Beyond kinetic scaling”, *Phys. Rev. A - At. Mol. Opt. Phys.* 81 (2010), arXiv: 0912.4183.
- [65] B. Nowak, S. Erne, M. Karl, J. Schole, D. Sexty, and T. Gasenzer, “Non-thermal fixed points: universality, topology, and turbulence in Bose gases”, in *Strongly interacting quantum systems out of equilibrium*, Vol. 99 (Aug. 2012), arXiv: 1302.1448.
- [66] I. Chantesana, A. P. Orioli, and T. Gasenzer, “Kinetic theory of nonthermal fixed points in a Bose gas”, *Phys. Rev. A* 99 (2019), arXiv: 1801.09490.
- [67] C.-M. Schmied, A. N. Mikheev, and T. Gasenzer, “Non-thermal fixed points: Universal dynamics far from equilibrium”, *Int. J. Mod. Phys. A* 34, 1941006 (2019), arXiv: 1810.08143.
- [68] S. Mathey, T. Gasenzer, and J. M. Pawłowski, “Anomalous scaling at nonthermal fixed points of Burgers’ and Gross-Pitaevskii turbulence”, *Phys. Rev. A* 92, 023635 (2015), arXiv: 1405.7652.
- [69] J. Schwinger, “Brownian motion of a quantum oscillator”, *Journal of Mathematical Physics* 2, 407–432 (1961).
- [70] L. V. Keldysh, “Diagram technique for nonequilibrium processes”, *Zh. Eksp. Teor. Fiz.* 47, [English translation: *JETP* 20, 1018 (1965)], 1515 (1964).
- [71] O. V. Konstantinov, and V. I. Perel, “A diagram technique for evaluating transport quantities”, *Zh. Eksp. Teor. Fiz.* 39, [English translation: *JETP* 12, 142 (1961)], 197 (1960).
- [72] L. P. Kadanoff, and G. A. Baym, *Quantum statistical mechanics, Green’s function methods in equilibrium and nonequilibrium problems* (Benjamin, 1962).
- [73] K. T. Mahanthappa, “Multiple production of photons in quantum electrodynamics”, *Phys. Rev.* 126, 329–340 (1962).
- [74] P. M. Bakshi, and K. T. Mahanthappa, “Expectation value formalism in quantum field theory. I”, *J. Math. Phys.* 4, 1–11 (1963).

-
- [75] P. M. Bakshi, and K. T. Mahanthappa, “Expectation value formalism in quantum field theory. II”, *J. Math. Phys.* 4, 12–16 (1963).
- [76] R. P. Feynman, and F. L. Vernon, Jr., “The theory of a general quantum system interacting with a linear dissipative system”, *Annals Phys.* 24, edited by L. M. Brown, 118–173 (1963).
- [77] E. A. Calzetta, and B.-L. B. Hu, *Nonequilibrium quantum field theory* (Cambridge Univ. Press, 2008).
- [78] G. Stefanucci, and R. Van Leeuwen, *Nonequilibrium many-body theory of quantum systems: A modern introduction* (Cambridge Univ. Press, 2013).
- [79] H. Kleinert, *Particles and quantum fields* (World Scientific, 2016).
- [80] W. Siegel, *Fields* (Dec. 1999), arXiv: hep-th/9912205.
- [81] T. Gasenzer, and J. M. Pawłowski, “Towards far-from-equilibrium quantum field dynamics: A functional renormalisation-group approach”, *Phys. Lett. B* 670, 135–140 (2008), arXiv: 0710.4627.
- [82] T. Gasenzer, S. Kessler, and J. M. Pawłowski, “Far-from-equilibrium quantum many-body dynamics”, *Eur.Phys.J. C* 70, 423–443 (2010), arXiv: 1003.4163.
- [83] D. Semkat, M. Bonitz, and D. Kremp, “Relaxation of a quantum many-body system from a correlated initial state. A general and consistent approach”, *Contrib. to Plasma Phys.* 43, 321–325 (2003).
- [84] I. De Vega, and D. Alonso, “Dynamics of non-Markovian open quantum systems”, *Rev. Mod. Phys.* 89, 015001 (2017), arXiv: 1511.06994.
- [85] N. Schlünzen, S. Hermanns, M. Scharnke, and M. Bonitz, “Ultrafast dynamics of strongly correlated fermions - Nonequilibrium Green functions and selfenergy approximations”, *J. Phys. Condens. Matter* 32 (2020), arXiv: 1902.07038.
- [86] L. V. Keldysh, “Real-time Nonequilibrium Green’s Functions”, in *Progress in Nonequilibrium Green’s Functions II* (2003).
- [87] H. van Hees, “Nonequilibrium relativistic many-body theory”, <https://itp.uni-frankfurt.de/~hees/publ/off-eq-qft.pdf>, [Online lecture notes; accessed 09-April-2021], 2017.
- [88] R. Dickinson, J. Forshaw, P. Millington, and B. Cox, “Manifest causality in quantum field theory with sources and detectors”, *J. High Energy Phys.* 2014, 49 (6), arXiv: 1312.3871.

- [89] F. M. Haehl, R. Loganayagam, and M. Rangamani, “The fluid manifesto: emergent symmetries, hydrodynamics, and black holes”, *J. High Energy Phys.* 01, 184 (2016), arXiv: 1510.02494.
- [90] F. M. Haehl, R. Loganayagam, and M. Rangamani, “Schwinger-Keldysh formalism. Part I: BRST symmetries and superspace”, *J. High Energy Phys.* 2017, 69 (2017), arXiv: 1610.01940.
- [91] F. M. Haehl, R. Loganayagam, and M. Rangamani, “Schwinger-Keldysh formalism. Part II: Thermal equivariant cohomology”, *J. High Energy Phys.* 070, 70 (2017), arXiv: 1610.01941.
- [92] P. Gao, P. Glorioso, and H. Liu, “Ghostbusters: unitarity and causality of non-equilibrium effective field theories”, *J. High Energy Phys.* 40, 1–20 (2020), arXiv: 1803.10778.
- [93] A. Das, *Finite Temperature Field Theory* (World Scientific, 1997).
- [94] D. Boyanovsky, H. J. de Vega, R. Holman, D. S. Lee, and A. Singh, “Dissipation via particle production in scalar field theories”, *Phys. Rev. D* 51, 4419–4444 (1995), arXiv: hep-ph/9408214.
- [95] B. Mihaila, J. F. Dawson, and F. Cooper, “Order $1/N$ corrections to the time-dependent Hartree approximation for a system of $N+1$ oscillators”, *Phys. Rev. D* 56, 5400–5412 (1997), arXiv: 9705354.
- [96] M. Brown, and I. Whittingham, “Two-particle irreducible effective actions versus resummation: Analytic properties and self-consistency”, *Nucl. Phys. B* 900, 477–500 (2015), arXiv: 1503.08664v3.
- [97] M. E. Carrington, B. A. Meggison, and D. Pickering, “The 2PI effective action at four loop order in ϕ^4 theory”, *Phys. Rev. D* 94, 025018 (2016), arXiv: 1603.02085.
- [98] A. Arrizabalaga, J. Smit, and A. Tranberg, “Equilibration in ϕ^4 theory in 3+1 dimensions”, *Phys. Rev. D* 72, 025014 (2005), arXiv: 0503287.
- [99] M. E. Carrington, W.-J. Fu, P. Mikula, and D. Pickering, “Four-point vertices from the 2PI and 4PI Effective Actions”, *Phys. Rev. D* 89, 025013 (2014), arXiv: 1310.4352.
- [100] M. Carrington, “Techniques for calculations with n PI effective actions”, EPJ Web Conf. 95, edited by L. Bravina, Y. Foka, and S. Kabana, 04013 (2015).
- [101] B. Garbrecht, and P. Millington, “Green’s function method for handling radiative effects on false vacuum decay”, *Phys. Rev. D* 91, 105021 (2015), arXiv: 1501.07466.

-
- [102] H. Kleinert, *Path integrals in quantum mechanics, statistics, polymer physics, and financial markets*, 5th (World Scientific, 2009).
- [103] A. Kamenev, *Field theory of non-equilibrium systems* (Cambridge University Press, 2011).
- [104] R. S. Souto, R. Avriller, A. L. Yeyati, and A. Martin-Rodero, “Transient dynamics in interacting nanojunctions within self-consistent perturbation theory”, *New J. Phys.* 20, 83039 (2018), arXiv: 1803.07372.
- [105] T. Prokopec, and D. Glavan, ”A pedestrian introduction to non-equilibrium QFT”, <https://webpace.science.uu.nl/~proko101/LecturenotesNonEquilQFT.pdf>, [Online lecture notes; accessed 04-April-2021], 2017.
- [106] J. M. Pawłowski, “Aspects of the functional renormalisation group”, *Annals Phys.* 322, 2831–2915 (2007), arXiv: hep-th/0512261.
- [107] M. Garny, and M. M. Müller, “Kadanoff-Baym equations with non-Gaussian initial conditions: The equilibrium limit”, *Phys. Rev. D - Part. Fields, Gravit. Cosmol.* 80, 85011 (2009), arXiv: 0904.3600.
- [108] J. P. Blaizot, J. M. Pawłowski, and U. Reinosa, “Exact renormalization group and Φ -derivable approximations”, *Phys. Lett. Sect. B Nucl. Elem. Part. High-Energy Phys.* 696, 523–528 (2011), arXiv: 1009.6048.
- [109] M. E. Carrington, “Renormalization group flow equations connected to the n -particle-irreducible effective action”, *Phys. Rev. D* 87, 045011 (2013), arXiv: 1211.4127.
- [110] M. E. Carrington, W.-J. Fu, D. Pickering, and J. W. Pulver, “Renormalization group methods and the 2PI effective action”, *Phys. Rev. D* 91, 025003 (2015), arXiv: 1404.0710.
- [111] D. F. Litim, and J. M. Pawłowski, “Completeness and consistency of renormalisation group flows”, *Phys.Rev. D* 66, 025030 (2002), arXiv: hep-th/0202188.
- [112] A. K. Cyrol, “Non-perturbative QCD correlation functions”, PhD thesis (Heidelberg U., 2017).
- [113] M. Geracie, F. M. Haehl, R. Loganayagam, P. Narayan, D. M. Ramirez, and M. Rangamani, “Schwinger-Keldysh superspace in quantum mechanics”, *Phys. Rev. D* 97, 105023 (2018), arXiv: 1712.04459.
- [114] T. R. Morris, “Momentum Scale Expansion of Sharp Cutoff Flow Equations”, *Nucl. Phys. B* 458, 477–503 (1996), arXiv: 9508017.

- [115] T. R. Morris, “The Exact Renormalisation Group and Approximate Solutions”, *Int. J. Mod. Phys. A* 9, 2411–2450 (1994), arXiv: 9308265.
- [116] M. J. Hyrkas, D. Karlsson, and R. Van Leeuwen, “Contour calculus for many-particle functions”, *J. Phys. A Math. Theor.* 52 (2019), arXiv: 1903.03489.
- [117] F. Haehl, R. Loganayagam, P. Narayan, and M. Rangamani, “Classification of out-of-time-order correlators”, *SciPost Phys.* 6, 001 (2019), arXiv: 1701.02820.
- [118] J. M. Pawłowski, private communication.
- [119] W. Metzner, M. Salmhofer, C. Honerkamp, V. Meden, and K. Schönhammer, “Functional renormalization group approach to correlated fermion systems”, *Rev. Mod. Phys.* 84, 299–352 (2012), arXiv: 1105.5289.
- [120] T. S. Evans, “What is being calculated with thermal field theory?”, in *9th Lake Louise Winter Institute: Particle Physics and Cosmology* (Mar. 1994), arXiv: hep-ph/9404262.
- [121] S. Huelsmann, S. Schlichting, and P. Scior, “Spectral functions from the real-time functional renormalization group”, *Phys. Rev. D* 102, 096004 (2020), arXiv: 2009.04194.
- [122] N. Wink, “Towards the spectral properties and phase structure of qcd.”, PhD thesis (U. Heidelberg, ITP, 2020).
- [123] R. Alkofer, and L. von Smekal, “The Infrared behavior of QCD Green’s functions: Confinement dynamical symmetry breaking, and hadrons as relativistic bound states”, *Phys. Rept.* 353, 281 (2001), arXiv: hep-ph/0007355.
- [124] M. Huber, “On gauge fixing aspects of the infrared behavior of yang-mills green functions”, PhD thesis (Graz U., 2010), arXiv: 1005.1775.
- [125] J. Berges, and B. Wallisch, “Nonthermal fixed points in quantum field theory beyond the weak-coupling limit”, *Phys. Rev. D* 95 (2017), arXiv: 1607.02160.
- [126] L. Shen, and J. Berges, “Spectral, statistical and vertex functions in scalar quantum field theory far from equilibrium”, *Phys. Rev. D* 101, 056009 (2020), arXiv: 1912.07565.
- [127] B. Mihaila, J. F. Dawson, and F. Cooper, “Resumming the large- N approximation for time evolving quantum systems”, *Phys. Rev. D* 63, 096003 (2001), arXiv: 0006254.
- [128] J. Berges, “Controlled nonperturbative dynamics of quantum fields out of equilibrium”, *Nucl. Phys. A* 699, 847–886 (2002), arXiv: 0105311.

-
- [129] J. Berges, and J. Serreau, “Parametric resonance in quantum field theory”, *Phys. Rev. Lett.* 91 (2003), arXiv: 0208070.
- [130] B. Mihaila, “Real-time dynamics of the $O(N)$ model in 1+1 dimensions”, *Phys. Rev. D* 68, 036002 (2003), arXiv: 0303157.
- [131] J. Berges, and D. Mesterházy, “Introduction to the nonequilibrium functional renormalization group”, *Nucl. Phys. B - Proc. Suppl.* 228, 37–60 (2012), arXiv: 1204.1489.
- [132] Y.-L. Wu, *Selected Papers of K. C. Chou* (World Scientific, 2009).
- [133] K.-C. Chou, Z.-B. Su, B.-L. Hao, and L. Yu, “Equilibrium and Nonequilibrium Formalisms Made Unified”, *Phys. Rept.* 118, 1–131 (1985).
- [134] S. Borsányi, and U. Reinosa, “Renormalized nonequilibrium quantum field theory: Scalar fields”, *Phys. Rev. D - Part. Fields, Gravit. Cosmol.* 80, 125029 (2009), arXiv: 0809.0496.
- [135] M. Garny, and U. Reinosa, “Renormalization out of equilibrium in a superrenormalizable theory”, *Phys. Rev. D* 94, 1–10 (2016).
- [136] H. van Hees, and J. Knoll, “Renormalization in Self-Consistent Approximations schemes at Finite Temperature I: Theory”, *Phys. Rev. D* 65, 025010 (2001), arXiv: hep-ph/0107200.
- [137] H. van Hees, and J. Knoll, “Renormalization of Self-consistent Approximation schemes Finite Temperature II: Applications to the Sunset Diagram”, *Phys. Rev. D* 65, 105005 (2001), arXiv: hep-ph/0111193.
- [138] J.-P. Blaizot, E. Iancu, and U. Reinosa, “Renormalization of Phi derivable approximations in scalar field theories”, *Nucl. Phys. A* 736, 149–200 (2004), arXiv: hep-ph/0312085.
- [139] L. Shen, “Universal dynamics and thermalization in isolated quantum systems”, PhD thesis (U. Heidelberg (main), 2020).
- [140] M. E. Carrington, S. A. Friesen, C. D. Phillips, and D. Pickering, “Renormalization of the 4PI effective action using the functional renormalization group”, *Phys. Rev. D* 99, 074002 (2019), arXiv: 1901.00840.
- [141] H. Collins, and R. Holman, “Renormalization of initial conditions and the trans-Planckian problem of inflation”, *Phys. Rev. D - Part. Fields, Gravit. Cosmol.* 71, 1–22 (2005), arXiv: 0501158.

- [142] J. F. Kokksma, T. Prokopec, and M. G. Schmidt, “Decoherence in an interacting quantum field theory: The vacuum case”, *Phys. Rev. D - Part. Fields, Gravit. Cosmol.* 81 (2010), arXiv: 0910.5733.
- [143] S. Swain, “Master equation derivation of quantum regression theorem”, *J. Phys. A. Math. Gen.* 14, 2577–2580 (1981).
- [144] J. F. Kokksma, T. Prokopec, and M. G. Schmidt, “Decoherence in an interacting quantum field theory: Thermal case”, *Phys. Rev. D - Part. Fields, Gravit. Cosmol.* 83, 085011 (2011), arXiv: 1102.4713.
- [145] J. Serreau, “Out-of-equilibrium electromagnetic radiation”, *J. High Energy Phys.* 8, 1873–1907 (2004), arXiv: 0310051.
- [146] J. Berges, J. Pruschke, and A. Rothkopf, “Instability-induced fermion production in quantum field theory”, *Phys. Rev. D* 80, 023522 (2009), arXiv: 0904.3073.
- [147] M. Schmidt, S. Erne, B. Nowak, D. Sexty, and T. Gasenzer, “Non-thermal fixed points and solitons in a one-dimensional Bose gas”, *New Journal of Physics* 14 (2012), arXiv: 1203.3651.
- [148] M. Karl, and T. Gasenzer, “Strongly anomalous non-thermal fixed point in a quenched two-dimensional Bose gas”, *New J. Phys.* 19, 093014 (2017), arXiv: 1611.01163.
- [149] F. Cooper, J. F. Dawson, and B. Mihaila, “Dynamics of broken symmetry lambda phi**4field theory”, *Phys. Rev. D* 67, 051901 (2003), arXiv: 0207346.
- [150] A. N. Mikheev, C. M. Schmied, and T. Gasenzer, “Low-energy effective theory of nonthermal fixed points in a multicomponent Bose gas”, *Phys. Rev. A* 99 (2019), arXiv: 1807.10228.
- [151] T. Gasenzer, private communication.
- [152] S. Mathey, T. Gasenzer, and J. M. Pawłowski, “Anomalous scaling at non-thermal fixed points of Burgers’ and Gross-Pitaevskii turbulence”, *Phys. Rev. A* 92, 023635 (2015), arXiv: 1405.7652.
- [153] J. M. Pawłowski and N. Wink, in preparation.
- [154] K.-c. Chou, Z.-b. Su, B.-l. Hao, and L. Yu, “Equilibrium and nonequilibrium formalisms made unified”, *Physics Reports* 118, 1–131 (1985).